TT 74-50028

The Publication of this Translation
was Supported by
THE UNITED STATES–ISRAEL
BINATIONAL SCIENCE FOUNDATION


Cat. No. 61028 3
ISBN 0 7065 1496 3



Translated by R. Kondor
Edited by P. Greenberg

Printed and bound by Keterpress Enterprises, Jerusalem

Available from the
U.S. DEPARTMENT OF COMMERCE
National Technical Information Service
Springfield, Va. 22151

N O T I C E

THIS DOCUMENT HAS BEEN REPRODUCED FROM THE BEST COPY FURNISHED US BY THE SPONSORING AGENCY. ALTHOUGH IT IS RECOGNIZED THAT CERTAIN PORTIONS ARE ILLEGIBLE, IT IS BEING RELEASED IN THE INTEREST OF MAKING AVAILABLE AS MUCH INFORMATION AS POSSIBLE.

## *FOREWORD*

Steady-state deflagration and detonation processes in condensed systems have now been investigated to a fair extent. Research on this problem began already at the end of the nineteenth century. Interest in the investigation of transient processes arose much later. The first papers dealing with this problem were written by Belyaev /1–5/, Andreev /6–8/ and Patry /9/, and appeared at the end of the thirties and beginning of the forties. Intensive research on the initiation and propagation of detonation has been carried out in the USSR and elsewhere (USA, England). The problem is far from completely solved, regardless of the advances made toward its better understanding.

Initiation of detonation under industrial conditions is a very dangerous phenomenon. Therefore, knowledge of the mechanism and conditions underlying transition from deflagration to detonation has not only scientific but major economic importance, especially when solving problems related to the provision of explosion-proof industrial plants.

This book is based on experimental data obtained by the authors between 1959 and 1970 at the Institute of Chemical Physics of the USSR Academy of Sciences. Moreover, this book systematizes and generalizes available literature data concerning this problem.

Transition from deflagration to detonation is a multistage process. The idea underlying the research was to separate and study each stage separately and to obtain information on the patterns of transition from one stage to another. Special attention was paid to the physical essence of the phenomenon. This approach was the most convenient, since in some cases (e.g., intensive impact (shock, impulse) excitation of a detonation) the individual stages last a very short time and some may be even absent. The approach given in this book proved fruitful and yielded a reasonably complete picture of the buildup of detonation from stable layer-by-layer deflagration to the initiation of a detonation.

The book includes an introduction and two parts. The introduction deals with the method of investigating rapid processes. The instrumentation and equipment used in research on transition from deflagration to detonation are described. The first part deals with solid porous explosives whose deflagration passes very readily over to detonation. These explosives are widely applied in practice to the production of propellant powders and monolithic explosive charges in the mining and construction industries.

Chapter I presents general properties of porous systems. The methods and principal results of the determination of the porosity, gas permeability, specific pore surface, and size distribution of the pores are reported. Chapter II deals with slow stable deflagration at a constant rate. The resulting experimental results are compared with the conclusions drawn from the theory of the deflagration of explosives and propellant powders.

The results of research on the initial stages of detonation (impairment of stable layer-by-layer deflagration) are given in Chapter III. The fundamentals of the theory of stable deflagration are examined. The effect of the main factors on the impairment of layer-by-layer deflagration are investigated. The theory of the limits of stability was developed; this theory permits one to derive the principles underlying the quantitative description of the tendency of diverse explosives to impair layer-by-layer deflagration conditions.

Data on the stability of a system which contains pores not connected with one another are reported in Chapter IV. Chapter V develops the main stages of the buildup of detonation to detonation. Special attention is devoted to convective deflagration, which results from an impairment in the stability.

Problems pertaining to the low-velocity (800–3500 m/sec) propagation of explosive transition are discussed. Results of research on transition from deflagration to detonation in explosives are reported. The effect of various factors on the size of the predetonation section are discussed for homogeneous and liquid explosives. The mechanism governing the initiation of detonation during ignition is considered. Data pertaining to the shock-wave initiation of detonations in porous explosives are presented.

The second part of the book consists of two chapters dealing with problems of the deflagration stability of liquid explosives.

The theory of the normal deflagration limit in low-viscosity liquid explosives is explained in Chapter VI. The conditions of normal transition from deflagration to perturbed conditions and the effects of liquid properties and combustion conditions on deflagration stability are analyzed. The phenomena characterizing the deflagration of liquid explosives beyond the stability limits are discussed. Chapter VII deals with experimental data on the hydrodynamic stability of the deflagration of individual homogeneous and mixed liquid explosives and the transition from perturbed deflagration to detonation. The results of experimental research on the deflagration laws governing two-phase (liquid–solid) systems are reported.

It is hoped that this book will promote the development of research in this intricate and interesting branch of physics. The authors express their thanks to M. K. Sukoyan, I. A. Karpukhin and A. V. Obmerin for their help in preparing the book.



CONTENTS

*Introduction*

## *METHODS OF INVESTIGATING TRANSITION FROM DEFLAGRATION TO DETONATION*

Transition from deflagration to detonation is a multistage nonsteady-state process. Comprehensive methods of research are required in order to study the very complicated pattern underlying this phenomenon and to obtain extensive information. The problem not only involves correct determination of the more important parameters (such as velocity, pressure, temperature), but also separation of the individual stages, since only such an approach will provide detailed data. The individual stages were separated by changing the experimental conditions.

The method used should satisfy a wide range of requirements, because the propagation velocity of the reaction ranges over seven orders of magnitude (from $10^{-1}$ cm/sec for normal deflagration to $10^{6}$ cm/sec in the final stage, if the process leads to detonation) whereas the corresponding pressure ranges over eight orders of magnitude (from $10^{-2}$ to $10^{3}$ atm).

We emphasize that research on the initiation of explosions in condensed systems is much more difficult than similar research on gaseous systems, due to the destructive action of high pressures. These difficulties increase for solid explosives which, in contrast to gases and liquid explosives, are not transparent; this considerably complicates the use of optical methods of study. The authors of this book have developed and applied new methods and instruments.

We now examine the equipment, methods and instrumentation for recording the more important process parameters employed in the study of transition from deflagration to detonation and the individual stages of this phenomenon. At low (especially atmospheric) pressures deflagration of most explosives follows the uniform pattern of normal layer-by-layer deflagration at a low constant rate. Above some elevated pressure (which depends on the density and properties of the explosive) layer-by-layer deflagration is impaired or ceases. Deflagration is therefore strongly accelerated and, under certain conditions, may pass to detonation.

Thus detonation arises if the explosive burns at a pressure above a certain limiting value.

## 1. HIGH-PRESSURE EQUIPMENT

The "constant-pressure" bomb (PB). The main purpose of this bomb, which is produced in several variants (up to 150, 350, 1000–5000 atm), is research on the deflagration of explosives and propellant powders. Such bombs are also used for studying the transition from deflagration of porous explosives to detonation. In non-Russian literature this equipment is termed the "Crawford bomb." The term "constant-pressure bomb" does not strictly define the equipment, since the pressure somewhat increases due to deflagration of the charge.

The bomb (Figure 1) comprises a thick-walled steel beaker (1) whose inner volume is 2–5 liters or more. The upper open part is hermetically sealed (using rubber packings) by a lid (2) just before the experiment begins. The deflagration process is observed and the propagation velocity measured mainly by an optical method. For this purpose the bomb is provided with a few transparent windows (3) made from optical glass or plexiglass. Electrical methods are also employed for determining the deflagration rate (see section 2). The pressure in the bomb used by the present authors was recorded by a specially developed, sensitive, quartz crystal probe (4). The explosive or powder sample (5) was fixed on a support connected to the lid of the bomb. The required pressure in the bomb was created by compressed nitrogen from a gas tank or by a compressor. This pressure was determined by a gauge connected to the interior of the bomb.

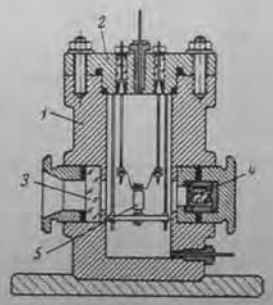


FIGURE 1. "Constant-pressure" bomb.

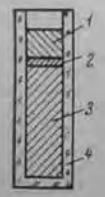


FIGURE 2. Schematic diagram of the "built-in charge."

It should be borne in mind that, unless special measures are taken, the pores of the investigated solid explosive charge become filled with nitrogen before the onset of deflagration, i. e., the pressure in the pores $p_p^0$ is equal to the pressure inside the bomb $p_0$. The pressure gradient $\Delta p$, which brings about penetration of the combustion products into the pores, arises during the combustion process, and usually $\Delta p \ll p_0$. The deflagration stability in this case is impaired by the jet mechanism (for a detailed treatment see section B, Chapter III).

Forced impairment of layer-by-layer deflagration of porous explosives (when gas flows into the pores under the action of a strictly defined and fixed pressure gradient produced prior to the onset of deflagration) was studied with the aid of a specially assembled explosive charge ("built-in charge") /10/, a schematic diagram of which is shown in Figure 2.

A solid auxiliary substance (1), functioning as the burning gas-impermeable partition, was pressed into a plexiglass shell (4) together with solid (2) and porous (3) samples. The lower end of the shell was glued on. This charge was placed in the bomb which, prior to the experiment, was filled with nitrogen to pressure $p_0$; the gas-impermeable partition was then ignited. Under these conditions the deflagration front approached the porous charge, when the initial pressure in the pores $p_p^0$ was equal to atmospheric pressure (usually $p_p^0 \ll p_0$, $\Delta p = p_0 - p_p^0 \simeq p_0$), and deflagration penetrates owing to the action of pressure $p_0$ inside the bomb. The "built-in charge" simulated deflagration of a porous inclusion in propellant powder charges. Therefore in some cases we ignited porous charge samples in model rocket chambers. Diverse variants of the rocket chamber were employed.

The deflagration process was recorded optically in addition to pressure $p(t)$. For this purpose a part of the chamber contains transparent windows.

Manometric bomb. The pressure in a manometric bomb is produced by combustion of the sample, which is placed in a small confined volume. This instrument is often termed a variable (increasing) pressure bomb. The manometric bomb makes it possible to determine the majority of the ballistic parameters of propellant powders and explosives (pressure dependence of deflagration rate, force of propellant powder, amount and composition of gases) and constitutes the most important instrument in interior ballistics laboratories. The fundamental laws governing standard deflagration of powders at high pressures (up to several thousand atmospheres) were determined by this instrument.

At present, various modifications of manometric bombs are widely employed for investigating the stability of the deflagration of propellant powders, solid rocket fuels, and explosives. The manometric bomb has a considerable advantage: the pressure increases during deflagration of the investigated charge. Therefore the critical pressure $p_0$ (at which stable deflagration is impaired) is easily attained.

One, presently used modification is shown in Figure 3a, and consists of a thick-walled cylindrical body (5) made from high-strength heat-treated steel. The solid sample in the form of tablets or powder in the form of a cartridge (3) was thoroughly cased along the lateral surface (4) and, with the exception of the upper end, placed into the duct of the bomb. The duct was hermetically sealed at its upper and lower ends with lids (1) and (7), clamped to the body of the bomb by slip rings (2).

The pressure in the bulk of the bomb is maintained by connecting the body to the lids by self-sealing copper rings (6). The lids are provided with insulated hermetically self-sealing electric terminals (8) and (11), capable of withstanding high pressures. The electric leads are in the form of a cone, whose base faces the inside of the bomb. The leads are insulated from the body of the bomb by conical plexiglass rings. The upper

lid is provided with a lead to supply electric current to the ignition device (9). This charge consists of a paper cartridge containing gunpowder or pyroxilin and a Nichrome spiral. The lower lid is provided with two insulated electric leads (11), which are used for measuring the propagation velocity of the process.

Specially developed, rapid-response piezoelectric probes (10) were used to record the time dependence of the pressure during the deflagration of the investigated charge (see section 3).

Figure 4 shows a typical $p(t)$ oscillogram in the bulk of the variable-pressure bomb when layer-by-layer deflagration ceases. The pressure increased smoothly with time as long as layer-by-layer deflagration proceeded. An abrupt pressure increase (the jump on the $p(t)$ curve) indicated that the critical pressure was reached, namely, the deflagration was impaired and broke through into the pores (the first peak on the curve is due to combustion of the ignition charge).

One of the bombs (Figure 3b) contained on its body (1) two plexiglass windows (2) for optical observation through a light conductor (3). This arrangement allowed additional information to be obtained on the process /11/ taking place in the sample (4). Probes (5) and (6) in this bomb allowed the respective pressures in the bulk of the bomb and in the pores of the combustion charge to be measured.

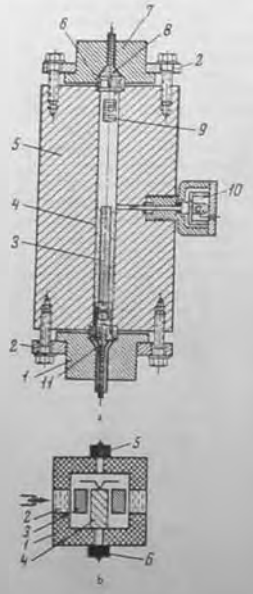


FIGURE 3. Manometric bomb with piezoelectric pressure probe (a) and with transparent windows (b).

Our investigations made use of a set of bombs with free volumes between 10 and 2000 $cm^3$. The charging density (ratio of the mass of burning substance to the free volume of the bomb) was not higher than 0.5 $g/cm^3$, while the maximum pressure was 6000–8000 atm.

Bomb for studying the development of deflagration in a single pore /12/. Research on the initiation and development of detonation in gas-permeable porous systems can be simplified by employing a controllable model – a single pore. As a rule the single pore (a slit) was comprised from two plane-parallel plates of a compact (nonporous) explosive. In some of the experiments one of the plates was replaced by a transparent plexiglass plate, which allowed optical methods to be used when recording the propagation of deflagration along the pore.




FIGURE 4. Curve of pressure $p(t)$ during the impairment of stable deflagration of a porous charge.

The slitlike charges were ignited in a specially developed manometric bomb (Figure 5) with a large free volume. Simultaneous optical recording of the process and of the pressure directly in the pore near the closed end was ensured. The bomb was provided with a transparent plexiglass window (6), two piezoelectric probes, one of which (3) recorded the pressure $p_b(t)$ in the bulk of the bomb, while the other (1) recorded the pressure $p_p(t)$ in the pore. The bomb also possessed a device (5) which extinguished the samples by removing the pressure. The pore (2) was ignited by a convective stream of burning gases, which are produced during combustion of the ignition charge (4) (pyroxilin + ammonium perchlorate); this charge created the initial pressure in the bomb within a very short time (5 msec). Thus the ignition charge produced essentially the filtration conditions of gaseous products in the pore, characteristic for the "built-in charge" system.

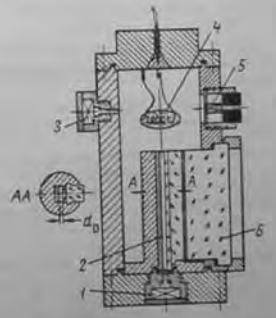


FIGURE 5. Bomb for studying the development of convective deflagration in a single pore.

We now consider instrumentation for investigating transition from deflagration to detonation. The charging density in the aforementioned

equipment was much lower than the initial density of the explosive; this limited the magnitude and rate $dp/dt$ of the pressure increase. Since the charge length was restricted and no solid shell was present, the nonsteady-state deflagration did not pass to detonation under these conditions. Andreev /6, 7/ developed one of the first instruments, intended for studying the initiation of detonation on ignition. At present, this equipment is known widely as "Andreev's tube."

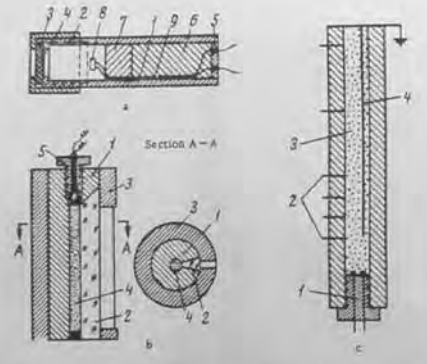


FIGURE 6. Instrumentation for investigating transition from deflagration to explosion or detonation:

a) Andreev's tube: 1) steel body; 2) steel lid; 3) lead disk; 4) asbestos plate; 5) steel bottom; 6) plaster of Paris; 7) explosive; 8) ignition device; 9) electric lead;
b) tube with ionization probe: 1) hermetic bolt igniter; 2) ordinary ionization probes; 3) explosive; 4) continuous ionization probe;
c) metallic shell with optical wedge: 1) steel cylinder; 2) plexiglass wedge; 3) steel shell; 4) sample; 5) bolt igniter.

Andreev's tube (Figure 6a). As a rule a steel beaker (diameter 40 mm, wall thickness 4–6 mm, height 200 mm) is used. The beaker has a lid with a large opening, closed by a metallic disk (usually made of lead) which is ejected when the critical pressure is attained. When the strength of the disk is low, deflagration leads to its ejection, so that the beaker remains intact. When the strength is large, regardless of the disk ejection, the beaker breaks into a larger or smaller number of pieces, corresponding to the pieces formed during detonation of the charge produced by a percussion cap detonator. The deformation of the beaker gives some idea about the nature of the detonation, while the minimum strength of the disk (at which the beaker is destroyed) is a measure of the tendency of the deflagration of the explosive to pass to explosion or detonation.



The disk strength is determined by igniting a coarse-grained smokeless powder in the tube. Such standardization determines the disk strength subject to slow pressure increase. The actual strength of the disk is usually higher than the measured value, because the pressure increase in the experiment is more rapid. The strength of the beaker of the above size is 1000 atm. The explosive charge is ignited by a cartridge of pyrotechnical composition. The charging density can be increased by filling the beaker to a certain height with plaster of Paris.

Andreev's tube allowed the first systematic data to be derived and, in the first place, enabled the various explosive powders to be compared as regards their tendency to pass from deflagration to detonation.

In Andreev's opinion, the main drawback of his method is that it gives only the final result of the experiment and, moreover, only in semi-quantitative form (number and size of the fragments), and does not illustrate the process kinetics. In addition, many explosives (low-sensitive explosive powders, cast and plastic explosives) do not detonate under such conditions. Subsequent refinement of Andreev's tube therefore involved an increase in the length and strength of the tube, and also application of modern recording methods in order to obtain reliable quantitative data.

The tests were carried out in thick-walled steel tubes, which were completely filled with explosives. Figure 6b shows a tube, used by Gipson and Maček /13/ for investigating transition from deflagration of cast explosives to detonation. The process rate was measured by conventional ionization probes and a continuous ionization probe, which is placed parallel to the charge axis (this probe is described in detail in section 2).

Tube with optical wedge /14/. We developed a tube with a plexiglass optical wedge, which allowed continuous recording of transition from deflagration to detonation (see Figure 6c). The tube consists of a steel cylinder (1) with a wedge-shaped slit (2) at its center. Plexiglass in the shape of the slit (2) was glued into it. The sharp edge of the wedge faced the side of the duct, so allowing the force acting upon the wedge to be decreased. The tube with the plexiglass wedge was placed in a steel shell (3) in order to increase the tube strength. The process was observed through a narrow slit opposite the plexiglass wedge. The sample of required density (4) was placed in the duct and, in the majority of cases, was pressed into the shell batchwise. The explosive sample was ignited via a hermetic bolt igniter (5) by a Nichrome spiral, heated by electric current.

This tube with the optical wedge made it possible to obtain high-quality continuous photographs of the transition from deflagration to detonation in explosive charges of diverse densities (see section 27).

Transition processes were also studied in transparent cylindrical plexiglass shells, and with equipment in which the explosive was (mostly in the form of a thin layer) squeezed between two plates /15, 16/, one of which was transparent (plexiglass). In contrast to the above equipment, the explosion was initiated by a spark or ignition of a thin metallic wire placed in the explosive by a capacitor discharge.

## 2. PROCESS RATE MEASUREMENT

Optical method. This method of determining the rate of self-propagation of the process. The image of the luminescent front is recorded on the film as an inclined line. The speed of the film $v_f$ is known, so the slope of the line representing the front determines the process rate $D$ in the form

$$D = v_f k' \tan \varphi,$$

where $k'$ is the ratio of the size of the object (length of the charge) to the size of its image on the film, i.e., the degree to which the photographic system has been reduced.

Deflagration processes (which are slow) are studied using low-speed photorecorders with a drumlike sweeping device and a film speed from several millimeters to several tens of meters per second. Universal photorecorders with a large range of speeds are usually used. An example of such a recorder is the FR-11, developed and constructed at the Institute of Chemical Physics of the USSR Academy of Sciences.

High-speed rotating-mirror cameras are used to study detonation processes. In this case the process is photographed on a stationary film with the aid of a rotating mirror, which enables the rate of photography to be increased. For this purpose, staff at the Institute of Chemical Physics designed SFR high-speed, ZhFR driven-sweep, and ZhLV driven slow-motion recorders, in which the mirror has the shape of a polyhedron. The ZhFR and ZhLV instruments do not have to be synchronized with the rotation of the mirror. When observing transient processes, it is sometimes convenient to use simultaneously two recorders with diverse rates of sweep /11/.

When filming deflagration or detonation of explosives by various types of cameras, the process rate is determined from the known frame frequency. The maximum frequency of the SKS-1M and SFR cameras (in the slow-motion variant) is $8 \cdot 10^5$ and $2.5 \cdot 10^6$ frames/sec.

Ionization probe method. The essence of the electric method with utilization of ionization probes is the ability of the combustion or detonation products to conduct electric current. Two or more spark gaps are placed in the explosive charge and a certain voltage fed. In the initial state the explosives are hardly conductive, so no electric current passes across the spark gaps. In the detonation wave or in the flame, the products are strongly ionized, and their resistivity is small (for



explosion products of typical explosives it is about 10–12 ohm/mm). Consequently the spark gaps are successively closed when a combustion or a detonation wave passes across them. An electric current is produced, and is recorded on the oscillograph screen. The mean process rate is determined from the known distance between the probes and the duration of the process occurring between them.

Continuous ionization probe method. A continuous method for determining the process rate has been developed /20–22/. A rheostatic probe is placed in the charge parallel to its axis. The resistance of this probe changes with the movement of the ionization front (front of the process).

The probe is a copper rod of 1.1 mm diameter with a close-wound spiral, made from PEVKT wire of 0.1 mm diameter /20/. One end of the winding is soldered to the copper rod and the other, together with the rod, is fixed to a coaxial cable. The probe together with a part of the cable is embedded in the explosive charge (cast charges or liquid explosive charges are most frequently used for this purpose). The free ends of the coaxial cable are connected to a cathode-ray oscilloscope, which records variations in the resistivity as the process takes place.

The process rate is determined from the record as follows. The length $L$ of the probe corresponds to the initial deflection $b_0$ of the oscilloscope ray. The sensitivity of the measuring section is then $\beta = b_0/L$. The time-dependent displacement of the front of the given process is $X(t) = \beta b(t)$, where $b(t)$ is the recorded curve of the investigated process. The process rate $D$ is determined from the equation

$$D = \frac{dX(t)}{dt} = \beta \frac{db(t)}{dt}.$$

Gal'perin and Shvedov /20/ estimate that the maximum error of the steady-state detonation speed determination does not exceed 2%. Another method /21, 22/, similar to that mentioned above, can be used to study transition from deflagration to detonation.

Method of determining normal deflagration ($u$) of solid samples by a piezoelectric detector. Belyaev et al. /23/ proposed a new method of determining the normal deflagration rate under the conditions prevalent in the manometric bomb. This rate is determined from the crests on the $p(t)$ curve. This method is very rapid and makes it possible to determine with a single experiment deflagration velocities at diverse pressures.

The method is as follows. The rate of pressure increase $dp/dt$ in a confined volume is determined by the rate of gas formation $u\rho S$ and the force of the powder $f$ ( $dp/dt \sim u\rho Sf$ ) comprising a combined charge containing substances with various rates $u$ and $f$ (the cross-sectional area $S$ = const). Therefore crests appear on the $p(t)$ record and correspond to the deflagration of each of the substances. The combined charge usually consists of cylinders of the auxiliary substances with a large value of $dp/dt$, the deflagration of which sharply increases the pressure in the bomb. The sample with a small value of $dp/dt$ is placed between these cylinders. The resulting curve $p(t)$ is shown on Figure 7, from which one can determine simultaneously the deflagration time of the cylindrical explosive sample of

known length and the mean pressure at which its deflagration occurs. Each successive explosive cylinder burns at a pressure higher than the preceding one.

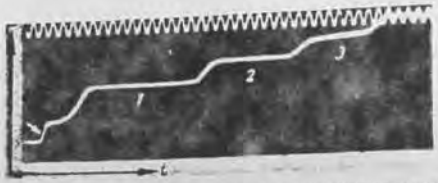


FIGURE 7. Function $p$ (t) during deflagration of a combined charge comprising three (1, 2, 3) cylinders consisting of the explosive sample (TNT).

Other tests employed a charge of the investigated explosive containing alternating (along the length) sections with small and large diameters and serving respectively as the fundamental (basic) and auxiliary (guiding pressure) elements. The $p(t)$ inflection method was used to determine the $u(p)$ function of several explosives and model mixtures up to 4000 atm /23/.

The method was modified so that it could be applied to the "constant-pressure" bomb. A highly sensitive piezoelectric detector was used; this detector recorded a slight pressure increase arising in the bulk of the bomb during deflagration of a charge, and consequently at the beginning and end of deflagration.

## 3. PRESSURE MEASUREMENT

Piezoelectric method. The piezoelectric method is based on the fact that the pressure $p$ measured by the piezoelectric transducer is converted into an electric voltage $U$ proportional to the pressure. The resulting signal is amplified and recorded by a loop or cathode-ray oscilloscope. The measured pressure acting on the piezoelectric transducer creates an electric charge $q = nF$ on its faces. This charge produces voltage $U$ at the amplifier input, where

$$U = \frac{q}{c_1 + c_p} = \frac{nF}{c_1 + c_p} = \frac{npS}{c_1 + c_p}.$$

Here, $n$ is the piezoelectric modulus; $p$ is the pressure to be measured; $S$ is the piezoelectric transducer area taking up the pressure, $c_1$ is the scale capacitance (capacitance at the amplifier input); $c_p$ is the piezoelectric transducer capacitance; $F$ is the force.

The design of a piezoelectric detector, which can be used for studying transition from deflagration to explosion or detonation, involves great



difficulties, because the detector must display the complete range of eigenfrequencies: from the lowest frequencies for recording deflagration, to the highest necessary for studying the fairly rapid predetonation processes. Moreover, such a detector must be mechanically strong and hermetic. The production of such a detector that satisfies the above criteria involves considerable difficulties. Nonetheless, a piston-type piezoelectric detector was produced at the Institute of Chemical Physics and permits one to record pressures up to 12,000 atm at rates of increase $dp/dt < 300$ atm/μsec /10/.

A schematic diagram of this detector is shown in Figure 8. The detector consists of a body (6), made from heat-treated steel and screwed into the bomb, a piston (8) which reacts to the gas pressure, and a lid with the piezoelectric unit.

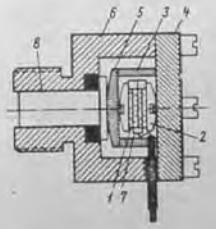


FIGURE 8. Schematic diagram of the piezoelectric detector.

The piston and the duct of the body are carefully polished. The piezoelectric unit consists of a steel plate (4), which serves as the base, arresting rings (3), two or four piezoelectric elements (1), two hemispherical bearings (2), a heat-treated steel membrane (5), and an electrode (7) placed between the piezoelectric elements. The body of the detector serves as the other electrode. It should be borne in mind that the detector can operate normally only when the parts of the piezoelectric unit are tightened with sufficient force. Piezoelectric quartz crystals with high mechanical strength and stable piezoelectric modulus were used ($n = 2.1 \cdot 10^{-12}$ coulomb/kg).

The compressive strength of piezoelectric quartz is about 1000 atm and 2000–3000 atm under static and dynamic conditions, respectively. Higher pressures arise in transient processes, so pressure compensation was achieved by using a rod whose area was considerably (6–10 times) smaller than the area of the quartz. In the majority of the detectors used the piston diameter was 3–4 mm and the diameter of the quartz disks, 10 mm. Thus such a detector should enable one, in principle, to measure pressures up to 15,000–20,000 atm. However, Bridgman /24/ noted that at pressures higher than 12,000 atm the piston detector may distort the results (they are too low) owing to the considerable lateral strain of the piston and because it is jammed in the duct of the detector body.

Low pressures (about $10^{-1}$ atm) can be recorded, when the detector does not have a piston and the pressure acts directly on the piezoelectric unit.

The electric signal emitted from the detector was amplified. Zverev designed a special electronic amplifier for this purpose. This amplifier possessed a large time constant, which permitted the piezoelectric equipment to be used also for long-term processes. At the same time it had a large bandwidth (about 350,000 Hz) and was also suitable for recording short-term high-frequency processes. The signal was fed from the detector to the amplifier by a cable arranged so as not to vibrate. The signal emitted from the detector was recorded by MPO-2 and N-107 loop oscilloscopes

(for slow processes) and PID-9 equipment, developed at the Institute of Chemical Physics by Sokolik and Stanilovskii /25/. The PID-9 equipment, based on the OK-24 two-channel cathode ray oscilloscope, was used to record the time-dependence of the pressure in the shock wave when studying explosions.

The different pressures were measured by inserting scaling capacitors of various capacitances at the input of the amplifier. The sensors were calibrated by a static-dynamic method. The piezoelectric detector was fixed in special equipment, and a press with oil was used to produce a certain pressure, measured by a standard gauge. The pressure was then removed for a short while (about $10^{-3}$ sec) and the resulting deflection recorded on the oscilloscope.

Though the instruments were calibrated under load-removal conditions, the results were not affected because piezoelectric quartz operates in the same fashion both on compression and unloading. All the applied detectors had linear amplitude characteristics. The error involved in the piezoelectric method of pressure measurement does not exceed 3%.

A tensometric probe is also used, but it is very sensitive to temperature variations and the necessity for regular probe calibration (after only a few experiments).

Consider now pressure measurement in the compression wave. Research on the structure of such waves, which arise in explosives on transition from deflagration to detonation, is very interesting in order to understand the mechanism of the phenomenon. The electromagnetic method /26, 27/ is the most reliable and simple way of recording compression wave parameters. This method enables one not only to observe the wave profile, but also to calculate the absolute pressure, since one measures simultaneously the velocity $D$ of the front and the velocity $U$ of the substance motion behind the front. Pressure is calculated by the formula $p = \rho_0 DU$ ($\rho_0$ is the initial density of the explosive). The method is mainly used to measure the velocity of substance motion.

Electromagnetic method. The principle of the electromagnetic method is the following. An electric conductor moving in a magnetic field gives rise to an induction emf in the conductor. This emf is given in terms of the velocity of the conductor, the length of the conductor, and the magnetic field strength by

$$\mathcal{E} = HLU \cdot 10^{-8},$$

where $\mathcal{E}$ is the emf (in V), $H$ is the magnetic field strength (in Oe), $U$ is the velocity of the moving conductor (in cm/sec), and $L$ is the length of the conductor (in cm).

This equation yields the velocity of the conductor. The conductor (here the probe) is a Π-shaped aluminum foil strip (thickness usually 0.05–0.25 mm) of width 10–15 mm whose crossbar $L$ is the working part of the probe. A sensor (2) is introduced into the charge (1) perpendicular to its axis and is then placed together with the charge into the field of a permanent magnet, so that when the probe moves its working plane intersects the lines of force of the field (Figure 9).

The compression wave passing through the charge sets the probe in motion. The emf induced at its ends is recorded on the cathode-ray



oscilloscope. For constant $H$ and $L$, the emf is only a function of the probe motion, which equals the mass velocity of the substance in the wave.

The magnetic field is produced by an electromagnet. The electromagnets used at the Institute of Chemical Physics create a uniform magnetic field strength of 400–800 Oe at the gap center to within 1%. The recorder consisted of an OK-17 two-channel cathode-ray oscilloscope with a frequency band of 10 mHz over the two channels and a transient response time of 0.035 μsec. The time of obstruction of the leading edge of the pulse from its onset until it attains its peak value is 0.07 μsec. The obstruction of the front may increase with increasing probe thickness, and with the specific gravity of the material from which the probe was produced.

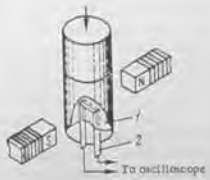


FIGURE 9. Schematic diagram of the electromagnetic method for measuring the mass velocity of a substance.

The wave front velocity is measured with either two probes, or with one probe which, however, must be step-shaped; such a probe was proposed by Dremin et al. /27/. Thus, in a single experiment we can measure simultaneously the mean wave velocity and the velocity of the substance motion behind this front. The electromagnetic method is used extensively for measuring detonation parameters and for studying the formation of a detonation wave in tests on shock initiation. However, its application for studying the mechanism of shock wave formation during transition from deflagration to detonation involves great fundamental difficulties, because this transition is usually observed when the explosive charge is enclosed within a sufficiently strong metal shell. The electromagnetic method may be used if the shell of the charge is made from nonmagnetic material, but this condition is often incompatible with the strength conditions.

Collapse probes. These probes were used to find the propagation velocity of a compression wave /13/. The probe consists of two wires separated by insulation. The principle of its application is based on the closing of an electric circuit as a result of the destruction of the insulation by the compression wave. The probes are calibrated with respect to fixed pressures. The advantage of these probes is that they make it possible to record the passage of a compression wave through the explosive whatever the shell material. However, they are unsuitable for recording the profile of a compression wave, since the probes are destroyed when the pressure exceeds some critical value (Gipson and Maček /13/ used probes which were triggered at threshold values of 800 and 2000 atm).

We note in conclusion that the possibilities of following a wave pattern are very restricted and far fewer than those used in gaseous systems, where very efficient, rapid-response schlieren instruments are used for this purpose.

## Chapter I

## GENERAL PROPERTIES OF POROUS SYSTEMS

Steady-state layer-by-layer deflagration of explosive systems is impaired by penetration of deflagration into the pores as a result of filtration of the combustion products /4–7/. Studies of the conditions of transition from deflagration to detonation will make use of the theory of filtration pertaining to the flow of natural fluids in porous systems. Some fundamental ideas and definitions to be examined in this book will be also applied.

A porous medium is a body containing pores (empty gaps). Fluid flow is only possible when at least some of the pores are in communication with one another and the system is gas-permeable. We treat only such porous media that remain unaffected by the molecular structure of the gas involved in the filtering process,* which takes place if the mean free path of the molecules does not exceed the pore size. This condition is satisfied for almost all systems, and is of interest when considering transition from deflagration to detonation.

### 1. FUNDAMENTAL PARAMETERS OF THE POROUS MEDIUM

A porous system is characterized by the following fundamental parameters: porosity, gas permeability, specific surface, pore size distribution, particle size.

The porosity $m$ is the ratio of the volume of the pores $V_p$ to the total volume of the sample $V_s$:

$$m = V_p/V_s = 1 - \delta, \qquad (1)$$

where $\delta = \rho/\rho_{max}$ is the relative density; $\rho$ is the density of the sample; $\rho_{max}$ is the maximum possible density of the explosive (single crystal density).

The value of $\rho_{max}$ for a mixture is determined by

$$\rho_{max}^{mix} = \frac{1}{\sum_i \frac{z_i}{\rho_{i\,max}}},$$

* Initiation and development of deflagration are determined mainly by the filtration patterns of the gaseous combustion products. The role of the melt will be discussed later.



where $z_i$ and $\rho_{i\,max}$ are the weight fractions and the maximum possible density of the $i$-th component.

The porosity is expressed as fractions of unity or as percents. We distinguish the absolute (physical) porosity, which is defined by formula (1) and includes both interconnected pores and closed pores. The porosity determined by the interconnected porous volume is termed open (effective) porosity. Here and later, the term "porosity" will mean absolute porosity, unless otherwise specified.

The gas permeability $k$ is the property of a porous medium which determines the possibility of gas flow in the sample. Gas permeability is expressed in units of (length)$^2$. The darcy is frequently used as the unit of measure, where 1 darcy $= 9.87 \cdot 10^{-13}$ m$^2$.

The specific surface of the sample, $S_w$ cm$^2$/g, is defined as the pore surface per unit mass of the solid (nonporous) substance.

The definition of pore size $d_p$ presents theoretical difficulties, since the pore surface generally has a very complex shape. However, from the geometric point of view the following definition is convenient: the pore diameter at any one point within the pore space is the diameter of the largest sphere which contains this point and which lies within the pore space /28/. On the other hand, the following definition corresponds best to the physical aspect of the problem: the pore diameter is the diameter of such a tube which, as regards its hydraulic properties, is equivalent to the given pore. This approach is used when designing diverse types of theoretical models of a porous medium. Naturally, the porous medium is characterized by a certain pore size distribution. Normal (Gaussian) distributions are used in the processing of the results.

Another important characteristic is the particle size – especially for porous systems, in which the particle shape and size do not change during preparation and burning of the sample.

All these parameters are determined experimentally. The methods and results of their measurement will be given below (section 5) for the explosives.

Theoretical ways of estimating the above parameters and establishing relationships between them are of considerable interest. For instance, it is sometimes necessary to estimate the mean pore diameter, particle size and specific surface from known gas permeabilities and porosities. Such estimates can be obtained by examining simplified theoretical models of a porous medium.

#### Theoretical models of the porous medium

The disordered structure is a distinguishing feature of a porous system. The Navier-Stokes equation for the flow of a viscous fluid cannot be solved in disordered systems. Therefore, in theoretical investigations a real porous medium is replaced by a simplified ordered model with equivalent hydraulic properties. The solution to the Navier-Stokes equation for fluid flow along a right circular tube is known and is used when designing the models.

The model of an ideal soil, consisting of identical cylindrical pores whose axes are parallel to one another, has become very popular /29/. In this model the mean hydraulic pore-diameter $d_p = 4S/\chi$ (where $S$ is the

cross-sectional area of the pore and $\chi$ is the wetted perimeter) is defined in terms of gas permeability and porosity by

$$d_e = 4\beta\sqrt{k/m}. \qquad (2)$$

The value of $\beta$ depends weakly on the pore cross-sectional shape; its mean value is taken as $\beta = 1.37$ (for a circular cross section, $\beta = 1.41$). Equation (2) permits one to estimate the mean hydraulic pore diameter, since it is assumed in this model that all the pores are identical. The ideal soil is an example of the capillary model of a porous medium.

The model proposed by Kozeny and refined by Carman is more complex. The porous medium in this model is a bundle of capillaries of a certain length but of diverse cross sections. This model allows a relation to be established between gas permeability, porosity, and specific pore area $S_w$:

$$k = \frac{m^3}{2S_w^2 \tau_{max}^2 (1-m)^2}. \qquad (3)$$

Kozeny's equation (3) is used for determining the value of $S_w$ and the particle size.

A simple correlation exists between pore diameter and particle size for porous systems consisting of identical spherical particles of diameter $r$. It follows from the theory of packing of spheres /28, 29/ that in this case the porosity is independent of particle diameter. Stable packing with minimum porosity $m = 0.259$ is "rhombohedral" packing. Stable packing with maximum porosity has not been found as yet (the literature reports stable packing of spheres with $m = 0.875$). The mean hydraulic pore diameter for a system consisting of identical spherical particles is /29/

$$d_p = \frac{2}{3}\frac{m}{1-m} r. \qquad (4)$$

For monodisperse systems consisting of arbitrary particles, the hydraulic pore diameter can be calculated /30/ by the formula

$$d_p = \frac{2}{3}\frac{m}{1-m} r' \sqrt{\frac{6.3(1-r'}{V'^{1/3}}}. \qquad (5)$$

where $V'$ is the particle volume, $s'$ is the particle surface, $r'$ is the diameter of a sphere equivalent in volume to the given particle.

An accurate estimation of the shape and size of the particles is extremely difficult. Nevertheless, the particles are characterized by some fixed size (see section 5).

Numerous unsuccessful attempts have been made to theoretically calculate gas permeability, but all the results differed considerably from experimental data. Attempts to determine a single universal relationship linking gas permeability and porosity were also unsuccessful. Therefore, gas permeability can only be determined experimentally.

We emphasize the important fact that when designing theoretical models of a porous medium it was assumed that all the pores are open to fluid flow.



Therefore, the porosity entering equations (2)–(5) must be interpreted as the open porosity.

### Some equations of gas filtration in a porous medium

Fluid flow in the pores is assumed to be laminar. The Navier-Stokes equation should be applied to the laminar filtration of a viscous liquid in a porous medium. Direct integration of this equation is impossible, owing to the complexity of the boundary conditions. Leibenzon /29/ derived a general equation for nonsteady laminar filtration of compressible fluid in a nondeformable ($k$ = const, $m$ = const), porous medium by substituting fictitious resistance forces in place of the viscosity effect. The equation for a gas assumes the form

$$\nabla^2 P = \frac{m\mu}{nk}\frac{1}{p}\frac{\partial P}{\partial t}. \qquad (6)$$

where $P = p^{n+1/n}$; $n$ is the polytropic index in the equation $p^{1/n} = \text{const}\cdot\rho$; $p$, $\rho$ and $\mu$ are the pressure, density and viscosity, respectively, of the gas.

Equation (6) is a parabolic, nonlinear second-order partial differential equation and can be integrated for one-dimensional flow under the following conditions:

1) if the filtration is isothermal ($n = 1$), equation (6) becomes

$$\frac{\partial^2 p^2}{\partial x^2} = \frac{2m\mu}{k}\frac{\partial p}{\partial t} \qquad (7)$$

(this equation was solved by Boussinesq);

2) if one can regard $p$ as constant ($p = p_a$) (for instance, when gas filtration takes place as a result of a pressure drop $\Delta p \ll p_a$). In this case the solution of the approximate equation

$$\nabla^2 p = \frac{m\mu}{nkp_a}\frac{\partial p}{\partial t} \qquad (8)$$

is the solution of the ordinary heat conduction equation.

Darcy's law is applicable to laminar flow, in which case the linear filtration speed is proportional to the pressure gradient:

$$v = -\frac{k}{\mu}\frac{dp}{dx}. \qquad (9)$$

The minus sign indicates that the flow direction opposes any increase in the pressure gradient.

Darcy's law is applicable for the Reynolds number $\mathrm{Re} = vd_p\rho/\mu$ ($d_p$ is the pore diameter or particle size), which determines the nature of the gas flow through the pores and does not exceed some critical value. According to different data this value lies between $\mathrm{Re} = 1$ and $\mathrm{Re} = 75$. Darcy's law is satisfied over a wide range of filtering speeds; deviations from this law

take place very slowly and are observed only at high and slow flow rates. In the first case this is due to the appearance of turbulent flow, and in the second case to molecular effects. The methods of determining the gas permeability of porous samples are based on Darcy's law.

The above brief, general information on a porous medium will be utilized later in the text.

Preparation of porous explosive systems. The minimum porosity which can be attained for uniform spherical particles is 0.259. The actual porosity of free-flowing explosive charges is generally much larger than the theoretical value (0.4–0.7). Various condensing methods are used to decrease the porosity.

One of the most popular methods of condensing explosives is dry pressing. This very simple method makes it possible to prepare samples whose gas permeability and porosity can be varied over a wide range. An advantage of this method is the possibility of obtaining samples which are homogeneous over their width and length, and possess the required, reproducible properties, provided certain rules of pressing are observed. Moreover, it will be shown below that the majority of the pore space is interconnected. For this reason explosive samples prepared by this method comprised the main objects used in the study of transition from deflagration to detonation.

Press molds with a circular cross section are usually used, but recently press molds with a rectangular cross section have also been employed. It has been found that uniform pressing over the bulk of the sample is achieved at an optimum sample height-to-diameter ratio of about 0.5. Therefore, we prepared elongated charges by connecting a considerable number of cylindrical tablets pressed by this method; fewer tablets were used for rectangular plates. The batch method was used to press the explosives into cylindrical form; this method consists of successive pressing (without extrusion) of the individual explosive samples. The height of each pressed charge was not larger than half its diameter.

When pressed, the substance was subject to conditions close to all-round compression. The applied load condenses the substance; the condensing process is limited by fracturing (crushing) of the particles and plastic strain. After extrusion, the sample is freed from the load, to the accompaniment of a small increase in volume. Charges with diverse porosities are obtained by changing the pressing pressure $P_0$. The minimum limiting porosity obtainable by blank pressing depends on the individual properties of the explosive, and especially on its strength parameters (see the table below).

| | TNT | Picric acid | PETN | Hexogen | Lead azide |
|---|---|---|---|---|---|
| Limiting porosity | 0,02 | 0,025 | 0,025 | 0,035 | 0,15 |
| Ultimate strength, $\sigma_{ult}$, kg/cm$^2$ | 340 | 520 | 600 | 820 | 1550 |

This table contains values of the minimum porosity of explosives, obtained at a maximum pressing pressure of 4000 atm, and also the ultimate strengths determined in /31/. The cited ultimate strengths were determined



when investigating the shock sensitivity of the explosive and, in the opinion of the authors, characterize the transcrystalline (inherent) strength of the explosive as a material. Regardless of the specific deformation conditions, the obtained values of the ultimate strength $\sigma_{ult}$ give some idea about the strengths of different explosives. For example, the lower the ultimate strength, the lower the minimum porosity and the higher the pressing ability of the explosives. It will be shown later (section 5) that the strength properties of explosives considerably influence the physical structure of the pore space.

The pressing density at a fixed pressure depends also on the particle size of the explosives, the introduction of the cementing additive, and on the ratio between the geometrical dimensions of the sample, the role of which is disregarded here. The above comments referred to the case when pressing was carried out at room temperature and without application of a solvent. When preliminary heating and special solvents are applied, samples can be used which are practically free from porosity.

The casting method can also be used to obtain charges of explosives and mixed propellant powders. The structure of a porous charge prepared by casting differs considerably from that obtained by blank pressing. Bubble- or cavitylike pores are characteristic of cast systems; most of the pores are interconnected. The porosity in cast charges depends on the cooling and polymerization regimes, and lies between 0.01 and 0.03 in the casting method. The possibility of employing the given method to obtain charges with a wide range of porosities is rather limited. Casting technology makes it very difficult to obtain homogeneous porous samples with predetermined properties.

Pressed porous systems are free of these drawbacks and open much wider possibilities for research workers. The term porous explosives or porous medium will subsequently be understood as systems obtained by pressing, unless otherwise specified.

## 5. METHODS AND RESULTS OF MEASURING FUNDAMENTAL PARAMETERS

Determination of porosity. The absolute porosity is usually measured by techniques based on density measurement. The porosity is calculated by equation (1). The sample density $\rho$ is determined by volume displacement, a nonwetting fluid (such as mercury) is used. Preliminary sample coating by a film of the corresponding material makes it possible to use a wider range of liquids. A correction is introduced for the volume of the coating. The volume of samples of low porosity may be determined by hydrostatic weighing, without coating. The volume of a porous sample of regular form is also determined by the geometric dimensions. There are many special methods of determining absolute porosity; the reader is referred to /28, 29/.

The saturation method or the gas expansion method is used for measuring open porosity. The first of these methods is based on the saturation of the porous sample with a liquid. We could use a liquid which penetrates well into the pores (such as kerosene), in which case the sample is saturated

in vacuo. Another liquid used for this purpose is mercury, which is directed into the exhausted sample under high pressure. The amount of liquid penetrating into the sample characterizes the size of the interconnected pore space.

The gas expansion method is based on direct measurement of the volume of air which has penetrated into the sample pores. For this purpose the sample is connected to an elevated pressure chamber of known volume. The variation in pressure in the sample – chamber system enables the volume of the interconnected pores to be calculated from the Boyle-Mariotte law.

The table below presents the results of measuring open porosity in TNT, tetryl, hexogen (initial particle size $r = 110-140\ \mu$) and ammonium perchlorate, obtained by the saturation method. The TNT, tetryl and hexogen samples were saturated with mercury,* and those of ammonium perchlorate with kerosene.

| | TNT | | | Tetryl | Hexogen | Ammonium perchlorate | | |
|---|---|---|---|---|---|---|---|---|
| Absolute porosity $m$ . . . | 0.16 | 0.08 | 0.05 | 0.05 | 0.05 | 0.2 | 0.1 | 0.01 |
| Open porosity $m_0$ . . . | 0.16 | 0.08 | 0.027 | 0.038 | 0.05 | 0.2 | 0.08 | 0.05 |

It follows from the data that the pores of all the investigated explosives are completely interconnected when porosity $m > 0.16-0.2$. The volume of interconnected pores is reduced with decreasing porosity; this is especially characteristic for explosives with the property of low strength (such as TNT and tetryl). However, the formation of closed (unconnected) pores is not observed in the case of the stronger hexogen even at low porosity, close to the limiting value. Thus, the structure of the pore space depends on the strength properties of the explosives, and hence on the deformation pattern of the explosives during pressing.

### Determination of pore size distribution

The method usual is to inject mercury into the pore system. The only distinction is the fact that the mercury volume in the pores is determined at different pressures. The porous sample is placed in a chamber with a strictly determined volume and then evacuated. The mercury is then injected at some elevated pressure and the volume of the mercury penetrating into the pores is determined; hence the volume $V_p$ of the pores of given dimensions are found. This operation is repeated at a higher pressure, when pores of smaller size are filled with mercury, and continued until the mercury fills all the pores. The pore size (diameter) $d_p$ is determined by the capillary pressure equation. This procedure yields an experimental dependence of the pore volume $V_p$ on pore size $d_p$, i.e., the integral pore curve of the pore size distribution $V_p(d_p)$. More frequently we use

* The open porosity and pore size distribution (see Figure 10) were determined by Ael'chikov and Volkov, who directed mercury into the pores.



differential curves $\alpha(d_p)$, where $\alpha$ is that part of the porous space which includes pores of sizes between $d_p$ and $d_p + \Delta d_p$.

Figure 10 presents the differential pore size distribution curve obtained by graphic integration of the experimental curves $V_p(d_p)$ (the derivatives $\Delta V_p/\Delta \log d_p$ are plotted on the ordinate axis). The data indicate clearly the characteristic pore dimensions.

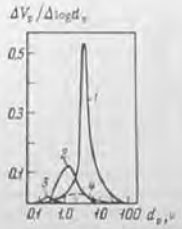


FIGURE 10. Differendal pore size distribution curves obtained by injecting mercury (initial particle size $r = 110-140\ \mu$).

1–3) TNT: 1) $m = 0.21$; 2) 0.16; 3) 0.05; 4) hexogen: $m = 0.05$.

It is of interest, above all, to observe the variation in pore size which corresponds to the distribution curve maximum in TNT samples of different porosity. Even at a comparatively high porosity ($m = 0.21$) the corresponding size is quite small (about 4 $\mu$), while at porosity $m = 0.05$ it decreases by one order of magnitude. The maximum pore size decreases from 50 to 1 $\mu$. The pore size in the hexogen sample was much larger than in TNT of the same porosity ($m = 0.05$) and initial dispersity, which is in agreement with the data discussed above.

We will show later (section 15 of Chapter III) that secondary explosives burn very stably, due to the formation of a continuous fused layer, which stabilizes combustion until its thickness is commensurable with the largest pore size. An estimate was carried out on the basis of this condition and yielded a pore size which was close to that obtained by direct determination of the pore size distribution.

### Gas permeability measurement

Gas permeability determines the gas flow over the pores and consequently the possibility of impairing deflagration. It therefore depends not only on porosity but also on the particle size, the type of particle packing, and the structure of the pore space. Thus no universal theoretical relationship exists between gas permeability and porosity, and its specific form is determined by experiment. Measurements of gas permeability are based on Darcy's law. Tests are carried out under steady-state conditions of isothermal gas filtration. The methods used differ only by modifications in the apparatus design.

Gas permeability in samples with small porosity ($m < 0.15$) was determined using the equipment shown on Figure 11a /10/. The main difficulty arising in this case of gas permeability measurement is to eliminate gas flow along the lateral surface of the sample. Consequently, the sample was placed into a well-polished conical press mold (4) at the required porosity. Prior to pressing the surface of the press mold was covered with a thin layer of bitumen, applied from a solution in benzene, which improved adhesion between the sample and the press mold. Application of a conical press mold prevented shifting of the porous sample (7) during the

test because of the pressure gradient. The press mold was fastened by means of rubber packing (6) and nuts (3). Special experiments indicated that these measures ensured airtightness of the whole assembly.

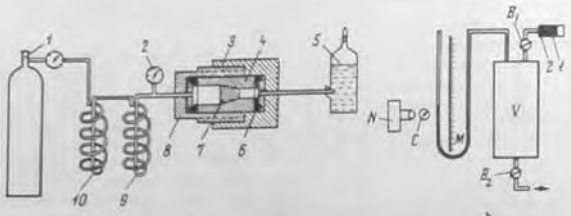


a b

FIGURE 11. Schematic diagram for gas permeability measurement in samples with low (a) and high (b) permeability.

The gas (mostly nitrogen) passed from a tank (1) via reducing valve (2) and coils (9) and (10) to the inlet of the porous sample (7). In coil (10) the gas is freed from water vapor by using dry ice. In coil (9) the dried gas is heated to room temperature, at which the measurements were conducted. The gas pressure $p_2$ at the inlet was measured with a standard gauge (2), while the pressure $p_1$ at the outlet was atmospheric. The pressure drop $\Delta p = p_2 - p_1$ at the ends of the sample was maintained stable and did not exceed 10 atm. A small gas meter (5) was employed to determine the rate at which the gas passed through the sample, its dissolution and absorption being prevented by preliminary saturation with water in the gas meter. The gas rate was measured under steady-state filtering conditions.

The permeability was measured on the basis of Darcy's law (9) with allowance for the gas compressibility. If equation (9) is expressed in the form

$$\frac{Q_{av}}{S} = \frac{k}{\mu}\frac{p_2 - p_1}{L}$$

and the gas filtration rate related to the average pressure $p_{av} = (p_1 + p_2)/2$ during isothermal flow in the form $Q_{av} = p_1 Q/p_{av}$, the initial formula for calculating the permeability is

$$k = \frac{2p_1\mu QL}{S(p_2^2 - p_1^2)}, \qquad (10)$$

where $k$ is the gas permeability (in darcys); $L$ is the sample length (in cm); $S$ is the mean cross-sectional area (in $cm^2$); $Q$ is the measured gas rate (in $cm^3$/sec) for atmospheric pressure at the outlet $p_1 = 1$ atm; and $\mu$ is the viscosity of the filtering gas (in centipoises).



It follows directly from (10) that the gas discharge $Q$ through the sample varies linearly with $p_2^2 - p_1^2$ when the geometrical dimensions of the sample remain constant.

The permeability in explosive samples with porosity $m = 0.15$–$0.03$ was measured on this equipment. The permeabilities lay between $10^{-2}$ and $10^{-4}$ darcys.*

Some of the results /10/ are shown in Figure 12. The ordinate denotes the reciprocal permeability (expressed in darcys) and the abscissa axis the absolute porosity.

The permeability in samples of high porosity ($m > 0.15$) was measured /22/ on equipment whose schematic diagram is shown on Figure 11b. The porous sample (1) was placed on a support (2) made from filter paper in order to obtain stable measurement results. Before testing, the container $V$ (about 1.5 liter) was evacuated with valve $B_1$ closed to a pressure $p_2$, which was 100–150 mm $H_2O$ below atmospheric pressure $p_1$. Valve $B_2$ was then closed and valve $B_1$ opened. Air began to flow through the explosive charge in container $V$. High-speed camera $N$ was employed simultaneously to record the time-dependence of the pressure from the readings of manometer $M$ and stopwatch $C$. Darcy's law as applied to the given experimental conditions is

$$k = \mu\left(\frac{LV}{S}\right)\cdot\left(\frac{dp}{dt}\cdot\frac{1}{p_1\Delta p}\right). \qquad (11)$$

Gas compressibility was ignored in the derivation of (11). Such a step was justified, since $\Delta p \ll p_1$. When processing the results, a correction was introduced to account for the drag of the support (2) and other parts of the equipment.

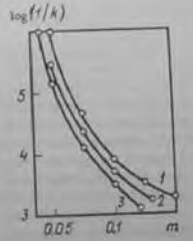


FIGURE 12. Plot of $\log(k^{-1})$ vs. $m$ (initial particle size $r = 5$–20 mm):

1) PETN; 2) stoichiometric mixture of trotyl with ammonium perchlorate; 3) trotyl.

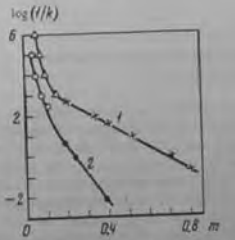


FIGURE 13. Plot of $\log(k^{-1})$ vs. $m$ for PETN samples pressed to particles of size 5 μ (1) and 500 μ (2).

○, △) data of /10/; ●, ×) data of /92/.

* A permeability $k \leqq 10^{-4}$ darcy is very low, far below the permeability of the majority of natural ores and soils.

The above equipment was employed to determine the permeability of a series of explosives over a wide range of porosities ($m = 0.8-0.03$); under these conditions the gas permeability varied over 7–8 orders of magnitude. The corresponding results for PETN at various porosities are presented on Figure 13. It follows that the dependence of the gas permeability of PETN on porosity varies considerably when $m = 0.1-0.2$. If the obtained data in log $(k^{-1})-m$ coordinates lie well on a straight line when $m > 0.15$ and are approximated by the function $k = a'e^{-bm}$ (where $a'$ and $b'$ are constants), then at lower porosities the curves are much steeper (an abrupt drop is observed in the gas permeability). It is logical that this effect is due to variations in the structure of the pore space.

The above data indicate that the permeability depends considerably on the initial size of the explosive particle. This result is trivial if applied to samples of high porosity. However, it is noteworthy that even at very low porosities ($m = 0.03-0.05$) the permeability of samples pressed from coarse grains continues to remain much higher. We might naturally expect that intensive crushing of the substance during pressing at high pressures (3000–4000 atm) destroys the dependence of the sample properties on the initial particle size. Our experience has shown that this is not so. The sample pressed to a high density continues to "remember" the history of its preparation. It will be demonstrated later that this effect of the particle size in very dense samples is found both during deflagration, and during initiation and development of detonation.

Since the relationships linking permeability to porosity are known for some explosives, we can compare stable deflagration for the same gas permeability and similar sample structure. Only such a comparison will reveal the role of the physicochemical and thermochemical properties of explosives when stable deflagration is impaired.

### Measurement of specific pore surface and particle size

The determination of the specific surface of pores is based on application of Kozeny's equation and of experimental relationships between permeability and porosity. In addition to this basic method, there are also various other ways /28/ of determining the specific surface (photomicrograph technique, a method based on application of vapor absorption by a solid surface, etc.).

The specific surface of pores is an important characteristic of explosives; its knowledge is necessary, especially when considering the problem of transition from deflagration to detonation. The dependence of specific surface on porosity is of special interest. Kozeny's equation (3) and experimental data on gas permeability (see Figure 13) were used to calculate the specific surface in PETN samples of various porosities and with initial particle diameters between 5 and 500 μ (Table 1).*

Computation of the specific surface for finely crystalline PETN is shown in Figure 14.

* The open porosity must be inserted in Kozeny's equation. When carrying out the calculation we therefore assumed that for porosity $m \geq 0.2$ the pores are completely interconnected ($m = m_0$), while for $m = 0.1$ in the case of fine crystalline PETN we assumed that $m_0 = 0.08$.



TABLE 1. Specific surface and mean particle size in PETN samples of different porosity

| | | Porosity $m$ | | | | | | |
|---|---|---|---|---|---|---|---|---|
| | PETN | 0.8 | 0.45 | 0.35 | 0.3 | 0.25 | 0.2 | 0.1 |
| Specific pore surface $S_{sp} \cdot 10^3$, cm²/g | Fine | 6.18 | 9.26 | 10.05 | 10.1 | 9.95 | 9.95 | 9.3 |
| | Coarse | — | 0.07 | 0.2 | 0.34 | 0.53 | 0.79 | 2.3 |
| Mean particle size $r = \frac{6}{S_{sp} \rho_{max}} \mu$ | Fine | 5.5 | 3.65 | 3.37 | 3.35 | — | — | — |
| | Coarse | — | 500 | 170 | 105 | — | — | — |

Note. Porosities of 0.8 and 0.45 correspond to free-flowing charges.

It follows from the above data that the dependence of specific pore surface on porosity for very fine explosives attains a peak at $m \simeq 0.3$.

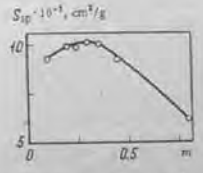


FIGURE 14. Specific surface of PETN samples of various porosities ($r \simeq 5$ μ).

Table 1 also shows calculation results of $S(m)$ for samples pressed from large crystals (initial particle size $r = 500$ μ). Comparison shows that, for samples from coarse crystalline PETN, the pore surface increases monotonically and considerably (by a factor of thirty) with decreasing porosity, and over the whole interval investigated it remains below the value for fine crystalline PETN. The increase in specific surface involves intensive crushing of large crystals; their degree of grinding increases with decreasing $m$, but does not reach the level characteristic of the preliminary finely ground substance. For this reason there is no peak on the $S(m)$ curve.

When the initial particles of the fine crystalline PETN are already very small, crushing, and hence increase in specific surface, is expressed more weakly. Further increase in pressing pressure (density of the explosives) does not lead to a decrease in particle size but alters the structure of the pore space. In particular, closed pores appear and the particles become larger, because contact between them improves. Hence the specific surface decreases and a peak is observed on the $S(m)$ curve.

The above ideas about crushing are supported by an evaluation of mean particle size in the sample, this is possible, because the specific pore surface is known.

The relationship between average particle size and specific surface can be derived from simple geometric ideas and also by combining expressions (2), (3) and (4):

$$r = \frac{6}{S_{sp} \rho_{max}}. \qquad (12)$$

Equation (12) is widely used for determining the mean particle diameter, especially of polydisperse explosive fractions (the PSKh laboratory

instrument is based on this principle). Mean particle sizes determined by (12) are presented in the last row of Table 1.

It should be noted that large crystals are crushed intensively even at comparatively low pressing pressures, i.e., pressures not exceeding 200 atm. Thus, the crushing effect is always present and cannot be neglected when working with pressed explosive charges.*

The particle shape and size remain unchanged if we use charges of free-flowing (bulk) density that are not subjected to mechanical loads during the test period. In addition to the above method of determining mean particle size from specific surface, we used also sieve and microscopic analysis for determining the initial particle size of monodisperse systems. Monodisperse fractions** are mainly obtained by sieving.

The sieve dimension of the particles is determined as the arithmetic mean of the dimensions of holes of two adjacent sieves. More frequently, the limiting values of the sieve openings are shown.

In microscopic analysis we determine the dimensions of a larger number of particles (no less than 100) over two directions, and then average the results. The mean microscopic dimension is, as a rule, larger than the mean sieve dimension for fractions consisting of elongated particles.

Sedimentation methods are also used in the determination of the particle size distribution of powders. The underlying principle is to determine the sedimentation rate of homogeneous particles in a viscous medium as a function of their size. Solid particles are usually precipitated under the effect of gravitational or centrifugal forces.

Table 2 lists the principal methods of measuring particle size and pore size, and also the limits of applicability of each method (the data are taken from [34]).

TABLE 2. Ranges over which particle size and pore size can be measured by various methods

| Method | Measurement range: | |
|---|---|---|
| | particle size, μ | pore size, μ |
| Optical microscope | 0.25—250 | 0.25—250 |
| Electron microscope | 0.0005—5 | 0.0005—5 |
| Sieve analysis | 40 and more | — |
| Precipitation in liquids | 0.5—300 | — |
| Precipitation in gases | 1—200 | — |
| X-ray scattering | 0.005—0.08 | 0.005—0.05 |
| Mercury—helium method | — | 0.005—10.0 |

An indirect method, which is based on measuring the gas permeability, enables pore sizes to be measured up to 0.1—1 μ, depending on the resolving power of the equipment employed. Equation (2) is used for this purpose.

* During transition from deflagration to detonation the explosive is subjected to compression waves, which may lead to additional crushing of the substance if such a possibility exists, i.e., if the limiting degree of crushing has not been reached. The problem of crushing explosive crystals under dynamic (shock) conditions of loading is studied elsewhere [33]. Explosive charges of free-flowing density with an initial particle size of about 1 mm were subjected to compression by a shock wave of 1500—2000 atm amplitude. The samples were sieved for a certain time and the particle size distribution determined. It was found that the final particle size corresponding to the distribution peak is 10—20 μ.

** Fractions of 100—140 and 320—400 μ are usually regarded as monodisperse.



*Chapter II*

## *STABLE DEFLAGRATION OF POROUS EXPLOSIVES*

Under certain conditions deflagration of porous explosives is stable, regular, and proceeds in a layer-by-layer manner. In this case the mass velocity of deflagration is close to the corresponding value for continuous nonporous samples.

A study of slow layer-by-layer deflagration of porous systems is of considerable theoretical interest and provides additional data on the mechanism of deflagration of explosives. Changes in density naturally lead to changes in heat propagation in the condensed phase, since the thermal conductivity and gas permeability of explosives depends on the density. The concentration of matter in the solid phase also changes. This fact possesses considerable importance for systems in which the basic reaction during deflagration takes place in the condensed phase. Research on stable deflagration of porous systems also helps one to understand the processes determining the onset of filtration instability.

It is assumed in modern theories of normal deflagration of condensed systems that heat is transferred from the reaction zone to the unreacted substance by conduction and radiation in the absence of convection (penetration of gaseous combustion products or melt). There is no reason to doubt this hypothesis as regards a nonporous system and its deflagration proceeds normally. However, it will be shown below that in porous systems penetration of the combustion products is known to occur sometimes, though deflagration is stable and regular. Naturally, such deflagration cannot be classified as normal.

Unlike solid systems, deflagration of porous systems is characterized by some specific features. We first note the more than one-dimensional character of the deflagration, determined by the geometric inhomogeneity of porous systems. Pores in the charge lead to curving of the burning surface. Consequently the heat and mass transfer conditions in the chemical reaction zone and the structure of the combustion products flowing from the surface change. The physical state of the hot surface exhibits the strongest effect on deflagration. The nature of deflagration is also determined by the disperse character of the porous medium surrounding the solid explosive and filling the pores with gas.

Experimental studies of stable deflagration of explosives with open (gas-permeable) porosity require some precautionary measures. Reliable data can be obtained only if burning proceeds subject to constant outside pressure. This condition is strictly fulfilled only if the sample is ignited in the atmosphere. The pressure increases during deflagration in a "constant

pressure" bomb, even when the free volume is sufficiently large (BD-150 and BD-1000 bombs), so that the combustion products penetrate into the pores. Moreover, unless special precautions are taken the pores of the explosive become filled with the gas (nitrogen) which was used to create the pressure in the bomb. The gas in the pores serves as a special inert additive to the explosive, whose mass increases with pressure. Both these factors may distort the result, but objective allowance for their influence on burning presents considerable difficulties. Therefore, only data obtained at constant (atmospheric) pressure will be examined.

## 6. EFFECT OF DENSITY OF AN EXPLOSIVE ON THE POSSIBILITY OF DEFLAGRATION

Andreev /35/ first showed that for fusible explosives there exists a limiting density below which burning is extinguished. Stable deflagration is observed at higher densities. Burning becomes irregular and pulsational near the limit of quenching. The density at the lower limit decreases with increasing charge diameter and crushing of the explosive particles. A change in density affects differently the burning of nitrocellulose, nitroglycerine powder, for which an upper density limit exists. Cessation of burning for a constant charge diameter is observed at a higher density, whereas burning of charges of lower density becomes stable.

The quenching of deflagration of porous charges may be explained by general concepts about the critical diameter of burning, a term introduced by Andreev /36/. The critical diameter $d'_{cr}$ characterizes the tendency of an explosive to burn and is defined as the smallest charge diameter for which the explosive can still burn. The inability to burn at a charge diameter below critical is due to noncompensating thermal losses from the heated layer and the zone of deflagration into the environment. Therefore, all these factors (increase in external pressure, initial temperature) which reduce the relative thermal losses and increase the deflagration velocity lead to a reduction in the critical diameter. An important effect is also exhibited by the shell of the charge – the thermal conductivity of its material and the wall thickness.

Let us examine how the critical diameter varies with density. Andreev /37, 38/ noted that an increase in the density of an infusible explosive (tetryl) increases the ability to burn ($d'_{cr}$ decreases), while the pattern is just the opposite for nitrocellulose.

Thus, unlike the effect of pressure and initial temperature, the effect of density on the critical diameter depends on the nature of the explosive. This is one of the specific features of deflagration of porous systems. This fact is very interesting and worth investigating. On the other hand, data on this problem is sparse /37, 38/. Preparation of charges with different density involves considerable methodical difficulties, so earlier tests were conducted with samples of maximum density (prepared nitroglycerine and nitropyroxilin powders) or with samples of free-flowing or close to free-flowing density.

Supplementary experiments were carried out in order to study the change in $d'_{cr}$ ($\delta$) over a wide density range /39/. The method of cones was used in



our preliminary estimation of $d'_{cr}$. The data obtained were refined by igniting cylindrical charges. The shell was produced from materials with low thermal conductivity (plexiglass, asbestos fabric) to decrease heat losses, and to prevent heating of the substance by propagation of the heat wave over the shell. We used a press mold of rectangular cross section, which enables us to obtain (after suitable processing) elongated (30–50 mm) cylindrical and conical high-density charges, which were then glued to the shell. The ignition system ensured regular ignition of the sample over the whole cross section of the surface.

The results are shown in Figure 15. The existence of a lower (for fusible explosives) and an upper (for "infusible" explosives*) quenching limit is a direct consequence of the diverse nature of the dependence of the critical diameter on the density. It will be shown below that the variation in the burning velocity with density also differs considerably for the considered explosives in accordance with the different form of the function $d'_{cr}$ ($\delta$).

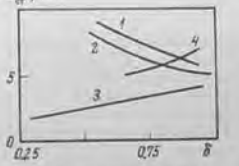


FIGURE 15. Dependence of critical diameter of deflagration on relative density ($p = 1$ atm):

1) hexogen, $r = 100–200$ μ; 2) tetryl, $r = 100–200$ μ; 3) 10% polystyrene + 90% ammonium perchlorate, $r = 15$ μ; 4) pyroxylin No. 1.

Consider now the factors determining the form of function $d'_{cr}$ ($\delta$). The approach employed here is to examine how the thermal losses vary during deflagration of charges with diverse densities, mainly thermal losses from the reaction zone to the substance.

The correct approach for a fusible explosive was outlined by Andreev /38/, who correlated the increase in $d'_{cr}$ at lower densities with the increase in thermal losses in the condensed phase by melt penetration into the pores. In fact, however, this is not quite correct, and the role of melting is not restricted by this phenomenon. Optical observations of the hot surface of hexogen show that in charges with lower density (close to the free-flowing value) the fused film continuously shifts over the surface and is accompanied by fluctuations in the flame. The movement of the melt is due to its entrainment by flowing gaseous combustion products as a result of inhomogeneities in the hot surface and of foaming, which occurs owing to the thermal expansion of gaseous bubbles.

The melt droplets moving over the surface and the individual formations containing the fused solid particles become larger owing to surface tension forces, and agglomeration occurs. Movement and agglomeration of the melt droplets lead to increased thermal losses and to a permanent destruction of the heated layer of the explosive prepared for burning. It is very interesting to observe the hot surface of hexogen when $d = d'_{cr}$. Burning may cease rapidly, if, for instance, conical charges are used. It was found that melts

* The term "infusible" explosive comprises substances whose burning surface is gas-impermeable. It follows from experiments (see section 8) that this condition is satisfied by pyroxylin, ammonium perchlorate, and ammonium perchlorate mixtures.

with inclusions of fused solid particles concentrate in one place, usually on the periphery, while the other part of the surface is free from melt. It is certain that the sharp reduction in the hot surface as a result of agglomeration of the individual droplets is the cause for interruption of burning.

With increasing density, the movement of melt and fluctuations of the flame cease, and the fused layer solidifies. Naturally, thermal losses due to shifting of the film cease, and consequently the ability to deflagrate increases with decreasing critical diameter (Figure 15). According to Annikov and Kondrikov /40/, on decreasing the diameter the burning velocity remains constant right up to quenching when melting secondary explosives with a low density, in contrast to liquid explosives. The disagreement with theory /41/, which predicts a decrease in the burning velocity as the limit is approached, was correctly attributed by Annikov and Kondrikov /40/ to thermal losses because of movement of the melt along the surface.

For "infusible" explosives with a "dry" burning surface, the main reason for the drop in $d_{cr}$ with decreasing density is the restricted penetration of gaseous combustion products into the pores. They are unable to ignite the explosive, so the penetrating gases heat them and change the heated layer. Additional heat supply to the explosive from the gaseous phase increases with decreasing density and compensates lateral thermal losses, so making possible stable deflagration in small-diameter charges. The effect of limited penetration of the products into the pores is observed (as explained in section 8) not only at low (free-flowing) densities, as was supposed by Andreev /38/ when considering the reasons for pulsating irregular burning, but also during deflagration of very dense charges.

Explanations of the increase in $d_{cr}$ with density must also take into account /38/ that, with increasing density, the thermal conductivity of explosives increases, as does consequent heat removal to the homogeneous phase.

## 7. DEFLAGRATION PATTERNS IN POROUS SYSTEMS

The approximate theory of deflagration proposed by Zel'dovich and Belyaev is most popular for condensed systems, so it will be explained here in brief. It is assumed in this theory that the reaction rate grows exponentially with temperature and that burning takes place in a narrow zone in the gaseous phase. The main evolution of heat is concentrated in a very narrow temperature range (width of the order of $RT_b^2/E$), close to the maximum burning temperature $T_b$. Heat transfer from the reaction zone to the unreacted substances takes place by conduction.

This theory was developed by Zel'dovich and Frank-Kamenetskii for the burning of gases /41, 42/. After the fundamental research of Belyaev, who proved that the combustion of volatile secondary explosives occurs in the gaseous phase and is analogous to the burning of homogeneous gaseous systems, this theory was extended without any restrictions or additions to the burning of volatile explosives. The most comprehensive and successful comparison of theory with experiment was carried out with volatile explosives /5/.



According to this theory, the expression for the mass velocity of burning is

$$u_m = up \sim \sqrt{\frac{2\lambda}{q^2}\,\Phi_{max}\,\frac{RT_b^2}{E}}, \qquad (13)$$

where $\lambda$ is the thermal conductivity coefficient of the substance emerging from the reaction zone; $E$ is the activation energy; $q$ is the heat of reaction; $\Phi_{max}$ is the rate of heat evolution in unit volume of the reaction zone at burning temperature $T_b$.

It is assumed in the theory that $\Phi_{max} \sim \exp(-E/RT_b)$. For the $n$-th order reaction $\Phi_{max} \sim C^n$ ($C$ is the concentration of the reacting substance). The gas phase reaction then satisfies the approximate expression

$$u_m \sim p^{n/2} \cdot \exp(-E/2RT_b).$$

In principle, the theory is also applicable when the reaction takes place in the narrow zone of the condensed phase.

Much research has been carried out on various aspects of steady-state burning, and the main results are fairly well explained in monographs /38, 44/. Modern ideas about burning mechanisms and the main trends in the development of the theory of burning are also contained in review articles /45–47/.

Let us consider the burning patterns of porous charges. It follows from the theory that:

a) the mass velocity of burning is independent of density for a volatile explosive ($u_m = \text{const}$) when the main reaction takes place in the gaseous phase*;

b) the mass velocity increases with density, if the reaction takes place in the narrow zone of the condensed phase. In this case $\Phi_{max} \sim \delta^n$. If we assume that the density of the substance $\delta$ does not change in the heating wave, then equation (13) yields

$$u_m \sim \sqrt{\lambda \delta^n}.$$

According to literature data, we can assume approximately that the thermal conductivity of explosives $\lambda \sim \delta^3$, in which case

$$u_m \sim \delta^{(n+3)/2}. \qquad (14)$$

The presence of thermal losses during burning leads to case a) or promotes case b), i.e., a drop in burning velocity with decreasing density.

The above comments hold in the absence of convective heat transfer from the deflagration zone to the unreacted substance, and hence the combustion products do not penetrate into the pores. We now examine available experimental data.

The linear burning velocity $u$ was usually determined in our experiments and denotes the visible travel velocity of the whole burning zone.

* A similar form of the function ($u_m = \text{const}$) should be observed for fusible secondary explosives, when the fused explosive burns preliminarily.

TABLE 3. Dependence of mass velocity of burning $u_m$ (g/cm²·sec) on relative density for some substances ($p = 1$ atm)*

| Substance | Initial particle size, μ | Charge diameter, mm | Relative density $\delta = \rho/\rho_{max}$ | | | | | | | Reference |
|---|---|---|---|---|---|---|---|---|---|---|
| | | | 0.3 | 0.4 | 0.5 | 0.6 | 0.7 | 0.8 | 0.9 | 0.95–0.98 | |
| Hexogen ($\rho_{max} = 1.80$ g/cm³) | 5 | 10 | — | — | 0.038 | 0.038 | 0.04 | 0.042 | 0.045 | 0.048 | Authors' data |
| Tetryl ($\rho_{max} = 1.78$ g/cm³) | — | 24 | — | — | 0.062 | 0.065 | — | — | — | — | /30/ |
| Poly(vinyl nitrate) | — | 8 | 0.13 | 0.137 | 0.145 | 0.155 | 0.162 | 0.172 | 1.92 | — | /52/ |
| 25% Al + 75% $Fe_2O_3$ ($\rho_{max} = 4.23$ g/cm³) | 20 | 10 | 1.2 | 1.6 | 1.95 | 2.4 | 2.85 | — | — | — | Authors' data |
| 70% (25% Al + 75% $Fe_2O_3$) + 30% $Al_2O_3$ ($\rho_{max} = 4.0$ g/cm³) | — | — | 0.28 | 0.31 | 0.4 | 0.55 | — | — | — | — | /1/ |
| Nitroglycerine powder NP ($\rho_{max} = 1.60$ g/cm³) | 400 | 10 | — | 0.07 | 0.075 | 0.08 | 0.095 | 0.09 | 0.092 | 0.095 | Authors' data |
| The same | 1500 | 10 | — | — | — | 0.22 | 0.14 | 0.09 | Absence of burning | — | |
| 10% polystyrene + 90% ammonium perchlorate ($\rho_{max} = 1.80$ g/cm³) | 15 | 10 | 0.163 | 0.172 | 0.162 | 0.15 | 0.142 | 0.14 | 0.14 | 0.14 | Authors' data |
| 2% $Cr_2O$ + 98% ammonium perchlorate ($\rho_{max} = 1.975$ g/cm³) | 15 | 10 | — | 0.11 | 0.132 | 0.145 | 0.12 | 0.09 | Quenching | | Authors' data |
| Pyroxylin No. 1 | — | — | 0.235 | 0.215 | 0.195 | 0.175 | 0.16 | 0.15 | | 0.15 | |
| Mercury fulminate ($\rho_{max} = 4.31$ g/cm³) | ~50 | 6 | Explosion | | | | 6.90 | 6.1 | 5.70 | — | /5/ |

* Some of the experimental data were read from graphs.



Deflagration of porous systems is usually characterized by the mass velocity $u_m$, which is obtained by multiplying the linear velocity by the density of the explosive: $u_m = up$. The mass velocity is equal to the mass of the substance deflagrating per unit time and unit cross-sectional area of the explosive charge.

Let $\xi = u_m(\delta)/u_m(\delta')$ denote the ratio of the mass velocity of burning at given density $\delta$ to the mass velocity at the highest density $\delta'$ used in the experiment. The value of $\delta'$ is usually less than the maximum density $\delta_{max}$, since it is difficult to obtain nonporous samples by the method of pressing. Moreover, at a high density the burning of some substances is interrupted, because the upper density limit is reached.

Table 3 presents data on the density dependence of the deflagration velocity (the tests were conducted at atmospheric pressure). Data for some substances are also shown in Figure 16.




FIGURE 16. Dependence of $\xi = u_m(\delta)/u_m(\delta')$ on relative density ($p = 1$ atm):

1) hexogen; 2) 25% Al + 75% $Fe_2O_3$; 3) poly(vinyl nitrate); 4) mercury fulminate; 5) 2% $Cr_2O$ + 98% ammonium perchlorate; 6) pyroxylin No. 1; 7) 10% polystyrene + 90% ammonium perchlorate.

It should be first noted that strict constancy of the mass velocity over a wide range of density variations was not observed for even one of the investigated explosives.

The investigated substances may be divided tentatively into two groups according to the form of function $u_m(\delta)$.

1. An increase in the mass velocity of burning with increasing density ($\xi < 1$) is observed for substances of the first group. This group includes secondary explosives (hexogen, tetryl), nitroglycerine powder (finely ground), poly(vinyl nitrate), thermite compositions. The distinguishing feature of substances in this group is that they melt or are liquefied during burning.

Another feature of this group is the large heat of evolution in the condensed phase during deflagration. Pokhil /50, 55/ found that an overall exothermal reaction occurs in the condensed phase during deflagration of nitroglycerine powder, and that a viscous liquid layer exists. This layer foams, because gas bubbles of the decomposition products evolve. The burning velocity of the thermite composition 25% Al + 75% $Fe_2O_3$, and especially of the gas-free composition 70% (25% Al + 75% $Fe_2O_3$) + 30% $Al_2O_3$, is determined by the chemical reactions in the melt /51, 53/. According to Maksimov and Merzhanov /52/, the main reaction during burning of poly(vinyl nitrate) also takes place in the liquid phase — in the foaming zone.

Consequently, the experimentally observed increase in the mass velocity of burning with increasing density corresponds to theoretical predictions. However, the function $u_m(\delta)$ is weaker than expression (14), which was derived on the assumption that the main burning reaction takes place in the condensed phase.

The decrease in $u_m(\delta)$ with decreasing density for the volatile explosive hexogen, whose main reaction during deflagration takes place in the gas

phase, is usually correlated /44/ with the decrease in the heat of evolution in unit volume and the corresponding increase in the role played by heat losses. It is assumed that this pattern is general for volatile explosives.

On the whole, the conclusions which follow from function $u_m(\delta)$ for substances of the first group can be correlated with existing concepts and can be explained by a single theory of deflagration.

2. The mass burning velocity of substances of the second group decreases with increasing density. This group includes "substances" which do not fuse during burning, such as pyroxylin, mercury fulminate, ammonium perchlorate (catalyzed), and ammonium perchlorate mixtures with a burning additive.

We mentioned above that the critical burning diameter for the given substances decreases with decreasing density (in contrast to the first group). Thus, some parallel features can be observed between changes in the mass velocity and in the critical burning diameter with density for certain representatives of these two groups. The burning patterns of substances of the second group are of considerable interest not only because they do not fit into existing concepts, but mainly because in deflagration of "infusible" systems we should expect the specific features characteristic of porous systems. At the same time there is a scarcity of data on this problem. For this reason we undertook a more exhaustive study of the stable deflagration of porous "infusible" systems.

## 8. DEFLAGRATION OF "INFUSIBLE" SUBSTANCES /39/

We selected as "infusible" substances pyroxylin, a mixture of ammonium perchlorate with a burning additive (polystyrene), ammonium perchlorate catalyzed with 2% $Cu_2O$ (the particle size of the components was $r \simeq 15\ \mu$).

There are no published data about the possibility of fusion of pyroxylin. As for ammonium perchlorate, it was maintained until recently that this substance sublimates during burning. However, in later works dealing with the burning mechanism of ammonium perchlorate it was found that $NH_4ClO_4$ fuses during burning. According to Beckstead and Hightower /54/ the melting point of ammonium perchlorate is high ($T_{melt} \simeq 850°K$) and the fused layer formed is small and discontinuous. These substances were assigned to the category of "infusible" explosive, since our experiments have shown that the burning surface of porous charges of the given substances are gas-permeable and consequently no continuous fused layer is formed.

The following parameters were determined in our tests: the dependence of the mass velocity of burning on density $u_m(\delta)$, the temperature distribution in the condensed and gaseous phases $T(x)$, and the pressure change in the pores of the deflagrating charge $p_k(t)$. We used tungsten-rhenium and copper-constantan thermocouples of thickness 30 $\mu$. The pressure in the pores was recorded at the closed bottom end of the charge by a sensitive open liquid pressure gauge (water, mercury). The tests were all carried out at atmospheric pressure.

The experimental results pertaining to the dependence of the mass velocity of burning of the examined substance on density are shown in Table 3 and Figure 17. The characteristic feature of the curve of $u_m(\delta)$



is that the mass velocity increases when the density is decreased beyond a certain point. As regards catalyzed ammonium perchlorate, we note a peak on the $u_m(\delta)$ curve. Deflagration is uniform and stable and the velocity values are well reproducible in the given density interval. The increase in mass burning velocity with decreasing density indicates the presence of convective heat transfer from the burning zone to the unreacted substance and limited penetration of the combustion products into existing pores. This possibility was first indicated by Belyaev /5, 48/ in applications to mercury fulminate. The results show that the penetration of combustion products during deflagration is not only characteristic for the rapidly burning mercury fulminate, but is a common feature of "infusible" explosives, including substances burning at a low velocity. The penetration of products is observed under burning conditions at a strictly constant low (atmospheric) pressure and, what is more important, during deflagration of high-density systems. The increase in $u_m$ for the perchlorate composition and pyroxylin begins when $\delta \simeq 0.7$–$0.8$, and for mercury fulminate when $\delta \simeq 0.9$.

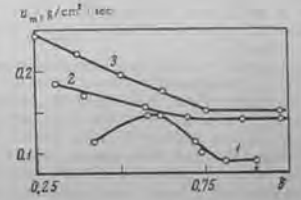


FIGURE 17. Dependence of the mass velocity of burning on relative density ($p = 1$ atm):
1) 2% $Cu_2O$ + 98% ammonium perchlorate;
2) 10% polystyrene + 90% ammonium perchlorate;
3) pyroxylin No. 1.

Before discussing results which confirm penetration of the combustion products into the pores, we first note a fact which is its indirect confirmation. If the density of the substance is reduced, then stable deflagration is impaired when $\delta < 0.65$ for mercury fulminate /5/ and $\delta < 0.12$ for pyroxylin /56/, and is characterized by a strong (one order or more) increase in the burning velocity. Burning becomes irregular and pulsational. In the case of the mixture based on ammonium perchlorate, burning at atmospheric pressure remains stable up to the minimum (bulk) density. However, the burning stability of the 10% polystyrene + 90% ammonium perchlorate mixture is impaired if the experimental conditions are somewhat modified, for instance, by igniting the mixture in an elongated gas tube, when a small (about $10^{-3}$ atm) pressure gradient arises at the tube walls owing to friction of the gas against the tube. It has now been convincingly

proved that the impairment in stability during deflagration arises due to filtration of gaseous products into the pores (see Chapter IV).

Thermocouple measurements carried out with a stoichiometric mixture of ammonium perchlorate and polystyrene ($\rho = 0.65$ g/cm$^3$) are now examined. First, we noted a considerable deviation in the temperature profile of the condensed phase from the Michelson profile; the thickness of the heated layer increases by a factor of 3–4.

We also measured the surface temperature $T_s$ (from the inflection on the $T(x)$ curve) and the temperature gradient in the gas phase close to the surface $(dT/dx)_{T=T_s}$. In this way it was possible to evaluate the amount of heat $q$ released during burning in the condensed phase.

If radiation (which is small) is neglected, the heat balance equation yields

$$q = c_p(T_s - T_0) - \frac{\lambda}{u_m}\left(\frac{dT}{dx}\right)_{T=T_s}, \qquad (15)$$

where $c_p$ is the heat capacity of the condensed phase; $\lambda$ is the thermal conductivity coefficient in the gas phase; $T_0$ is the initial temperature. Substitution of $c_p = 0.35$ cal/g·deg, $\lambda = 1.6 \cdot 10^{-4}$ cal/cm·sec·deg, and the experimental values $T_s = 600°C$, $(dT/dx) = 3.1 \cdot 10^4$ deg/cm into equation (15) yields $q \simeq 175$ cal/g.

It should be borne in mind that the heat in the condensed phase consists of two components: heat is introduced by the penetrating combustion products and heat is released by chemical reactions /48/. A sharp division of these components is very difficult, since they act simultaneously. Therefore, only an approximate evaluation can be conducted. According to measurements, the thermal effect of the overall exothermal reactions in the condensed phase during burning of monolithic samples is about 100 cal/g. This is the peak value, since a decrease in the density of the reagents gives rise to heat release as a result of reactions in the condensed phase, and this heat release decreases according to (14). However, even if this value (which is known to be too high) is selected, we see that at least 75 cal/g is introduced by combustion products penetrating into the pores.

Our measurements of the pressure $p_g(t)$ in the pores of a burning charge provided interesting data (a schematic diagram of the test equipment and the results are shown in Figure 18).* It was found that on burning pyroxilin and an ammonium perchlorate-additive mixture, the pressure in the pores is lower than the external atmospheric pressure, $\Delta p = p_g - p_s < 0$. Rarefaction increases at the initial instant after ignition, after which the limiting value sets in ($\Delta p = \Delta p_l$). The pressure in the pores does not change, regardless of the fact that deflagration continues.

The effect of the density of the samples and the composition of the ammonium perchlorate + polystyrene mixture was studied in order to obtain an explanation for this phenomenon. It was found (see Figure 18) that with increasing density (decrease in pore diameter $d_p'$) rarefaction

* This experimental series made use of charges possessing a larger diameter ($d = 16$ and 20 mm), which prevented any distorting effect of the supplementary free volume that unavoidably arose when connecting the pressure gauge.



$\Delta p_l$ increases, reaches its peak value, and then decreases sharply. For instance, the largest rarefaction $\Delta p_l \simeq 0.1$ atm is observed for the mixture 10% polystyrene + 90% ammonium perchlorate at a sufficiently high density $\delta \simeq 0.8$. It is noteworthy that at approximately this density the mass velocity of burning increases with decreasing density (see Figure 17). When $\delta < 0.8$, $\Delta p_l$ is inversely proportional to the mean hydraulic diameter of the pore: $\Delta p_l \sim 1/d_p'$, where $d_p'$ is determined by relationship (2).

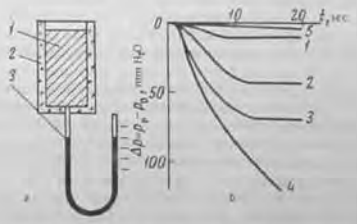


FIGURE 18. Schematic diagram (a) of the test equipment and the results (b) of measuring the pressure $\Delta p_g(t)$ in the charge pores during deflagration of samples consisting of 10% polystyrene + 90% ammonium perchlorate of diverse porosity ($p = 1$ atm).

a: 1) charge; 2) plexiglas shell; 3) pressure gauge; b: 1) $\delta = 0.35$; 2) 0.5; 3) 0.61; 4) 0.8; 5) 0.9.

In high-density charges ($\delta = 0.9–0.95$) no rarefaction is observed in practice. Thus there exists an optimum pore diameter at which the observed effect is strongest.

Rarefaction was found to depend not only on pore size, but also on the composition of the mixture. A pattern similar to the above was observed also during deflagration of pyroxylin.

The initiation of rarefaction in the pores of a burning charge is, at first glance, in contradiction to the penetration of combustion products into the charge pores. The physical nature of the observed effect is explained by examining some possible hypotheses.

Only two such hypotheses are noted. The jet hypothesis is particularly attractive. According to this approach, suctioning off of air contained in the pores is due to the ejecting action of the jet of the effluent products formed during deflagration of the individual particles. However, in this case the rarefaction should not exceed $10^{-4}$ atm, which is several orders lower than the experimental value.

The other hypothesis, in our opinion, corresponds more to reality. The hot combustion products enter the charge at a pressure close to $p_s$, fill the pores, impart heat to the surrounding substances, and are cooled. This process must be accompanied by a pressure drop in the half-closed pore

space. Condensation of the products also promotes the pressure drop. This hypothesis was confirmed by direct measurement. Hot nitrogen at various temperatures, or combustion products were blown into a porous sample, which consisted of an inert substance MgO with a gas-impermeable bottom. Rarefactions, which increased with the temperature of the gas blown in, were observed in these tests. In accordance with this theory the pressure drop in the pores should be stronger, the higher the degree of gas cooling and the concentration of the condensation products. The effect of pore size and mixture composition can be explained from this aspect.

The whole set of reported data indicates that combustion products almost always penetrate into the pores during burning of porous "infusible" substances, and the deflagration of such systems is no longer normal.* It is noteworthy that layer-by-layer burning was considered, when penetrating combustion products did not ignite the inner pore surface.

The data examined in sections 6–8 correspond to burning at strictly constant atmospheric pressure. Deflagration of porous explosives at pressures above atmospheric have been studied /37, 38, 82/. The samples were ignited in a "constant-pressure" bomb. Unfortunately, the results were not analyzed from the standpoint of the potential effect of the penetrating combustion products corresponding to the pressure increase in the bomb during deflagration of the charge.** The effect of nitrogen, which fills the pores of the substance, was disregarded. The available data are therefore difficult to interpret.

## 9. DYNAMIC INCREASE IN PRESSURE ON THE HOT SURFACE

The pressure $p'$ on the burning surface of condensed substances may exceed the pressure $p_0$ in the surrounding volume, if the release of heat takes place completely or partially in the gas phase. The pressure increase created on the hot surface is usually called the dynamic increase $\Delta p_d = p' - p_0$.

Unlike detonation, deflagration proceeds with decreasing pressure and expansion of the reaction products. The lower branch of the Hugoniot adiabat corresponds to constant-velocity deflagration. The velocity of the combustion products moving away from the surface increases in accordance with the nature of the heat release over the tongue of the flame. Thus a pressure gradient $\Delta p_d$ exists between the sections enclosing the deflagration zone; the pressure is highest on the burning surface.

In the past much attention was devoted to the evaluation of $\Delta p_d$ /4–8, 38/, which is related to the following facts. It was assumed earlier that the dynamic pressure increase is the main cause for impairing stable burning. Though (as shown later) this cause is not the fundamental and universal one (the actual causes are much more comprehensive and diverse, see section 12), in certain conditions (such as burning under constant external pressure) $\Delta p_d$ must not be neglected. Moreover, the fact that $\Delta p_d$ exists was used to explain the pressure dependence of the burning rate of rapidly burning explosives /58/.

Let us determine the pressure drop at the hot surface using the laws of mass conservation and momentum conservation. For simplicity we consider one-dimensional burning of a nonporous explosive and characterize the state of the gas in the immediate vicinity of the surface by pressure $p'$, density $\rho'$, velocity $v'$, and temperature $T'$ ($v'$ is the velocity of the gases released from the surface, in general $v' \neq 0$; $T'$ is the temperature of the surface). The gas in the given cross section contains the gasification (evaporation) products of the condensed phase. The corresponding parameters of the final products after the burning zone are denoted by $p_1$, $\rho_1$, $v_1$ and $T_1$. It is assumed that no condensed particles are present during deflagration.

The pressure $p_1$ in the final reaction products is determined by the boundary conditions at infinity, and for subsonic flow is equal to pressure $p_0$ in the surrounding volume ($p_1 = p_0$). The pressure gradient thus arises only due to ignition of the gasification products near the surface.

The equations of conservation of mass and momentum assume the form

$$\rho u = \rho' v' = \rho_1 v_1,$$
$$p' + \rho u v' = p_1 + \rho u v_1,$$

whence

$$\Delta p_d = p' - p_1 = (\rho u)^2 \left(\frac{1}{\rho_1} - \frac{1}{\rho'}\right). \qquad (16)$$

If $\Delta p_d \ll p_1$, which holds for the majority of explosives, equation (16) becomes

$$\Delta p_d = \frac{(\rho u)^2 R}{p_1}\left(\frac{T_1}{M_1} - \frac{T'}{M'}\right), \qquad (16')$$

where $M'$ and $M_1$ are the molecular weights in the corresponding sections of the gas streams.

It follows from (16') that a considerable increase in the pressure at the burning surface may occur for a rapidly burning explosive even when the quantity $(T_1/M_1) - (T'/M')$ varies considerably.

If the gasification and combustion products contain condensed particles whose weight fraction is $\varepsilon'$ and $\varepsilon_1$, respectively, while their velocity equals that of the gas, then, according to Bakhman's calculations /57/,

$$\Delta p_d = (\rho u)^2 R\,\frac{(1-\varepsilon_1)\,T_1/M_1 - (1-\varepsilon')\,T'/M'}{p_1 - (1-\varepsilon_1)(\rho u)^2/\rho_1}. \qquad (17)$$

If the external pressure decreases and the resulting burning velocity decreases at a rate slower than linear, then the velocity at which the products move away, namely $v_1 = u\rho/\rho_1$, increases. However, it cannot exceed the sonic velocity $c = \sqrt{\gamma R T_1/M_1}$. Hence the pressure in the products cannot be lower than some minimum value given by

* In addition to the thermal effect the penetrating products may also act catalytically.

** If a continuous fused layer is formed on the burning surface, gaseous combustion products do not penetrate into the pores. This occurs, for instance, in deflagration of secondary (fusible) explosives with low porosity.

$$P_{min} = (1 - \varepsilon_1)\rho u \sqrt{\gamma R T_1 / M_1}. \qquad (18)$$

Thus as the sonic velocity is reached, the pressure in the products $P_{min} = P_1 > p_s$ remains constant and independent of further decrease in the external pressure.* In this case the pressure at the charge surface is $P_{min} + \Delta p_d$, where $\Delta p_d$ is given by expression (17). This fact limits the minimum pressure at which explosives deflagrate /5/ and is especially important during burning in vacuo.

In order to determine $\Delta p_d$ we need not, in principle, allow for the multistage nature of the burning process. It is sufficient to consider transition from the initial stage of the combustion products (near the surface) to the final stage. A correct determination of the temperature and composition of the combustion products in the considered sections is of special importance.

We considered one-dimensional burning, which takes place if the explosive charge is placed into a shell. In the absence of a shell the products moving away expand laterally and the flow is no longer one-dimensional. In this case the increase in pressure is higher than in one-dimensional burning. In the simplest case, when the burning surface is plane and the zone in which heat is released is conical with apex angle $\varphi$, the pressure gradient can be determined from (17), where we replace $(\rho u)^2$ by $\left(\rho u \sin \frac{\varphi}{2}\right)^2$.

The general problem dealing with the pressure gradient at the front of an oblique wave was treated by Shelkin and Troshin /86/.

Consider now experimental data on the excess pressure at the hot surface. We mainly investigated initiating and rapidly burning explosives, since $\Delta p_d$ for secondary explosives and powders is so small that it cannot be recorded. It should be noted at the very outset that available experimental data are very sparse and were usually obtained by a method based on measuring the reaction $F$ exerted by the hot charge on an elastic support. It was assumed that the pressure gradient is given by $\Delta p = F/S$ ($S$ is the cross-sectional area of the charge) and that a dynamic increase in pressure exists. Belyaev /5/ used this method to determine $\Delta p_d$ for some rapidly burning explosives at atmospheric pressure.

The tests were carried out with 4-mm samples; their lateral surface was encased in collodion. It is of interest that the measured values of $\Delta p_d$ were very low (see Table 4).

Most interesting are the data on mercury fulminate, whose deflagration mechanism was investigated rather exhaustively /5, 49/. It was found that mercury fulminate burns in two zones. The burning velocity is determined by the low-temperature (800—1000°K) zone adjoining the burning surface. There is practically no luminescence in this zone and no more than 20—25% of the initial substances. The remainder is dispersed and is combusted to the final products in the second high-temperature luminous zone, which is situated far from the surface. The dark zone and the most coarsely dispersed particles in the form of separate luminescent tracks are shown in Figure 19 /93/. The width of this dark zone increases with decreasing pressure, and at 40—50 mm Hg the brightly luminescent flame ceases.

* According to an estimate carried out by Bakhman /67/ $P_{min}$ = 4—8 mm Hg for mercury fulminate (without allowance for the effect of solid particles on the sonic velocity). The much higher value, $P_{min}$ = 4 atm, is obtained for the very rapidly burning lead styphnate.



TABLE 4. Mass rate of burning $u_m$ and dynamic pressure increase $\Delta p_d$ for some initiating and rapidly burning explosives ($p_s$ = 2 atm)

| Substance | $u_m$, g/cm² · sec | $\Delta p_d$, mm Hg | Literature |
|---|---|---|---|
| Trinitroazidobenzene $C_6(NO_2)_3(N_3)_3$ | 3.1 | 4 | /5/ |
| Tricycloacetone peroxide $C_9O_6(CH_3)_6$ | 1.18 | 4 | /5/ |
| Potassium picrate $C_6H_2(NO_2)_3OK$ | 2.74 | — | /5/ |
| | 1.3 | 5 | /5/ |
| | (in shell) | | |
| Mercury fulminate $Hg(ONC)_2$ | 5.9 | 15 | /5/ |
| | | 10—15* | /39/ |
| | | 85—90** | |
| Lead styphnate $C_6H(NO_2)_2O_2Pb \cdot H_2O$ | 100 | — | /38/ |

* In a shell less than 40 mm in length.
** In a shell more than 40 mm in length.

The dependence of the burning velocity on pressure (when $p < 1$ atm) is approximated by a linear function of the type $u = A + Bp$. Analysis of the gaseous combustion products for the low-temperature zone gives the mean molecular weight of the products $M \simeq 120$. A tentative thermodynamic calculation for the high-temperature zone (without allowance for dissociation) according to the recommended equation $Hg(ONC)_2 = Hg + 2CO + N_2$ gives $T_1 \simeq 3500$°K, $M_1 \simeq 70$, $T_1/M_1 \simeq 50$.

FIGURE 19. Photograph of deflagration of mercury fulminate ($p$ = 1 atm).

At (below atmospheric) pressure $p_s$ Belyaev /5/ determined experimentally the dependence of $\Delta p_d$ on external pressure $p_s$ (Figure 20); its form is characteristic. Such a curve (with a minimum) follows from expression (16) when function $u(p)$ assumes the form $u = A + Bp$. However, the calculated values of $\Delta p_d$ lie much lower than the experimentally determined ones (the calculation was conducted with allowance for the low-temperature zone alone, which is only correct for burning in vacuo).

Sulimov and Korotkov /39/ obtained an interesting result concerning the ignition of mercury fulminate samples pressed to a high density ($\delta$ = 0.97) in thin-walled tubes of various lengths $L_{tu}$ (Figure 21). The sample height was maintained constant (6 mm). A piezoelectric probe was used to measure the reaction. It follows from Figure 21 that when $L_{tu}$ is larger than 40 mm pressure $\Delta p_d$ increases considerably from 10—15 mm Hg (which agrees with data of Belyaev /5/) to 85—90 mm Hg.*

It is natural to assume that the results are due to the zonal nature of the deflagration process, so that when $L_{tu} > 40$ mm the high-temperature zone in

* This fact cannot be explained by the friction of the products against the tube walls.

the tube, in which the disperse particles burn to the end and the main part of the heat of reaction is evolved, is also displaced. In this case the excess pressure is determined by the total action of both zones (the whole burning zone) with the last zone predominating.* Confirmation of this point of view is the satisfactory agreement between experimental ($\simeq 90$ mm Hg) and theoretical ($\simeq 130$ mm Hg) values of $\Delta p_d$, especially if we remember that a high value of $T_1/M_1 \simeq 50$ was used, corresponding to the products of total combustion.

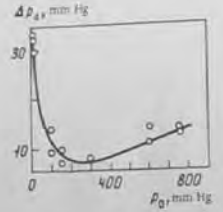


FIGURE 20. Dependence of dynamic pressure increase $\Delta p_d$ at the burning surface of mercury fulminate on external pressure $p_0$.

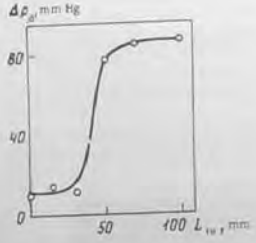


FIGURE 21. Dependence of $\Delta p_d$ on the length of the gas outlet in the case of mercury fulminate ($p = 1$ atm).

We mention a special feature characteristic of rapidly burning explosives /5/. At the initial instant of mercury fulminate burning there is a substantial pressure jump on the $\Delta p_d(t)$ curve, while the optical oscilloscope records a higher burning rate along a section covering several (up to 2–4) mm, after which deflagration propagates at a constant rate.**

This effect is also found both when igniting with a spiral and via a layer of slowly burning substance. It can be explained in terms of the nonsteady-state theory of burning /43/ and involves the creation of a sufficiently thick heated layer in the rapidly burning explosive on ignition and its accelerated combustion. Thus rapidly burning explosives represent a very good model with which to study nonsteady burning processes.

In conclusion, it should be mentioned that the results reported here refer to the burning of high-density explosives.

* In a short ($L_{to} < 40$ mm) tube the pressure gradient created is determined by the low-temperature burning stage.

** An increase in the burning rate at the initial stage was also noted for other rapidly burning explosives (lead styphnate and picrate /58/).



*Chapter III*

## *IMPAIRMENT OF STABLE DEFLAGRATION OF GAS-PERMEABLE POROUS SYSTEMS*

Stable steady-state deflagration of explosives is impaired under certain conditions. The impairment is expressed by a significant increase (by a factor of $10^1$ to $10^2$) in the mass velocity of burning. This chapter deals with a group of problems related to the mechanism of acceleration, and to the laws and critical conditions governing impairing of the stability of deflagration — the initial stage of detonation onset.

### 10. FUNDAMENTAL THESES OF STABILITY THEORY

The stability of steady-state burning of condensed systems was investigated theoretically by Belyaev and Andreev /4, 5, 8/. The theory is based on equilibrium between gas supply and gas removal during deflagration. The impairment of stable deflagration was shown to be a consequence of the simple laws of gas dynamics.

Naturally, the dynamic pressure increase that arises at the charge surface during ignition (section 9) must somewhat increase the burning velocity, since the burning velocity usually increases with pressure and produces further pressure increase, etc. The problem is therefore to determine conditions under which equilibrium cannot be established in the process under examination, i.e., under which burning becomes unstable while the burning velocity and the pressure at the surface increase continuously. It was assumed that, in principle, this way of producing instability is also possible in the deflagration of nonporous explosive charges.

Belyaev /4/ employed mercury fulminate to first compute the critical burning velocity which corresponds to the stability limit, subject to the conditions of stability of gas supply and gas removal and under the assumption that $u_m(p)$ is linear.

Stability theory was further developed by Andreev /8/. Burning of a cylindrical charge at its ends was examined on the assumption that the pressure dependence of the burning velocity is given by $u_m = A' + Bp^\nu (\nu < 1)$. Andreev used an expression for gas removal that is valid for the critical (sonic) efflux of the combustion products,* which is established when the pressure near the surface is approximately double the external pressure. It was shown that burning is stable if, when the gas supply equals the gas

* It was noted earlier that the efflux regime can be realized during burning of an explosive in vacuo, or for very rapidly burning explosives like lead styphnate.

removal, the gas supply increases more rapidly with pressure than does the gas consumption, i.e., the derivative of the mass velocity of burning with respect to pressure ($du_m/dp$) does not exceed some limit. The value of this limit is equal to the discharge coefficient:

$$A = \sqrt{\frac{\gamma}{RT}\left(\frac{2}{\gamma+1}\right)^{(\gamma+1)/(\gamma-1)}}$$

where $T$ is the gas temperature (°K), $\gamma = c_p/c_v$, and $R$ is the gas constant; the value of $A$ is 7–7.6 g/cm$^2$ · sec · atm.

It was found that for all secondary explosives $du_m/dp$ is 50–200 times smaller than the gasdynamic limit. For initiating explosives which can deflagrate when pressed to a high relative density, $du_m/dp$ is also lower than the critical value, but approaches this value. It is noteworthy that initiating and rapidly burning explosives (such as mercury fulminate and lead styphnate) for which stability impairment is expected owing to their high burning velocity, are characterized by weakening of the $u_m(p)$ dependence at elevated pressures /38/.

Thus one of the fundamental results of our theoretical examination was to provide theoretical explanations underlying the ability of the majority of investigated explosives to undergo stable deflagration. It was assumed that the area of gas introduction (burning surface) is equal to the area of gas removal (end of the hot charge); this is fulfilled, if a hot nonporous substance burns. At the same time, instability was experimentally observed not only during burning of initiating explosives, but also of secondary (slow-burning) explosives, which, of course, required an explanation. The hypothesis was advanced /4, 6/ that the fundamental cause is the increase in the burning surface, which can arise in several ways. The burning surface must increase by a factor of at least $B/A$ in order to impair the stability.

The surface increases for porous systems, because burning penetrates into the pores of the charge. It was shown elsewhere /10–12, 59–70/ that this acceleration mechanism occurs on a very large scale and is most characteristic for solid explosives. This approach was used to derive very interesting and important results, which form the main topic treated in this chapter.

Andreev considered the other possible mechanism of increase in the burning surface to be more important. This mechanism is realized if the explosive burns with intensive dispersion, which results in the formation of a suspension of particles with a developed surface in the combustion products /38, 72/. The dispersion process may be due not only to chemical causes (gas-formation reaction in the condensed phase), but also to physical causes (explosive particles may be formed owing to cracking of crystals by thermal shock as a result of the release of vapors of volatile impurities, etc.). This mechanism of increase in the gas supply is very interesting, especially as far as solid explosives are concerned. Unfortunately, there are very few and fragmentary data in the literature (see section 19).

The main mechanism governing the acceleration of burning in liquid explosives is the theory of spontaneous eddy formation, developed by Landau /73/. According to this theory the deflagration front is unstable when subjected to infinitely small perturbations, in which case the small curved sections of the deflagration front grow spontaneously.



Belyaev also emphasized that during burning of liquid explosives which are nonhomogeneous in structure, an important acceleration mechanism is based on the penetration of burning into the bulk through existing inhomogeneities (bubbles) /4/. From this standpoint Belyaev explained how detonation arose in hot methyl nitrate at low pressure when the liquid boiled, and was accompanied by the formation of bubbles and absence of detonation at higher pressures when no boiling took place /2/.

We note in conclusion that, for a gaseous system, the acceleration of burning is also due to the increase in the burning surface. Fundamental research of Shchelkin /75/ has shown that the main cause of the acceleration of the flame is vortex formation of the uncombusted gas moving ahead of the flame front, which leads to bending and eventual destruction of the deflagration front. The unreacted mixture moves owing to expansion of the combustion products. Accelerated burning is observed when the Reynolds number, related to the flow of the uncombusted gas, exceeds some critical value, i.e., when vortices must arise. During ignition of the gas in the tube the vortices in the gases begin to form at the tube walls and propagate toward the axis. Convincing proof of this point of view is the abrupt acceleration of burning in rough tubes (in comparison with smooth tubes), so increasing the turbulence of the flow. According to Zel'dovich /76/, curving (extension) of the flame front also accelerates burning of the gaseous mixture. The flame in the central part of the tube moves more quickly than near the walls.

When gaseous mixtures are ignited in large-diameter tubes, spontaneous eddy formation becomes as important as in liquids.

As regards solid substances, penetration of burning into the pores (bulk) of the explosive is the main mechanism governing the impairment of deflagration.*

The first experimental research on the stability of deflagration of condensed systems was carried out by Andreev /6, 7/ and Belyaev /5/. Andreev /6, 7/ demonstrated that detonation arises during ignition of porous secondary explosives in a confined space (Figure 6a) if a sufficiently high pressure is achieved during deflagration. According to Belyaev /5/, burning of initiating explosives (mercury fulminate) when $\delta < 0.65$ becomes unstable, even at atmospheric pressure.

The scarcity of observations, which, moreover, are mostly of a qualitative nature, did not permit the creation of a unique and physically justified quantitative scheme of the phenomenon and did not provide answers to some practically important problems connected with explosion safety in the production of explosives and propellant powders. For this reason the following trends were adopted when studying impairment of the stability of deflagration of porous systems /10–12, 59–70/: 1) study of the mechanism governing penetration of burning into pores under typical ignition conditions; 2) determination of the critical conditions of the impairment of stability for various groups of explosives and propellant powders; 3) study of the effect of the charge parameters (gas permeability, porosity, geometrical dimensions) and the physicochemical and thermochemical properties of explosives during deflagration stability; 4) establishment of quantitative laws governing losses in stability.

* Subsequently, the terms "penetration of burning into the pores," "impairment of stability of burning (deflagration) of gas-permeable porous systems," and "onset of filtration instability" are synonymous.

This chapter will deal with fundamental (mostly experimental) data on the onset of filtration instabilities in porous gas-permeable systems. Later chapters will be devoted to the other important aspect of the problem, namely, the development of the instability.

## 11. FORMULATION OF THE PROBLEM

Impairment of the stability of deflagration is a complex nonsteady-state phenomenon which includes gasdynamic, thermophysical and physico-mechanical processes. The decisive processes are the filtration of combustion products into the pores, and ignition of the explosives. In some cases, when the sample in the stable deflagration stage is subjected to the effects of mechanical loads, allowance must also be made for sample deformation.

Thus, in general form, the theoretical formulation of the problem requires the simultaneous solution of the equation of nonsteady nonisothermal filtration into a deformed porous medium and of the equations describing heat transfer and ignition of explosives. Allowance is also made for the specific mechanism of deflagration of explosives, so it is evident that great difficulties are encountered in the theoretical formulation of the problem. It is therefore hardly surprising that no general solution to the problem yet exists. Thus it is only natural to seek a simplified theoretical formulation (sections 13, 14). The following main simplifications are introduced.

1. Deformation of the charge is generally neglected, i.e., it is assumed that the initial permeability, porosity and pore size remain unchanged during stable deflagration. This assumption is justified for the overwhelming majority of high-density crystalline explosives.

2. We consider separately a) filtration of gases into pores, and b) the problem of ignition of the porous explosive; the gasdynamic pattern of the gas flow is assumed.

3. The ignition conditions of the pore walls /70/ are described by the ignition theory of Zel'dovich /43/ developed for volatile explosives; this theory disregards exothermal reactions in the condensed phase.

We now specify the term "impairment of stability of deflagration." The condition necessary for impairment of stable deflagration of gas-permeable systems is the movement of the gaseous combustion products ahead of the deflagration front. In other words, penetration of the gases is ensured by seeing that the mean velocity of the outflowing gases $V_g$ relative to the pore walls exceeds the linear burning velocity of layer-by-layer charge deflagration $u$ ($V_g > u$).

This condition is necessary, but by no means denotes loss of stability. The earlier example of burning of an "infusible" explosive (section 8) demonstrates that though restricted penetration of products into the pores took place (i.e., the required condition was fulfilled), burning remained stable.

The following condition is sufficient to impair stability: the hot gaseous products that overtake the deflagration front produce ignition of the porous substance, which propagates at a velocity surpassing the deflagration velocity.



Fulfillment of the required condition involves the problem of gas filtration into the pores, while satisfaction of the sufficient condition involves the problem of the thermal action of gases on substances and of possible ignition regimes. From this standpoint we are entitled to consider separately each of the above problems.

It follows that it is convenient to speak about impairment of stability only in respect of specific ignition conditions, which determine the filtration and heat transfer processes.

## 12. MECHANISM OF GAS PENETRATION

Before dealing with gas flow through pores we must examine the cause or driving force behind the penetration and see what makes the combustion products flow into the pores. The driving force behind penetration of the products determines the mechanism governing the impairment of deflagration stability as a whole.

The forced mechanism appears to be the fundamental one, in which the inflow of gases is due to the pressure difference. During forced flow, the pressure $p'$ at the surface of the hot charge exceeds the pressure $p_s$ in the pores: $\Delta p = p' - p_s > 0$ or $\Delta p = p - p_s > 0$ (if the dynamic pressure increase $\Delta p_s$ is ignored in comparison with the external pressure $p$). The pressure gradient depends on the ignition conditions. Subscript "0" will denote the initial pressure value; the absence of subscript "0" will denote the instantaneous value.

Consider the following characteristic cases, which correspond to typical ignition conditions:

1. Burning of the "built-in charge" (see Figure 2) (external pressure is maintained constant, $p = p_s = \text{const}$; initial pressure in pores $p_s^0 = 1$ atm, $p_0 \geqslant p_s^0$).

2. Burning at increasing external pressure in a manometric bomb (see Figure 3) ($p(t) \neq \text{const}$; $dp/dt > 0$; $p_s^0 = 1$ atm).

3. Burning at constant external pressure ($p = p_s = \text{const}$, $p_s = p_s^0$).

Cases (1) and (2) are the most interesting, because they correspond to practice. At the same time we can observe the onset of instabilities in samples whose porosity varies widely ($m$ greater than 0,03–0,05). The pressure gradient arises naturally under these conditions, since $p > p_s$.

The "built-in charge" simulates burning of a porous inclusion in propellant charge during operation of a rocket engine. The special feature of this scheme is that the initial and boundary conditions are defined. This was used in the theoretical consideration of the gas efflux. Application of this scheme enables the burning stability to be observed at a strictly defined pressure gradient which is easily obtained by changing the external pressure.

Increasing-pressure conditions are realized in practice during random burning of explosives in industrial equipment during ignition in various types of capsule detonators, etc. The advantage of this increasing-pressure technique is its good reproducibility and simple equipment. Similar results are obtained by the given method and by the "built-in charge." Therefore, the manometric bomb method is applied widely in experimental research on the impairment of stability.

As regards burning under constant pressure (case 3), the gradient is created during the actual burning process by a far from trivial technique. On igniting the charge the gas pressure in the pores is equal to the external pressure ($p_p^* = p_0$), which is maintained constant during burning ($p_0$ = const).* In this case, penetration of the first gas portions into the pores is essentially due to the dynamic pressure increase $\Delta p_d$, which arises at the moment of ignition and which (in the picturesque words of Andreev) "plays the role of an unconventional triggering mechanism."

Experiments carried out recently have enabled our ideas about the mechanism of gas penetration under these conditions to be extended. As noted earlier, the surface of the hot porous sample is not planar in the general case. A jet system issues from the surface and originates at the individual burning grains of the explosive. Jets are formed due to curving of the burning surface; they are inclined at different angles to each other and hence give rise to a "cumulative" interaction /10, 61/. Collision of the jets gives rise to new jets, some of which are directed into the pores of the explosive (Figure 22). Where the jets collide, one observes a local pressure increase which does not exceed $\Delta p_d$. However, it is significant that, during jet interaction, gas at a temperature above that in the immediate vicinity of the surface penetrates into the pores, since the gases flow in from the deflagration zone, which is situated farther from the surface.

a b

FIGURE 22. Schematic diagram (a) and photograph (b) of jet interaction at the pore inlet.

It was shown in section 8 that hot products penetrating into the pores are cooled, while the pressure, maintained at a constant level prior to burning of the gas in the pores, decreases more intensively the higher the extent of cooling ($T/T_0$) ($T$ is the temperature of the jet flowing into the pores). Thus, in contrast to the first and second cases, the pressure gradient during deflagration of "infusible" substances under constant pressure arises mainly owing to the drop in internal pressure in the pores. At the same time its magnitude may be several orders larger than the dynamic pressure increase (see Figure 18). The resulting gradient is self-sustained at the same level and controls the gas flow throughout burning of the gas.

Consequently, in this case, too, gas penetration is forced, but the pressure gradient is specially produced. Therefore, this penetration mechanism

* The condition of constancy of the external pressure is strictly determined during burning in the atmosphere.



is best termed the jet mechanism (spontaneous) and regarded as a variant of the overall, forced penetration mechanism.

The existence of the jet mechanism is confirmed by the following experimental results. It was found that the factors facilitating the formation of an instability during deflagration are: a) artificial formation of a groove at the pore inlet /10/ and increase in the angle between the colliding jets /61/; b) increase in temperature of the penetrating gases. Only by the jet mechanism can the impairment of burning stability at a decreasing external pressure (observed by Bobolev et al. /61/) be explained.

Spontaneous penetration of burning will be examined in detail later (section 16). We mention only that the range of its action is limited, since the jet mechanism cannot ensure high pressure gradients. The given mechanism is essential when low-density samples burn at constant external pressure ($p_0$ = const) and when $p_p^* = p_0$.

### A. FORCED PENETRATION OF BURNING INTO PORES

The onset of filtration instabilities is mostly determined by the flow pattern of the combustion products along the pores. Let us therefore consider some problems of gas filtration as applied to typical specific ignition conditions. It is thus possible not only to establish the flow pattern, but also to sometimes conduct quantitative estimates. The role of the melt, formed during burning of fusing explosives, will be considered in section 15.

## 13. GAS FILTRATION

Let us consider gas filtration as applied to the conditions governing the "built-in charge" /10/. In the general case we must treat nonsteady and nonisothermal filtration of gas into a porous medium, which is very difficult since the flow is described by nonlinear equation (6).

We introduce the following simplifying assumptions. The filtration will be assumed isothermal and one-dimensional (in the direction of the $x$-axis). The initial pressure in the pores is neglected.

A very strong assumption is the hypothesis that the process is isothermal. On the other hand, it is physically justified in two limiting cases of combustion: 1) when the effective heat-transfer path of the gas $L_{cool} \ll L$ ($L$ is the length of the charge), i.e., when the gas is cooled in a narrow surface layer; 2) when $L_{cool} > L$, i.e., the temperature of the filtering gas is practically constant. Neglect of the initial pressure $p_p^*$ in the pores is justified for the very interesting case of burning of low-porosity charges, the impairment of the stability of which is observed at high pressures $p_0$ (tens or hundreds of atmospheres), and consequently $p_0 \gg p_p^*$.* The problem is formulated as follows (Figure 23). We are given an interface ($x = 0$)

* Impairment of the stability of deflagration of charges with low density, close to the bulk density, takes place, as a rule, in the presence of small pressure gradients: $\Delta p \ll p_0$. In this case the gas flow is described by heat conduction equation (8').

to one side of which ($x < 0$) is gas with viscosity $\mu$ and at constant pressure $p_0$, and to the other side of which ($x > 0$) is an undeformed porous medium with given gas permeability $k$, porosity $m$, and initial pore pressure $p_p^* = 0$. Nonsteady (at $t > 0$) laminar flow of the gas is examined in an undeformed porous medium, which satisfies the Boussinesq equation (7).

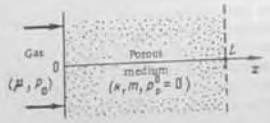


FIGURE 23. Calculation of gas filtration during burning of a "built-in charge."

**Filtration into an unbounded porous medium**

On the basis of the above assumptions we have

$$\frac{\partial p}{\partial t} = C^2 \frac{\partial^2 p^2}{\partial x^2}, \tag{19}$$

$$p(x, 0) = 0, \tag{19a}$$

$$p(0, t) = p_0. \tag{19b}$$

A similarly formulated problem was solved by Barenblatt /77/, who obtained analytical expressions for the coordinate of the leading edge of the gas $X(t)$ and for the pressure distribution $p(x, t) = p_0\varphi(\xi)$, where $\xi = \frac{x}{C\sqrt{p_0 t}}$ is the self-similarity parameter. Function $\varphi(\xi)$ for approximate calculations can be expressed in the form $\varphi(\xi) = 1 - \xi/\xi'$, where $\xi'$ is a constant equal to 2.29 for given initial (19a) and boundary (19b) conditions. Hence, approximately,

$$p(x, t) = p_0\left(1 - \frac{x}{\xi' C\sqrt{p_0 t}}\right), \tag{20'}$$

i.e., we may assume that the pressure drops linearly.

The gas penetration depth is determined by the coordinate of the leading edge:

$$X(t) = \xi'\sqrt{\frac{kp_0 t}{2m\mu}} = 1.62\sqrt{\frac{kp_0 t}{m\mu}}, \tag{20}$$

while the velocity of the front motion is

$$U_x(t) = 0.81\sqrt{\frac{kp_0}{m\mu t}}. \tag{21}$$



Expression (20) can be employed in order to obtain in explicit form the condition governing impairment of the stability of burning. If, during the time of combustion of the heated layer $\tau = \varkappa/u^2$, the gas penetrates to a depth exceeding the thickness of the heated layer $\varkappa/u$, the condition that must be satisfied is

$$X(\tau) > \varkappa/u, \tag{22}$$

where $\varkappa$ is the thermal diffusivity of the explosive and $u$ is the velocity of layer-by-layer deflagration.

Hence relationships (20) and (22) imply that the required condition is satisfied if

$$\frac{kp_0}{m\mu\varkappa} > 0.38. \tag{23}$$

Substitution into (23) of the characteristic values $p_0 = 50$ atm, $\mu = 3 \cdot 10^{-4}$ poise, $\varkappa = 10^{-3}$ cm$^2$/sec, $k = 10^{-5}$ darcy $\simeq 10^{-16}$ cm$^2$ and $m = 0.05$ proves convincingly that the required condition governing impairment of the stability is clearly satisfied for samples with very low permeabilities. We shall return later to this very important result, which is confirmed by experiment for "infusible" explosives.

**Filtration into a bounded porous medium**

In this case we must construct a supplementary condition on the gas-impermeable boundary (at $x = L$):

$$\left.\frac{\partial p}{\partial x}\right|_{x=L} = 0, \tag{19c}$$

and rewrite the initial condition in the form

$$p(x, t') = 0, \tag{19d}$$

where $t'$ is the time taken for the leading edge of the gas to reach the impermeable boundary.

This problem is solved by expressing pressure $p(x, t)$ as the trinomial

$$p(x, t) = \bar{a} + \bar{b}x + \bar{c}x^2, \tag{24'}$$

where $\bar{a}$, $\bar{b}$ and $\bar{c}$ are functions of time defined so that $p(x, t)$ in form (24') satisfies the integral equation of nonsteady filtration

$$\int_0^L \frac{\partial p}{\partial t}\,dx = C^2 \int_0^L \frac{\partial^2 p^2}{\partial x^2}\,dx,$$

subject to initial (19d) and boundary (19b and 19c) conditions.

Omitting the computation details, the final solution can be written as

$$p(x, t) = p_0 - \frac{p_0}{L^2} \exp\left[-\frac{3kp_0}{m\mu L^2}(t - t')\right] \cdot (2Lx - x^2). \qquad (24)$$

When $t < t'$ the pressure distribution is described by (20') according to /77/, and when $t > t'$ by expression (24) (Figure 24).

The pressure change at the gas-impermeable boundary ( $x = L$ ) is found from

$$p(L, t) = p_0\left(1 - \exp\left[-\frac{3kp_0}{m\mu L^2}(t - t')\right]\right). \qquad (25)$$

Thus, as the leading edge of the gas reaches the impermeable boundary the pressure on it increases in accordance with (25), while the pressure gradient $\partial p/\partial x$ and, consequently, the inflow rate of the gas in the sample decrease. It is evident from (25) that with increasing permeability $k$ and decreasing sample length, the rate at which the pressure in the sample pores becomes equal to the external pressure increases.

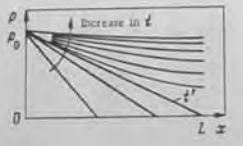


FIGURE 24. Pressure distribution in time and length when gas flows into a porous charge with an impermeable bottom.

The time $t_{r.p.}$ during which the relative pressure at the closed end $p_0'/(p_0 - p)$ increases by a factor of $e$ will be termed the characteristic equalization (relaxation) time. Hence equation (25) yields

$$t_{r.p.} = t - t' = \frac{m\mu L^2}{3kp_0}. \qquad (26)$$

Thus, the presence of a closed end stabilizes the flow and may increase the burning stability, if the pressure relaxation takes place prior to ignition in the pores.

The correctness of the calculations was checked with the aid of special tests in which we determined the time at which the leading edge of the gas reached the closed end of the charge during stable burning. Charges consisting of a mixture of 10% polystyrene + 90% ammonium perchlorate, the burning surface of which is permeable, were ignited in a special bomb by an igniter which produced pressure $p_0 < p_0$ during a short time (5 msec); this pressure was maintained constant during burning. Two piezoelectric probes were used, one of which recorded the pressure in the bulk of the bomb and the other in the pores of the hot charge near the closed end. The time $t'$ was determined from the beginning of the collapse of the probe. Values of $t'$ (sec) obtained at pressure $p_0 = 25$ atm are listed below for samples of porosity $m = 0.15$ and a permeability $k = 10^{-3}$ darcy.

| Charge length, cm | Calculation by equation (20) | Experiment |
|---|---|---|
| 1 | 0.07 | 0.05 |
| 2 | 0.28 | 0.24 |



Satisfactory agreement between $t_{calc}$ and $t_{exp}$ shows that the assumptions introduced in the calculation were justified.

The above comments refer to conditions under which the external pressure $p_0$ unexpectedly increased over the porous charge but did not change with time.

Filtration under burning conditions subject to increasing pressure. This problem was solved by Barenblatt /77/ in a formulation similar to that employed in the problem about filtration into a medium without boundaries but with boundary conditions of the type $p(0, t) = p_0 t^n$ $(n > 1)$. Consider the simpler case, when filtration takes place into a confined medium while the pressure in the pores remains below the variation in external pressure. The latter requirement is satisfied if the characteristic time of pressure relaxation in the pores $t_{r.p.}$ is much smaller than the relaxation time of the external pressure, i.e., when $t_{r.p.} < t_{r.e.}$, where $t_{r.e.} = \frac{p}{dp/dt}$. In this case filtration may be considered as quasi-steady, and the expression

$$V_g = \frac{L}{p}\frac{dp}{dt}\frac{T_g}{T_0} \qquad (27)$$

can be used /61/ to calculate the velocity of the inflowing gas, where $T_g$ is the filtering gas temperature, $T_0$ is the initial temperature of the porous medium, and $dp/dt$ is the rate of change of the external pressure. Equation (27) was derived from the equation of mass conservation and is valid when $dp/dt < 3kp^2/m\mu L^2$.

Let us estimate the limits for which the latter inequality is satisfied. We assume that when $k = 10^{-3}$ darcy, $m = 0.15$ ( $d_p' = \sqrt{\frac{\Sigma_p}{m}} \simeq 0.5\ \mu$ ), $p = 50$ atm and $L = 5$ cm; the limiting rate of change in external pressure $dp/dt < 50$ atm/sec. Thus, the assumption about the quasi-steady nature of the filtration is satisfied over a fairly wide range of parameters. The quasi-steady approach is justified when the gas flows into pores which are not excessively wide and whose bottom is impermeable.

Having treated the conditions of gas inflow into pores, we now turn our attention to the aftereffects of the penetration of combustion products.

## 14. CONDITIONS OF PORE WALL IGNITION

It was determined experimentally that the most typical result of the thermal effect of inflowing hot gases is ignition of the pore walls /10, 12/. The ignition conditions were investigated theoretically by Margolin and Chuiko /70/.

Their data /70/ enable us to consider the simplified problem concerning heating of the walls of pores of constant cross section (hydraulic diameter $d_p$) by a gas flow moving at velocity $V_g$ relative to the pore walls and possessing initial temperature $T_g$, specific heat $c_g$, thermal conductivity coefficient $\lambda_g$, and density $\rho_g$. In a coordinate system linked to the burning surface of the charge, the gas flows into the pores with velocity ( $V_g - u$ )

where $u$ is the linear burning velocity of the explosive. The inflowing gas gradually cools and its temperature drops with $T_g$ until it attains the wall temperature $T_0$. To a first approximation it is assumed that the gas temperature does not vary smoothly but jumpwise: at some section $L_{cool}$ from the inlet it is $T_g$, and then $T_0$. It is further assumed that the wall temperature at the section $L_{cool}$ is constant and equal to $T$. The heat balance equation then assumes the form

$$(V_g - u)\, c_g \rho_g (T_g - T)\, \frac{d_p^2}{4} = \frac{\mathrm{Nu}\, \lambda_g}{d_p} (T_g - T)\, L_{cool} d_p. \qquad (28)$$

where Nu is the Nusselt number of the gas entering the pores.

Equation (28) determines the distance $L_{cool}$ over which the gas releases heat:

$$L_{cool} = \frac{(V_g - u)\, d_p^2}{4\,\mathrm{Nu}\, \varkappa_g}; \quad \varkappa_g = \frac{\lambda_g}{\rho_g c_g}. \qquad (29)$$

The values of $V_g$ and Nu are measured or calculated (section 13) starting from the gas inflow regime. According to Kutateladze /113/, in the case of laminar flow when $\frac{x}{d_p} \frac{1}{\mathrm{Re}\, \mathrm{Pr}} > 0.1$ the Nusselt number can be regarded as constant (here, $x$ is the distance from the gas inlet into the pores; Re and Pr are the Reynolds and Prandtl numbers, respectively): Nu = 3.66. It follows from (29) that, with small pore diameters, the depth over which the gas flowing into the pores is cooled is very small.* For example, at $V_g = -1$ m/sec and atmospheric pressure, $L_{cool}$ assumes the following values:

$$L_{cool}(d_p = 1\,\mathrm{cm}) \simeq 30\,\mathrm{cm}; \quad L_{cool}(d_p = 100\ \mu) \simeq 30\ \mu;$$
$$L_{cool}(d_p = 10\ \mu) \simeq 0.3\ \mu.$$

The pore walls are heated during time $\tau_0$, given by

$$\tau_0 = L_{cool}/u. \qquad (30)$$

The time $\tau_1$ until temperature $T'$ is attained on the surface is obtained by constructing the heat balance equation at the pore walls:

$$\frac{\mathrm{Nu}\, \lambda_g}{d_p} L_{cool} d_p (T_g - T')\, \tau_1 = (T' - T_0)\, \rho_s c_s L_{cool} (d_p \sqrt{\varkappa_s \tau_1} + \alpha \varkappa_s \tau_1) \qquad (31)$$

($\alpha = 0$ for slitlike pores and $\alpha = 1$ for circular pores). Subscript "s" refers to the solid phase. It is here assumed that the penetration depth of the heated layer $l = \sqrt{\varkappa_s \tau}$ is constant on the whole section $L_{cool}$.

Hence equation (31) yields

$$\tau_1 = \frac{d_p^2}{\varkappa_s} \left( \frac{\beta}{\mathrm{Nu} - \alpha\beta} \right)^2, \quad \beta = \frac{\lambda_g}{\lambda_s} \frac{T' - T_0}{T_g - T'}. \qquad (32)$$

* The depth of cooling may increase considerably, if heat is evolved in the condensed phase during deflagration.



The time $\tau_2$ during which a thermal layer $l_0 = \varkappa_s/u$ forms and corresponding to steady-state deflagration conditions is

$$\tau_2 = l_0/u = \varkappa_s/u^2. \qquad (33)$$

If relationship (30) is combined with the expression $l_0 = \sqrt{\varkappa_s \tau_0}$, we obtain the equation

$$l^2 = L_{cool} l_0. \qquad (34)$$

According to the theory developed by Zel'dovich /43/ (who disregards the reaction in the condensed phase), ignition of propellant powder includes: 1) creation in the condensed phase of a sufficiently deep, heated layer; 2) heating to surface temperature $T'$, at which intensive gasification of the powder begins; 3) ignition of the gasification products. Zel'dovich proved that the heat required for ignition of the gasification products is much less than the heat necessary for heating the powder.

In accordance with this theory /43/, the following inequalities must be fulfilled:

$$l/l_0 > 1, \qquad (35)$$
$$\theta_0 = \tau_0/\tau_1 > 1. \qquad (36)$$

Comparison of (35) and (36) indicates that (35) is equivalent to the following:

$$L_0 = L_{cool}/l_0 > 1 \quad \text{or} \quad \tau_0/\tau_2 > 1, \qquad (35')$$

i.e., the requirement of a sufficient thickness of the thermal layer is the same as the condition that the effective heat transfer path of the gases $L_{cool}$ exceeds the thickness of the thermal layer $l_0$.

Substitution of equations (30), (32) and (33) into (35) and (35') yields the ignition conditions in the form

$$L_0 = \left( \frac{l}{l_0} \right)^2 = \frac{L_{cool}}{l_0} = \frac{(V_g - u)\, u d_p^2}{4\,\mathrm{Nu}\, \varkappa_g \varkappa_s} > 1, \qquad (37)$$

$$\theta_0 = \frac{(V_g - u)\,\mathrm{Nu}}{4u} \frac{(\rho c \lambda)_g}{(\rho c \lambda)_s} \left( \frac{T_g - T'}{T' - T_0} \right)^2 \left( 1 - \frac{\alpha\beta}{\mathrm{Nu}} \right)^2 > 1. \qquad (38)$$

The ignition temperature $T'$ depends on chemical kinetics, the thermophysical characteristics of the substance, its initial temperature, and the heat transfer conditions. It can be seen from (37) and (38) how the fundamental characteristics of the deflagration of inflowing gas and of the explosive affect the ignition conditions. In particular, ignition is only possible when $V_g - u$ is greater than zero.

Interesting qualitative results follow from the above discussion. Their physical sense corresponds to experimental observations and, in principle, these results may be derived independently from general considerations. The resulting data become very clear, if they are represented graphically (Figure 25). The ignition conditions (37) and (38) are represented in gas pressure $p$ – pore diameter $d_p$ coordinates by curves 1 and 2, respectively.

Inequalities (37) and (38) are satisfied above these curves. In this case the coordinate plane is divided into the following characteristic regions, each of which corresponds to a certain thermal regime.

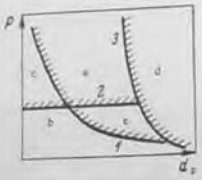


FIGURE 25. Dependence of pressure $p$ of pore-wall ignition by inflowing gas on pore diameter $d_p$.

Stable layer-by-layer deflagration occurs at low pressures and not too wide pores (region b); however, no gases penetrate since not one of inequalities (37) and (38) is satisfied. Region b covers the case of stable burning during the stage preceding the impairment of stability.

Pores of medium size are ignited on increasing the pressure (region a); this situation is characteristic for impairing the stability of the thermal conditions. Both inequalities are satisfied in this case.

In region c (high pressures and narrow pores) forced burning occurs (pyrolysis of the explosive), in which case condition (37) governing the formation of a sufficiently thick heated layer is not satisfied.

Condition (38) is not satisfied in region e: long-term heating of the explosives takes place. It may be assumed that the given region corresponds to thermal explosion (flashes) of the explosive heated to a sufficient depth.

Finally, region d (to the right of curve 3) corresponds to turbulent burning of the half-combusted gaseous products which, under certain conditions, may fill the wide pores of the burning charge. The conditions were obtained under which deflagration propagating over the half-combusted gaseous products may ignite the pore walls /70/. In conclusion, we note that rigorous quantitative calculation of the ignition conditions involves considerable difficulties.

## 15. EXPERIMENTAL STUDY OF THE IMPAIRMENT OF STABLE BURNING

The experimental investigations were carried out mainly by the increasing-pressure method. Porous samples were ignited in manometric bombs (see Figure 3) with continuous recording of the pressure in the bulk of the bomb by piezoquartz /10, 11/ or tensometric /64/ pressure probes. The process was also recorded optically through transparent windows in the bomb /10, 63/. Special experiments were conducted to record the pressure in the pores of the hot charge.

The lateral surface and the lower end of the charge were cased. The upper end was ignited by a wire, heated by an electric current or an igniter, so producing a small pressure increase leading to a further pressure increase in the bulk of the bomb owing to deflagration of the porous charge. It should be emphasized that reliable data can only be obtained with this setup if the igniter does not give rise to perturbations. In particular, the



pressure produced by the igniter must be much lower than the critical pressure. The igniter must ensure stable and simultaneous ignition of the charge over the whole surface with a minimum delay. We used as igniter finely ground gunpowder, pyroxylin, and a pyroxylin-ammonium perchlorate mixture.

Figure 26 shows a typical $p(t)$ plot obtained in the bulk of the bomb, and also an optical record, during impairment of stable layer-by-layer deflagration of the porous charge. As long as stable burning lasted, we observed a smooth pressure increase, and the burning rate of the charge was close to the burning rate determined in the Crawford bomb. The sharp increase in pressure and velocity (inflection on the curve) indicated that critical conditions were reached, that stable burning in parallel layers was impaired, and that burning broke through into the pores. Impairment of stable burning may be characterized by critical values of the pressure in the bulk, of the burning velocity, or of the permeability. The main characteristic used was the critical pressure $p_*$ at which stable burning collapsed, which is preferable under increasing-pressure conditions and for the "built-in charge" system. Naturally, under forced penetration the pressure alone determines the rate of gas flow (see equation (21)) and, consequently, the final inflow effect. The extent of burning and the temperature distribution in the gas phase are also pressure-dependent. The critical pressure is determined directly from the $p(t)$ oscillogram. However, optical measurements of the critical burning velocity cannot always be obtained, especially when high-pressure manometric bombs are employed.


FIGURE 26. Optical oscillogram (a) and $p(t)$ recording (b) during impairment of stable deflagration in a manometric bomb.

Impairment of stable deflagration of "fusible" secondary explosives is usually accompanied by a sharp break in the $p(t)$ curve, from which we also determined the collapse pressure. During long-term stable burning and also for some "infusible" explosives, the appearance of an instability takes the

form of a smooth increase in pressure and burning velocity, and for this reason there is no sharp break on the $p(t)$ plots. The critical pressure was determined from these oscillograms. The data were presented in order to facilitate processing in log $p - t$ coordinates, or they were compared with records of the stable burning of a solid (reference) charge.

This simple variant of the manometric bomb method with continuous pressure recording $p(t)$ made it possible to investigate and compare the burning stability of various groups of explosives and propellant powders.

### Effect of porosity and gas permeability

Impairment of the burning stability of very porous ($m > 0.15$) explosive charges was studied elsewhere /11, 32, 62–69/. The main attention of Belyaev et al. /10, 60/ was devoted to the appearance of instability in samples with low porosity ($m = 0.15$–$0.03$) and permeability ($k = 10^{-3}$–$10^{-6}$ darcy) for the following reasons. For porosity $m < 0.15$, charge deformation during layer-by-layer deflagration can be neglected, since stability is impaired at pressures far below those at which the samples were pressed. Moreover, the results correspond to impairment in the stability of burning of unrestricted charges, when the cased lower end displays no effect. Finally, it will be clear from our further comments that at lower porosities its effect on the stability of physicochemical properties of the explosives will be especially strong.

Let us now consider the results of Belyaev et al. /10, 60/. Porous samples (diameter 5 and 10 mm, length 40–70 mm) were used. The initial particle size was mainly between 5 and 20 $\mu$. The charging density was constant (50 kg/m$^3$). The rate at which the pressure changed for layer-by-layer deflagration was $dp/dt = 0.1$–$10$ atm/msec.

The burning stability was shown to be independent of the length of the section of layer-by-layer deflagration, but uniquely determined by the critical collapse pressure. The experimental data are therefore expressed in the form of collapse pressure as functions of the main parameters of the charge.

Figures 27 and 28 present the critical pressure as a function of porosity for secondary explosives and mixed composition (stoichiometric ratio of the components). The points on the curves denote the average values of 3 or 4 measurements. Burning is stable in the pressure region below the curve, and unstable above it.

Listed below are the main results, which follow from the data obtained.

1. Stability of burning of secondary explosives (TNT, DINA, picric acid, PETN) over the whole porosity interval under investigation is impaired at pressures much higher than in the case of pyroxylin, and mixed compositions based on potassium and ammonium perchlorates.

2. Burning of compositions based on ammonium perchlorate is stable at pressures of 100–200 atm, if the sample porosity does not exceed 0.05.

3. Similar critical pressures were obtained for the investigated mixed compositions with various fuels (polystyrene, bitumen, TNT) at the same porosity. This result indicates that impairment of the stability of such a system is determined mainly by the properties of the oxidizer.



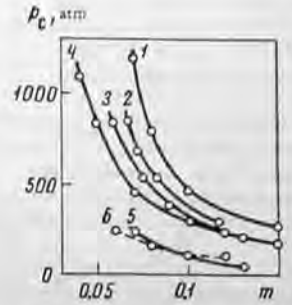


FIGURE 27. Critical pressure of collapse as a function of porosity for secondary explosives ($d_{charge}$ = 10 mm, r = 5–20 $\mu$):

1) TNT; 2) picric acid; 3) DINA; 4) PETN; 5) hexogen; 6) pyroxylin No. 1.

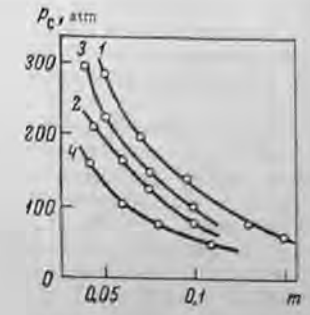


FIGURE 28. Critical pressure of collapse as a function of porosity for mixed explosives ($d_{charge}$ = 10 mm, r = 5–20 $\mu$):

1) bitumen + $KClO_4$; 2) polystyrene + $KClO_4$; 3) TNT + $NH_4ClO_4$; 4) bitumen + $NH_4ClO_4$.

4. The critical pressure increases with decreasing porosity; $p_c(m)$ is best described by the hyperbolic function

$$p_c(m - b) = a, \tag{39}$$

where $a$ and $b$ are constants, the values of which are tabulated below.

| | a | b |
|---|---|---|
| TNT | 24 | 0.05 |
| Picric acid | 15 | 0.05 |
| PETN | 20 | 0.025 |
| Mixed compositions | 5–7 | 0.025 |

The value of constant $a$ is determined by the physicochemical properties of the substance and experimental conditions. Constant $b$ approximately characterizes the closed (gas-impermeable) porosity. This follows by comparing the above data with the dependence of gas permeability on porosity (see Figure 12): the sample permeability is very small (about $10^{-6}$ darcy) at porosities $m = 0.03$–$0.05$. According to (39), stable burning should be maintained up to high pressures at porosity $m \leqslant b$, as confirmed by direct experiment. Stable burning of PETN samples and mixed compositions with porosity $m = 0.02$–$0.03$ was observed up to the maximum pressure (3000–4000 atm) used in our tests /23/. An insignificant increase in porosity to 0.05 leads to instability (see Figure 28). Thus, transition from stable deflagration to unstable burning proceeds very sharply over the given range of porosities.

Consider now the effect of gas permeability, since this parameter determines the possibility of filtration of combustion products into the pores. The corresponding data are shown in Figure 29; the dependence of permeability on porosity was determined by a method described earlier (section 5).

It is noteworthy that differences in the burning stability of the investigated explosives are most apparent at small permeabilities ($k \sim 10^{-5}$ darcy). As the permeability (porosity), and hence the pore size, increases, the differences in critical pressure decrease. This indicates that the role of the physicochemical properties as a factor influencing stability is very important, especially for small pore sizes.

The burning stability of mixed explosives with small permeability ($k = 10^{-5}$ darcy) is impaired at low pressures ($p_c = 100$–$200$ atm), which is in qualitative agreement with the above computation results (see p. 51). No such agreement exists for secondary explosives. Note that the burning stability of the powerful explosive PETN is much higher than the stability of mixed explosives. Furthermore, the effect of the collapse pressure on gas permeability differs considerably. For mixed explosives it is comparatively weak and has the form

$$k \exp(p_c/F) = G, \qquad (40)$$

where constants $G$ and $F$ depend weakly on the nature of the fuel. In secondary explosives we observe, as a rule, a stronger and more complex dependence of the collapse pressure on permeability. These special features in the behavior of the observed systems are due to differences in the mechanism of their deflagration, mainly in the physical state of the burning surface.

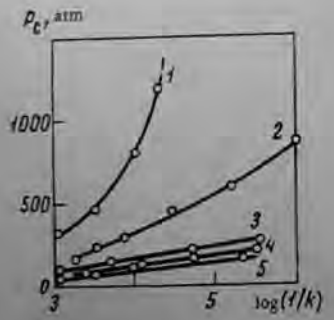


FIGURE 29. Critical pressure of collapse as a function of the logarithm of the reciprocal gas permeability ($d_{charge}$ = = 10 mm, $r$ = 5–20 μ):

1) TNT; 2) PETN; 3) bitumen + $KClO_4$; 4) TNT + $NH_4ClO_4$; 5) bitumen + $NH_4ClO_4$.

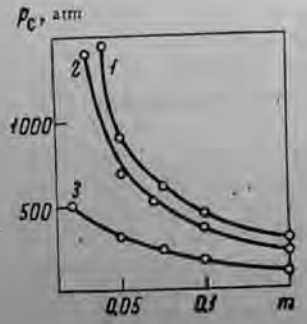


FIGURE 30. Critical pressure of collapse as a function of porosity for PETN with various initial particle sizes ($d_{charge}$ = 5 mm):

1) $r$ = 5–20 μ; 2) $r$ = 120 μ; 3) $r$ = = 500 μ.



The above data were obtained for systems which were pressed from particles of the same size ($r \simeq 5$–$20\ \mu$).

We now examine the effect of the initial particle size of an explosive (PETN) on the impairment of deflagration. The dependence of the collapse pressure on porosity and permeability for PETN samples with various initial pore sizes is shown in Figures 30 and 31 (the data of Figure 13 were used to plot the $p_c$ (log $1/k$) curve), which indicate that an increase in particle size at constant sample porosity or permeability leads to a considerable decrease in the collapse pressure. This result shows that neither porosity nor permeability uniquely determine the stability of deflagration. In addition to gas permeability, the pore size distribution (or, more correctly, the presence of large pores) affects the impairment of stable burning.

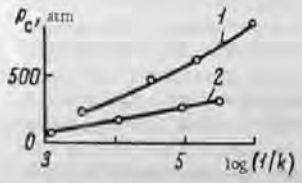


FIGURE 31. Critical pressure of collapse as a function of the logarithm of the reciprocal gas permeability of PETN ($d_{charge}$ = 10 mm):

1) $r$ = 5–10 μ; 2) $r$ = 500 μ.

### Stability series

Our studies were carried out under identical conditions and permit the classification of individual explosives by their degree of stability. The burning stabilities of samples with a gas permeability of $10^{-5}$ darcy were compared for identical initial particle size, geometrical charge dimensions and ignition conditions. The results are summarized below for permeability $k = 10^{-5}$ darcy, initial particle size $r$ = 5–20 μ, charge length $L$ = 40–70 mm, charge diameter $d_{charge}$ = 10 mm, and charging density equal to 0.05 g/cm³; the collapse pressure is in atmospheres.

| | | | |
|---|---|---|---|
| Secondary fusible explosives | | Infusible substances | |
| TNT | 2000 | pyroxylin | 200 |
| picric acid | 800 | ammonium perchlorate-based compositions | 100–175 |
| PETN | 550 | Initiators | |
| hexogen | 250 | mercury fulminate | 100 |
| | | lead azide + 2% paraffin | detonates at any pressure |

(Sample porosity $m$ = 0.06–0.07 corresponds to crystalline and ammonium perchlorate explosives with particle size 5–20 μ and gas permeability $k = 10^{-5}$ darcy.)

Secondary explosives are the most stable, while initiators are the least stable. Changes in the properties of a substance in the stability series are governed by a strictly determined pattern: the tendency to fuse decreases, while the role of reactions in the condensed phase becomes larger.

The majority of secondary explosives tend to fuse during deflagration without any considerable decomposition in the condensed phase. A study of the burning surface of extinguished porous samples and the simultaneous record of the pressure in the bulk and in the pores of the hot charge showed that the high burning stability of very dense secondary explosives (TNT, picric acid, DINA, PETN) is due to the existence of a continuous fused layer on the hot surface /10, 59, 60/.* During stable burning, when the pressure is subcritical, the fused layer functions as a gas-impermeable partition and prevents filtration of gaseous products into the pores: the pressure in the pores remains practically equal to the atmospheric pressure right to the end of deflagration, i.e., until the deflagration front approaches the probe at the end of the charge. The continuous melt is broken at near-critical pressure. Under these conditions the penetrating gases are cooled intensively owing to heat taken up for fusing and vaporization of the substance, and this, too, stabilizes burning.

To a first approximation, it can be assumed that the burning of fusible explosives is stable, as long as the fused layer remains continuous. The continuity condition of the fused layer implies that its thickness $x$ should be no less than the maximum pore size:

$$x \geqslant d_{p\,max}. \tag{41}$$

Interesting results follow from this expression. First, we see that the calculated thickness of the fused layer corresponds to the experimentally determined stability series of secondary explosives.

The thickness of the fused layer can be calculated by the formula

$$x = \frac{\lambda}{up\bar{c}} \ln \frac{T_x - T_0}{T_{melt} - T_0}, \tag{42}$$

where $u\,p$ is the mass velocity of burning; $\lambda$ is the thermal conductivity of the melt; $c$ is the specific heat; $T_x$ is the critical temperature; $T_{melt}$ is the melting point; $T_0$ is the initial temperature.

Published /78–80/ values of the quantities entering equation (42) show that at a pressure of 100 atm the thicknesses of the fused layer for TNT, picric acid, PETN and hexogen are 30, 35, 13 and 5 $\mu$, respectively, while at 300 atm they are 18, 12, 3 and 2 $\mu$. The fact that the above explosives appear in the same sequence as in the stability series again confirms that our concepts are correct.

Moreover, equation (41) allows one to estimate the maximum pore size. For instance, in the case of TNT with porosity $m = 0.15$ the collapse pressure is $p_c \simeq 300$ atm. At this pressure the thickness of the fused layer, and hence the maximum pore size, corresponds to $d_{p\max} = 18\,\mu$. It follows from the pore size distribution (see Figure 10) that the directly measured value of the same porosity in TNT samples is similar or equal to 10 $\mu$.

The series of decreasing stabilities to the right of secondary explosives includes substances in the deflagration of which either the fused layer is

* Independently of the authors, Taylor /82/ advanced the hypothesis about the stabilizing effect of the fused layer during burning of fused porous explosives.



not formed at all (pyroxylin, mercury fulminate) or is not continuous (mixtures based on ammonium or potassium perchlorate). During burning, $NH_4ClO_4$ and $KClO_4$ fuse with decomposition at a high temperature. At atmospheric pressure the melting point of ammonium perchlorate is 850°K /54/, whereas for potassium perchlorate it is 883°K /81/.

Instabilities are also caused by exothermal reactions in the condensed phase, which are important during the burning of pyroxylin/50/, compositions based on ammonium perchlorate /48/, and mercury fulminate /5/. The gaseous decomposition products formed in the condensed phase produce dispersion of the substance, permanent destruction of the formed layer, and thus make it impossible to form a continuous fused layer, even if a liquid film is produced. On the other hand, heat release in the condensed phase increases the heat transfer path of combustion products penetrating into the pores and facilitates ignition of the internal pore surface.

The temperature of penetrating products is important in impairment of deflagration, and depends on the combustion temperature of the explosive and the temperature distribution near the surface. Andreev /37/ correctly regarded a high combustion temperature as the cause of an increased tendency to detonate. Our experiments showed that the increase in the burning temperature, achieved by introducing the fuel into pure ammonium perchlorate, led to a decrease in the collapse pressure.

However, the temperature distribution in the gas phase has a decisive effect on the collapse of burning /10/, since, first of all, the gaseous products adjacent to the surface penetrate into the pores. The narrow temperature range, which is characteristic for systems based on ammonium perchlorate /81, 161/, was found to be responsible for the low stability of their burning. Together with the above factors, we see that compositions based on ammonium perchlorate do not differ in their stability from mercury fulminate. A large temperature gradient near the surface ensures ignition of a porous substance by a hot gas and makes possible burning in the narrow pore.

The following fact must be emphasized. During impairment of the burning stability of "infusible" substances according to the forced mechanism, the mass velocity of layer-by-layer burning is not important (unlike during impairment by the spontaneous mechanism, see sections 12, 16). Thus, at similar stabilities, the mass burning velocity of mercury fulminate is one order higher than the corresponding velocities of the perchlorate compositions.

The above comments clearly imply that the stability of burning is closely related to the burning mechanism and depends on the set of physicochemical properties.

Let us determine the critical pore size (diameter) $d_{cr}$ at which penetration of burning into the pore is observed. For this purpose we employ the condition of stabilization of burning by the fused layer: $d_{cr} = x$. When $d_{cr} > x$ burning penetrates into the pores, while when $d_{cr} < x$ this does not happen. For instance, the collapse pressure in the case of PETN is 300 atm at charge porosity $m \simeq 0.1$. At the given pressure, the size of the fused layer and, consequently, the critical pore diameter corresponds to $d_{cr} = 3$.*

* Let us compare the obtained value of $d_{cr}$ with the mean hydraulic diameter of the pores. The investigated porous medium will be described by the ideal soil model. In accordance with Ch. I, for PETN at critical porosity $m = 0.1$ and gas permeability $k = 1.5 \cdot 10^{-4}$ darcy, we have $d_p \simeq 0.2\,\mu$, which is one order of magnitude smaller than $d_{cr}$. This difference arises because impairment of layer-by-layer deflagration begins in the largest (not the average-size) pores of the charge: $d_{cr} = d_{p\max}$.

The critical pore diameter decreases with increasing pressure and burning velocity. Allowance for the fact that $d_{cr} = x - 1/u$ and $u \sim p$ for fusible explosives yields

$$d_{cr} \sim 1/u \sim 1/p,$$

whence $ud_{cr} = \text{const}$, or $pd_{cr} = \text{const}$. These relationships are approximately satisfied for fusible explosives.

The relationship $pd_{cr} = \text{const}$ also holds in the deflagration of porous systems which do not form a solid fused layer. However, in this case the value of the constant is much lower. This means that penetration of burning into identical-size pores of infusible explosives takes place at lower pressures. If for PETN burning penetrates into 3-$\mu$ pores at a pressure of 300 atm, it does so when $p_c < 100$ atm for pores of similar dimensions.

The burning stability of low-density explosive charges was studied elsewhere /64–68/. The following substances were investigated: TNT, xylyl, picric acid, trinitrobenzene, hexanitrodiphenol, tetryl, octagen, PETN, mercury fulminate. A very dense ($\delta = 0.95$–$0.97$) charge was used as reference. Experimental data were represented as pressure in the bulk vs. time, $p(t)$ curves. The fundamental parameter was the critical density. It was found that for a relative density $\delta = 0.7$ ($r = 50$–$100\ \mu$) the burning stability of all the studied explosives is impaired at a pressure not exceeding 50 atm. The pressure produced by the igniter that ignited the charge was 50 or 100 atm, i.e., it was close to, or exceeded, the critical value. Therefore, these data are interesting from the viewpoint of burning beyond the stability limit. These results, which correspond to burning of high-density charges and which give an idea about the relative burning stability of various explosives, are more or less in agreement with the above explanation.

The effect of a flegmatizer. Bobolev et al. /63/ studied the burning stability of a hexogen-paraffin mixture. The particle size of the hexogen was 200 $\mu$. The results are illustrated in Figure 32, from which it follows that the introduction of 10% paraffin does not affect the collapse pressure. Tests with larger flegmatizer amounts were not carried out. We are of the opinion that the main effect of introducing a flegmatizer is to considerably change the pattern of the process development after impairment of deflagration and to eliminate detonations arising in pure explosives.


FIGURE 32. Impairment of stable burning of a hexogen ($r = 200\ \mu$) + paraffin mixture.

1) pure hexogen; 2) hexogen + 10% paraffin.

## Role of the geometrical dimensions of a charge

Belyaev /10/ et al. studied the effect of the charge diameter $d_{charge}$ and length $L$. Charges with a gas-impermeable bottom were investigated.

Experiment has shown that in a manometric bomb, the burning stability of samples with gas permeability $k < 10^{-3}$ darcy (used by Belyaev et al. /10/) is practically independent of the length of the layer-by-layer burning section preceding the appearance of convective burning. Burning stability is determined by the collapse pressure (at the instant the critical pressure is reached, the length of the remaining charge was 15–20 mm, as a rule). This result indicates that, for a sufficient length, the presence of an impermeable boundary at the lower end does not affect the filtration process of the products and the collapse of deflagration.

Thus, the data of Belyaev et al. /10, 60/ correspond to the impairment of layer-by-layer deflagration of unbounded porous charges. It must be emphasized that under these conditions the collapse pressures determined in a manometric bomb and by the "built-in charge" method are in agreement.

On the other hand, ignition of the filtering gas at the lower end of the charge, so leading to equalization of the pressure in the pores and decrease in the filtration rate, may stabilize burning. Stabilization occurs, if combustion products penetrating along the charge are unable to ignite the inner surface of the pores.

Theoretical analysis indicates (section 13) that the effect of the impermeable boundary increases with decreasing charge length and increasing permeability. The stabilizing effect of the closed end was studied by conducting experiments with the aid of a "built-in charge" (see Figure 2) in which low-density charges ($m > 0.2$, $k > 10^{-3}$ darcy) of various lengths were ignited.

The experiments were carried out with a mixed system (based on ammonium perchlorate) at constant pressure $p_0$, which was higher than the critical pressure $p_c$ determined for the given charge. The results are presented schematically on Figure 33 (charge length $L$ was plotted on the abscissa axis and the delta function $\Delta'$ on the ordinate axis; burning is stable when $\Delta' = 0$ and unstable when $\Delta' = 1$). There exists a threshold value of the charge length ($L'$) below which layer-by-layer burning was stable and its mass velocity close to the velocity of the nonporous sample. Convective burning conditions arise on increasing the charge length ($L > L'$). A similar effect was observed by Andreev and Gorbunov /64/.

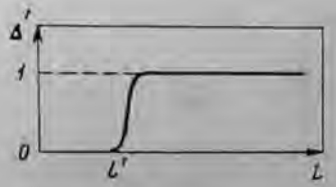


FIGURE 33. Effect of charge length on impairment of stable burning.

Transition from stable to unstable burning was observed over a narrow range of charge lengths. In the transition region, convective burning beginning at a low velocity was usually decelerated and replaced by layer-by-layer deflagration (Figure 34 shows the $p(t)$ curve and the oscillogram obtained in a single experiment with identical recorder sweep rates).

Thus the existence of a threshold charge length $L'$ when $p_0 > p_c$ is due to very rapid pressure equalization in the pores. For instance, for a charge with $m = 0.3$, $k = 10^{-2}$ darcy, length $L = 0.3$ cm at pressure $p_0 = 50$ atm, the characteristic relaxation time of the pressure in the pores in accordance with (26) is very small and given by $t_{rel} \simeq 0.5 \cdot 10^{-3}$ sec, which is much lower than the usually observed ignition delay.

We studied the effect of charge diameter (Figure 35) with PETN in a manometric bomb. The constant charging density during sample ignition

was attained by using a set of manometric bombs with diverse [illegible]. It can be seen from Figure 35 that an increase in the charge diameter in the interval $d_{charge} = 3$–$10$ mm decreases the stability of burning. Further increase in diameter has a negligible effect. A similar charge-diameter effect was observed when studying other explosives.

FIGURE 34. Record of pressure $p(t)$ and optical oscillogram during burning of a "built-in charge."

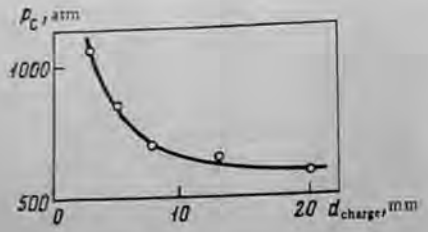


FIGURE 35. Effect of charge diameter on impairment of stable burning.

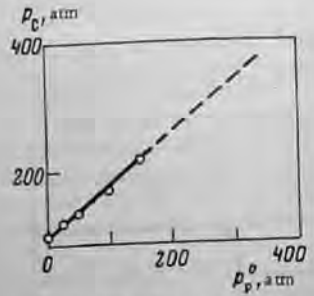


FIGURE 36. Dependence of critical pressure on the initial nitrogen pressure in the pores.

The function $p_c(d_{charge})$ was compared with data on the effect of the initial particle size (see Figures 30 and 31). A decrease in the stability of burning with increasing charge diameter and initial particle size for identical sample permeability indicates that layer-by-layer deflagration is not impaired simultaneously over the whole front, but in individual centers – the largest pores into which burning first penetrates.* An increase in the charge diameter and initial pore size led to an increase in the number of large pores, and consequently the number of centers into which burning penetrates, which is also the cause of the decrease in deflagration stability. The important role of the pore size distribution follows from these data. For this reason the permeability, which is the integral parameter of a porous medium, does not uniquely determine the impairment possibilities of the stability of layer-by-layer deflagration. The fact that we must allow for the pore size distribution in macroscopically homogeneous porous systems is a specific feature of the phenomenon under investigation.

* This is also confirmed by the type of optical record of convective burning (see Figure 34), which is characterized by an unequal "ragged" front due to penetration of burning over the individual pores into the central part of the charge with subsequent emergence of burning onto the lateral surface of the charge.



### Effect of experimental conditions /10/

The possibility of impairing layer-by-layer deflagration depends on the experimental conditions, which determine the causes leading to the filtration of combustion products into the pores (see section 12). The burning stability of identical porous samples was compared in a manometric bomb and in a "constant-pressure" bomb (the pores were filled with nitrogen). It was found that in the latter case layer-by-layer deflagration is impaired at pressures 5–15 times as large; moreover, the nature of the produced convective burning differs considerably (see section 23).

The burning of porous charges is now examined under these conditions. The increased burning stability in the "constant-pressure" bomb is due to filling of the pores with a cold inert gas during the production of the pressure. Special tests were undertaken, in which nitrogen was initially directed into the manometric bomb and filled the pores of the explosive. The charge was then ignited by a wire fed by electric current. The results for the specific case of PETN ($m = 0.24$, $r \simeq 20\ \mu$) are shown on Figure 36 (the initial pressure in the pores $p_p^0$ is plotted on the abscissa axis). It is seen that the stability of layer-by-layer deflagration increases with increasing pressure in the pores. During burning of the same charge in the manometric bomb ($p_p^0 = 1$ atm) the collapse pressure is $p_c = 100$ atm, while in the "constant-pressure" bomb (when the pores are filled with nitrogen) $p_c$ is much larger (700 atm).

Thus the collapse pressure of layer-by-layer deflagration (or, what is the same, critical pore size) in the manometric bomb of the "built-in charge" system is much lower than in the "constant-pressure" bomb, because under these conditions the mechanism of combustion-product penetration into the pores changes (see section 12).

## B. SPONTANEOUS PENETRATION OF BURNING INTO PORES

Layer-by-layer deflagration is impaired by the spontaneous (jet) mechanism, where there is no forced penetration of gases and the structure of the burning zone and the gas stream are not one-dimensional and unsteady in the immediate vicinity of the charge surface.

Suppose the gas flow over the burning surface is one-dimensional, and the temperature and velocity of the gases increase with increasing distance from the surface. In this case, it follows from Hugoniot's adiabat that the pressure will gradually decrease with increasing distance from the surface. A local pressure increase may therefore arise only during unsteady and

more than one-dimensional burning. The existence of spontaneous penetration of gases was determined in subsequent experiments.

Deflagration was studied subject to decreasing pressure. It is clear that no forced penetration of gases will arise under burning conditions at constant, and especially decreasing, pressure. In this case, penetration (if it takes place at all) should occur due to the spontaneous penetration mechanism.

Charges with a gap of 40 mm length and ~0.1 mm width were prepared between the plate of the secondary explosive (hexogen) and a plastic plate. This gap simulated the pore. Charges were also used with a supplementary volume $V_{sup}$ added to the "pore." The charge was ignited in a 2-liter bomb, in which the pressure was created by nitrogen. A control valve made it possible to obtain the required rate of pressure variation during charge deflagration, including $dp/dt = 0$ and $dp/dt < 0$. The pressure change in the bomb was fixed by a piezoelectric detector and recorded on an oscillograph. At the same time high-speed pictures were taken through the plastic plate. It was found that during deflagration of the charge without a supplementary volume and with a completely closed valve, burning propagates into the pores when the pressure does not exceed 25 atm at the instant of charge ignition. Penetration into the pores is much easier on increasing $p$. Table 5 shows some typical results when $p = 45$ atm. In this table, $V_0$ is the intrinsic pore volume and $u_b$ is the mean burning propagation velocity in the pore. $V_g$ is the velocity of forced gas inflow into the pores without allowance for spontaneous inflow, and is given by the expression

$$V_g = \frac{V_0 + V_{sup}}{S} \frac{dp}{dt} \frac{1}{p} \frac{T_g}{T_0},$$

where $S$ is the cross-sectional area of the pore inlet.

TABLE 5. Burning of a slitlike charge

| $dp/dt$, atm/sec | 25 | 90 | 70 | 40 | 0 | -5 | -15 | -5 | -15 | -18 | -15 |
|---|---|---|---|---|---|---|---|---|---|---|---|
| $V_g$, cm/sec | 125 | 80 | 55 | 35 | 0 | -4.5 | -74 | -135 | -540 | -900 | -400 |
| $V_0/(V_0 + V_{sup})$ | 5.5 | 1 | 1 | 1 | 1 | 1 | 5.5 | 30 | 40 | 55 | 30 |
| $u_b$, cm/sec | 330 | 210 | 190 | 160 | 120 | 88 | 30 | 60 | 1.2 | 1.2 | 1.2 |
| Result | Burning penetrates into pores | | | | | | | | Burning does not penetrate into pores | | |

It can be seen from Table 5 that burning penetrates into the pores not only when $dp/dt > 0$, but at a truly constant and even decreasing pressure. Under decreasing pressure conditions, the increase in the supplementary volume, in contrast to the effect at increasing pressure, leads to a more difficult penetration of burning into the pores. At some value of $V_{sup}$ and for the given rate of pressure drop burning did not propagate at all into the pores. This paradoxical effect of the supplementary volume (destabilization of burning under increasing pressure conditions and stabilization under decreasing pressure conditions) is explained by the fact that, when $dp/dt < 0$, cold gas flows from the pores outward and prevents penetration of gases from the outside, whereas when $dp/dt \geq 0$ we have forced



penetration of gases into the pores. This is also confirmed by data, according to which the value of $p_c$ (the critical pressure of impairment of normal burning) does not correlate well with $dp/dt$ or $V_0/(V_0 + V_{sup})$ but correlates well with the gas flow velocity $V_g$, the expression for which includes both $V_0/(V_0 + V_{sup})$ and $dp/dt$. Under decreasing pressure conditions, normal burning may occur at pressures which considerably exceed the critical pressure determined under normal conditions. For instance, normal burning of the above charge was observed at $V_0/(V_0 + V_{sup}) = 300$, $p_0 = 65$ atm and $dp/dt = -12$ atm/sec. Tests on the burning of the charge with a pore subject to decreasing pressure showed that normal burning can be impaired also in the absence of forced penetration. Under these conditions penetration of gases is caused by the structure of the zone near the burning surface and proceeds spontaneously. During burning at decreasing or truly constant pressure, spontaneous penetration is the only cause that impairs normal burning. Heat transfer by spontaneous inflow of gases must also be allowed for during burning under slightly increasing pressure.

There are additional facts that confirm the existence of spontaneous gas penetration. On burning an explosive charge in air (i.e., at a truly constant pressure) the burning gases flow only into the half-space above the charge surface. A divergent gas jet issues from the charge surface. If a wall or another hot charge is brought toward the hot charge, the gas jet interacts with the wall or with the gas jets issuing from the second charge and the gases fill the gap between the wall and the charge (or between the two charges, see Figure 22). In this case not only the gases, but also the combustion products may penetrate into the gap. The gas penetrates without a doubt, because the gas jets collide with the wall or with one another. We know from the theory of jets that when two jets collide at an angle another two jets are formed, the gas of which moves to the opposite side in the direction of the bisector of the angle of convergence.

Belyaev et al. /10/ found that the rounded edges of charges facing the gap facilitate propagation of burning into the gap. This result was explained on the basis of the jet mechanism. Tests showed that quiet burning of the charge or intensive propagation of burning into the gap can be brought about, to some degree, by changing the angle between the charge surface and the wall. A similar effect is also observed at elevated pressures: a decrease in the angle between the charge surface and the wall from 60° to 10° leads to a 20–40% increase in $p_c$. These experiments led to the conclusion that the jet mechanism is fundamental among the spontaneous mechanisms of gas penetration. The jet mechanism may also explain Bakhman's results /109/, which established that, on burning a charge in air, there exists some gap size for which burning penetrates most easily into the gap between the wall and charge.

It is noteworthy that especially favorable conditions for spontaneous penetration are created during deflagration of powder charges: the irregular nature of the deflagration front always gives rise to colliding jets of gas and facilitates conditions for the ejection of explosive particles.

## 16. PENETRATION CRITERIA

The criteria for spontaneous impairment of the stability of normal burning should include conditions governing penetration of gaseous combustion products into the pores of the charge and its effect on the combustion products. It should be expressed in terms of relationships involving dimensionless numbers describing the combustion of a burning charge. The pore diameter $d_p'$ may serve as the dimensionless parameter in the form of a relationship to another quantity with dimensions of length, characterizing the deflagration process. Such quantities are the widths of the characteristic burning zones $l$ (there may be several such zones $l_1$) and the characteristic grain sizes of the substance $r$.* Moreover, the criterion will include dimensionless numbers characterizing gas flow and heat exchange (Nusselt number, Prandtl number, Lewis-Lykov number):

$$d_p'/l = F(l/l_1;\ l/r;\ \mathrm{Pr_1};\ \mathrm{Nu};\ \mathrm{Lu};\ T_g/T';\ T_T/T_0;\ \lambda_T/\lambda_g). \qquad (43)$$

Here, $\lambda_1$ and $\lambda_g$ are the thermal conductivity coefficients of the condensed and gaseous phases; $T_0$, $T_g$ and $T'$ are the initial temperature, combustion temperature, and temperature on the surface of the condensed phase during burning, respectively.

For narrow zones, or when parameter $l/r$ has a weak effect, we have for a given substance

$$d_p'/l = \mathrm{const} = \mathrm{An} \quad \text{when} \quad l/r \to 0. \qquad (43')$$

In fact, the condition $l/r \to 0$ is not always satisfied. When the dimensions of particles forming the charge are small, especially if $r \sim l$, ignition of the walls is considerably facilitated, in the same way as the presence of a roughness of optimal dimensions leads to the ignition of the surface of a powder grain /70, 175/. Consequently, the stability of burning of charges made from finely disperse particles is lower when $d_p'/l > \mathrm{An}$ and $r \sim l$.

If the criterion for a group of substances depends weakly on the dimensionless numbers in the parentheses of (43), it will have the form of (43'). Analysis of experimental data shows that $d_p'/l$ is usually the most important parameter in (43), since the other combinations vary over a much narrower range. Therefore, in a first approximation, relationship (43') is used as the criterion of the impairment of normal burning. We know from the theory of combustion that the width of the heating zone of the condensed and smoke-gas phases $l_g$ and $l_1$ is $l \sim \lambda/\rho u c$. The width of the chemical reaction zone in the condensed and smoke-gas phases is proportional to the width of the heating zone; only the width of the zone of termination of burning may deviate somewhat from this value. In line with the above comments and specifying condition (43'), we obtain

$$\rho u d_p' (c/\lambda) > \mathrm{const} = \mathrm{An}, \qquad (44)$$

* Belyaev /5/ first advanced the hypothesis concerning the possibility that the penetration of burning into pores is determined by a relationship linking pore size to the distance between the burning surface and the reaction zone.



where $c/\lambda$ may refer either to the condensed or to the gas phase.

Condition (44) indicates that if the product of the mass velocity of burning $\rho u$ and the hydraulic pore diameter $d_p'$ is smaller than some constant, normal burning is stable. If, on the other hand, this product exceeds some critical value $\varphi'$, burning penetrates into the charge pores. Since the ratio of the specific heat $c$ to the thermal conductivity coefficient $\lambda$ of explosives varies over a rather narrow range, criterion (44) can be approximately simplified to the condition

$$\rho u d_p' = \varphi > \varphi' = (\rho u)' d_p'. \qquad (44')$$

Analysis showed /90/ that both the requirement of the formation of a heated layer of the condensed phase in the pore wall and the conditions of its ignition (or pyrolysis) are determined by the same set of dimensionless numbers entering dimensionless equation (43). It was assumed in the derivation of (44') that the difference in the chemical kinetics of substances completely takes into account the burning velocity $\rho u$, and temperatures $T_g$ and $T'$. This assumption appears justified, since Zel'dovich proved that the ignition process, which is affected by chemical kinetics to the greatest extent, can be approximately determined by quantities $\rho u$ and $T'$ /43/. Moreover, it is assumed that the process is essentially independent of the parameter $\rho_g/\rho_1$.

The stability criterion of burning of porous charges was first obtained by Margolin /90/. Later, Belyaev /60/ proposed that $l$ in (43) should be employed as the width of the melting layer for fusible explosives, and as the width of the heating zone of the gases for infusible substances; he also proposed that the condition governing the stability of burning should assume the form $pd \leqslant \mathrm{const}$ or $p(1-\delta) \leqslant \mathrm{const}$. Bobolev et al. /11/ examined the conditions determining the impairment of the completeness of the fused layer on the surface of substances that fuse during burning. They found that the critical burning rate $u'$ is given by

$$u' = \frac{128 x (\rho - \rho') u_1}{(1-\delta) r \rho},$$

where $\rho$ and $\rho'$ are the densities of the initial substance and the melt; $x$ is the thickness of the melting layer; $u_1$ is the burning rate at 1 atm; $\delta$ is the relative density of the charge. At lower densities, $u'$ usually corresponds to very low pressures.

Analysis of experimental data. Processing of experimental data in the form of (44') has made it possible to show /62, 90/ that the first-approximation theory correctly reflects the pattern of the phenomenon, while quantity $\varphi'$ can be represented as a sufficiently representative characteristic of the burning stability of porous charges. At the same time, introduction of the critical value of $\varphi'$ provides the basis for further specification of the role of various factors not entering (43'). Table 6 shows the mean critical values of $\varphi'$ for some individual substances and homogeneous mixtures. The table also contains secondary explosives, initiating explosives, and two ballistic powders. The table was compiled from published experimental results. Altogether, it contains data of tests on charges with relative porosities from 0.25 to 0.7 at comparatively large particle sizes of

50 to 730 μ (including polydisperse charges /62/). The critical burning velocity lies between 0.33 and 8 g/cm²·sec, and the pressure between 1 and 750 atmospheres.*

TABLE 6. Critical parameters of normal burning of homogeneous substances

| Substance | φ', 10³, g/cm·sec | $d'_p$, μ | | h | |
|---|---|---|---|---|---|
| | | 10 atm | 100 atm | 10 atm | 100 atm |
| TNT | 13.2 | 1400 | 178 | 1 | 1 |
| Picric acid | 12.81 | 940 | 136 | 1.5 | 1.3 |
| Nitrocellulose | 9.8 | 330 | 100 | 4.25 | 1.8 |
| PETN | 11.1 | 540 | 55 | 2.6 | 3.3 |
| Powder N | 4.35 | 120 | 40 | 11.7 | 4.5 |
| Powder NS | 7.0 | — | — | — | — |
| Tetryl | 7.1 | 235 | 48 | 6.0 | 3.7 |
| Hexogen | 6.9 | 163 | 21 | 8.6 | 8.7 |
| Octogen | 6.5 | 140 | 24 | 10 | 7.5 |
| Ammonium perchlorate | 3.7 | 110 | 20 | 12.7 | 8.9 |
| Mercury fulminate | 11.4 | 11.5 | 4.3 | 12 | 41 |
| Ammatol 80/20 | 14.4 | — | — | — | — |

Note. The pore size was calculated by (2), (4) and (5). The data of Tables 6, 7 and 8 were obtained in a "constant-pressure" bomb (when the pores were filled with nitrogen).

Experimental data were employed to calculate the pore diameter $d'_p$. When this value was exceeded, normal burning was impaired under the given conditions (pressures 10 and 100 atm). This characteristic allows one to evaluate the relative tendency of various substances toward spontaneous impairment of normal burning. By arranging the substances as a series by decreasing values of $d'_p$ at a given pressure (in Table 6, at 10 and 100 atm) we see that (without allowance for ammatol) TNT and picric acid burn in the most stable fashion, while mercury fulminate is the least stable from this standpoint. The quantitative characteristic can be selected as $h$, i.e., the ratio $d'_{p1}/d'_{p2}$, where $d'_{p1}$ refers to the given substance and $d'_{p2}$ to TNT at standard temperature and the same pressure. Quantity $1/h$ may be termed the TNT coefficient of stability of porous-charge burning from the aspect of the critical pore diameter:

$$h(p) = \frac{d'_{p1}}{d'_{p2}} = \frac{\lambda_1 c_1 (\rho u)_2}{\lambda_2 c_2 (\rho u)_1} \simeq \frac{(\rho u)_2}{(\rho u)_1}.$$

It should be borne in mind that, owing to the nonlinear nature of the burning velocity—pressure function for some explosives, the series arranged by the degree of burning stability obtained for one pressure need not coincide with the series for another pressure; this is evident from Table 6. Therefore, any comparison of the relative burning stability of explosives must

* In addition to the data collected elsewhere /90/, it is noteworthy that for mercury fulminate with $\delta = 0.89$ and $s = 50$ μ, we found $p_c = 70$ atm, $(\rho u)' = 26.2$ g/cm²·sec, i.e., $\varphi' = 11.4$ mg/cm·sec. Table 6 is more accurate than the table reported in /90/.



clearly indicate the pressure range, which is sometimes the decisive factor.

Table 6 shows that the value of the critical constant $\varphi'$ differs somewhat from substance to substance and lies between 13.2 and 4.35 mg/cm·sec. The mean value for nitro esters is 10.5 ± 0.7, and for nitroso compounds 7.5 ± 1 mg/cm·sec. Without ignoring the observed deviations, it is noteworthy that, on the whole, the values of $\varphi'$ lie in a fairly narrow range. The observed deviation is doubtlessly due to factors disregarded in (44'), including certain experimental facts. However, the value of plotting a series by the relative burning stabilities is one possibility of comparing and introducing various effects. For instance, when comparing values of $\varphi'$ for powder charges, and for charges with an artificial slitlike pore with a very smooth surface, $\varphi'$ is 1.5—2 times larger in the latter case. At the same time, charges made from finely disperse PETN ($r \sim 20$ μ) possessed a value of $\varphi'$ which was a factor of 2 smaller than the mean value for coarsely disperse particles /90/. These facts are in agreement with the above-mentioned effect of small particles when $r \sim l$.

Substitution of the mean value $\varphi' = 8$ mg/cm·sec and the typical value $(\lambda/c)_s = 1.5 \cdot 10^{-3}$ g/cm·sec into (44') yields the value of the constant An = $= (c/\lambda)_s \varphi' \simeq 6$. Calculation of the constant in line with (35) (condition for ignition of the pore wall) gives about 1.5—2 for $V_s = (\rho u)/\rho_s$. Thus the theoretical value is in reasonable agreement with experiment. We note that the value of the constant of the order of 2 corresponds to the smallest value of $\varphi'$ observed in the experiment. In other words, the theory gives a lower threshold estimate whereas, in practice, the burning is more stable, as a rule.

Babaitsev et al. /171/ examined a possible correlation between An and the combustion temperature of substances. It is noted that TNT, for which the highest value of $\varphi'$ is observed, has the lowest combustion temperature among secondary explosives. The behavior of potassium picrate is explained /171/ by the increase in pressure with temperature: when $\rho = 0.85$ g/cm³, this substance has two ranges of accelerated burning — at 7—20 atm, where $\varphi' = 13.6$ mg/cm·sec, and above 60 atm, where $\varphi' = 7.7$ mg/cm·sec. Similarly, the value of $\varphi'$ at higher pressures in pyroxylin is twice as large as at atmospheric pressure. It was noted earlier and elsewhere /62, 90/ that the effect of parameters $T_s/T_0$, $T_s/T'$ and $\rho_s/\rho_s$ was disregarded in expression (44'). However, it is evident that the experimental observations are in good agreement with the expected effect of pressure on the possibility of the impairment of the normal regime via the degree of burning.

Let us note another fact. If $c$ and $\lambda$ in (44) refer to the gas phase, relationship (44) becomes an analog of the Peclet number ($\rho u$ is the burning velocity). Substitution of $(\lambda/c) = 2 \cdot 10^{-4}$ g/cm·sec into (44) yields the critical Peclet number $Pe' = (\rho u d)' \cdot (c/\lambda)_s = 40$—$45$. In the general case, the condensed and gaseous phases affect the stability of burning. If we consider, as above, that $\lambda_s/\lambda_s = \text{const}$ for a group of substances, we can insert $\lambda_1$ and $\lambda_s$ into (44).

We now examine the data on heterogeneous systems. The above evaluation of the critical conditions was developed for homogeneous systems. In heterogeneous and, especially, in polydisperse systems supplementary characteristic parameters enter that are disregarded in (44'). Boboley et al.

/62/ studied typical heterogeneous systems consisting of a mixture of fuels (saccharose, urotropine) and oxidizers: ammonium perchlorate and potassium perchlorate. Potassium perchlorate, unlike ammonium perchlorate, cannot burn independently. The selected substances differ considerably from each other in their physicochemical properties, and especially in the fact that urotropine and ammonium perchlorate do not fuse during burning, while potassium perchlorate and saccharose, as a rule, do so on the surface layer of the condensed phase of the hot mixture. The experimental results are summarized in Table 7.

TABLE 7. Normal limits of burning of fuel-oxidizer mixtures

| Components | Composition, wt% | δ | $d_p'$, μ | $p_c$, atm | $(\rho u)'$, g/cm² · sec | φ', mg/cm · sec |
|---|---|---|---|---|---|---|
| Ammonium perchlorate (100—160 μ)—saccharose (100—160 μ) | 100:0 | 0,537 | 67 | 20 | 0,535 | 3,58 |
| | 90:10 | 0,58 | 62,5 | 13 | 0,608 | 3,80 |
| | 80:20 | 0,58 | 62,5 | 8 | 0,627 | 3,90 |
| | 70:30 | 0,568 | 66 | 7 | 0,674 | 4,43 |
| Ammonium perchlorate (210—160 μ)—urotropine | 85:15 | 0,683 | 69,5 | 7 | 0,752 | 5,22 |
| | 75:25 | 0,634 | 57,5 | 6 | 0,655 | 3,78 |
| | 65:35 | 0,687 | 47 | 9 | 0,705 | 3,33 |
| Potassium perchlorate (160—250 μ)—saccharose (160—250 μ) | 90:10 | 0,595 | 119 | 14 | 0,76 | 9,0 |
| | 80:20 | 0,555 | 110 | 7 | 0,825 | 9,05 |
| | 70:30 | 0,540 | 116 | 6 | 0,775 | 8,95 |
| | 60:40 | 0,567 | 105 | 6,5 | 0,88 | 9,20 |
| Potassium perchlorate (63—100 μ)—urotropine | 75:25 | 0,598 | 62 | 9 | 1,6 | 9,9 |
| | 65:35 | 0,63 | 57 | 10 | 1,86 | 10,65 |
| | 55:45 | 0,654 | 55 | 12 | 1,87 | 10,4 |
| | 45:55 | 0,60 | 45 | 16 | 2,15 | 9,6 |

Note. Particle size of urotropine ~ 100 μ.

The results for the ammonium perchlorate-hexogen mixture are presented in Table 8. Both components of this mixture can burn independently and display diverse critical pressures.

TABLE 8. Limits of normal burning of ammonium perchlorate + hexogen mixtures

| Ammonium perchlorate: hexogen ratio, wt% | δ | $d_p'$, μ | $p_c$, atm | $(\rho u)'$, g/cm² · sec | φ', mg/cm · sec |
|---|---|---|---|---|---|
| 100:20 | 0,535 | 119 | 12 | 0,315 | 3,74 |
| 75:25 | 0,543 | 115 | 3,5 | 0,350 | 4,05 |
| 50:50 | 0,544 | 113 | 2,8 | 0,553 | 6,25 |
| 25:75 | 0,562 | 107 | 5 | 0,607 | 6,48 |
| 0:100 | 0,564 | 106 | 12 | 0,83 | 6,65 |

Note. Particle size of both components is 160—250 μ.



A study of the effect of the mixture composition on its burning stability (Tables 7 and 8) established that the addition of both fusible saccharose and infusible urotropine in amounts of 30—35 wt% to ammonium perchlorate leads to a very slight change in the critical value of φ' characteristic for pure ammonium perchlorate. It may be similarly concluded that both the composition and the properties of the fuel affect the φ' value of mixtures based on potassium perchlorate. Table 7 indicates that φ' ≃ 9—10 mg/cm · sec for potassium perchlorate mixtures with saccharose and urotropine. This value is close to the value for a typical secondary explosive /90/. The critical value of φ' for an ammonium perchlorate-saccharose mixture tends to increase with increasing fuel level, whereas in the mixture with urotropine φ' passed through a maximum to decrease somewhat.

A change in the particle size of the components did not affect the values of φ'. Thus, in the test with the 80:20 ammonium perchlorate-saccharose mixture containing a lower particle size ($r$ = 50—63 μ, $\delta$ = 0.557, $d_p'$ = 30 μ), we obtained φ' = 3.96 g/cm · sec, $p_c$ = 23 atm, $u\rho'$ = 1.28 g/cm² · sec; this value of φ' is the same as that for mixtures with particle size 100—160 μ.

Burning of the ammonium perchlorate-hexogen mixture (see Table 8) was studied over a wide range of component ratios. It was found that the critical value of φ' is not an additive function of the composition, but is determined by the component whose volume content in the mixture is larger.

It is important that a change in the composition, e.g., of the ammonium perchlorate-saccharose mixture, leads to a very strong variation in the calculated combustion temperature of the products (in the 80:20 mixture it was twice the value in the 100:0 mixture). Nevertheless, φ' was unaffected.

Margolin and Chulko /90/ showed that the critical values of φ' for such readily fusible substances as TNT and nitrocellulose (respectively, 13 and 10 mg/cm · sec) do not differ considerably from the value of φ' for infusible nitrocellulose. It follows from Tables 7 and 8 that the ability of the fuel to fuse is not the decisive factor which determines the stability of burning and the possibility of its penetration into the charge pores, namely, when no continuous fused layer is present on the burning surface.

Andreev /68, 172/ has illustrated that the addition of a small amount of finely disperse aluminum to ammonium perchlorate facilitates transition from deflagration to detonation. Tests showed that the critical value of φ (under burning conditions at constant pressure) for the ammonium perchlorate-aluminum mixture ($r$ — 25 μ) is not lower than, but even exceeds, the value of φ' for pure ammonium perchlorate. Hence the introduction of aluminum increases the deflagration stability of the considered mixture in comparison with pure ammonium perchlorate in constant-pressure experiments. On the other hand, in these experiments with the same mixture but with burning at increasing pressure, the introduction of aluminum facilitated transition from deflagration, beyond the stability limit, to detonation. Similar results were obtained /171/ when investigating the effect of dispersity on aluminum. It was found that An' = 20 for a mixture of coarse ammonium perchlorate with 5% Al ($r$ — 14 μ), while An' = 1.6 for a mixture of fine ammonium perchlorate with powder ($r$ = 1 μ). For a mixture of coarse ammonium perchlorate with 10% lampblack An' = 2.5, whereas for a mixture with coke ( = 150—250 μ) An' = 34. Therefore some heterogeneous systems, including components unable to burn independently, require allowance for

more factors affecting the burning process than those entering condition (44). As for a mixture of oxidants with organic fuels, and also a mixture of substances able to burn independently, their burning stability is described by (44) to a sufficient extent. It is noteworthy that tests with ammonium perchlorate + aluminum powder mixtures indicate that the same factor may at the same time increase the critical value of $\varphi'$ and lead to intensification of convective burning of the charge beyond the stability limit.

Deviations from (44) are also observed in burning of powder charges made from small particles ($r \simeq 15\ \mu$). According to Lobanov, $\varphi'$ is equal, respectively, to 0.45, 0.4, 1.5 and 3 mg/cm·sec for 10% polystyrene + + 90% ammonium perchlorate, 2% $Cu_2O$ + 98% ammonium perchlorate, pure ammonium perchlorate, and PETN.

Leipunskii /92/ showed that better results are obtained when using the pore diameter derived from an experimental determination of the gas permeability of charges. He concluded that the decisive role is played by pores of average size, whose number is largest during spontaneous impairment of normal burning of porous systems.

In concluding this chapter, we recommend that An or $\varphi'$ be refined for new systems, if only at one point, since condition (44) is more accurately satisfied for one system than for the whole set of substances.



*Chapter IV*

## *BURNING OF SYSTEMS WITH UNCONNECTED PORES*

This chapter deals with the burning of systems containing closed pores, not connected to one another, when the system as a whole is gas-impermeable. The shape of the pores may differ: they may be individual pores, or pores distributed over the bulk in the shape of spheres or elongated, cylindrical and flat pores (fissures).

Pores form for fundamentally different reasons. We shall examine only some of them.

Unconnected pores form in propellant powders and explosives during production (technological bubble porosity, cavities) and also during their storage or combustion (cracks, porosity). The physicomechanical properties of the system considerably influence pore formation. Bills and Wiegand /124/ report that multicomponent propellant powders tend to form such types of pores. These powders are a heterogeneous mixture which contain components with very different properties, such as an elastic fuel-binder, crystalline oxidizer (ammonium perchlorate) and metal additives. When a channel-type charge is firmly fixed to an engine and burns, and powder expands owing to the action of the powder gases, and leads to impairment of the adhesive bond between the fuel and oxidizer, layers around the filler particles are peeled off (voids are created). Peeling-off of the binder from the oxidizer is the fundamental physical process that determines pore formation /124/. This process takes place not only due to mechanical stresses, but also to thermal stresses. The linear expansion coefficient of the composite powder (about $10^{-4}$ deg$^{-1}$) is one order of magnitude larger than the corresponding coefficient for steel, so tensile thermal stresses arise in the charge-steel body system during cooling. The linear expansion coefficients of the individual components of the powder also differ. Consequently, a "frozen" porosity arises at low temperatures /160/. Stress concentration at the sites where the binder is peeled off or destroyed may lead, under certain conditions, to the combination of pores and to the formation of fissures.

Pores and fissures may also form during charge ignition, owing to the action of large temperature and pressure gradients.

Naturally, penetration of burning into unconnected pores is much less dangerous than in the case of gas-permeable systems. On the other hand, the presence of pores in the sample leads to bending of the combustion front, increase in the burning surface, and consequent increase in the pressure in the engine.

The steady-state pressure in an engine is defined by the equation

$$p_0 = \left(\frac{b\rho S_0}{A\sigma}\right)^{1/(1-\nu)}, \qquad (45)$$

where $S_0$ is the burning surface; $A$ is the discharge coefficient; $\sigma$ is the cross-sectional area of the nozzle; $\rho$ is the powder density; $b$ and $\nu$ are constants in the burning velocity law, $u = bp^\nu$.

It is evident from (45) that a change in the burning surface may give rise to a considerable increase in the pressure in the engine (especially for high values of $\nu$) exceeding the maximum permissible value. Consequently, the engine may be destroyed by throttling, due to the limited (supplementary) burning surface $\Delta S$ in the presence of pores.

Suppose $\nu < 1$. After the burning surface increases from $S_0$ to $S = S_0 + \Delta S$, gasdynamic equilibrium is again established at a pressure given by

$$p = p_0 (S/S_0)^{1/(1-\nu)}. \qquad (45')$$

Since $p = p_0 + \Delta p$, $S = S_0 + \Delta S$, the quantity $(S/S_0)^{1/(1-\nu)}$ can be expanded in series form. If only the first two terms are retained, we obtain from (45')

$$\frac{\Delta p}{p_0} = \frac{1}{1-\nu}\frac{S}{S_0}.$$

This expression makes it possible to calculate the relative pressure increment with an accuracy sufficient for practical purposes.

If the pore surface is defined, simple geometrical relationships can be used in the calculation of $\Delta p/p_0$ and it may be assumed that the burning velocity in the pores does not differ from the burning velocity outside them. If necessary, we can introduce the increased gas supply from the pore surface, due to the creation of excess pressure inside the pore (see section 22). This approach to the determination of $\Delta p/p_0$ is justified when the pores cannot grow (the initial depth cannot increase) during the burning process. The problem of pore growth during burning will be considered in section 22.

Thus, for normal operation of an engine it is very important to decrease $\nu$, to improve the physicomechanical properties of the propellant powder, and to ensure correct engine design in order to prevent pore formation at every stage of the charge "life."

## 17. CRITICAL CONDITIONS FOR BURNING TO PENETRATE INTO A SINGLE PORE

The critical size of a pore into which burning can penetrate was estimated in section 15. Data on the impairment of the burning stability of gas-permeable porous systems was employed in this calculation. However, burning in closed pores is characterized by some specific features, which must be taken into account when considering critical conditions of penetration.



Ignition of gas near the closed end of the pore stabilizes the flow of combustion products and makes penetration of burning more difficult. On the other hand, good conditions are produced for inflow of gases according to the spontaneous mechanism, since there is no periodic impairment of the notches (characteristic for pressed systems) which generate the combustion products in the pores.

The authors of this book carried out some direct tests. They used flat slitlike charges (Figure 37), which were ignited in a manometric bomb. The $p(t)$ curve in the bulk of the bomb was recorded and the penetration process photographed. The authors determined the critical pressure $p_c$ at which burning penetrated into a pore of width $d_0$. The tests were mostly carried out with the charges shown in Figure 37a (pore formed by plates of the explosive and plexiglass*).

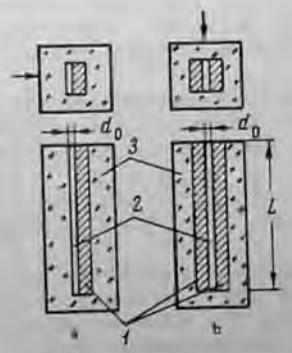


FIGURE 37. Schematic diagram of slitlike charges:

a) closed pores formed by a plate made from solid explosive and a plexiglass plate;
b) closed pore formed by two plates made from solid explosive:
1) explosive; 2) pore; 3) plexiglass casing; $d_0$ is the pore width; $L$ is the pore length; the arrow shows the direction of photography.

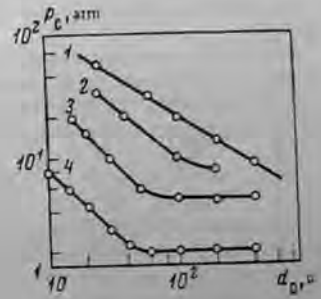


FIGURE 38. Dependence of critical pressure on pore width:

1) hexogen; 2) nitroglycerin powder; 3) slow-burning composite propellant powder; 4) fast-burning composite propellant powder.

The results of experiments with nitroglycerin, composite propellant powder of two brands and hexogen are shown in Figure 38. Burning of the high explosive, hexogen, is the most stable, followed by the nitroglycerin powder and the composite propellants. The stability of the composite powders decreases with burning velocity; this can be seen when comparing data for three slow-burning and four fast-burning explosives. Thus, the burning rate possesses considerable importance when comparing the

* It was shown that $p_c$ does not change when the pores shown in Figure 37b (formed by two plates made from explosives) burn.

burning stability of explosives or propellant powders of one group over a narrow interval of pressure changes.

On the whole, the results agree with the data of section 16, both in absolute value and from the standpoint of the comparative stability.

The low burning stability of composite powder in comparison with nitroglycerin powder is explained by differences in the temperature profile of the gas phase. It is known /81, 83, 163/ that the distance $h_m$ between the burning surface and the high-temperature gas zone for composite powders is one order of magnitude lower than for nitroglycerin powder (when $p_0 \simeq 40$ atm, the values of $h_m$ are 2 and 0.1—0.2 mm, respectively). Moreover, the pressure at which the substance is completely combusted differs considerably (10—20 and 40—50 atm, respectively). This implies that the temperature of the gas flowing into the pores of the composite powder, even at low pressures, is higher than the temperature of the gas flowing into the nitroglycerin powder. This was confirmed by direct measurement of the temperature in the pores /12, 59/. This difference is also evident in the nature of the pore ignition after penetration (section 22).

The $p_c(d_0)$ curve for composite powders displays two sections: a strong dependence for small pores and a weaker dependence for large pores.

It follows from the ignition conditions examined in section 14 (see (38)) that we can expect a function of the type

$$p_c^{1+3\nu} d_0^2 = \text{const}. \qquad (46)$$

Comparison of calculated with experimental data shows that agreement is satisfactory for small $d_0$: the slope of the curve corresponds to the theoretical value and is equal to $-2/(1+2\nu)$. The relationship between the critical pressure and the pore size for the studied powders ($\nu \simeq 0.5$) is hyperbolic /12/: $p_c \cdot d_0 = \text{const}$. It is of interest that for hexogen ($\nu = 1$) function $p_c(d_0)$ is weaker than for the powders, in accordance with relationship (46). The disagreement between theory and experiment at high $d_0$ (the section of the weak $p_c(d_0)$ dependence) apparently arises because the dependence of the Nusselt number on the velocity of the effluent gas ($\mathrm{Nu} \sim \mathrm{Re}_x^{0.5}$) should be taken into account.

The effect of pore surface roughness was also studied. Tests were conducted with hexogen plates to which various degrees of roughness were imparted. It was shown that, in accordance with the theory, the presence of roughness reduces stability: the critical pressure decreases from 35 to 20 atm at a mean pore diameter $d_0 = 40\ \mu$ and a roughness size of about 10 $\mu$. Variations in the roughness dimensions have a weak effect on the critical pressure. The effect of pore roughness arises because the projections become heated more rapidly and to a higher temperature than a smooth surface, and act as ignition centers.

## 18. BURNING OF SYSTEMS WITH BUBBLELIKE POROSITY

Belyaev /59/ studied burning of samples of propellant powders, which contained bubblelike (spherical) pores of diameter 0.1—0.5 mm, distributed uniformly throughout the volume. Samples with diverse porosities were



obtained by varying the technological process of their production. Cylindrical charges (diameter 10 mm, height $H = 15$—$20$ mm), which were cased over the lateral surface, were ignited in a BD device. Belyaev calculated the linear burning velocity $u = H/t$, where $t$ is the combustion time. The mass velocity of burning was calculated by multiplying the linear velocity by the density. Quantity $u_m = u\rho$ is the amount of substance combusted in unit time from unit cross-sectional area (without allowance for the surface relief).

The results are presented in Figure 39. The density and porosity of the sample are plotted on the abscissa axis, and the linear ($u$) and mass ($u_m$) velocity of burning on the ordinate axis. The tests were carried out at pressures between 1 and 42 atmospheres.

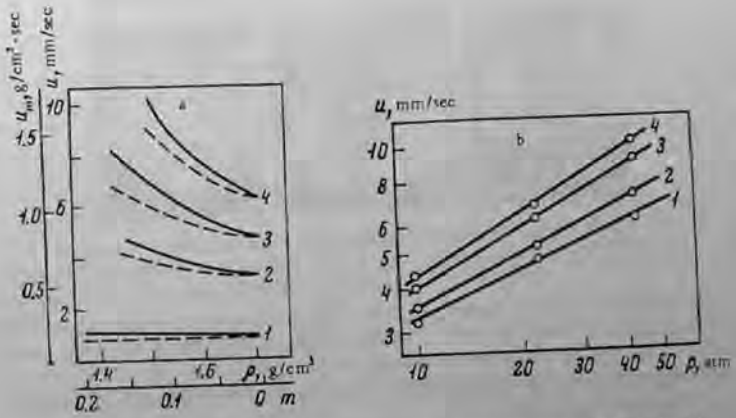


FIGURE 39. Effect of closed (bubblelike) porosity on linear ($u$) and mass ($u_m$) velocity of burning:

a: 1) 1 atm; 2) 10 atm; 3) 22 atm; 4) 42 atm; solid curves refer to $u$, dashed curves to $u_m$; b: 1) $m = 0$, $\nu = 0.45$; 2) $m = 0.05$, $\nu = 0.57$; 3) $m = 0.10$, $\nu = 0.67$; 4) $m = 0.125$, $\nu = 0.6$.

It follows from these data that $u_m$ is density-independent at a pressure of 1 atm. At higher pressures, both the linear and the mass burning velocities increase with increasing porosity, the increase is stronger, the higher the pressure.

Processing of the data in log $u$ — log $p$ coordinates (Figure 39b) showed that the presence of closed pores in the charge leads to a change in the law of burning, $u = bp^\nu$. The tentative burning velocity $b$ at $p = 1$ absolute atm is practically independent of porosity, while exponent $\nu$ increases with porosity.

Photographic observations of the burning of individual pores were carried out by Chuiko, who showed that in accordance with the data of Figure 39, at low pressures, the inner surface of the pores is ignited

after a long delay and bending of the burning front is insignificant. Burning, as it were, does not respond to the presence of pores. As the pressure increases, the delay of ignition becomes shorter and bending of the surface increases (Figure 40).

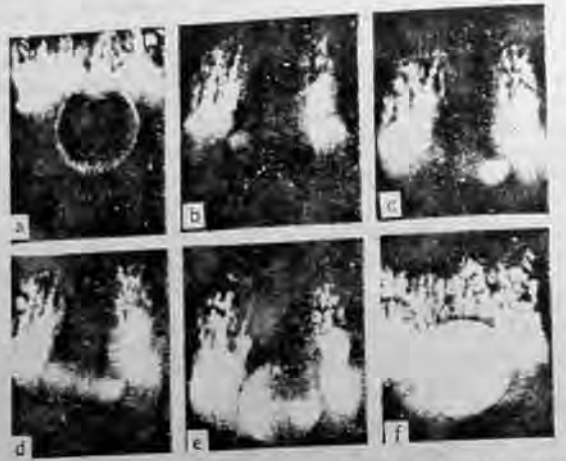


FIGURE 40. Motion pictures of the ignition of a spherical pore ($d$ = 4mm, $p$ = 50 atm).

Equalization of the pressure in the spherical pore upon the approach of the burning front proceeds very rapidly, and consequently the heat reserve introduced by the combustion products is insignificant. The fact that the pore is nevertheless ignited indicates the important role of heat supply from the combustion zone.

The decrease in the delay of pore ignition with increasing pressure permits us to explain the experimentally determined, stronger effect of porosity at higher pressures (see Figure 39).

The data can be explained somewhat differently /59/ (see Figure 39) when we use the simplified scheme of burning of a porous charge (Figure 41), and assume that all the heat is released in a narrow zone of the gas phase and transferred into the condensed phase by conduction.

When the principal reaction takes place in the gas phase, the amount of combusted matter per unit surface of the burning front at a given pressure assumes a specific value. Under steady-state burning conditions this amount of intermediate products flows from the condensed phase into the gas phase; the flame with the given surface can "process" these products independently of the density of the initial substance. "Automatic regulation" of the supply of the required quantity of intermediate products is realized by changing the distance between the reaction zone of the gaseous products and the surface of the substance, and by the corresponding change in the heat flow.

At low pressures, the reaction zone is far from the charge surface and the burning front in the gas phase is not curved but plane (position 1 in



Figure 41). Therefore, the mass velocity is only determined by the pressure and not by the density of the original substance. The linear burning velocity is inversely proportional to the density. Evidently, in order to ensure the required inflow of intermediate products, the flame must be somewhat closer to the surface of the porous sample than to the surface of the nonporous one. This is one limiting case.

In the other limiting case (at sufficiently high pressures) the distance between the reaction zone in the gaseous phase and the charge surface becomes much smaller than the pore size and the surface of the flame completely reproduces the outline of the charge surface (position 3 in Figure 41). The ratio of the mass burning velocity of the porous charge (calculated relative to the cross section of the charge) to the mass burning velocity of the nonporous charge is the same as the ratio of the surface of the porous charge to the surface of the nonporous one. This ratio for an idealized distribution of pores of the same diameter at the lattice points of a cubic lattice is $1 + \sqrt[3]{36\pi m^2}$. Comparison with experiment (Figure 39) shows that this limiting case is not realized even at peak pressure (42 atm).

Between these extreme cases there lies the region of intermediate pressures in which, with increasing pressure, the flame front (position 2 in Figure 42) approaching the surface of the condensed phase changes from planar to assume its most curved shape. The position of the boundaries of this region depends on the pore size or, more precisely, on the ratio of the pore size to the distance between the charge surface and the reaction zone in the gaseous phase. When a system with closed pores deflagrates in this pressure region, a "geometrical" increment (owing to the increase in the curvature of the flame with pressure) is added to the "chemical" increment in the burning velocity with pressure (owing to the increase in the rate of reaction in the flame). This also leads to a higher exponent in the burning law $u = bp^{\nu}$.

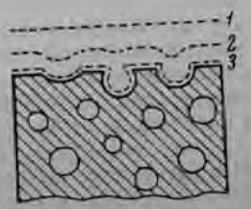


FIGURE 41. Schematic diagram of burning of a system with closed pores at various pressures.

The dashed curve shows the position of the reaction zone relative to the surface at various pressures $p_1 < p_2 < p_3$.

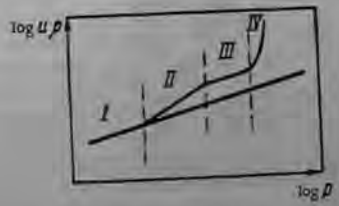


FIGURE 42. Pressure dependence of the mass burning velocity for a system with closed porosity.

The upper curve corresponds to $m > 0$, and the lower to $m = 0$ (nonporous sample).

In the general case, the pressure dependence of the mass burning velocity for a system with closed pores should have the form shown in

Figure 42. To clarify the explanation, this function $u = bp^{\nu}$ is assumed to be linear over the whole range of pressures, i.e., $\nu = \text{const}$. The position of the boundaries between the regions depends on the physicochemical properties and mechanical characteristics of the system and on the pore size.

Regions I, II and III correspond to positions 1, 2 and 3 in Figure 41. In region III, the pores are so rapidly ignited that the burning velocity of the sample is only determined by the complete combustion of the partitions between the pores. Therefore, $\nu$ for both the porous and nonporous samples remains unchanged. Separation of pores by gas-impermeable partitions prevents penetration of burning into the bulk of the sample. However, this stabilization of the process can only be realized until a certain pressure is reached.

At high applied pressures the partitions are mechanically destroyed, the pores become connected, and burning penetrates into the bulk. This process is accompanied by a sharp increase in the burning velocity of the charge (region IV).

It should be borne in mind that the effect of the destruction of the partitions when the flame front approaches the pores is observed at relatively low pressures (about 40 atm). However, the thickness of the impaired saddle is small, it depends on the physicomechanical properties of the system and comprises about 10–20% of the pore diameter.

We have considered the burning of an industrially produced system with closed pores. This case also comprises burning of deformed samples. We mentioned earlier that the fuel binder is peeled off ammonium perchlorate crystals during expansion of composite propellant powders, owing to impairment of the adhesive bonds. This peeling-off begins on the large crystals. Thus, closed pores are formed in the expanded samples and so increase the burning velocity. According to Bills and Wiegand /124/ it is possible in present-day composite powders to localize the damage, because removal of the binder from the oxidizer is uniform in character, as is evident in the photograph, Figure 43. The relation between porosity and the largest of the principal normal strains $\varepsilon$ has the form

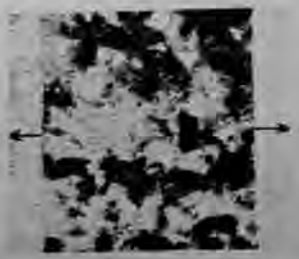

FIGURE 43. Pore formation during expansion of composite propellant powder.

Strain $\varepsilon = 50\%$; arrows indicate the direction of the expansion; dark regions show the formation of voids around the oxidizer particles, which are white.

$$m = \varepsilon(1 - 2\mu') - \mu'\varepsilon^2(1 - \varepsilon),$$

where $\mu'$ is Poisson's ratio.

Sorkin /94/ reports the following expression for the dependence of burning velocity on the strain:

$$u_\varepsilon = u_0(1 + \xi\varepsilon^n), \qquad (47)$$

where $\xi$ and $n$ are coefficients that depend on the propellant composition.

Consequently, the burning velocity of propellant powder in the general case does not only depend on pressure, initial temperature and gas flow velocity, but also on the strain, which is allowed for in the interballistic computation of a rocket engine with a charge attached firmly to the body.



The above comments refer to conditions when burning is not the direct cause of the formation of pores (fissures) and burning served only to "bring to light" existing structural defects.

## 19. THERMAL SHOCK DURING BURNING

In nonporous brittle systems, and especially in crystalline explosives, fissures may be formed during burning because of thermal shock, namely, thermal stresses created in the heated layer of the explosive /38/. The stress increases with temperature gradient, and hence with burning velocity.

Bowden et al. /88/ observed bursting of single crystals of explosives during burning. Whittaker and Barham /96/ observed a similar effect for single crystals of ammonium perchlorate that were ignited at 42 atm.

The problem has been treated theoretically by Irwin et al. /174/, who correlated the experimentally observed sharp increase in the burning velocity ($\nu > 1$) of ammonium perchlorate samples at $p > 350$ atm /95/ with the formation of fissures.* Their calculation /174/ showed that throughout the whole pressure range (350–1600 atm) bursting of ammonium perchlorate is due to thermal stresses and not shearing stresses, as assumed earlier.

Bursting of crystals of explosives when temperature drops are present in the absence of burning was investigated experimentally by Andreev and Gorbunov /97/. The explosive crystallites were immersed in water at various temperatures and the temperature drop $\Delta T$ which led to the appearance of fissures was determined. It was established that larger crystals of explosives are fairly sensitive to thermal shocks – sudden heating on the surface cracks the crystals at small temperatures drops. For PETN and hexogen, fissure formation was observed for drops $\Delta T$ as low as 15–20°C, whereas for less sensitive explosives (such as picric acid and TNT) $\Delta T$ was 40–50°C.

Much higher temperature drops are produced during burning. On the other hand, there is no published material that reports bursting of powders and polycrystalline explosives during the combustion process. Research on the burning of samples of secondary and initiating (mercury fulminate) explosives, pressed to the maximum possible density, showed /23, 36, 80/ that no anomalous changes occur in the pressure dependence of the burning velocity between 1000 and 4000 atm (where such effects should be expected**). This result indicates that the mechanism of fissure formation during combustion of explosive polycrystals apparently differs from the mechanism for single crystals, and that the burning process has considerable importance. It is quite possible that the fusion process prevents formation and development of fissures during burning of secondary explosives. We can further assume that the thermal shock arises under

* However, according to Glazkova /158/ the shape of the $u(p)$ curve for ammonium perchlorate in the 350–1000 atm range depends strongly on the type of casting and the presence of a catalyst, which shows the important role played by chemical factors. For instance, the $u(p)$ curve becomes normal ($\nu = 0.8$) when 5% $K_2Cr_2O_7$ is introduced. The explanation of Irwin et al. /174/ is therefore not exhaustive.

** The thermal stresses increase with the burning velocity, because the temperature gradient increases.

especially favorable conditions, for instance, when a high-temperature gas stream is blown past the burning sample, so increasing the heating intensity of the solid phase. In any case, available indirect data give reason to believe that such an assumption is valid.

We note in conclusion that the available data in the literature do not permit one to formulate the mechanism and pattern of fissure formation during burning. Therefore, much theoretical and experimental research on this interesting problem remains to be carried out.



*Chapter V*

*GROWTH OF EXPLOSION*

## 20. GENERAL SCHEME

Chapter III dealt with studies of the initial stages in the onset of explosions — impairment of layer-by-layer deflagration. This chapter deals with data which explain the mechanism and pattern of propagation of the process after the loss of stability, in order to answer the fundamental question as to how the explosion grows and how detonation arises. The term "explosion" is here meant in the wider sense of the term and includes the sequence of different regimes (stages) preceding detonation.

Early studies, showing the theoretical possibility of transition from the deflagration of solid explosives to detonation, were carried out 30 years ago by Andreev /6, 7/, Belyaev /1—5/, and Patry /9/. It was found already then that if this transition is easy (ignition in air) for initiating explosives (like mercury fulminate) of low density, in the case of homogeneous explosives this transition can only take place when the explosive is ignited and burns under high-pressure conditions in a strong closed casing. The Andreev tube (see Figure 6a) is still used in one variant for studying transition from deflagration to detonation.

Growth of explosion in applications under conditions of mechanical action (when a pendulum hammer hits an anvil) was studied exhaustively by Bowden and Yoffe /15/. The tests were carried out with a thin layer of explosives confined between flat surfaces held in place by high pressure. The authors revealed the general outline of the growth of explosion from the hot spot of the reaction and established the complicated stagewise nature of the propagation of the process: deflagration — rapidly accelerating burning — low-velocity detonation (1000—2500 m/sec) — normal detonation.

Normal detonation arises, as a rule, when burning proceeds from the ignited layer to the incompletely ignited explosive. Though the general outline of the growth of explosion has been established, no detailed research on the individual stages was carried out owing to the small volume in which the process takes place.

The work of Bowden was further advanced by Bobolev et al. /16, 126, 127/.

In recent years, transition from deflagration to detonation has been studied for pressed /14, 142—144/ and cast /13, 121, 125, 131/ explosives confined in strong closed casings. These studies shed light on the physical essence of the transient phenomena and clarified the general growth prior to detonation.

According to modern ideas, transition from deflagration of solid explosives to detonation can be represented by a general, very simplified

schematic diagram (Figure 44) and includes the following stages: I — stable layer-by-layer deflagration; II — convective burning; III — low-velocity (800–3500 m/sec) region of transition by explosion*; IV — steady-state normal detonation. Each stage differs by the mechanism of heat transfer and initiation of the reaction. The main form of heat transfer during layer-by-layer deflagration is molecular thermal conduction, while in convective burning it is forced convection. The low-velocity regime is initiated by compression waves, and detonation by a shock wave. In the general case the growth of the process is accelerated. The final result of the accelerated growth is the formation of a shock wave, which initiates detonation of the explosive if its amplitude exceeds the critical value and if the system is able to detonate (the charge diameter is larger than the critical diameter of detonation). The existence and spatial extent of the individual stages depends on the structure of the charge, the physicochemical (individual) properties of the explosives, and the experimental conditions. For instance, convective burning may pass directly to detonation by omitting stage III. The process may also terminate upon the establishment of the low-velocity regime with a constant velocity and the absence of detonation.

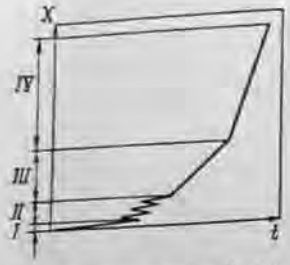


FIGURE 44. General scheme of transition from deflagration of solid explosives to detonation.

Subsequent explanation will be simplified by examining separately convective burning, wavelike low-velocity regimes, and shock initiation of detonation. This approach is also important because each stage possesses its own topics of interest. On the other hand, until quite recently our knowledge about the individual stages was very fragmentary and limited. Separate investigations of the individual stages have recently yielded new results, which fill (though incompletely) gaps in our knowledge. The spatial extent over which each of these stages takes place is achieved by appropriate design of the experiment, so that transition from one stage to another is made more difficult. The experiment can be set up so that the process develops in a stable fashion subject to convective burning or low-velocity regimes only. This approach considerably simplifies the research and provides a detailed analysis of the individual stage.

The difficulties involved in drawing conclusions from data on transition from deflagration of solid explosives to detonation arise because, frequently, the available information was obtained under different conditions which make comparison difficult, and with different types of systems. Therefore, we attempted to explain the fundamental features in order to reveal the influence of the physical structure of the charge or the chemical nature of the explosives. Special care was taken to report results obtained with the same experimental design.

* The propagation velocity in the low-velocity regime is considerably lower than the velocity of normal (high-velocity) detonation. At present, there is no commonly accepted terminology for this stage. The following terms are used: low-velocity detonation (for explosive powders), wavelike burning, low-velocity regime. We shall use mainly the term "low-velocity regime of transition by explosion," since in high-density charges the propagation velocity is usually a fraction of the sonic velocity in the original explosive.



### A. CONVECTIVE BURNING

The convective burning regime arises after impairment of stable deflagration. The inner pore surface is ignited by gaseous combustion products penetrating into them. The penetration velocity is 10 to $10^4$ times higher than the layer-by-layer deflagration velocity. Before examining the main results of research work on convective burning of porous systems, let us discuss contemporary ideas about the ignition mechanism of solid explosives and powders.

## 21. FUNDAMENTAL IDEAS ABOUT THE IGNITION MECHANISM

Until recently, little attention was devoted to the ignition of propellant powders and solid explosives. However, during the last decade scientists became much more interested in this problem after the construction of solid-propellant rocket engines. Many papers were published dealing with experimental and theoretical research on the ignition process, mainly of various types of propellant powders. Nonetheless, many aspects of the ignition mechanism still remain unclear. The literature contains comprehensive discussions as to where the propellant is ignited, and which role is played by processes arising in the condensed and gaseous phases.

The ignition mechanism depends to a large extent on the physicochemical properties of the investigated system, the intensity of heat supply, and the state of the environment. At present, the gas-phase /43, 102, 104/ and solid-phase /98–100/ theories of ignition are very popular.

Gas-phase theory. The approach of Zel'dovich /43/ is the simplest one for setting up this theory. His approach is based on the burning mechanism of volatile explosives /5/, which have a clearly defined gasification temperature equal to the boiling point. It is here assumed that the substance is heated to the gasification temperature at the expense of the energy of the source. As of this instant the substance is gasified, and the principal reaction leading to ignition takes place in the gaseous phase at a certain distance from the surface. An indispensable condition for ignition is the production of a heated layer in the condensed phase. The layer depth must be sufficient to ensure the required critical temperature gradient near the surface (the theory of Zel'dovich was briefly reviewed by us when deriving the equations for pore ignition in section 14). In this theory, heat release in the condensed phase and the hydrodynamic patterns of the environment are taken into account. However, the theory considers transition from ignition to deflagration. The ideas of Zel'dovich were further developed by Librovich /102/. At present, attempts are being made to refine the given model (as applied to composite propellant powders) by taking into account, for example, diffusion of the oxidizer to the fuel.

Experiments with powders at high heat flows are the basis for creating gas-phase theories. The more important role played by gas phase processes with increasing heat flow intensity is indicated by the stronger influence of the oxygen concentration in the environment and the pressure on the arrest period and energy of ignition /104/.

Solid-phase theory. There exist several variants of the theory developed by Zel'dovich /98/, Hicks /99/ and Merzhanov et al. /100/. In this theory the principal reaction takes place in the condensed phase. It accounts well for the low-temperature regimes of thermal action under which the substance behaves inertly for a considerable time after introducing the heat flow, and under which (at a certain temperature) the reaction in the condensed phase sets in and the surface temperature $T_s$ rises abruptly. The temperature at which the $T_s(t)$ curve has a break is taken as the ignition temperature. The small effect of gas-phase processes at low-temperature ignition is demonstrated by experiments in which, under these conditions, the time lag before ignition depends weakly on the oxygen concentration.

The problem of transition from ignition to steady-state deflagration is neglected in the solid-phase theory.

Merzhanov et al. /100, 101/ used the tools of the solid-phase theory to determine the effective kinetic parameters of heat release ($E$, $k_0$, $Q$) from experimental data on low-temperature ignition. They proposed /100/ an ignition criterion, according to which the condensed substance is ignited when the rates of heat supply from the external source and of the chemical reaction become equal:

$$q(t_i) = Qk_0\int_0^\infty \{\exp|-E/RT(x,t_i)| - \exp(-E/RT_0)\}\,dx, \qquad (48)$$

where $x$ is the distance from the surface; $q$ is the heat flux from the external source; $T_0$ is the initial temperature; $E$ is the activation energy; $R$ is the gas constant; $k_0$ is the preexponential factor; $Q$ is the heat effect of the reaction (per unit volume); $t_i$ is the time lag before ignition.

A study of the ignition of pyroxylin and a composition consisting of ammonium perchlorate (90%) + polyethylene (10%) showed /101/ that for heat flow intensity $q = 1-10$ cal/cm$^2$·sec good agreement was found between calculated (using equation (48)) and measured time lags before ignition. This indicates that the theory and criterion (48) can be used to describe ignition under these conditions.

Low-temperature regimes of thermal action are thus described by the solid-phase ignition theory, and high-temperature regimes by the gas-phase theory, although there are no distinct boundaries separating high and low intensities. At present, there is a tendency to create a unified theory, which would allow for exothermal transitions both in the condensed and in the gaseous phases. Difficulties in establishing such a theory arise because we have no physical pattern of the ignition process, especially at high intensities.

Simple regimes of heat supply are generally applied in experimental ignition studies.

Research on ignition by the action of convective heat flows is interesting from the standpoint of transition from deflagration of porous systems to



detonation. Baer et al. /105/ studied the ignition of composite propellant powders by convective flows of sufficiently high intensity (10–100 cal/cm$^2$·sec); they used a shock tube with gas efflux through a controllable nozzle. The gas velocity above the investigated propellant sample was varied between 50 and 100 m/sec. The time lag before ignition $t_i$ was defined as the period between the instant the heat flow was applied and the instant luminescence appeared (luminescence was fixed by a photomultiplier). The dependence of $t_i$ on the mean heat flow $\bar{q}$ for a propellant based on ammonium perchlorate is shown in Figure 45 (the propellants were ignited at air and nitrogen pressures of 17.5 and 25 atm, and at oxygen pressures of 10 and 17.5 atm). In pure oxygen $t_i$ decreased more, the higher the pressure. Function $t_i(q)$ differs for the various propellants. The tests showed that the physical properties of the propellant (type of binder, nature of the adhesion between binder and oxidizer, dispersity of ammonium perchlorate) have a considerable influence. The time lags before ignition were 5–45 msec for $q = 10-100$ cal/cm$^2$·sec.

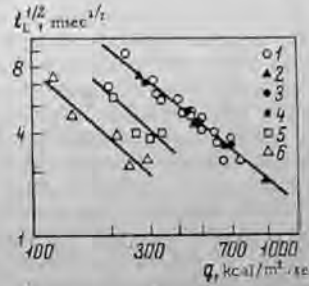


FIGURE 45. Dependence of the time lag before ignition of composite propellant powder on the heat flux /105/:

1) air, 17.5 atm; 2) air, 25 atm; 3) $N_2$, 17.5 atm; 4) $N_2$, 25 atm; 5) $O_2$, 10 atm; 6) $O_2$, 17.5 atm.

Merzhanov et al. /101/ described the ignition of composite propellant powders, model compositions and pyroxylin by lower intensity convective flows.

Information about the ignition of explosives is sparse; only two papers are noteworthy.

Bryan and Noonan /164/ determined the ignition energy of some explosives for a strictly determined time of action of the igniter (3 msec). Heated gas (mainly helium) was passed over the samples. The resulting data (reported below) give some idea as to the relative ability of explosives to be ignited.

| Explosive | TNT | Tetryl | Hexogen | PETN | Lead azide | Lead styphnate |
|---|---|---|---|---|---|---|
| Ignition energy, cal/cm$^2$ | >0.38 | 0.32 | 0.33 | 0.23 | 0.081 | 0.044 |

Andreev and Rogozhnikov /112/ proposed a method for determining the flammability of explosives. The method is based on establishing the minimum weight of the igniter required to excite stable deflagration of the explosive charge in a manometric bomb. The igniter comprised a mixture of pyroxylin No. 1 and ammonia saltpeter (50:50) yielding gaseous products on combustion. This method served to determine the flammability of several explosives. They can be arranged in the following sequence of decreasing flammability: potassium picrate, tetryl, 62% dynamite, xylyl, ammonium perchlorate, TNT, trinitrobenzene, and ammonites. The method

is simple and rapid, and enables a comparative evaluation of the flammability of diverse explosives to be carried out. However, Andreev and Rogozhnikov correctly note that a theoretical treatment of the results involves difficulties, due to the complex nature of the thermal action associated with the nonconstancy of the pressure and temperature of the gases created by the igniter.

## 22. GROWTH OF BURNING IN A SINGLE PORE

Penetration of burning into a pore involves 1) ignition of a suitable section of the pore subjected to the action of hot combustion products, and 2) propagation of the burning front along the pore length from the hot spot of ignition. The first aspect of the problem can be solved in principle, with the aid of contemporary notions developed in the preceding section. At present, however, there is no mathematical model or sufficiently complete physical understanding of the burning front propagation along the surface of the explosive. This problem is not solved for the practically important question of the ignition of the channel of the powder charge during the operation of rocket engines. Some approaches to this problem were outlined by Raizberg /106/, who assumed that the propagation velocity of the burning front is the same as the displacement velocity of the leading edge of the zone in which critical ignition conditions were attained. Raizberg assumed that the surface element is instantaneously ignited when a critical surface temperature is reached or when a critical amount of heat (relative to unit area of the surface of the heated layer) is accumulated. The effect of the ignition mechanism is neglected in this approach. The mathematical analysis of the phenomenon is carried out using some simplifications and the results are not compared with experimental data.

We tried to solve this problem by an experimental approach with allowance for the complex nature of the phenomenon.

Studies of the onset and growth of convective burning in disordered porous systems are difficult because (as shown below) the front of convective burning is not plane. Therefore optical methods (specifying luminescence on the lateral surface of the charge) do not give a sufficiently complete and objective pattern of the process growth in the case of nontransparent (solid) explosives. It was assumed that the fundamental laws governing the propagation of convective burning can be obtained with the aid of a simplified ordered model, the single pore. This model facilitates experimental research on all the successive stages of the onset and growth of convective burning.

Consider a single pore (fissure) into which ignited products arrive from one side. After ignition of one end of the pore the boundary dividing the ignited and nonignited parts of the surface propagates as a burning front along the pore. Thus, only the burning front velocity need be determined along the surface (ignition velocity) and its dependence on various parameters: properties of the system, geometrical dimensions of the pores (width, length, shape of pore), pressure, conditions at the opposite end of the pore (open, closed end).



### Pore ignition

Experimental method. The slitlike charges used are illustrated in Figure 37. We used mostly a closed, flat pore formed by two plane-parallel disks made from a nonporous substance with smooth surfaces. The ignition process was studied with one of the disks replaced by a plexiglass plate (Figure 37a), which made it possible to record the propagation of burning by optical methods. The pore was ignited at the upper end. The geometrical dimensions were defined by the length (depth) $L$ and distance $d_0$ between the disks made of the substance, and characterizes the equivalent pore diameter $d_p$ (for a flat pore $d_p \simeq 2d_0$).

The slitlike charges were combusted in a specially developed manometric bomb (see Figure 5), described in detail on p. 5. The pore is ignited by the convective flow of a hot gas, formed during combustion of the igniter. The process was at the same time recorded optically by a high-speed motion-picture camera or photorecorder. In this way the time lag before ignition $t_L$ and the pore ignition velocity $u_{ig}$ could be measured and the pressure $p_p(t)$ in the pore near the closed end of the charge recorded directly.

Some of the tests were carried out in a "constant-pressure" bomb (Crawford bomb), when the initial pore pressure was equal to the pressure in the bulk of the bomb. The ignition of both a closed and an open pore was studied in this experimental series. The pore was ignited by a Nichrome spiral fed by an electric current. In addition to optical recording of the propagation of burning in the pore we measured the temperature in the pore with the aid of thin (30 $\mu$) tungsten-rhenium thermocouples. The temperature was measured by the method of Zenin /183/.

The initial pore width $d_0$ was larger than the critical width $d_{cr}$ in all the experiments, in order to ensure flame penetration into the pore. Composite and ballistic powders were mainly studied.

General pattern of pore ignition. The ignition regime, which propagates in the form of successive displacements of the burning front (Figure 46), is the most typical.* Application of optical methods yielded a detailed pattern and the characteristic features of the flow of the products in the zone adjoining the ignition front. The flow pattern is very clear when metal particles are introduced into the powder. It was found that the combustion products move at a high velocity in advance of the ignition front, heat the surface of the pore, and are cooled during this process. The combustion products always moved ahead of the ignition front, which separated the products moving along the pore from the stream of products flowing out from the pore.

The products in the pore with the open end move forward, in the main (in the direction of propagation, see Figure 46a). In the initial stage, the ignition velocity increases sharply along the pore; the ignition is like an avalanche (Figure 47), since the ignition front propagates along the preliminarily heated substance. However, the velocity is limited if the pore length is sufficient.

* Under certain conditions, when the products moving along the pore contain condensed particles, face-type ignition may be observed: the condensed particles falling onto the surface produce ignition before the main front. Experiments have shown that the minimum size of particles producing face-type ignition is 85–100 $\mu$.


FIGURE 46. Motion picture of the ignition of a single pore:

a) open pore; b) closed pore.

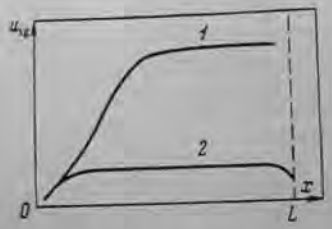


FIGURE 47. Variation in ignition velocity along closed (1) and open (2) pores.

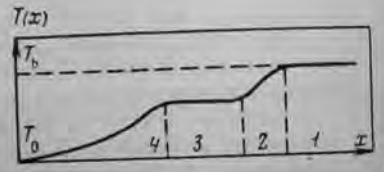


FIGURE 48. Temperature distribution $T(x)$ along an open pore during ignition (composite propellant powder, $p = 1$ atm; $d_0 = 4$ mm).

In the closed pore, the movement of the products in advance of the ignition front is more complex; circulation currents (see Figure 46b) are observed when the products move in a direction opposite to the propagation of the ignition front. These currents are very important in heat transfer during ignition of the closed pore. They arise because the ignition front is not plane: its individual sections move at different velocities. The combustion products from the sections ahead of the front are also the source of circulation jets. A detailed investigation of the structure of the ignition front and temperature measurements showed that, in the case of a composite propellant powder, the following characteristic zones are observed (Figure 48): the flame zone (1), the weakly luminescent zone (2),



the mixing zone (3), and the condensation zone (4). The ignition front corresponds to the boundary between zones 1 and 2. Circulation of the products starts in zone 4. The gases in this zone consist of the pyrolytic products of the propellant and can burn in the air. In the closed gap, the extent of the temperature zones hardly varies as the flame propagates. It is of interest that the ignition velocity of the closed pore is practically constant over a long section of the pore (see Figure 47). This experimental fact was established by Bakhman /109/. A decrease in velocity was observed at the closed end.

The spatial extent of the zones is simultaneously reduced with increasing external pressure and, at the same time, the temperature of the combustion products increases. The gas temperature in the pore of the composite propellant is as high as the maximum burning temperature, even at comparatively low pressure (10–20 atm) and in sufficiently narrow pores ($d_0 \simeq 0.1$ mm). This result agrees with published data, according to which the maximum burning temperature of an ammonium perchlorate-based composition is reached at a distance $h_м$ from the surface of the order of $10^{-3}$ cm.

The small distance $h_м$ between the surface and the high-temperature zone considerably facilitates not only impairment of burning (see section 15), but also the growth of convective burning along the pores. This is explained by the fact that the flame in the case of the composite propellant penetrates into identical pores at lower pressures than in the case of substances having larger $h_м$ (such as nitroglycerin powder), and at a higher velocity. It is known /81, 83, 163/ that $h_м$ is one order higher for the composite propellant than for the nitroglycerin powder.

Temperature measurements in a pore of nitroglycerin powder of width $d_0 < 2h_м$ showed (Figure 49) that, at a pressure of 30 atm, the temperature at the instant immediately after penetration is sufficiently low (about 1000°K) and increases as the pore begins to burn. Burning of the powder in the pore is flameless in the initial stage and, up to $d_0 \simeq 2h_м$, takes place at a velocity lower than the normal velocity /84/.


FIGURE 49. Temperature $T(t)$ (1) and pressure $\Delta p(t)$ (2) recordings in the bulk of the bomb when burning penetrates into the open pore (nitroglycerin powder, $p = 30$ atm, $d_0 = 100$ μ).

Burning in the pore is unstable under certain conditions, as indicated by repeated ignition of the pore followed by quenching. Anomalous burning in the pore is observed at lower, near-atmospheric pressures.

Figure 50 shows photographs of anomalous burning. The ignition front on frame 1 propagates along the whole pore length. The substance burns for $10^{-3}$ sec and is then quenched after a very short time $t < 2 \cdot 10^{-3}$ sec. At the instant of being quenched there is a considerable increase in the luminous intensity of the flame. The substance did not burn 0.004 sec, whereupon ignition started at individual points (frames 2, 3) and propagated throughout the pore.

FIGURE 50. Photographs of anomalous burning of the substance in the pore.

Repeated pore ignition (after quenching) resulted either from gradual propagation of the front, or from growth of burning at individual points. The latter case is characteristic of composite powders and points to the important role of processes resulting from subsequent quenching in the condensed phase.

Anomalous burning may be explained by concepts developed by Zel'dovich /107/ and applied to burning of powder in a semiconfined volume, since the igniting pore is a divergent nozzle (more accurately, a combination between a divergent and a thermal nozzle) with a very small free volume. Zel'dovich showed that under critical efflux conditions, when the relaxation time of the chamber is much shorter than the relaxation time of the heated layer (i.e., at low pressure), burning of the powder in a chamber with a small free volume is unstable and anomalous.

Another possible reason for the anomalous burning is that stable burning of the substance cannot take place in the narrow pore in the absence of an active (leading) combustion zone.

Effect of various factors on the ignition velocity of a closed pore. We now deal only with a closed pore, the ignition velocity of which is maintained constant over its length.

Bakhman /109/ found that the dimensionless propagation velocity of burning $\chi = u_{ig}/u$ into the gap between the wall and the burning powder charge increases with decreasing gap width until a limiting value is reached. After passing the maximum it falls abruptly to unity ($u_{ig} = u$). Our experiments showed that, with increasing external pressure, the maximum of function $\chi(d_0)$ is shifted to the region of smaller pore sizes; at the same time the propagation velocity increases (Figure 51). We mainly investigated the section of the $\chi(d_0)$ curve to the right of the maximum. As expected, the ignition velocity $u_{ig}$ as a function of the conditions varies very widely (from some tens of millimeters per second to hundreds of meters per second).

It is convenient to study the effect of different factors on the ignition velocity when penetration of burning does not produce a large excess pressure. This can be accomplished if the slit charges of types $a$ or $b$ (see Figure 37) (but for large values of $d_0$) are combusted in a Crawford bomb. Under these conditions the charge burns according to the spontaneous mechanism.



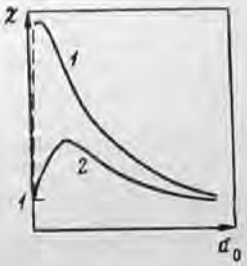


FIGURE 51. Dimensionless ignition velocity as a function of the closed pore width at different pressures:

1) $p_1$; 2) $p_2$. $p_1 > p_2$.

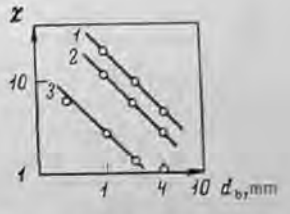


FIGURE 52. Ignition velocity as a function of pore width:

1) $p_0 = 30$; 2) 10; 3) 1 atm.

Tests in a Crawford bomb. We studied the effect of the bomb pressure $p_0$ and gap width $d_0$ on the mean propagation velocity of burning over the closed gap. The results for a composite propellant powder are shown in Figure 52: the velocity of pore ignition increases with increasing pressure and decreasing pore width.

Processing of the data yields

$$\chi d_0 p_0^{0.8} = 0.25 \text{ cm} \cdot \text{atm}^{0.8},$$

A similar type of function can be derived from the theory. In contrast to the initial pressure, changes in the initial temperature of the powder from +20° to −70°C have hardly any effect on the velocity of pore ignition.

A series of experiments was conducted in which the composition of the powder was varied. The physicochemical properties of the organic fuel in an ammonium perchlorate-based composite propellant was found to have some effect on the ignition velocity of the pore surface. As fuel we used polystyrene, poly(methyl methacrylate), bitumen, and polyester. A metallic fuel (aluminum) has a special effect. Aluminum particles with a mean mass diameter of about 15 $\mu$ were used. They replaced the oxidizer in the 15% bitumen + 85% ammonium perchlorate system. The resulting data are represented below ($p_0 = 50$ atm, fissure diameter $d_0 = 0.1$ mm, $L = 30$ mm).

| Al, % | 0 | 5 | 10 | 20 |
|---|---|---|---|---|
| Ignition velocity, m/sec | 1 | 1.33 | 0.97 | 0.56 |
| Dimensionless ignition velocity | 59 | 74 | 64 | 42 |

When aluminum is introduced in amounts up to 5–10% the ignition velocity increases, while higher levels display a flegmatizing effect. A similar effect was observed earlier by Andreev and Rogozhnikov /68/, who performed tests with binary ammonium perchlorate + Al mixtures in the powdered state.

Another experimental series was conducted to study the role of the geometrical pore size. Comparative research on charges of types a and b (see Figure 37) and on charges with different fissure depth $L$ showed that the ignition velocity of fissures possessing equal ratios $L/d_0$ differs.* The ignition velocity increases in passing from charges of type a to charges of type b, and with increasing fissure depth.

The ignition velocity depends essentially on the pore shape. If a flat pore (fissure) is replaced by a cylindrical pore with the same hydraulic diameter, $u_{ig}$ is much lower. At present, there is no satisfactory explanation for this phenomenon. It may be assumed, however, that the growth of circulation currents of the combustion products is impeded in the cylindrical channel.

The ignition velocity increases considerably in pores with rough walls. Penetration of burning in this case becomes more intensive, because the heat transfer coefficient increases in the region of the projections. Moreover, the projections are more rapidly heated and more readily ignited.

Experiments in a manometric bomb. If tests are performed in narrow and sufficiently deep fissures, they are ignited at such high velocities that considerable excess pressure is produced in them /59, 110/. In this case the experiments should be performed in a manometric bomb (Figure 5), which enables one to record the pressure in the fissure. The pores were confined in a strong shell made of plexiglass and steel. It was found that excess pressure inside the pore has a tremendous effect on the ignition process, since the ignition velocity and the pressure in the pore are strongly correlated. The above nature of the effect of various factors on the ignition velocity of the fissures is also valid in this case, the only difference being that the general pattern is more pronounced. The onset of excess pressure in a narrow pore brings about an interesting paradox: with decreasing fissure width (to $d_0 = d_{cr}$) the ignition velocity and the maximum excess pressure in the pore ($p_p^*$) increase continuously. On the other hand, upon a slight reduction in $d_0$ burning does not penetrate into the fissure, i.e., the section of the $\chi(d_0)$ curve to the left of the maximum becomes so narrow that it cannot be observed (Figure 51).

Some idea about the absolute ignition velocity of a fissure in a composite propellant powder is given by the figures cited below ($p_0 = 50$ atm, $L = \text{const}$). The velocity of normal burning at $p_0 = 50$ atm is about 10 mm/sec.

| | | | |
|---|---|---|---|
| $d_0$, mm | 0.6 | 0.4 | 0.2 |
| $u_{ig}$, m/sec | 55 | 100 | 300 |
| $p_p^*$, atm | 300 | 700 | 1800 |

The ignition velocity may be two or three orders of magnitude higher than the normal burning velocity and may reach several hundred meters per second. This result is noteworthy, because such high convective burning velocities are observed for nondetonating systems, such as composite propellant powders /160/.

Experiments with composite powders at various external pressures $p_0$ showed that the ignition velocity increases with increasing pressure, whereas the time lag before ignition $t_i$ drops abruptly:

* In the case of fissures of type b we used half the real value of the width in the calculation of $L/d_0$; in other words, we allowed for the "one-sided" character of the fissure.



| | | | |
|---|---|---|---|
| $p_0$, atm | 10 | 30 | 100 |
| $t_i$, msec | 20–40 | 5 | 2.0 |
| $u_{ig}$, m/sec | 0.2 | 70 | 100 |
| $p_p^*$, atm | 10 | 300 | 400 |

Ignition of the fissure in the manometric bomb corresponds to conditions of intensive heat supply, when gas phase processes play an important role. This is confirmed by the decrease in the time lag before ignition with pressure and by the estimate of the heat flux. The heat flux at the inlet part of the fissure was calculated from the expression $q = \alpha(T - T_w)$ for $p_0 = 50$ atm and $d_0 = 0.1$ mm and found to be about 200 cal/cm$^2$·sec. In this equation, $\alpha$ is the heat transfer coefficient, calculated from the Nusselt number /113/; $T$ is the temperature of the filtering gases and taken equal to the combustion temperature of the igniter, $T_w$ is the mean wall temperature. The time lag before ignition for a composite propellant powder measured under these conditions was 5 msec.

The question naturally arises as to the maximum possible limiting ignition velocity of a narrow pore of constant cross section when the pressure drop is large. It follows from general considerations that the ignition velocity cannot be higher than the velocity of the gas moving along the pore, i.e., the sonic velocity in the products (1000–1200 m/sec).* The maximum pore ignition velocity was about 600–700 m/sec in our experiments.

## Aftereffect of penetration of burning into a fissure /12, 59, 110/

Determination of excess pressure in a nondeformed fissure. It can be shown that pore ignition at a velocity considerably exceeding the normal burning velocity of substances must lead to excess pore pressure $\Delta p = p_p - p_0 \neq 0$; this was confirmed experimentally elsewhere.** The pressure in the pore is a function of various fundamental parameters:

$$p_p = f(u_{ig}/u',\ d/h_w,\ L/d,\ \varkappa,\ x/L), \qquad (49)$$

where $u'$ is the pore deflagration velocity; $L$ and $d$ are the pore depth and width, $\varkappa$ is a coefficient allowing for resistance to outflowing products; $x$ is the coordinate whose zero corresponds to the pore inlet.

The first two parameters in (49) are associated with burning and ignition, and the others with the geometrical dimensions of the pore and the state of its surface.

The fissure pressure was studied experimentally in a manometric bomb (Figure 5). The fissure was formed from two thin (2–3 mm) powder disks confined in a firm plexiglass-steel shell. This practically prevented deformation of the fissure during burning. Figure 53 shows a schematic diagram (Figure 53a) and oscillograms (Figures 53b, c) of pressure recordings in the fissure near the closed bottom end (lower curve 1) and in the

* This applies when no shock wave arises in the pore and the friction of the gas against the pore wall is disregarded.

** Serebryakov /111/ analyzed quenching after shooting of Kimberlevel gas powder and suggested that excess pressure arises in the narrow channels.

bulk of the bomb (upper curve 2). The pressure increases from the bottom to the top, and the time from left to right. The pore pressure curve $p_p(t)$ is recorded as follows. During a period of the order of $10^{-3}$–$10^{-4}$ sec after the beginning of the pressure increase in the bulk of the bomb the pressure in the pores begins to be equalized, because the combustion products penetrate into it. The break on the $p_p(t)$ curve indicates that the pore begins to ignite after time $t_L$.

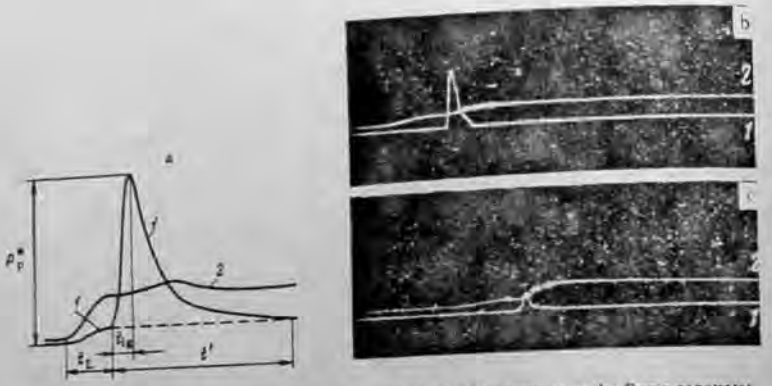


FIGURE 53. Schematic diagram (a) and oscillograms (b, c) of the pressure as the flame penetrates into the pore:

1) record of the pressure at the closed bottom end; 2) record of the pressure in the bulk of the bomb; $t_L$ is the time lag before ignition; $t_{ig}$ is the pore ignition time; $t'$ is the time during which excess pressure exists in the pore.

During period $t_{ig}$ the pressure in the pore increases and reaches its peak value $p_p^*$. The pressure then decreases, due to pore ignition and mechanical destruction of the fissure walls. The time during which there exists excess pressure $\Delta p \neq 0$ in the pore is $t' \simeq 10^{-4}$–$10^{-2}$ sec. Simultaneous optical recording of the process and of the pressure in the pores showed that, in narrow fissures, $t_L$ and $t_{ig}$ correspond approximately to the time lag before ignition and the ignition time of the fissure. It was established that all the factors bringing about an increase in ignition velocity lead to a pressure increase in the fissure.

The pressure in the fissure was studied as dependent on parameter $L/d_0$, which is the ratio of the burning surface to the area over which flow occurs (the Pobedonostsev parameter). Some of the results for a composite propellant powder are shown in Figure 54, which shows that with increasing $L/d_0$ ($d_0$ is decreased while $L$ = const) a gradual pressure increase in the pore is noted starting from some critical value $(L/d_0)_{cr}$. There is no simple geometrical similarity: in pores with the same geometry ($L/d_0$ = const) the pressure increases with depth, due to the difference in the ignition velocities of geometrically similar pores.

The experimental data are satisfactorily described over a wide range of variations by the function*

* This equation is correct for both subsonic and sonic (critical) efflux velocities of the combustion products.



$$\Delta p_m = 1.1 p_0 [L/d_0/(L/d_0)_{cr}]^n - p_0, \qquad (50)$$

where $(L/d_0)_{cr}$ is the value at which $\Delta p_m = 0.1\, p_0$; $n$ is a constant whose value depends on the fissure depth ($n$ is close to unity for a fissure a few centimeters deep).

Equation (50) automatically allows for the nature of the pore ignition and also for the nonsteady-state effects of the burning of powder in the fissure.

The values of $\Delta p_m$ when $L/d_0$ is smaller than $(L/d_0)_{cr}$ can be calculated by the following equation, which was derived from the law of conservation of mass and momentum for an incompressible liquid without allowance for friction at the wall*:

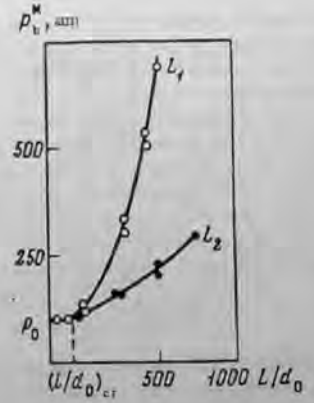


FIGURE 54. Excess pressure in fissures of various depths as a function of parameter $(L/d_0)$, $L_1 > L_2$.

$$\Delta p_m = c \frac{u_0^2}{p_0} \left(\frac{L}{d_0}\right)^2, \qquad (51)$$

where $c = \rho_p^2 RT/M$ ($\rho_p$ is the density of the powder; $M$ and $T$ are the molecular weight and temperature of the combustion products); $u_0$ is the normal burning velocity.

For small pressure increments $\Delta p_m \ll p_0$ the burning velocity $u_0$ in expression (51) depends only on the pressure $p_0$ in the rocket chamber.

If typical values of the parameters are inserted into (51) we obtain

$$\left(\frac{L}{d_0}\right)_{cr} = 20 p_0/u_0. \qquad (52)$$

When $(L/d_0) > (L/d_0)_{cr}$, equation (51) gives lower results than experiment. This indicates that our computations must allow for the dependence of the ignition velocity on pressure, the velocity of the gas flow,** and on the nature of flame propagation along the fissure.

Unlike composite powders, the excess pressure in the fissure of nitroglycerin powder at low bomb pressures is so small that it cannot be determined, though the flame also penetrates into the fissure. However, a large excess pressure arises in the fissure if we combust a slitlike charge at elevated pressures. This result may be explained if we allow for differences between the burning mechanisms of composite propellant and ballistic powders.

Fissure deflagration /12, 59/. When a gas stream flows past a powder, its burning velocity increases. This effect is termed erosive burning. An increase in the burning velocity is usually associated with eddy formation in the surface layer of the gas, and leads to an increase in the heat flux into the condensed phase of the powder.

* Equation (51) was first verified by Leipunskii /92/ for the burning of an inserted cylindrical charge in a rocket engine.

** Such a computation was performed by Kirsanova /117/.

The gas supply from the hot surfaces of the fissure increases, due to excess pressure and erosive effects. The oscillogram of Figure 53c indicates that the onset of the pressure increase in the fissure is related to a considerable increase in pressure in the bulk of the bomb; it can also be seen how the erosive peak is formed on curve 2. The height of this peak determines the mean (during the action of the excess pressure) burning velocity of the powder in the slit. The variation in the gas supply in the fissure can thus be related to the excess pressure impulse $\int_0^{\tau} \Delta p\, dt$.

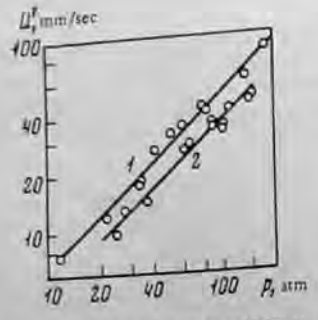


FIGURE 55. Erosion burning velocity as a function of pressure in the sonic flow of the products:

1) nitroglycerin powder; 2) composite propellant powder.

A special feature of erosive burning of the fissure is the presence of high gas velocities (up to sonic) and high pressures. At high pressures the erosive effect becomes considerable, since experiment has shown that the pressure dependence of the erosive burning velocity $u'$ becomes stronger. For instance, in sonic flow (when the gas velocity is equal to the sonic velocity in the products) function $u'(p)$ assumes the form (see Figure 55)

$$u' \sim p^{0.8} \qquad (53)$$

independently of exponent $\nu$ in the normal burning law $u = bp^{\nu}$. For powders $\nu$ is much less than 0.8. A function of type (53) was also established by Pokhil et al. (cited in /59/). It can be derived theoretically starting from the ratio between the Nusselt and Reynolds numbers, describing heat transfer in turbulent gas flow /113/.

When the pressure is considerably increased ($\Delta p \gg p_0$) we observe mechanical destruction of the fissure walls in the inlet part. The zone of destruction is usually bell-shaped. Completion of burning of the ejected powder particles led to an abrupt pressure increase in the bulk of the bomb.

These results were obtained when the fissure was practically undeformed and could not grow. The slitlike charge, formed by thin disks of the powder, was placed in a strong casing. We shall now examine what happens during burning with a fissure of limited size enclosed in the bulk of the powder, when there is a possibility that the fissure can grow.

### Fissure growth

Burning penetrates into narrow pores (fissures) at a high velocity and consequently gives rise to excess pressure in the fissure. Our experiments showed that, in principle, the local pressure increase in the burning fissure may under certain conditions lead to its growth (increase in its depth). Special theoretical and experimental research /110, 114, 117/ was based on data of Belyaev et al. /12, 59/.



We studied the behavior of fissures in the bulk of the powder when there is the possibility of extension (deformation)* and intergrowth of fissures. The solution of the problem must take into account the burning process in the fissure and the ability of the powder to resist the growth of fissures. We determined the size of the fissures, which grow (unstable fissures) when burning penetrates into them. No growth occurs in the case of stable fissures.

The mechanical stability of burning fissures in powder was studied theoretically by Leipunskii and Kirsanova /114/, whose main results are reported below. They considered (Figure 56) a flat fissure, extending to infinity in the direction of the $z$ axis. The fissure was arranged in the $xy$ plane perpendicular to the burning surface in the semiinfinite space of the powder. The fissure was subjected from all sides to hydrostatic compression by pressure $p_0$. It was assumed that ignition of the fissure surfaces and efflux of the combustion products into the steady-state zone take place instantaneously. It was further assumed that the pressure increase in the fissure is small in comparison with the pressure in the chamber $p_0$, so the burning velocity of the powder in the fissure was regarded as constant: $u(p) = u(p_0)$.

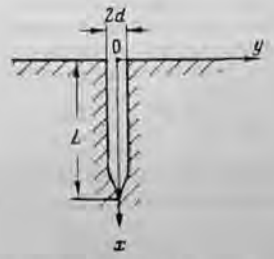


FIGURE 56. Schematic diagram for computation of the mechanical stability of a burning fissure.

First, Leipunskii and Kirsanova determined the magnitude and distribution of the pressure in the planar burning channel and then considered the equilibrium of the fissure, which is expanded by the excess pressure. The problem was solved in a static formulation, i.e., the excess pressure was regarded as time-independent. They applied the mathematical theory of equilibrium fissures, constructed by Barenblatt /115/. According to this theory the contour of the fissure remains immobile as long as the loads acting on it are small and balanced by molecular adhesive forces, acting in the small end region of the fissure, namely, the region where the edges of the fissures are so close to each other that the molecular forces are very large. With increasing load the adhesive forces increase (because of deformation) to their limiting values. Such a fissure may be termed the limiting equilibrium fissure. The overall characteristic of the limiting value of the adhesive forces proposed by Barenblatt has the form $K = \int_0^a \frac{g(x)\,dx}{\sqrt{x}}$, where $g(x)$ is the distribution of the limiting adhesive forces in the end region $a$ of the fissure; $K$ is termed the modulus of adhesion. A further increase in load leads to fissure growth.

The distribution of excess pressure in a flat fissure of length $l$ and width $2d$ was determined from the conditions of conservation of mass and momentum flows:

* The deformation of the fissure is naturally accompanied by a decrease in excess pressure in comparison with burning in an undeformed fissure of the same depth.

$$\Delta p(x) = p(x) - p_0 = \Delta p_m (2x/l - x^2/l^2), \tag{54}$$

$$\Delta p_m = \frac{\gamma - 1}{\gamma} q \frac{\rho^2 u^2 l^2}{p_0 d^2},$$

where $\Delta p_m$ is the pressure near the bottom ($x = l$) end of the fissure ($\gamma$ is the adiabatic exponent and $q$ the heating power of the powder).

The equilibrium condition of a fissure of length $(-l, l)$* kept open by symmetric pressure $\Delta p(x)$ has the form /115/

$$\frac{K}{\sqrt{2l}} \geqslant \int_0^l \frac{p(x) - p_0}{\sqrt{l^2 - x^2}} dx. \tag{55}$$

The modulus of adhesion $K$ is determined experimentally under appropriate conditions. Integration of (55) yields the half-width $d$ of the stable fissure of length $l$:

$$d > \sqrt{\frac{\gamma - 1}{\gamma} q \frac{\rho^2 u^2}{p_0 K} \sqrt{2} \left(2 - \frac{\pi}{4}\right)} \cdot l^{3/4}. \tag{56}$$

The equality in (56) determines the limiting dimensions of the stable fissure. Substitution of (56) into (54) permits calculation of the pressure in the limiting stable fissure. When $x = l_{sp}$,

$$\Delta p_m = \frac{K}{\sqrt{2 l_{lim}} \left(2 - \frac{\pi}{4}\right)}. \tag{57}$$

The pressure inside the fissure leads to its deformation (widening). This fact is taken into consideration by setting

$$d = d_0 + \Sigma, \tag{58}$$

where $d_0$ is the initial half-width of the fissure, while $\Sigma$ is the displacement arising from pressure $\Delta p(x)$ given by (54).

The displacement of the edges of a flat fissure in a powder with Young's modulus $\varepsilon$ and Poisson's ratio $\mu$ was calculated on the basis of classical elasticity theory /116/. When $|x| \leqslant l$, it yields an equation of the type

$$\Sigma = \frac{\Delta p_m l}{\varepsilon} (1 - \mu^2). \tag{59}$$

It follows from equations (57) and (59) that the opening of the limiting stable fissure is

$$\Sigma = \frac{K}{\varepsilon} \frac{(1 - \mu^2)}{\sqrt{2} \left(2 - \frac{\pi}{4}\right)} \sqrt{l_{lim}}. \tag{60}$$

* It has been shown /114/ that the pattern remains unchanged, if additional interaction of region $x \geqslant 0$ with region $x < 0$ is introduced.



Kirsanova and Leipunskii /114/ finally employed relationships (56), (58) and (60) to determine the boundaries of the region of stable flat fissures in the form

$$d_0 = l_{lim}^{3/4} \sqrt{\frac{\gamma - 1}{\gamma} q \frac{\rho^2 u^2}{p_0 K} \sqrt{2} \left(2 - \frac{\pi}{4}\right)} - \frac{K (1 - \mu^2) \sqrt{l_{lim}}}{\varepsilon \sqrt{2} \left(2 - \frac{\pi}{4}\right)}. \tag{61}$$

This equation is presented graphically in Figure 57 (curve 1). To the right of curve 1 lies the region of stable fissures and to the left the region of unstable (growing) fissures. The larger the modulus of adhesion, the wider the stability region. It is interesting that short fissures are stable at a reasonably small initial width ($d_0 \to 0$) for which burning can still penetrate. The adhesive forces compensate widening of short fissures. The size of stable fissures of zero width ($d_0 = 0$) is determined from (61) as

$$l' = \left[ \frac{K}{\sqrt{2} \left(2 - \frac{\pi}{4}\right)} \sqrt[3]{\frac{\gamma}{\gamma - 1} \frac{p_0}{q} \left( \frac{1 - \mu^2}{\rho u \varepsilon} \right)^2} \right]^2. \tag{62}$$

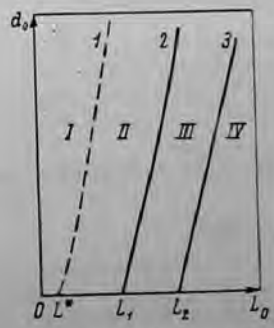


FIGURE 57. Stability regions of a burning fissure:

I—IV) stability regions; 1—3) stability boundaries.

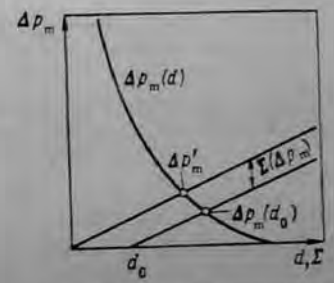


FIGURE 58. Graphical determination of excess pressure in a deformed fissure.

Such fundamental calculations of the mechanical stability of a burning fissure /114/ were based on the fact that fissure growth is due to excess pressure, which is created when the flame penetrates into it.

A few comments are in order before examining experimental research on the stability of pores /110/. Calculation of pressure increase in the deformed fissure $\Delta p_m$ is of independent interest, for instance, when estimating the increase in gas supplied from the burning surface, since, in general, the burning velocity in the fissure exceeds the burning velocity outside the fissure.

It will be clear from the following that we must know $\Delta p_m$ in fissures whose depth exceeds the limiting depth, corresponding to the boundary of

mechanical stability (curve 1, Figure 57). On the other hand, direct experimental determination of $\Delta p_m$ in a closed fissure placed in the bulk of the powder presents considerable difficulties.

The method proposed by Kirsanova and Leipunskii /114/ is used to calculate $\Delta p_m$ in a deformed pore /110/. However, the experimental function (50) is employed in place of expression (54) for $\Delta p_m(l/d)$ (which holds for small $\Delta p_m$). It was thus possible to determine the excess pressure $\Delta p_m$ over a wide region ($0.1\ p_0 < \Delta p_m < p_0$) up to the onset of sonic efflux. Moreover, expression (50) allows for ignition, the pressure dependence of the burning velocity, the gas velocity in the fissure, and also for nonsteady-state effects. Therefore, no special assumptions need be introduced about the ignition conditions and the nature of burning of the powder in the fissure. Finally, the calculation does not involve consideration of the mechanical stability of the fissure and consequently the results may be applied to growing fissures.

We considered system of equations (50), (58) and (59), and solved it by graphical (Figure 58) and analytical methods.

A maximum possible pressure increment $\Delta p'_m \geq \Delta p_m(d_0, l_0)$ (see Figure 58) was found to exist for each powder. Quantity $\Delta p'_m$ is a function of the physicochemical and physicomechanical characteristics and holds in fissures of width $d_0 = 0$ for any initial $l_0$.

Simultaneous solution of (50) and (59) for $n = 1$ and $d = \Sigma$ yields

$$\Delta p'_m = \frac{p_0}{2}\left[\sqrt{1 + \frac{4.4e}{p_0(1-\mu^2)\left(\frac{l}{d}\right)_{cr}}} - 1\right], \qquad (63)$$

where $\Delta p'_m$, $p_0$ and $e$ are expressed in kg per cm$^2$.

With allowance for (52), equation (63) yields the empirical equation

$$\Delta p'_m = 6.5 \cdot 10^{-2} \frac{(u_0 e)^{1/3}}{p_0^{2/3}}. \qquad (64)$$

This equation holds for $1.7\ p_0^2 < u_0 e < 30\ p_0^2$, where $u_0 = u(p_0)$ is expressed in mm/sec. It follows from (64) that for $p_0 = \text{const}$ the excess pressure is only determined by the burning velocity and Young's modulus (the effect of both these quantities on $\Delta p_m$ is identical).

When $d_0 \neq 0$, the relationship between $\Delta p_m$ and the initial dimensions of the flat pore is described in a first approximation by

$$\Delta p_m = \Delta p'_m\left[1 - \frac{d_0}{l_0}\left(\frac{l}{d}\right)_{cr}\right]. \qquad (65)$$

Let us now return to the problem of fissure growth. Our experiments /110/ showed that impairment of mechanical stability does not bring about catastrophic growth of the fissure. There are some features which are specific to the growth process of burning fissures and are disregarded by Kirsanova and Leipunskii /114/. First, allowance must be made for the time factor. The period during which increased pressure acts in the burning fissure is very short (of the order of $10^{-2}$ sec), owing to the ignition. The velocity with which the fissure begins to grow is therefore very important.



It was found that the loss in stability of burning fissures has very different aftereffects, depending on the excess pressure developed in it. Three characteristic situations may arise:

1. The increase in fissure depth while the pressure pushes open the fissure is negligibly small. Fissures that are unstable in the mechanical sense (to the right of curve 1 in Figure 57) practically retain their stability. This occurs when

$$\frac{K}{\left(2-\frac{\pi}{4}\right)\cdot\sqrt{2l_0}} < \Delta p_m < \frac{K'}{\left(2-\frac{\pi}{4}\right)\sqrt{2l_0}}. \qquad (66)$$

2. The increase in fissure depth during the action of the excess pressure is finite. Interruption of the growth is caused by the finite duration of the excess pressure, whereas the growth rate is short relative to the burning velocity. Such growth is termed restricted growth, and arises when

$$\frac{K'}{\left(2-\frac{\pi}{4}\right)\sqrt{2l_0}} < \Delta p_m < \frac{K^*}{\left(2-\frac{\pi}{4}\right)\sqrt{2l_0}}, \qquad (67)$$

where $K^* > K' > K$.

3. The increase in depth due to growth compensates the increase in fissure width in such a way that the pressure increment remains sufficient to ensure continuation of the growth. This case is observed when

$$\Delta p_m > \frac{K^*}{\left(2-\frac{\pi}{4}\right)\sqrt{2l_0}}. \qquad (68)$$

It should be noted that the deviation in the values of $K^*$ and $K^*$ from $K$ is due to the requirement that the growth rate be taken into account and that it is independent of the time-dependence of the modulus of adhesion. The boundaries of the practical stability and of the self-sustaining growth cannot be obtained by calculation alone without experiment, since calculation of the growth rate at the present state of the theory is impossible.

Insertion of the maximum pressure, given by (65), into (66)–(68) yields a relationship linking the stability of fissures during burning to their initial dimensions. The results are shown in Figure 57. The $L_0, d_0$ plane is divided by curves 1, 2, 3 into four regions /110/: I – region of absolute (mechanical) stability /114/; II – region of practical stability; III – region of organic growth; IV – region of self-sustaining growth.

The values of $L'$, $L_1$ and $L_2$ are determined in terms of $K$, $K'$ and $K^*$ and the limiting pressure increase $\Delta p'_m$:

$$L' \simeq \tfrac{1}{2}\left(\frac{K}{\Delta p'_m}\right)^2; \quad L_1 \simeq \tfrac{1}{2}\left(\frac{K'}{\Delta p'_m}\right)^2; \quad L_2 \simeq \tfrac{1}{2}\left(\frac{K^*}{\Delta p'_m}\right)^2.$$

The wider stability region in comparison with the region obtained by mechanical calculation is caused mainly by the low growth rate of the

fissure together with the short-term existence of the excess pressure in the burning fissure.

It is noteworthy that the possibilities of growth interruption (automatic stabilization) of the pore, arising when the growth rate does not strongly exceed the burning velocity, have also been discussed /114/.

Our experiments revealed the role of burning in the growth of the fissure. In the initial stage burning leads to fissure growth, since the flame penetrates the pores (formed at the end part of the fissure) at a high velocity. In the final stage burning may exert a stabilizing effect, because the carrier of the fissures (the sites where the stresses are concentrated) is completely combusted.

The data discussed in this section refer to the case when the charge contains only one pore.

## 23. PROPAGATION OF CONVECTIVE BURNING IN POROUS EXPLOSIVES

We now consider convective burning in disordered systems, in which the charge contains a group of interconnected pores prior to burning. The development of burning after impairment of stability will be dealt with. We emphasize at the very outset that this problem has been insufficiently investigated. The conclusions reached here are based on experiments described elsewhere /10, 12, 32, 56, 63, 65–69, 120/.

The experiments were conducted with explosives which were poured or pressed batchwise into plexiglass or steel casings. The charges were usually ignited from the upper, open end so that a convective regime was produced. The process was photographed from the lateral surface of the charge.

Characteristic features of convective burning. Typical photographs of convective burning, obtained under different experimental conditions, are shown in Figure 59. It is interesting to note how nonuniformly the ignition front shifts (this is very clear when the "built-in charge" system is used, see Figure 59a). The size of the nonuniformity is fairly large and may attain several charge diameters. When the sample is combusted in a Crawford bomb (no "built-in charge") the nonuniformity is smaller (Figure 59b, c). In some cases the trace has the form of steps (Figure 59b): the burning velocity first increases sharply, then decreases. The luminescent part of the flame has a striated structure. The nonuniform nature of the recorded luminescence is due to the fact that ignition of the inner pore surface by the penetrating gaseous jets of the combustion products does not proceed as a continuous front (uniform velocity) but at different velocities /10, 32/. First, the pores in the central part of the charge are ignited, then the burning front at some points reaches the lateral surface and propagates to all sides (this can be seen on the photographic records in the form of "tongues," Figure 59a). This outline was confirmed by high-speed motion pictures. It was noted earlier (section 15) that stable burning is not simultaneously impaired over the whole front, but only at individual centers which comprise the largest pores of the charge. This fact, and also the optical traces of convective burning, imply



that first large pores are ignited into which combustion products readily penetrate and which are most prepared for ignition. Further propagation of burning over the large pore is promoted by the pressure increase in it, which also leads to penetration of the flame into smaller pores.* Thus the pore size distribution (powder inhomogeneity) and the potential interaction between the pores are of considerable importance in the propagation of convective burning. These ideas are supplemented also by the following experimental data. Andreev and Chuiko /32/ performed experiments in which thin paper served as the bottom of the charge. In convective burning the paper is nonuniformly ignited at several points, whereas in stable burning ignition was uniform. Moreover, the flame was quenched by removing the pressure from samples burning in the convective regime, which indicated the existence of a system of branched channels in which were traces of burning /63/.

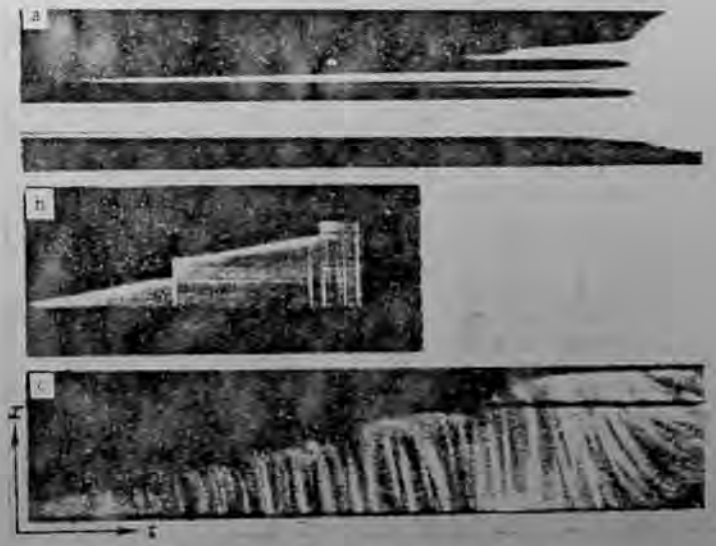


FIGURE 59. Typical photographs of convective burning of porous charges: a) 10% polystyrene + 90% ammonium perchlorate ("built-in charge"); b) 10% polystyrene + 90% ammonium perchlorate; c) tetryl; combustion was in a Crawford bomb in the last two cases.

Consequently, all the data indicate that the convective burning front is not straight but curved.

A characteristic feature of the convective burning regime is that penetration into pores is accompanied by intensive dispersion (ejection) of substance as individual grains or whole pieces, which are entrained by gaseous products flowing away from the charge surface.

* For such development, the pore must have maximum size and its depth must be sufficient.

The ejection of substance, whose residues are frequently observed at the bottom of the bomb, is clear on high-speed motion pictures. At the moment of ejection one usually observes a weakening of the luminous intensity. Subsequent ignition takes place on surface sections undamaged by ejection /63/.

Ejection arises from the presence of excess pressure in the pores. It is very pronounced during burning of pressed charges characterized by low mechanical strength.

This process gives rise to some interesting aftereffects. First, the burning zone is widened: particles ejected from the charge surface burn in a considerably thick layer. Also, ejection of substance restricts the pressure increase in the pores and is one of the stabilizing factors permitting high-speed deflagration without transition to detonation. In this sense the tests of Chulko /63/ and Kondrikov /56/ are very representative. They attempted to increase adhesion between particles of the substance and at the same time to make entrainment of the particles more difficult. In these tests, a rapid increase in velocity was observed when the charge consisted of free-flowing particles which were not connected to each other.

However, the stabilizing effect of ejection appears when no possibility exists for completely combusting the ejected particles, e.g., when the charge casing is short. The essence of the matter is that ejection of the substance leads to formation of a reactive suspension, which is combusted to the end product provided the gas outlet is sufficiently long. Accelerated burning of the suspension is accompanied by a rapid pressure increase over the charge surface, which leads to stronger penetration of high-temperature gases into the pores. Its consequence is a further increase in the surface and the burning velocity.*

Thus, convective burning of powder chips placed in long tubes proceeded at the outset with a low and almost constant velocity. The process velocity increased by a factor of a hundred as burning penetrated from the upper plane of the tube into the bulk of the material /56/.

It follows from the aforementioned that the convective burning model can be represented by the following simplified scheme. The leading edge of the gaseous combustion products, like the ignition front moving at a lower velocity, is uneven and very curved. The burning zone is very elongated and contains a large volume of explosive material, whose size decreases due both to burning at the surface and to the destruction of individual pieces of explosives by excess pressure in the pores. The growing burning surface presupposes the existence of high propagation velocities. As a result of erosion, the presence of a gas stream flowing past the explosive particles leads to an increase in their burning velocity which, together with the high pressure, leads to intensive complete combustion of the suspension. This model is similar to that of large-scale turbulent combustion of gaseous systems. Therefore, methods employed in the theory of turbulent burning can be applied to the theory of convective burning.

* The pressure during burning of suspensions may increase so rapidly, that the remainder of the explosive detonates. Andreev /32/ regarded the explosion of the suspension produced by burning as one of the most important ways for transition from deflagration to detonation. The possibility of such a mechanism for free-flowing charges is proved experimentally below (see section 22).



Convective burning regimes. There are various propagation regimes, depending on the experimental conditions and especially on the gas supply/gas removal ratio. As a rule the process is nonsteady: the velocity of convective burning increases or decreases along the charge. However, if the sample is ignited in air or in a Crawford bomb (the pores are filled with inert gas) convective burning of porous charges with a closed bottom proceeds at a practically constant velocity along the charges (Figure 59c). Complete analogy is observed with the ignition of a single closed pore. This regime, which is termed quasi-steady, was investigated to the greatest extent.

* Quasi-steady regime of convective burning. The general outline of the propagation of the quasi-steady regime is examined. Andreev and Chulko /32/ studied the effect of the density, particle size of the explosive, charge diameter and pressure on the velocity of convective burning. Homogeneous explosives (PETN, hexogen, tetryl) were pressed into plexiglass tubes (diameter 5 mm, height 35 mm) with a closed bottom and ignited in BD-1000 bombs at pressures of up to 1000 atm.

The pressure dependence of the burning velocity for PETN samples of different dispersity and density are shown in Figure 60. The low-pressure range displays stable layer-by-layer deflagration, whose velocity is almost independent of the density and increases linearly with pressure. On attaining the critical pressure the velocity abruptly increases, and the convective regime is established. Its characteristic feature is the strong pressure dependence of the burning velocity: $u_в = bp^\nu$, where $\nu > 1$. Some weakening of the $u_в(p)$ dependence at higher pressures is connected with the dilution of powdered explosive by gas (nitrogen), which serves as the inert additive, reducing the temperature of the combustion products penetrating into the pores. The mass of the nitrogen increases with decreasing density of the explosive and with increasing pressure.

It is of interest that the density dependence of the velocity of convective burning (at constant pressure) (Figure 61) has a form similar to that observed on ignition of a single pore (see Figure 51). As the density increases (the pore diameter decreases), the velocity of convective burning increases and then drops again. This velocity is highest at some optimal density, which is close to the density at which the highest specific pore surface is observed (Figure 14).

Unlike normal burning, the charge diameter considerably affects the velocity of convective burning (Figure 62) /32, 56/. The increase in burning velocity with charge diameter is evident at low densities, and is not related to changes in lateral thermal losses.

Equilibrium between gas supply and gas removal is established in the quasi-steady burning regime and remains stable for a limited charge length. An attempt will be made to establish the law governing variations in the quasi-steady velocity of convective burning on the basis of available experimental data and results derived in section 16. In the case of large pores, subject to the jet mechanism of flame penetration into charge pores, the following estimation variants are possible.

1. We assume that the burning velocity $u_в$ beyond the stability limit is higher than the normal velocity $u_0$, due to the increment $\Delta S$ in the burning surface $S_0$ arising from ignition of the pores to some depth, i.e., $N = u_в/u_0 = 1 + \Delta S/S_0$. After appropriate substitution and introduction of

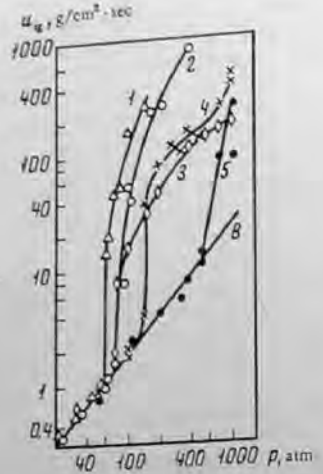


FIGURE 60. Pressure dependence of the burning velocity for PETN of different dispersity and density:

8) relationship for the high-density explosive. Particle size (μ) and density (g/cm³): 1) 200 μ and 1.08 g/cm³; 2) 200 and 1.17; 3) 20 and 0.5; 4) 20 and 0.71; 5) 20 μ and 1.17 g/cm³.

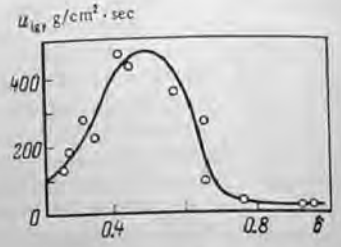


FIGURE 61. Dependence of the mass velocity of convective burning on relative density at 1000 atm (PETN, r= 20 μ).

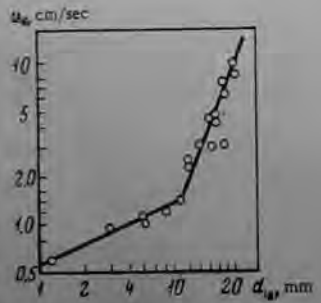


FIGURE 62. Dependence of the velocity of convective burning on charge diameter (hexogen, r = 130 μ, ρ = = 1.15 g/cm³, p =40 atm).

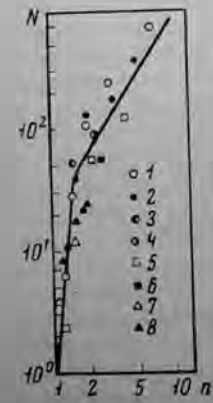


FIGURE 63. Generalized dependence of the quasi-steady convective burning velocity of powder charges:

1, 3, 4) PETN /32/; 2) hexogen; 5, 8) octogen /176/; mean particle diameter (μ) and density (g/cm³): 1) 200 μ and 1.17 g/cm³; 2) 200 and 1.08; 3) 200 and 1.07; 4) 20 and 1.15; 5) 400 and 1.2; 6) 110 and 1.05; 7) 70 and 1.07; 8) 60 μ and 1.08 g/cm³.



the variable $n = \varphi/\varphi'$ ($\varphi = \rho u d$), which shows how far burning proceeds beyond the stability limit, we obtain $N \sim n(1 + a_1 n)$. For large $n$, i.e., far from the limit, the ratio of the velocity of convective burning to the velocity of normal burning increases as $n^2$.

2. We apply the results of Krasnov et al. /162/, who obtained the following relationship for the velocity $u_{ig}$ of the ignition front immediately following the gas flow that enters the pore with velocity $v$:

$$\frac{v}{u_{ig}} = 1 + \frac{4\mathrm{Nu}\,\varkappa_g \varkappa_s}{u^2 d_p^2}. \qquad (69)$$

If $v$ is equal to the velocity of the jet of combustion products flowing into the pores, $N \sim n^2/(pn^2 + a_2)$, where $a_2$ is a constant depending on the charge characteristics. When $pn^2 \ll a_2$ we have $N \sim n^2$, but when $pn^2 \gg a_2$, $N \sim 1/p$, i.e., the velocity of the ignition front decreases with increasing pressure.

Figure 63 shows experimental data processing of work /32, 82/ on the burning of some powder charges of some explosives. Some correlation, similar to that expected, was obtained, regardless of the large scatter of experimental data due to poor reproducibility of the convective burning velocities. It would be of great interest to obtain results in the parameter range over which $N \sim 1/p$. Margolin's experiments with mercury fulminate are noteworthy here. He observed a decrease in the mechanical effect of convective burning of charges when the pressure increases considerably (300–500 atm). It is quite possible that the drop in the propagation velocity of convective burning together with nitrogen penetration into the pores may be responsible for this phenomenon. This situation is also probable, because at these elevated pressures $N$ was of the order of $10^2$ whereas in experiments with other substances $N$ was seldom higher than ten.

This problem has been investigated only to a very slight extent. It must be formulated and specified so that account is taken of the real pattern of convective burning, when the flame front does not propagate continuously but in the form of jets that enter the bulk of the charge.

Consider the propagation of convective burning when igniting a charge under increasing-pressure conditions; a "built-in charge" scheme is used. Under these conditions burning develops in a nonsteady fashion. At near-critical pressure convective burning, which started with a low velocity, may be retarded and pass to layer-by-layer deflagration (see Figure 34). Damping of the process is caused by ignition of the gaseous combustion products ahead of the ignition front near the closed bottom end.

When conditions are far from critical and elongated charges are used, the velocity of convective burning increases as it propagates and the process is accelerated. The accelerated regime of convective burning is characterized by deep pulsations (see Figure 59a), which indicate strong bending of the ignition front.

The pores present in the charge play a decisive role in the growth of convective burning. The pores over which convective burning propagates may also form during the burning process. This is observed, for instance, when an explosive charge burns in a closed deformable casing /120/. This effect is of considerable importance, especially during burning of high-density (cast or pressed) charges. The pores form as a result of widening of the inner channels due to the wedging action of the elevated pressure in it.

A general outline of pore formation was obtained from tests in which some of the explosive pressed to a high density $\delta = 0.98$ were directly replaced in the casing by an inert material. Analysis of the inert material (after ignition) showed that the gas penetrated into the gap between the casing and the charge, and also over the system of pores formed on the lateral surface of the charge.

The existence of this effect was also confirmed by the following experiment. Charges with diameter $d_{charge} = 10$ mm and made from ammonium perchlorate and polystyrene ($\delta = 0.98$) were ignited and the $p(t)$ curve recorded during burning. In some of the experiments the mixture was pressed into a thin-walled ($\Delta = 5$ mm) steel casing. In other experiments, an inserted charge encased on all sides with the exception of the upper front was used, and was not in direct contact with the thick-walled ($\Delta = 20$ mm) casing. In the latter case the charge was subjected to bulk compression. The charging density was kept constant. During burning of the charge pressed directly into the thin-walled casing the $p(t)$ trace showed an abrupt break, indicating process acceleration at $p \simeq 1$ kbar.* Burning of the inserted charge not in contact with the casing took place in layer-by-layer fashion, while the pressure in the casing exceeded 4000 atm.

Thus analysis of the growth of detonation must make allowance for the propagation of convective burning over pores formed by peeling-off of the charge from the casing.

The pressure increases continuously in the combustion zone in accelerated nonsteady-state propagation of convective burning in a porous charge and leads to further increase in the process rate. It follows from earlier considerations (p. 99) that an infinite increase in velocity is impossible. The process must be stabilized when the velocity of convective burning in the products is near-sonic. However, on igniting a porous charge of sufficient length this limiting case of the propagation of convective burning is practically not realized at the closed end. This is due to the fact that, with increasing process velocity, the intensity of the compression waves ahead of the ignition front increases and at a given threshold velocity the compression wave is able to initiate a chemical reaction. The initiation mechanism of the reaction changes and the regime of convective burning passes to the low-velocity wavelike system. The threshold velocity is determined by experiments in which the explosive charge was completely disengaged from the inert material plate (steel, plexiglass) /122, 125/. The plate prevents penetration of gaseous combustion products, and consequently interrupts convective burning but does not prevent the passage of compression waves. This approach allows one to separate convective burning from the wavelike low-velocity regime. The threshold velocity (maximum velocity of convective burning) for condensed high explosives (PETN, hexogen) was found to be 700–800 m/sec /120, 127/, i.e., much lower than the velocity at which stabilization of the convective regime can be expected.

Figure 64 shows a typical photograph of the process that arises when igniting PETN ($\rho = 1.45$ g/cm$^3$) in a plexiglass casing. It can be seen that practically immediately after ignition the convective burning regime sets in

* The calculation based on the equations of elasticity theory shows that at $p = 1$ kbar widening of the inner channel of the steel casing ($d_{charge} = 10$ mm, $\Delta = 5$ mm) is about 10 $\mu$.



FIGURE 64. Growth of explosion during ignition (PETN, $\rho = 1.45$ g/cm$^3$, $r = 500$ $\mu$, charge = = 5 mm).

FIGURE 65. Photograph of process propagation when separating the charge by an inert partition introduced into the low-velocity zone (PETN, $\rho = 1.45$ g/cm$^3$, $r = 500$ $\mu$, $d_{charge} = 5$ mm).

with the characteristic "staggered" front,* whose velocity increases with propagation and attains tens and hundreds of meters per second. This is accompanied by a decrease in pulsations at the luminous front. A further increase in velocity up to 900–1000 m/sec is characterized, as a rule, by a change in the slope of the trace due to the onset of the low-velocity regime. Naturally, when introducing a steel plate to separate the explosive charge in this zone, the process is transmitted through the plate at a somewhat lower velocity. The velocity then increased to its former value (Figure 65), while the plate remained unbroken.

### B. LOW-VELOCITY WAVELIKE REGIME OF EXPLOSIVE TRANSITION

Convective burning passes to the low-velocity regime of explosive transition in line with the scheme of the growth of explosion (Figure 44), and in the majority of cases precedes the onset of normal detonation. Figure 66

* Layer-by-layer deflagration of short duration, since the pressure in the closed system increases rapidly and attains the critical detonation value.

shows a photograph of transition from deflagration to detonation when the growth of explosion passes through the following stages: convective burning — low-velocity regime — detonation.

FIGURE 66. Photograph of transition from deflagration of PETN to detonation ($\rho = 1.55$ g/cm$^3$).

The speed of the low-velocity regime is much lower (2—10 times) than that of normal detonation. The wavelike nature of the low-velocity regime has been proved: the chemical reaction is initiated by the compression wave propagating over the explosive charge /120, 125—127/. Low-velocity regimes arise both during ignition of an explosive in a casing, and by the action of a weak shock wave on an explosive.

Apin and Bobolev /132/ were the first to observe propagation of the low-velocity regime in powdered explosive charges.* It was proved much later that the low-velocity regime also applied to high-density (cast and pressed) explosive charges /13, 120, 122, 125—129, 131, 159/.

The existence of low-velocity regimes was established for a wide range of homogeneous, composite and initiating explosives. As a rule, low-velocity regimes arise in systems capable of normal detonation.

Until quite recently, it was generally believed that the low-velocity regime represents an unstable process which either will be damped or will pass over to normal detonation. A very interesting result of recent research is that conditions could be determined subject to which the low-velocity regime propagates in a stable manner at a constant velocity along the charge and over a considerable distance (40—50 charge diameters).

Separation of the stability region made it possible to conduct systematic and detailed research on the propagation of the low-velocity regime. In the first place such research was carried out with powdered, and later with high-density, explosive charges.

* The low-velocity regime in powdered explosives is usually termed low-velocity detonation.



## 24. STABLE PROPAGATION OF THE LOW-VELOCITY REGIME

The term "low-velocity detonation" will be applied to powdered charges, and the term "low-velocity regime" to high-density charges (see the footnote on p. 88).

### Propagation of low-velocity detonation in powderlike explosives /122, 134 — 136/

Mainly homogeneous explosives (TNT, tetryl, PETN, hexogen) were studied in detail. Coarse crystalline powders were put into thin-walled casings made from cellophane or plexiglass. Low-velocity detonation was initiated by a weak shock wave, produced by the explosion of an especially active charge. Parfenov /135/ found that if a stable process sets in, its velocity is independent of the initiating power. The steady-state nature of the process propagation was also investigated by varying the charge length; the largest length over which stable low-velocity detonation was observed was 500 mm.

Stable propagation of low-velocity detonation was observed at certain particle diameters of the explosive and charge diameters. The dependence of process velocity on charge diameter for tetryl and PETN powders of various dispersity are shown in Figure 67.

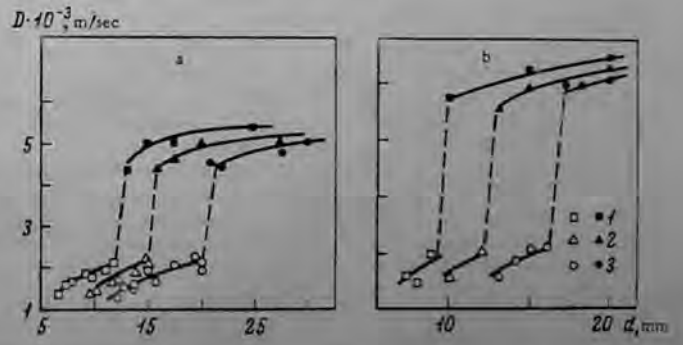


FIGURE 67. Rates of low-velocity (open circles) and high-velocity (full circles) detonation as functions of charge diameter /135/:

a) tetryl, $\rho = 0.92$ g/cm$^3$; 1) $r = 0.5$; 2) 0.8; 3) 1.3 mm; b) PETN, $\rho = 0.95$ g/cm$^3$; 1) $r = 1.5$; 2) 2.0; 3) 4.2 mm.

The top and bottom boundaries of the stability region of propagation are given by those values of the charge diameter whose magnitude is approximately proportional to the particle size of the explosive.

For small diameters, the process is damped outside the region of stable propagation, whereas for large diameters low-velocity detonation passes over to normal high-velocity detonation. The highest speed of low-velocity detonation (2000–3000 m/sec) is independent of the dispersity of the material and remains practically unchanged for all explosives.

Figure 67 shows that the rate of stable low-velocity detonation increases with charge diameter and decreasing particle diameter.

The pressure in the low-velocity detonation wave was measured by the "aquarium" /135/ and electromagnetic /122, 136/ methods. The results are summarized in Table 9. The pressure in the normal detonation wave of the investigated powder charge is about 50 kbar.

TABLE 9. Pressure in the low-velocity detonation wave

| Explosive (density 0.92–1.0 g/cm³) | Charge diameter, mm | Particle diameter, mm | Rate of low-velocity detonation, km/sec | Pressure, kbar | |
|---|---|---|---|---|---|
| | | | | aquarium method /135/ | electromagnetic method /122, 136/ |
| TNT | 20 | 0.5 | 2.12 | 14.8 | – |
| | 28 | 0.4–0.8 | 1.67 | – | 7.5 |
| Tetryl | 20 | 1.3 | 2.14 | 14.5 | – |
| | 20 | 1.0–1.6 | 2.0 | – | 13.4 |
| Hexogen | 20 | 2.0 | 1.98 | 10.4 | – |

It follows from Table 9 that the pressure in the low-velocity detonation regime is about 7.5–15 kbar and considerably lower than the pressures reached by normal detonation with the same charge diameters. Another feature of the process is that only an insignificant part of the total energy is evolved during propagation of low-velocity detonation; according to published data /135, 136/, heat evolution does not amount to more than 30–35% of the energy of normal detonation.

Other results /134, 135/ can be explained by the model of "explosive" burning /167/, according to which the chemical reaction takes place in the form of surface burning of the individual grains of the explosives. One fundamental reason in favor of the model is that the lower and upper charge diameters bounding the stability region of low-velocity detonation are proportional to the initial particle diameter.

Effect of charge density. Published data on low-velocity regimes were obtained with the aid of free-flowing or high-density systems. Systems of intermediate densities were not investigated.

We have shown experimentally that stable propagation of low-velocity regimes at intermediate charge densities is possible. The density dependence of the velocity of the regime was thus determined for PETN. Stable propagation of the low-velocity regime was observed when PETN, with initial particle diameter $r = 1.0–1.25$ mm, was encased in a low-strength plexiglass casing. The charge density was varied from 0.95 to 1.68–1.70 g/cm³; the regime was not present at densities exceeding 1.70. The results are illustrated in Figure 68, where the regime velocity in charges of density 1.45–1.70 g/cm³ is seen to be practically density-independent /120/.



At lower densities, the velocity increases with decreasing density (approximately, $W \sim 1/\rho$).

Low-velocity processes can therefore be propagated stably in charges of different densities by suitable selection of the experimental conditions.

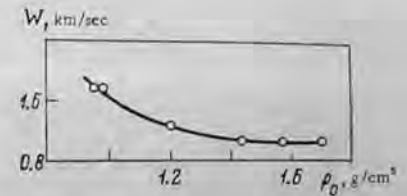


FIGURE 68. Density dependence of the rate of the low-velocity regime (PETN, $r = 1.0–1.25$ mm, $d_{charge} = 5$ mm, plexiglass casing).

Research on the propagation of the low-velocity regime in high-density explosive charges is very interesting because, unlike low-density explosives, the specific volume of the substance at the front of the compression wave does not change and the phenomenon is not distorted by the complex pattern created when the pores are suddenly closed. It was assumed that low-velocity regimes in high- and low-density systems have the same nature. This determined the approach to the problem of Sulimov et al. /166/, based on an attempt to reveal the main outline and to understand the nature of the low-velocity regime with the aid of a model as simple as the high-density explosive charge. Such an approach is convenient, especially because, at present, there exists no theory or physically justified mechanism of the low-velocity process.

### Propagation of low-velocity regimes in high-density charges

Stable propagation of low-velocity regimes in homogeneous high-density explosive charges was investigated elsewhere /127–129, 131, 166/. Bobolev et al. /127/ noted that the corresponding propagation velocity in a PETN layer ($\delta = 0.95$) clamped between flat plexiglass plates was about 1000 m/sec. Propagation in cast TNT encased in a steel tube (wall thickness 10–15 mm) took place at a constant velocity of 1800–2200 m/sec /131/. The observed propagation velocities were lower or close to sonic in the original explosive and varied over narrow limits. Some investigations /127, 131/ were carried out with invariant casing parameters. However, it should be emphasized that stable propagation of the low-velocity regime in high-density secondary explosives is observed only when the explosive is surrounded by a sufficiently strong casing, thus demonstrating the important role of the casing in the propagation of the low-velocity regime.

Systematic research was conducted with a view to explaining the effect of the casing on the speed of the low-velocity regime /128, 129, 166/.

Optical methods were employed in the case of PETN to study the propagation speed $W$ of the stable low-velocity regime on the wall thickness $\Delta$ of the steel casing. PETN of particle size 500 $\mu$ was pressed batchwise into the casing (made from steel 45) to density $\rho = 1{,}73$ g/cm$^3$ (relative density $\delta = 0.875$). The inner diameter of the casing was 5 mm and the charge length, 150–250 mm. The wall thickness was varied at intervals of 0,5 mm. These easy-to-design experiments not only made it possible to reveal the role of the casing, but also to obtain some essentially new results about the propagation patterns of the low-velocity regime.

The low-velocity regime was initiated mainly by ignition at the closed end of the charge by a bolt igniter or by a weak shock wave of known amplitude produced by detonation of a special charge. It was found that the regime velocity is independent of the initiation method. A driven photorecorder was used to measure the regime velocity over the steady-state interval of the process via radial openings (diameter 0.8 mm) in the casing situated 20 mm apart. The photographs were taken in natural light.

In addition to measuring the speed of the low-velocity regime, we determined the dynamic strength of the casings under loading conditions that approached those arising during the onset of the low-velocity regime. For this purpose the piezoelectric method was employed to directly measure in separate tests the maximum pressure $p'$ which arises in the channel of the casing at the instant of its destruction. The pressure was recorded near the ignition point, close to which (at a distance of 10–15 mm) the casing was destroyed. The piezoelectric probe and recording instruments used made it possible to record pressures up to 12 kbar at a growth rate $dp/dt < 0{,}3$ kbar/$\mu$sec.

The results demonstrate that the low-velocity regime in PETN is established 20–30 mm from the ignition point and propagates stably over the remainder of the charge (about 30–40 $d_{charge}$) at a velocity that is constant over the charge length.* Figure 69 shows characteristic photographs. Figure 70 presents the dependence of the regime velocity on the wall thickness of the steel casing /166/. These results correspond to the steady-state process. Each point on the $W(\Delta)$ curve represents the average value of 3–5 tests.

It can be seen that the speed of the low-velocity regime changes continuously from 1300 to 3300 m/sec. On increasing the steel casing thickness from 1,3 to 2 mm the speed increases from 1300 to 2000 m/sec; when $\Delta = 2$–$4$ mm a section with retarded velocity increase is observed. For a casing with $\Delta > 4$ mm the velocity increases again and reaches (at $\Delta \simeq 8$ mm) the limiting value of 3300 m/sec. Further increase in the outer diameter of the casing to 40 mm ($\Delta = 17{,}5$ mm) did not alter the speed of the regime.

Consequently, the use of casings made from one particular substance (steel 45) but with different wall thicknesses permits one to vary the speed of the low-velocity regime in high-density charges over a wide range.

* A casing with wall thickness $\Delta < 6$ mm was destroyed during the experiments; casings with thicker walls remained whole.



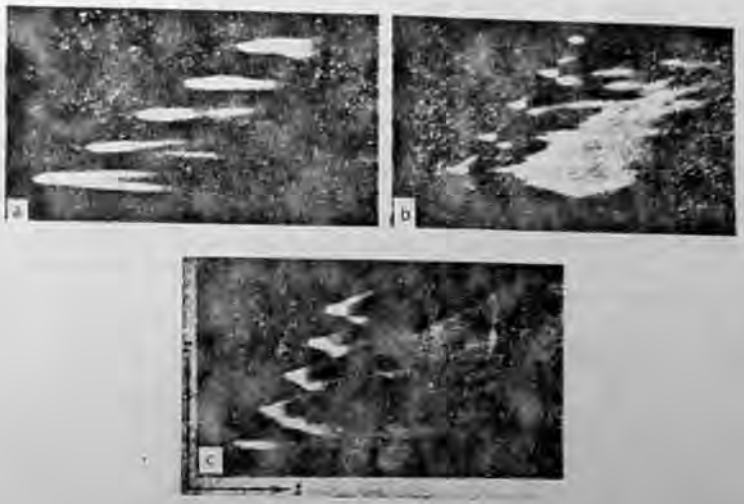


FIGURE 69. Photographs of the propagation of the low-velocity regime at different speeds (PETN, $r = 500$ $\mu$, $\rho = 1.73$ g/cm$^3$, $d_{charge} = 5$ mm, steel shell):

a) $W = 1500$ m/sec, $\Delta = 1.5$ mm; b) $W = 2400$ m/sec, $\Delta = 4.0$ mm; c) $W = 3300$ m/sec, $\Delta = 12.5$ mm.

In this respect solid explosives differ from liquid explosives, where the propagation of low-velocity detonation changes discretely. For instance, in nitroglycerin it is 1000 and 2000 m/sec, depending on the sonic velocity in the casing /122/.

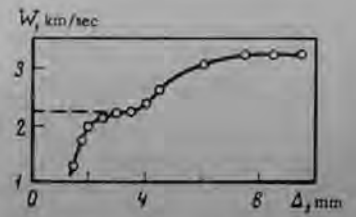


FIGURE 70. Dependence of the speed of the low-velocity regime ($W$) on the wall thickness of the steel casing (PETN, $r = 500$ $\mu$, $\rho = 1.73$ g/cm$^3$, $d_{charge} = 5$ mm).

Another important result of our research is that the speed of the low-velocity regime may be both higher and lower than the sonic velocity in the original explosive.* The dashed line in Figure 70 corresponds to the longitudinal sonic velocity in PETN with given density and particle size ($C_l = 2250$ m/sec); it was measured by ultrasonic techniques.** It is noteworthy that in earlier papers subsonic /125/ or near-sonic /131/ propagation was considered to be typical for the low-velocity regime in high-density explosives. The obtained data can also be used to explain the disagreement between the regime speeds observed in different tests

* Naturally, the subsonic process cannot be regarded as a detonation process.

** This value is the longitudinal sonic velocity in an infinite medium. The sonic velocity was determined with an UDM-1M instrument.

employing the same explosive. Function $W(\Delta)$ in Figure 70 becomes weaker at near-sonic speeds $C_1$ of the low-velocity regime.

Measurements of pressure $p'$, to which the steel casings of different wall thickness are subjected, are illustrated in Figure 71. The measurements were carried out for casings of wall thicknesses 0.7–2.7 mm with pressures $p'$ varying from 4 to 10 kbar. The results are described satisfactorily by the equation $p' = p_0\Delta^{0.7}$. The dashed section of the curve $p'(\Delta)$ in Figure 71 corresponds to extrapolation of the obtained data. The extremal point on the extrapolation curve was obtained from experiments with shock wave initiation and corresponds to the shock wave pressure at which the low-velocity regime with maximum speed (3300 m/sec) is still initiated. An insignificant increase in shock wave intensity will bring about detonation.

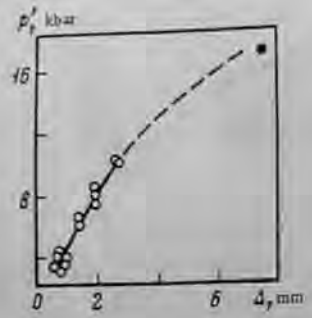


FIGURE 71. Dependence of the dynamic pressure $p'$ destroying the casing on the wall thickness (material of the shell is steel 45, $d_{charge}$ = 5 mm).

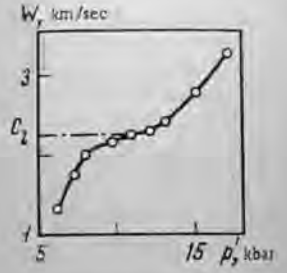


FIGURE 72. Function $p'(W)$ for PETN ($r = 500\ \mu$, $\rho = 1.73\ g/cm^3$, $d_{charge}$ = 5 mm).

The data presented in Figures 70 and 71 yielded the speed of the low-velocity regime as a function of the pressure in the casing $W(p')$ (Figure 72). Three sections can be distinguished on the $W(p')$ curve: 1) a subsonic section ($W < C_1$) with a strong $W(p')$ dependence; 2) a near-sonic section ($W \simeq C_1$) in which the regime velocity depends weakly on $p'$; 3) a supersonic section ($W > C_1$), where $W(p')$ becomes strong again.

The data indicate that the speed of the low-velocity regime is determined by the pressure attained in the casing and, eventually, by the amplitude of the compression wave propagating in the explosive. The main function of the charge casing is to maintain the pressure in the wave at a certain level. The fact that the strength of the casing (i.e., the resistance determined by the adhesive forces) has a decisive influence on the regime velocity was also confirmed by subsequent experiments. Surrounding a thin-walled ($\Delta$ = 1.3 mm) casing by a massive, but not strong water shell does not change the process velocity. The low-velocity regime does not propagate in PETN when employing a massive, but low-strength lead casing.



Additional tests were conducted in casings which were not as strong as steel casings. In thick-walled casings made from plexiglass, duralmin and brass, the limiting speeds of the regime were 1100, 1200 and 2600 m/sec, respectively, which are in agreement with the yield points of the materials used.

Function $W(p')$ (Figure 72) gives some idea about the effect of the shock wave amplitude on the regime velocity, since there are grounds to assume that the amplitude of the compression wave in the explosive does not exceed $p'$. The following fact speaks in favor of this assumption. In a casing with $\Delta$ = 1.3 mm ($W$ = 1300 m/sec) (see Figure 72) the pressure $p'$ = 6 kbar is close to (somewhat exceeds) the pressure reported by Bobolev et al. /127/ when the amplitude of the compression wave, measured directly by another (electromagnetic) method, was 5 kbar at $W$ = 1200 m/sec. Unfortunately, there are at present no direct measurements of the pressure in the compression wave of the low-velocity regime at its different propagation speeds.

During stable propagation, the speed of the low-velocity regime does not change over considerable charge lengths, which implies that the amplitude of the compression wave leading the process is maintained at a constant level. This situation arises when dynamic equilibrium exists between gas supply (owing to the chemical reaction) and gas removal (owing to deformation (widening) of the casing).

No detonation took place in our experiments; this can be explained by comparing $p'$ (see Figure 72) with the critical pressure $p_{cr}$ initiating shock-wave detonation. The value of $p_{cr}$ was measured in experiments with transmission of detonation through an inert (copper) partition (see section 29). We determined the minimum amplitude of the shock wave that propagated in the explosive and initiated detonation. The critical pressure was found to be 17 kbar for the investigated PETN charges ($\delta$ = 0.975) with steel casing.* If the pressure in the initiating wave was somewhat less than $p_{cr}$ (which was achieved by a small increase in the thickness of the partition), low-velocity regimes were created whose speed corresponded to the casing thickness. In a casing with $\Delta \simeq 8$ mm, a low-velocity regime could be initiated with a limiting speed of 3300 m/sec when the shock wave propagating in the explosive attained a pressure of about 17 kbar. This value is marked in Figure 71.

Comparison of $p'$ with $p_{cr}$ shows /128/ that, when the low-velocity regime propagates, the pressure in the casing is lower than the critical detonation pressure: $p' < p_{cr}$. Therefore, propagation of the low-velocity regime is stable if we create conditions under which the pressure in the compression wave is kept constant and below the critical pressure that initiates detonation.

The results of investigating the low-velocity regime in one explosive (PETN) and with one design of the experiment were examined here /128, 129, 168/. Let us now examine published material. The low-velocity regime of explosive transition to detonation was observed /13, 125/ during ignition of cast explosives (pentolite, DINA) in strong steel tubes. This regime propagated more stably in the less sensitive TNT /125/.

Babaitsev, Kondrikov, and Tyshevich /131, 159/ investigated in detail stable propagation of the low-velocity regime in cast TNT. It was found

* Under these conditions, the speed of normal high-velocity detonation of PETN is 8500 m/sec.

that in strong steel tubes propagation at a speed constant over the length (1800–2000 m/sec) takes place over a considerable distance up to 50 cm. The pressure in the compression wave was measured by the "aquarium" method and found to be 5–8 kbar.

Table 10 lists values of the maximum speed of the low-velocity regime for various high-density explosives, and also the longitudinal sonic velocities in the explosives. All available data in the literature are included.

TABLE 10. Maximum speeds of the low-velocity regime in high-density explosives ($\rho$ — density, g/cm³; $d_{charge}$ — diameter, mm; $L$ — length, mm; $\Delta$ — wall thickness, mm)

| Explosive | Parameters of cylindrical casing | Longitudinal sonic velocity in explosive, m/sec | Nature of process | Maximum speed of low-velocity regime, m/sec | Reference |
|---|---|---|---|---|---|
| Pressed PETN $\rho = 1.73$ $d_{charge} = 5$ $L = 200$ | Plexiglass, $\Delta = 45$ mm | 2250 | Stable | 1100 | /120/ |
| | Brass, $\Delta = 20$ mm | | " | 2600 | /128/ |
| | Steel 45, $\Delta = 2-4$ mm | | " | 2000–2400 | /129/ |
| | Steel 45, $\Delta = 8$ mm | | " | 3300 | /129/ |
| | Steel 30 KhGSA, $\Delta = 8$ mm | | Transition to detonation | 3300 | /129/ |
| Pressed hexogen $\rho = 1.75$ $d_{charge} = 5$ $L = 200$ | Steel 30 KhGSA. | 2500 | " | 2400 | /126/ |
| Cast DINA $d_{charge} = 12.7$ $L = 300$ | Steel, $\Delta = 9.5$ mm | — | " | 2000–2300 | /13/ |
| Cast 50/50 pentolite $d_{charge} = 12.7$ $L = 300$ | Steel, $\Delta = 9.5$ mm | 2430 | " | 2100–2500 | /125/ |
| Cast TNT $d_{charge} = 9-15$ $L = 500$ | Steel, $\Delta = 5-13$ mm | 2300 | Stable | 2200 | /[illegible]/ |

Note. The low-velocity regime in TNT was initiated by a weak shock wave, and in all other tests by the wave arising during ignition. The longitudinal sonic velocity in PETN, hexogen and TNT was measured by an ultrasonic method.

It can be seen from Table 10 that the most common and typical maximum speeds of the low-velocity regime were obtained for various explosives under different conditions, and approach the longitudinal sonic velocities (2000–2500 m/sec) in the original explosives.



## 25. THE LOW-VELOCITY REGIME IN HIGH-DENSITY EXPLOSIVES

It was noted earlier that the low-velocity regime has a wavelike nature. We shall now deal with experimental data justifying this assumption. First, it is necessary to detect the role of the compression wave propagating over the explosive charge and its casing.

A special experiment was designed to reveal the effect of wavelike perturbations. In this test the steel casing was completely cut apart in the plane perpendicular to its axis and then separated by a porous rubber sheet (thickness 5 mm), which attenuated the compression wave traveling along the casing. It was found that in such a casing the low-velocity regime in PETN ($\rho = 1.73$ g/cm³) propagated stably along the whole charge. Stable propagation of the low-velocity regime was unimpaired, if the explosive charge was separated from the casing by a porous rubber layer. Consequently, unlike liquid explosives the compression wave in the original substance is the decisive factor in the propagation of the low-velocity regime; perturbations moving along the charge are much less important. This conclusion is confirmed by the fact that propagation of the low-velocity regime is observed in uncased substances, such as crystals of initiating explosives (lead azide and silver azide) /223/ or charges of secondary explosives (cast TNT) /27/. The low-velocity regime in cast TNT due to the action of a shock wave is unstable (it is quenched or passes over to detonation) /27/.

The profile of the compression wave in an explosive during low-velocity propagation is therefore of interest. There is, however, a scarcity of relevant data.

Profile of the compression wave. Gipson and Maček /13/ determined the velocity of the pressure front (with the help of collapse probes) and the front of the chemical reaction (with the help of ionization probes). The probes were placed in one plane at different distances along cast DINA and pentolite charges. It was found that the reaction arises behind the shock wave after a considerable delay. The results of one of these tests, in which the probes were placed in the low-velocity zone, is shown in Figure 73. Transition to detonation was not observed in this experiment. We see that the compression wave (1), measured by a collapse probe actuated at about 0.8 kbar, leads the reaction front (2) by about 40 mm. It is interesting that the distance between the fronts as propagation proceeded at 1400 m/sec was practically constant, i. e., the reaction zone and the individual points of the pressure front move over the charge at an approximately equal velocity. When sturdier collapse probes (actuated at about 2 kbar) were used under such conditions, they recorded smaller separations between the two fronts during the low-velocity stage. The pressure front is more easily reproduced than the reaction front.

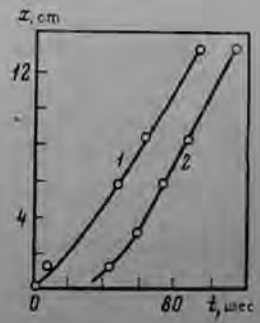


FIGURE 73. Propagation of the compression (1) and flame (2) fronts in the low-velocity regime (cast DINA, $d_{charge} = 12.7$ mm).

A sensitive initiating explosive (lead azide) was used as indicator in order to trace the passage of compression waves /120, 127/. A thin layer of the indicator was placed so that it separated a high-density PETN charge over the whole cross section. Detonation of the lead azide led the luminescent reaction front by 5–10 mm at a regime velocity $W \simeq 1000$ m/sec. The complete profile of the compression wave was measured electromagnetically at one point along the charge by Bobolev et al. /127/. A typical record under steady-state propagation conditions (1200 m/sec) is shown in Figure 74, which indicates that the pressure increases gradually to some peak value. The measured amplitude of the compression wave was 5 kbar, which is in agreement with the results of determining $p'$.

FIGURE 74. Oscillographs of the mass velocity $v(t)$ during propagation of the steady-state regime at 1200 m/sec (marker separation, 2 μsec).

Thus, all the reported data indicate that during subsonic propagation of the low-velocity regime in high-density explosives the wave is not a shock wave and is characterized by a stretched profile with smooth increase in pressure. The existence of a compression wave without any pressure jumps at its front was determined long ago when studying the propagation of explosive waves in soils /133/.

At higher (near-sonic or supersonic) regime velocities the complete profile of the compression wave was not measured. This is due to the fact that stable regimes with given velocities are only observed in strong metallic casings, whose presence very much complicates study of the wave profile in the explosive. However, the supersonic nature of the regime indicates that, under these conditions, the regime propagates via a shock wave. These are the fundamental experimental results.

As yet, there is no complete theory of the low-velocity regime.* Therefore, we first attempted to establish a consistent working hypothesis which would explain, at least formally, the experimental results obtained with high-density explosives.

After analyzing existing data we proposed the following working hypothesis /168/: the speed of the low-velocity regime is equal to that of the compression wave along the explosive; the self-sustaining compression wave – chemical reaction zone complex may be stable. It was assumed that the results of studying low-velocity regimes can be explained with the aid of data on the propagation of the compression wave in solid (explosive or inert) substances.

* Many attempts have been made to construct a theory of low-velocity detonation. Most interesting is the paper of Kuznetsov /119/, who also includes a critical study of earlier papers on this problem.



The proposed hypothesis was justified by comparing the propagation of the low-velocity regime and weak (with amplitude 1–20 kbar) compression waves in solid substances.

Let us examine what happens at the initial instant after applying constant pressure to the surface of a flat solid body /130/. Suppose the stress (pressure $p$) – specific volume ($v$) diagram pertaining to this solid body (explosive) for the state behind the wave front has the form shown in Figure 75. The state corresponding to the line $0-1'$ satisfies Hooke's law and corresponds to small deformations and pressures. At higher dynamic loads, when the pressure is higher than some value (yield point $p_y$), the solid body passes into a flowing state similar to a liquid. This state is characterized not by a complete absence of shearing stresses, as in a liquid, but by the absence of tangential stresses when the shearing strains are increased. Line $1'-2$ with a smaller slope corresponds to the flowing state of the solid body. The propagation velocity of the compression wave for an elastic body (section $0-1'$) is equal to the longitudinal sonic velocity $C_l$ in an infinite medium. On transition to the flowing state (section $1'-2$) the wave propagates with volumetric velocity

$$C_0 = V\overline{(\partial p/\partial \rho)_s} = V\overline{-V^2(\partial p/\partial V)_s}.$$

Various variants are possible, depending on the relationship between the wave amplitude and the dynamic yield point (Figure 75). If $p < p_y$ one elastic compression wave propagates at velocity $C_l$ (Figure 76a, state 1 on the $p,v$ diagram). If, on the other hand, $p > p_y$, state 2 on the $p, v$ diagram is attained. However, in this case two waves propagate over the body: an elastic wave with amplitude $p_y$ in the state behind the front (1'), and after it a plastic wave in the state behind the front (2) (Figure 76b). The plastic wave does not overtake the elastic one, since $C_0 < C_l$. The wave does not split into two in the case of a strong shock wave ($p \gg p_y$) with velocity $D > C_l$.

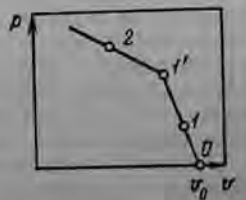


FIGURE 75. Stress (pressure)–volume diagram for a solid body.

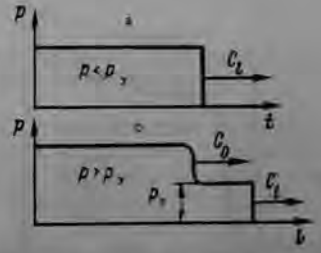


FIGURE 76. Two cases of compression wave propagation in a solid body:

a) one elastic wave; b) an elastic and a plastic wave.

This is the general pattern, which is to be expected during the propagation of compression waves at different intensities. Quantitative relationships can be obtained only experimentally. The pressures in the compression waves of interest lie between 1 and 20 kbar. Unfortunately, it is just in this pressure range that the dynamic compressibility of solid bodies has been insufficiently studied and that there is a scarcity of data. The compressibility of high-density TNT was studied elsewhere /27, 156/. It was proved that a wave with amplitude $p > 10$–$20$ kbar has a shock profile, whereas the adiabatic shock curve of TNT is described by a conventional linear equation. Dremin and Koldunov /27/ observed a deviation from the linear law at low pressures. When $p < 7$–$10$ kbar the wave splits into an elastic and a plastic wave /27, 156/; the plastic wave propagated at subsonic velocity. However, no systematic and detailed investigation of the compressibility of explosives at low pressure has been conducted. Therefore, additional experiments were set up to investigate the propagation of compression waves with amplitude 1–20 kbar /166/.

We studied high-density TNT ($\rho = 1.60$ g/cm$^3$) whose compressibility was close to that of PETN, and also the inert organic substance plexiglass. The electromagnetic method was employed, so the whole compression wave profile could be recorded. The magnetic field intensity at the center of the electromagnet gap of 200 mm width was 450 oersted to within 1%. We used two Π-shaped probes made from 0.07-mm aluminum foil; they were mounted perpendicular to the axis of the investigated sample, which had a diameter of 50–60 mm. The samples were not encased. The signals from the probes were recorded on an OK-17 double cathode-ray oscilloscope. The wave velocity ($D$) and the mass velocity of the substance ($U$) were measured.

We developed a method of producing a flat low-intensity shock wave in the sample substance. A pressure of 1–10 kbar was produced by an air shock wave, initiated by detonation of a TG 50/50 spherical charge. Stronger waves were produced by detonating a cylindrical charge made from a TNT–NaCl mixture, which was brought into contact with the sample substance. Waves of different intensities were obtained by changing the distance between the sample and spherical charge, or the percentage content of the NaCl in the mixture.


FIGURE 77. Dependence of the shock-wave propagation velocity on the pressure amplitude:

I) pressed TNT, $\rho = 1.60$ g/cm$^3$; II) plexiglass, $\rho = 1.18$ g/cm$^3$; 1) data of /166/; 2) /27/; 3) /173/.

The data were presented as a wave velocity ($D$) vs. pressure in the wave ($p$) plot, since the velocity of motion and the profile of the wave are determined by its intensity. The results are shown in Figure 77 and the characteristic oscillograms $U(t)$ in Figure 78. For comparison, we plotted in Figure 77 also other data /27, 173/, which correspond to pressure $p > 7$ kbar and agree satisfactorily with our results.

It can be seen from Figure 77 that the form of the $D(p)$ curves is identical for both substances. The $D(p)$ curve consists



of three characteristic sections. The subsonic branch corresponds to plastic wave propagation, whose velocity depends strongly on the wave amplitude (as follows from our data). It was found that splitting of the shock wave on formation of an elastic and a plastic wave takes place for TNT and plexiglass at similar pressures (about 7 kbar). The elastic wave propagates at a velocity equal to the longitudinal sonic velocity ($C_l = 2300$ m/sec for TNT and $C_l = 2800$ m/sec for plexiglass). Its amplitude is not constant, but depends on the total pressure in the wave.* The pressure increase in the plastic wave takes place within 1–10 μsec, depending on the amplitude.

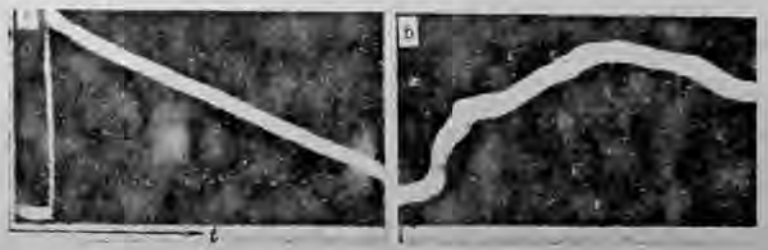


FIGURE 78. Oscillogram of the mass velocity in pressed TNT:

a) shock wave ($p = 10$ kbar); b) elastic + plastic wave system ($p = 5$ kbar).

The pressure region from 7 to 15 kbar corresponds to the section of weak dependence ("plateau") on the $D(p)$ curve; the wave propagates with a velocity that is close to the longitudinal velocity of sound and has a shock profile. Any variation in the shock wave amplitude over this range has practically no effect on the wave velocity. At a pressure exceeding 15 kbar we see a stronger dependence of $D(p)$, and the adiabatic shock curve of the substance is described by a conventional linear equation.

The compressibility of TNT and plexiglass is described by similar curves. The given form of the $D(p)$ or $D(u)$ curve may be typical for a solid confined material.

Let us compare the obtained data with the results of our study of the low-velocity regime. We compare the data of Figure 72 and Figure 77. The shapes of the curves $W(p')$ and $D(p)$ are the same. In addition, the pressure at which the characteristic bends on both curves occur are in agreement.

The qualitative agreement in the propagation of the low-velocity regime in weak compression waves confirms the validity of our hypothesis. It furnishes additional proof that the main role in the propagation of the low-velocity regime in solid explosives is played by the wave propagating over the explosive charge, not by the wave propagating over the casing.

Our results may serve as a theoretical basis for the quantitative calculation of the speed of the low-velocity regime; for such a calculation

* Corresponding data for the elastic wave are not shown in Figure 77.

we require the compressibility of the explosive and the compression wave parameters. In particular, we managed to obtain for PETN satisfactory agreement between the experimental and theoretical maximum speeds of the low-velocity regime (3300 and 3100 m/sec, respectively). In our calculation we used the adiabatic shock curve for PETN and assumed that, in accordance with the ideas developed, the experimental maximum speed of the regime is the same as the propagation velocity of the shock wave, whose amplitude is equal to the critical initial pressure of normal detonation ($p_{cr} = 17$ kbar).

The above approach allows one to explain the existence of subsonic low-velocity regimes, which are caused by the movement of a plastic wave in the explosive. This wave has no pressure jump at its front, in agreement with direct measurements of the front profile in this case /127/ (cf. Figure 74). Explanation of this fact from the standpoint of the wavelike nature of low-velocity processes has already presented great difficulties.* It is now understandable why different investigators who experimented under different conditions and with various explosives (TNT, pentolite, PETN, hexogen) found the most typical velocities of the regime at values (2000—2500 m/sec) that approached the longitudinal sonic velocity (see Table 10). This value is the most probable, since it corresponds to the "plateau" on the $W(p')$ curve.

Finally, we should expect an increase in the speed of the regime if we use explosives with high $p_{cr}$ and maintain a high pressure in the wave (e.g., by using casings made of superstrong materials). We verified our hypothesis by carrying out experiments with PETN-agate ($\rho = 1.76$ g/cm$^3$) for which $p_{cr}$ is much higher than for pressed explosives, if casings made from 30 KhGSA high-strength steel are used. In this case the speed of the low-velocity regime increased up to 3500 m/sec.

Rapid unstable propagation of the low-velocity regime can also be observed when a high-intensity shock wave (which ensures "forced" propagation of the process) acts upon the explosive. For instance, Dremin and Koldunov /27/ performed experiments with cast TNT charges of 60-mm diameter (without casing) and noted that, during the action of a critical shock wave ($p_{cr} = 35$ kbar), a process was initiated (in our terminology, the low-velocity regime) whose speed remained constant (3600 m/sec) over 1—2 charge lengths and later passed to detonation. It is interesting that the propagation velocity of the regime measured by an optical method was in agreement with the shock wave velocity measured by electromagnetic probes placed along the axis of the charge. This fact indicates directly that the speed of the low-velocity regime is equal to the propagation velocity of the shock wave over the explosive charge. Under the same conditions, but subject to a subcritical shock wave, the process was quenched.

The stable low-velocity regime in high-density secondary explosive charges was only observed when a casing was present. In this connection it is noteworthy that the pressure in the compression wave in the steady-state regime not only depends on the strength of the casing, but also on the nature of the heat release immediately behind the wave.

* It should be taken into account, too, that the plastic wave moves over a substance, the structure of which may differ from the original structure due to the action of the elastic compression wave.



At present, the stability and the steady-state nature of the self-sustaining complex consisting of the compression wave and the wide zone of the chemical reaction, have been studied neither theoretically nor practically, the mechanism governing maintenance of the compression wave is, to a large extent, unclear. On the other hand, it is just these questions that are very important when working out a theory of the low-velocity regime.

The above comments related to high-density explosives. It is quite possible that the results may be useful, too, for investigating the law governing the propagation of low-velocity "detonation" in powdered explosives. In this respect, the paper of Bolkhovitinov and Vasil'ev /154/ is interesting. They proved that shock compression of TNT powder in the nonsteady detonation wave has a complex character and two waves are observed. Bolkhovitinov and Vasil'ev are of the opinion that, first, the pores are closed, after which the homogeneous substance is further compressed.

With allowance for these data, low-velocity "detonation" in powders may be represented simply. The substance behind the front of the first wave is compressed to near-maximum density and moves with a velocity equal to the mass velocity of the substance. A second wave then propagates along the moving substance behind the front of which a chemical reaction arises. This explains the increase in speed of the low-velocity regime with decreasing density (Figure 68) and allows one to estimate the expected difference ($\Delta W$) in the propagation speeds of the low-velocity regime in high- and low-density charges. To a first approximation, this difference can be assumed equal to the mass velocity of the substance ($U_1$) behind the front of the first wave. Published data /150/ for PETN ($\rho \simeq 1.0$ g/cm$^3$) with $p_1 = 5$ kbar* yield $U_1 \simeq 500$ m/sec, which does not differ strongly from the value $\Delta W \simeq 700$ m/sec observed in experiment. The real pattern of the process growth during propagation of low-velocity detonation is doubtless much more complex. First, the onset and growth of the reaction is facilitated so that stable low-velocity regimes in powders propagate when a strong casing is absent.

Chemical reaction during propagation of a low-velocity regime in high-density systems. It is now generally accepted that when a weak shock wave acts on an explosive a chemical reaction takes place at individual localized hot spots. An estimate of the temperature of the shock compression of the explosive in a wave at a pressure of about 30 kbar shows that heating of the substance in the bulk is negligible, not exceeding a few dozen degrees. Available data indicate that pores (inhomogeneities) present in the charge are the hot spots of the reaction during propagation of the low-velocity regime in high-density systems. These data are set out in more detail below.

The presence of a small number of pores in a charge (a few percents) has a considerable influence on the possibility of low-velocity regime propagation. This is especially pronounced in charges encased by low-strength casings. For instance, with a plexiglass casing, the low-velocity regime is observed in PETN for charge density $\rho < 1.70$ g/cm$^3$ ($m > 4\%$). The process does not propagate at higher densities. The low-velocity regime

* According to Sobolev et al. /139/, unrotopine powder is compacted to maximum specific-weight density at pressure $p_1 \simeq 5$ kbar.

may propagate in PETN charges with a density of 1.73–1.76 g/cm³, only when a strong stable casing is used.

Low-velocity regime propagation also depends on the initial particle size of the explosive and, consequently, on the pore size. It was found that when decreasing the initial particle size from 500 to 20 μ the speed of the low-velocity regime decreases from 2250 to 2000 m/sec (the charge used had a diameter of 5 mm, a density of 1.73 g/cm³, and was placed in a casing with a wall thickness of 3.5 mm). Babaitsev et al. /159/ note that the process which was stable in large-crystalline TNT is quenched when fine-crystalline TNT is used.

The theory dealing with a focus of thermal explosion /123/ can be used to estimate the size of the hot spot and to compare it with the size of the pores present in the charge.

The critical size of the hot spot is determined by the expression

$$r_{cr} \simeq 3.48 T_{cr} \sqrt{\frac{\lambda R}{zQE}} \exp(E/2RT_{cr}) \left[\ln \frac{E}{RT_{cr}^2}(T_{cr} - T_0)\right]^{0.5}. \quad (70)$$

The critical temperature is found from the equation relating $T_{cr}$ to the critical induction period:

$$\tau_{ind} \simeq \frac{2c\rho RT_{cr}^2}{QEz} \exp(E/RT_{cr}). \quad (71)$$

In these two expressions, $E$ is the activation energy, $z$ is a preexponential factor, $Q$ is the heat produced by the reaction, $T_0$ is the initial temperature of the substance, $c$ is the specific heat, $\rho$ is the density, and $\lambda$ is the thermal conductivity coefficient.

The delay $\tau_{ind}$ in the initiation of the reaction was determined by tests, in which the motion of the low-velocity regime to the explosive–plexiglass interface was photographed against a bright screen. The value of $\tau_{ind}$ is determined as the period during which the compression wave emerges from the explosive (this instant coincides with the time at which the interface begins to move) and approaches the luminous reaction zone.

For PETN at $W = 1000$ m/sec, $\tau_{ind} = 10^{-5}$ sec.

We shall assume for PETN that $E = 39{,}500$ cal/mole, $z = 10^{18}$ sec$^{-1}$, $Q = 10^3$ cal/cm³, $c = 0.3$ cal/g·deg, $\rho = 1.7$ g/cm³, and $\lambda = 2{,}4 \cdot 10^{-4}$ cal/cm·sec·deg. In this case, relationships (70) and (71) yield $T_{cr} = 400°C$, and the critical hot-spot size $r_{cr} = 2 \cdot 10^{-4}$ cm.

Let us compare the obtained value of $r_{cr}$ with the size of pores present in the charge. There are no direct data on PETN in the literature. However, measurements of the pore size distribution (see Figure 10) show that pressed high-density ($\delta = 0.95$) TNT and hexogen samples contain pores whose size is of the order of $10^{-4}$ cm.

On the other hand, the inhomogeneities at which the reaction is excited may be formed, too, in the originally nonporous explosive during the propagation of the low-velocity regime. Bobolev et al. /127/ relate the variation in the transparency of cast PETN before the luminous front of the low-velocity regime was observed by them with deformations and destruction of the substance.



Bobolev et al. /127/ emphasize the standpoint according to which hot spots are formed by stable destruction of the nonporous explosive in the shock wave. This process is similar to the process arising during mechanical action, especially by impacting.

At present, the question as to how a hot spot arises and what is the specific physical mechanism underlying its formation has not yet been solved. The most probable mechanism of heating is friction due to the difference between the velocity of the substances filling the pore (inhomogeneity) and the mean velocity of the explosive behind the front of the compression wave.

Propagation of the reaction from hot spots in high-density systems, as in powders, apparently takes place in the form of surface explosive burning /167/. This hypothesis is confirmed to a certain degree by experiments in which the effect of the state of the surface of the explosive particles on the velocity of the regime and the boundaries of its propagation was studied. Coating of PETN particles ($r = 500\mu$) by a thin (a few microns) paraffin layer led to a considerable decrease in the speed of the low-velocity regime until the process completely ceased, regardless of the fact that charges with higher porosity (up to 5%) were used.

## C. TRANSITION FROM DEFLAGRATION TO DETONATION

### 26. TRANSITION FROM THE LOW-VELOCITY REGIME IN HIGH-DENSITY EXPLOSIVES TO DETONATION

Stable propagation of the low-velocity regime is observed at certain densities, explosive particle sizes, charge diameters, and casing strengths. Variation of one of these parameters (such as decrease in explosive density, increase in charge diameter or casing strength) leads to instability of the process, which may pass over to detonation. A necessary and sufficient condition for the onset of detonation is the formation of a shock wave of critical intensity $p_{cr}$ in a charge whose diameter exceeds the critical value.

The fundamental relationship determining transition to detonation is that relating the pressure $p'$ in the casing to the critical pressure initiating detonation.

We have shown in the foregoing section that the low-velocity regime is stable, if the pressure in the casing is smaller than the critical pressure:

$$p' < p_{cr}.$$

It should be expected that transition from the low-velocity regime to detonation will take place if*

$$p' > p_{cr}.$$

A critical-intensity wave may form in this case. Transition to detonation is thus promoted by all those factors that increase $p'$ and decrease $p_{cr}$. Available experimental data will now be examined.

* Price and Wehner /125/ show that detonation sets in when this inequality is satisfied.

Pressed high-density explosives. Obmenin et al. /120/ studied transition from the low-velocity regime to detonation in PETN of various densities. Variations in charge density enable one to change widely the critical pressure initiating detonation.

Tests were carried out in plexiglass or steel (with an optical wedge, see Figure 6c) casings, and continuous optical recordings were made of the process arising after charge ignition. A typical photograph of transition from the low-velocity regime to detonation is shown in Figure 79. Transition from the low-velocity regime to detonation in pressed PETN is seen to be jumpwise. The average speed of the low-velocity regime in the stage preceding detonation was determined in these tests.

FIGURE 79. Photograph of transition from the low-velocity regime to detonation (PETN, $\rho = 1.45$ g/cm$^3$, $r = 500$ u, $d_{charge} = 5$ mm).

The critical pressure initiating detonation in the encased PETN charges was also measured (Table 11). It was found that the low-velocity regime passes over to detonation when $p' \geq p_{cr}$; prior to detonation, the speed of the regime increases with $p_{cr}$. Thus the onset of detonation does not allow high speeds of the low-velocity regime to be attained in charges of reduced density.

TABLE 11. Transition from the low-velocity regime to detonation

| Parameter | Plexiglass casing | Steel casings with optical wedge | | |
|---|---|---|---|---|
| Relative density of PETN | 0.82 | 0.9 | 0.96 | 0.975 |
| Charge diameter, mm | 10 | 5 | 5 | 10 |
| Mean speed of the low-velocity regime prior to onset of detonation, m/sec | 1100 | 1500 | 2200 | 3300 |
| Critical pressure initiating detonation, kbar | 5 | 8 | 11 | 17 |
| Pressure destroying the casing $p'$, kbar | 6 | | 15—17 | |

Note. The steel casing with the optical wedge is equivalent in dynamic strength to a steel casing with wall thickness $\delta \simeq 8$ mm.



An increase in charge length or charge diameter promotes instability not far from the limiting conditions ($p' \simeq p_{cr}$). For instance, with a plexiglass casing the low-velocity regime in PETN ($\delta = 0.82$) did not pass over to detonation at a charge length of 150 mm; at the same time, the speed of the low-velocity regime increased slightly along the charge (from 800 to 1000—1100 m/sec). However, transition was observed when the charge length was increased to 300 mm (see Figure 79). A similar pattern was obtained when the charge diameter was increased.

The wave steepness and amplitude grow continuously during transition to detonation. The ideas developed in section 25 give reason to assume that in the stage preceding the onset of detonation the speed of the low-velocity regime should change in accordance with the established $W(p')$ dependence (see Figure 72). Tests carried out with PETN ($\rho = 1.73$ g/cm$^3$) naturally showed that the regime velocity increases monotonically over the length, and we observe sections with subsonic, near-sonic and supersonic velocities.

Cast explosives. Transition from deflagration of cast explosives to detonation was investigated by Maček and Gipson /13, 121/ and Price and Wehner /125/. Their research dealt mainly with transition from the low-velocity regime to detonation. Onset of detonation was observed if the explosive (DINA, pentolite 50/50) was cast into heavy steel tubes (inner diameter 12.7 mm, outer diameter 31.8 mm) of sufficient length (343 mm). The schematic diagram of the experiment and the distribution of the probes is shown in Figure 6b. The propagation velocity of the reaction front was determined by conventional ionization probes. The ionization method does not possess the advantage of the optical method, namely, continuous observation of process growth. However, in combination with collapse probes, which recorded the passage of the compression wave, the methods used made it possible to obtain comprehensive information about the investigated process.

The pressure was recorded by strain gauges cemented to the outer surface of the tube near the ignition point /121, 125/. The gauges were calibrated under static conditions.

Price and Wehner /125/ set up experiments to study the effect of the charge casing on transition from deflagration to detonation, and to obtain additional information about the low-velocity regime. In addition to the above method they used high-speed motion pictures of the destruction of the tube and probes in order to determine the radial deformation of the outer tube surface.

Measured values of the propagation velocity of the process, obtained by the ionization probes, are shown in Table 12. The data show that the onset of normal detonation is preceded by the low-velocity regime (1000—2300 m/sec) with propagation period 30—80 μsec. Accordingly, the length of the predetonation run [the induction distance] varied between 6 and 18 cm, the most typical value being about 10 cm. The peak velocity prior to the onset of detonation was 2000—2300 m/sec and close to (somewhat lower than) sonic in the explosive. It can also be seen that the velocity increases along the charge, especially in the initial period. However, the authors interpret their results regarding the nature of the velocity variation of the regime along the charge in another manner. Gipson and Maček note that "the acceleration, however, is seldom sufficiently pronounced to give the appearance of a smooth transition into steady-state

detonation." Price and Wehner /125/ in referring to this paper, wrote that Gipson and Maček demonstrated the existence of a low-velocity regime which propagates at constant speed in their experiments on the transition from the deflagration of DINA to detonation.

TABLE 12. Changes in velocity along the charge on transition of cast explosives (DINA, pentolite) to detonation

| $h_1$, mm | $D_{1k}$, mm/μsec | $h_2$, mm | $D_{2k}$, mm/μsec | $h_3$, mm | $D_{3k}$, mm/μsec | $h_4$, mm | $D_{4k}$*, mm/μsec | $h_5$, mm | $D_{5k}$, mm/μsec | $h_6$, mm | $D_{6k}$, mm/μsec |
|---|---|---|---|---|---|---|---|---|---|---|---|
| DINA /13/ | | | | | | | | | | | |
| 32 | 1.1 | 25.4 | 2.3 | 50.8 | 7.3 | 76.2 | 7.6 | 152.4 | 7.6 | 228.6 | — |
| 32 | 1.1 | 25.4 | 1.8 | 50.8 | 2.0 | 76.2 | [3.7] | 152.4 | 7.6 | 228.6 | — |
| 32 | 1.0 | 25.4 | 0.89 | 50.8 | 1.4 | 76.2 | [4.8] | 152.4 | 7.6 | 228.6 | — |
| 38 | 1.3 | 19.1 | [2.0] | 44.5 | 7.6 | 95.3 | 8.0 | 146.1 | — | — | — |
| 38 | 2.4 | 19.1 | 7.3 | 44.5 | 7.8 | 95.3 | 7.8 | 146.1 | — | — | — |
| 32 | ⊖ | 19.1 | 1.1 | 44.5 | 7.7 | 69.9 | [3.2] | 120.7 | 7.1 | 171.5 | — |
| 20 | 1.6 | 12.7 | 0.82 | 38.1 | ⊖ | 63.5 | [>2.1] | 88.9 | 7.7 | 114.3 | 7.7 |
| 20 | 0.91 | 12.7 | 1.2 | 38.1 | 1.3 | 63.5 | ⊖ | 88.9 | [>2.0] | 114.3 | 5.4 |
| Pentolite /125/ | | | | | | | | | | | |
| 33.3 | 1.95 | 12.7 | [2.6] | 63.5 | 7.3 | 114.3 | 7.1 | 177.8 | 7.6 | 254 | |
| 33.3 | 1.27 | 12.7 | 2.1 | 63.5 | [3.4] | 114.3 | 7.5 | 177.8 | 7.6 | 254 | |
| 33.3 | 0.36 | 12.7 | 1.37 | 63.5 | [3.4] | 114.3 | 7.9 | 177.8 | 6.9 | 254 | |
| 33.3 | 3.6 | 12.7 | 1.35 | 63.5 | [2.5] | 114.3 | 5.8 | 177.8 | 6.4 | 254 | |

Note. $h$ denotes the distance between the igniter and the first probe, $h_i$ the distance between the first and $i$-th probes, $D_{ij}$ the mean velocity between the $i$-th and $j$-th probes, $[\overline{D_{ij}}]$ the velocity along the section where the low velocity passes over to the high velocity; ⊖ denotes recording failure.

The data in Figures 72 and 77 enable the results to be interpreted so as to eliminate the above contradictions. The velocity increases along the charge in the initial stage of subsonic-regime propagation. As the sonic velocity is reached any velocity changes are seen to be absent, so that the onset of detonation is preceded by some section over which the velocity is practically constant (near-sonic). Transition from the regime propagating at constant velocity can be explained if we bear in mind that the pressure increase in the shock wave hardly alters the speed of the low-velocity regime on the "plateau" of the function $W(p')$.

Transition from the low-velocity regime to steady-state detonation takes place in a jumpwise manner in cast explosives /13/, since the smallest



transition distance was 13 mm with a corresponding time of 4 μsec. However, research on the detonation wave formation in cast TNT during shock initiation was carried out by Dremin and Koldunov /27/ and showed that detonation arises in the form of a smooth increase in the wave parameters up to the detonation parameters. In experiments carried out by Babaitsev et al. /131/, transition from deflagration of cast DINA to detonation also took place in the form of a smooth increase in velocity.

Simultaneous measurements of the velocities of reaction and pressure fronts (Figure 80) are of special interest. They show that the compression wave leads the reaction front. The record in Figure 80a, obtained by the use of sensitive collapse probes (0.8 kbar), shows that the probes were activated by a weak decaying pressure pulse, or possibly by one of a series of weak pulses which was overtaken by a stronger compression wave (or shock wave) near the region of onset of steady-state detonation. Application of sturdier collapse probes (actuated at 2 kbar) (Figure 80b) showed that the onset of detonation is realized by pressure waves whose parameters increase smoothly.

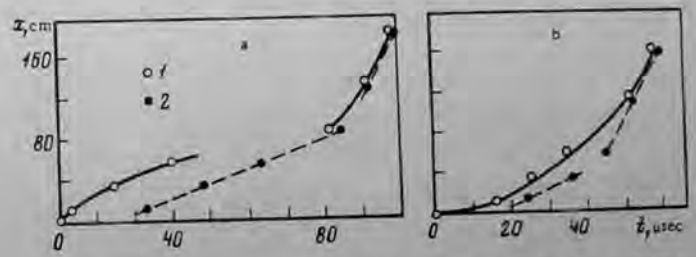


FIGURE 80. Simultaneous recording of compression (1) and flame (2) fronts on transition from the low-velocity regime to detonation:

a) DINA; b) pentolite.

Unfortunately, this sparse and fragmentary information does not give a comprehensive notion about the wave pattern preceding the transition from the low-velocity regime to detonation, and shows only the complex nature of the phenomenon.

It has been noted elsewhere /13, 121/ that the rate of pressure increase $dp/dt$ in the combustion zone has a considerable influence on transition from deflagration to detonation. The pressure for the investigated explosives increased according to the exponential law $p = p_0 e^{bt}$ (for pentolite $p_0 = 1$ kbar, $b = 8.856 \cdot 10^4$, $t$ was expressed in seconds). The pressure was measured up to 4 kbar. When the pressure increase was slower, the section before detonation increased or detonation was altogether absent.

High-speed motion pictures together with other recording methods /125/ made it possible to establish that detonation took place prior to destruction of the tube. Deformation of the tube was symmetrical, while a strong detonation was observed 28 μsec after a pressure of 1 kbar was attained

in the casing. Extrapolation of the $p(t)$ curve to 28 μsec enabled the pressure $p^*$ at which the tube is destroyed to be estimated (20 kbar). This value exceeds the critical initiation pressure of shock wave detonation, which was 11 kbar (for DINA) and 19 kbar (for pentolite)*. Transition of these explosives from deflagration to detonation could thus be explained.

It was assumed implicitly in these papers that layer-by-layer deflagration of explosives passes over directly into the low-velocity regime. This problem was not specially investigated. Therefore, it is not certain whether convective burning on the explosive–casing interface (discussed in section 23) preceded the low-velocity regime, so the question remains open.

In his earlier paper Maček /121/ proposed an elementary theory of the phenomenon: transition from deflagration of solid explosives to detonation, as in gases, is due to the shock wave that arises in the noncombusted explosive, because of coalescence of the compression waves initiated by the flame front. Below, we shall term this mechanism the gas or "piston" mechanism.

These constitute the fundamental results about the onset of detonation in high-density regimes, when transition to detonation takes place according to the following scheme: layer-by-layer deflagration – convective burning – wavelike low-velocity regime of explosive transition – normal high-velocity detonation.**

## 27. TRANSITION FROM DEFLAGRATION OF LOW-DENSITY EXPLOSIVES TO DETONATION

In this case deflagration passes over to detonation by the following scheme: layer-by-layer deflagration – convective burning – normal detonation. In strong casings the low-velocity regime is absent, as a rule, or has a very short duration. Typical optical photographs of transition from deflagration of PETN to detonation are shown in Figure 81 /14/.

1. A characteristic feature of transition from deflagration of low-density products to detonation is the onset of detonation ahead of the convective flame front. This fact was first established experimentally by the Soviet investigators Petrovskii, Sokolov and Aksenov /143/. Their result is one of the fundamental arguments in favor of applying to porous explosives the "gas" mechanism of transition from deflagration to detonation.

The photographs in Figure 81 show the developed regime of convective burning with the characteristic staggered front. This form of recording is due to the fact (see section 23) that the convective burning front is not flat, while ignition takes place in the individual (large) pores present in the charge. In powders, detonation arising ahead of the combustion zone does not lead to the formation of a retonation wave moving in the reverse direction (toward the side of the combustion products). Between the detonation region and the combustion zone there remains a section of nonreacting

* Unfortunately, the paper does not report the conditions under which reproducible values of $p_{cr}$ were obtained.
** Convective burning is of short duration when igniting a high explosive charge at the closed end in a strong casing.



substance, which is seen on the photograph (Figure 81a) as an interruption in the luminescent zone. Sokolov and Aksenov /143/ showed by an indirect method that the explosive is compressed in the section ahead of the flame front. This conclusion was drawn from an analysis of the condensed residues of the explosive remaining after the experiments.

Special experiments, in which the retonation wave was produced artificially, were carried out /14/ in order to obtain more information about the state of the substance, and especially to provide direct proof of compression in the given zone. The following technique was applied. A small amount (about 0.1 g) of slightly compressed lead azide was placed into the investigated explosive charge at the site where the detonation was produced. Otherwise, the experimental techniques were identical in all the tests. The compression waves leading the flame front brought about explosion of the lead azide, which initiated detonation both of the initial-density and of the compressed explosives. An optical record of one of these tests is shown in Figure 81d, which indicates that the velocity of the retonation wave in the explosive is considerably larger than the velocity of the detonation wave. For powdered PETN charges (crystal size 0.5 mm) the velocity of the detonation wave is 4700 m/sec and corresponds to an initial density of $\rho = 1.0\,g/cm^3$, while the virtually constant retonation velocity is 7800 m/sec and corresponds to density $\rho = 1.55\ g/cm^3$. This result is direct proof of the strong compression of the powdered explosive ahead of the flame front under the action of the compression wave. In our opinion, the absence of a retonation wave during the natural onset of detonation is due to this fact. If we compare the result with the critical initiation pressure of detonation which, according to Seay and Seely /150/, is 2.5 kbar for PETN ($\rho = 1.0\ g/cm^3$), we conclude that the explosive is compressed to a considerable density in a compression wave of relatively low intensity. This conclusion agrees with results of Aleksandrov et al. /33/, who analyzed samples of porous explosives remaining after application of a shock wave. It was found that when a 1.5–2-kbar shock wave acted, not only was the explosive crushed but its density increased from 1.0 to 1.5 $g/cm^3$.

Figure 81d depicts another interesting result: the boundary separating sections with different detonation velocities is fairly clear. This indicates that the compression wave initiating detonation has a steep leading edge. It is evident that the effect of compression is especially strong at low densities.

The above comments were based on the type of photograph of transition from deflagration to detonation.

2. In the majority of experiments the detonation front is formed very near to the accelerating flame front. Frequently, an increase in luminescence is observed at the point of detonation onset (Figure 81c); in our opinion this is connected with the formation of a localized explosion. The thermal explosion of a limited volume of explosive is the direct cause of the onset of detonation. Explosion of PETN, leading to the formation of a detonation wave, was also observed under other experimental conditions /16/.

This indicates that the onset of localized explosions takes place everywhere and is an essential and integral part of the transition from deflagration to detonation. It was found that on transition from deflagration

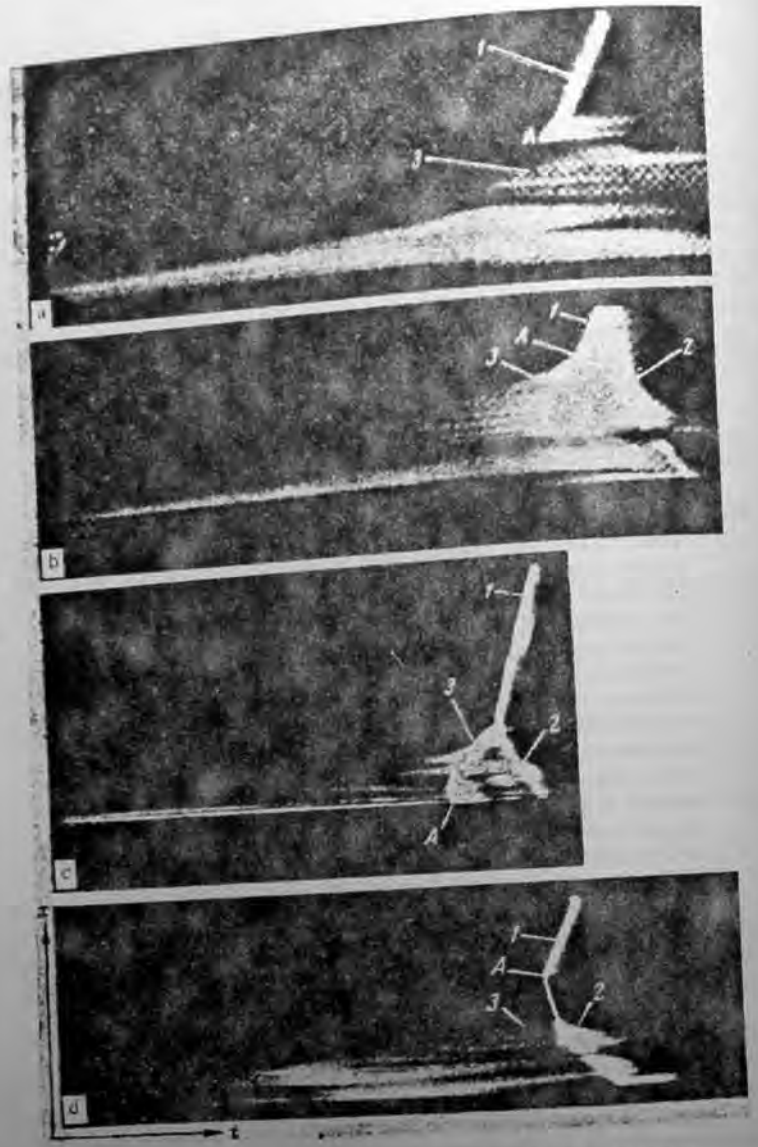


FIGURE 81. Typical photographs of transition from deflagration of PETN to detonation:

a) $D$ = 4700 m/sec, $W$ = 750 m/sec ($\delta$ = 0.56, $r$ = 500 μ); b) $D$ = 4300 m/sec, $R$ = = 2800 m/sec, $W$ = 800 m/sec ($\delta$ = 0.4, $r$ = 20 μ); c) $D$ = 7800 m/sec, $R$ = 3200 m/sec ($\delta$ = 0.80, $r$ = 20 μ); d) $D$ = 4700 m/sec, $R'$ = 7800 m/sec, $W$ = 250 m/sec ($\delta$ = 0.56, $r$ = 500 μ). 1) detonation wave ($D$); 2) retonation wave in the explosion products ($R$) or in the explosive ($R'$); 3) process preceding detonation ($W$).



of PETN to detonation localized explosions not only take place near the flame front, but at a certain distance behind the front, in the burning material (Figure 81c). Explosion $A$ arises in the convective burning zone with the characteristic "staggered" front and leads to the formation of a shock wave, which propagates at a velocity of 2800 m/sec, overtakes the flame front, and after a short delay (~ 2 μsec) produces detonation ($D$ = 7800 m/sec). The probability of the formation of volumes of uncombusted or partially combusted substance capable of exploding is very high, since the convective burning front is not planar but very much curved.

The onset of localized explosions was also observed in the transition from the deflagration of free-flowing charges of ammonium perchlorate with polystyrene to detonation (Figure 82). The experiments were performed with the participation of A. V. Obmenin and I. N. Lobanov. Unlike the above experiments, in these tests the charge was ignited in the atmosphere near the open end. A long gas outlet (its diameter equal to the charge diameter) was fixed to the open end. The tests show that, after ignition, convective burning sets in and ejects the substance into the free volume of the tube. The volume combustion in the tube led to the rapid pressure rise. Consequently, localized explosions that brought about detonation of the mixture were produced in the zone of convective burning. In such a scheme deflagration passes over to detonation when a weak casing surrounds the charge.


FIGURE 82. Photograph of transition of a 10% polystyrene + 90% ammonium perchlorate mixture to detonation ($r$ = 15 μ, $\rho$ = 0.65 g/cm$^3$, $p$ = 1 atm, open tube of length 100 cm).

It should be noted that Patry /9/ observed the onset of detonation in a burning explosive, when he studied transition from deflagration of an initiating explosive (mercury fulminate) to detonation.

Recent research on transition from deflagration of gaseous systems to detonation were carried out by the schlieren method /138, 141/ and showed that the main cause for the onset of detonation is the localized explosion of the adiabatically compressed volume of the mixture ahead of the turbulent flame zone.

Table 13 shows characteristic schemes of the growth of explosion in porous explosives.

TABLE 28. Typical schemes of the growth of explosion in pressed explosives

| State of explosive | Properties of casing | Scheme of growth | Characteristic features |
|---|---|---|---|
| High-density charges (independent of initial dispersity of explosive) | Strong compact casing ($p' > p_{cr}$)* | Layer-by-layer deflagration—low-velocity regime—detonation | Jumpwise nature of transition from low-velocity regime to detonation |
| | Low-strength casing ($p' < p_{cr}$) | The same, but without detonation | Stable propagation of low-velocity regime |
| Low-density charge | Strong casing ($p' > p_{cr}$) | Layer-by-layer deflagration—convective burning—detonation | Detonation wave formed ahead of or very close to flame front. Compression of explosive in front of flame front is essential. Detonation sets in due to growth of localized explosion in convective burning zone. |
| Explosive charges of bulk density with particle size of several millimeters | | Layer-by-layer deflagration—low-velocity regime—detonation** | Observation of stable low-velocity regime depends on properties of casing (low-velocity detonation when $p' < p_{cr}$) |

* $p'$ is pressure destroying the casing, and $p_{cr}$ critical pressure initiating detonation of encased charge.
** See Sokolov and Aksenov /143/.

## 28. INDUCTION DISTANCE

A quantitative characteristic of the tendency toward the transition from deflagration of explosives to detonation is the induction distance $L_{ind}$, i. e., the distance between the point of ignition and the point of onset of detonation. This parameter enables different classes of explosives to be compared by their tendency to detonate.

The induction distance has been measured elsewhere /14, 142—144, 165/. The value of $L_{ind}$ may be easily determined from continuous optical traces. However, optical recording is not always feasible and considerably complicates the experimental technique. A simple method has therefore acquired wide popularity /14, 142, 165/ and is based on a study of the damaged channel of a thick-walled metallic casing, which is not destroyed in the experiment. Such a study can be carried out if the casing is cut along the axis of the channel after performing the experiment. Figure 83 shows a schematic diagram (a) and a photograph (b) of the channel of the thick-walled casing deformed after the test; $A$ denotes the ignition point of the porous sample, $AD$ the induction distance, and $DE$ the detonation section.

In the induction region, the channel expands smoothly and after some distance $AC$ the diameter has a constant value, which remains practically unchanged. It was found that, together with the channel widening, the color of its inner surface changes /14/. Behind the widened channel outlet with constant $C$ one observes a distinct boundary $D$, which is perpendicular to the charge axis and separates two regions differing in color: a light zone $BD$ corresponding to the induction region, and a dark zone $DE$ corresponding to the detonation section. Comparison of the obtained imprints with optical



recordings showed that boundary $D$ corresponds to the site of the onset of detonation. The change in color is apparently connected with the different deformations of the casing in the ignition region and in the detonation section, and the different composition of the explosion products. In the detonation section there is intensive destruction of the channel and formation of striations. Intergrowth of the striations partially overlaps the "light" zone in the induction region.


FIGURE 83. Schematic diagram (a) and photograph (b) of the inner channel of the casing after transition from deflagration to detonation.

In some cases the channel diameter in section $CD$ of the "light" zone is slightly larger than the channel diameter in section $DE$ (shown in Figure 83a by a dashed line). Moreover, the point where the channel diameter expands to a constant value does not usually correspond to the site of the onset of detonation ($AC$ is less than $AD$, see Figure 83a). For this reason, determination (after Griffiths and Groocock /142/) of the induction length from the point at which the diameter begins to assume a constant value leads to reduced values of $L_{ind}$.

As a rule, the ignition point $A$ corresponds to the onset of convective burning. When the explosive is ignited at the closed end the layer-by-layer deflagration stage is absent because the pressure grows rapidly and reaches the critical collapse pressure $p_c$. Korotkov et al. /14/ used the "built-in charge" system (see Figure 2) when the charge was ignited at the open end. The sample of porous explosive was ignited through a solid (gas-impermeable) layer at pressure $p > p_c$, so that convective burning arose immediately. The encased charge was ignited in a bomb with a large free volume; the required pressure in the bomb was produced by preliminary combustion of an auxiliary charge.

The results for homogeneous explosives will be illustrated by the example of PETN, whose deflagration readily passes over to detonation.

Effect of parameters of homogeneous explosive charges. Figure 84 shows the dependence of the induction distance on porosity for PETN with initial particle diameters $r = 20\,\mu$ and $r = 500\,\mu$. The porosity was varied from 0.7 to 0.04. Data were obtained with ignition at the open end according to the above system; the charge was situated in a brass casing of 20-mm wall thickness. The scatter of the induction distances are noteworthy, especially for fine crystalline PETN. A large number of tests were set up; their results were averaged and served for plotting the curves in Figure 84. The dashed curve in Figure 84 is the averaged curve for the 20-$\mu$ PETN. The function $L_{ind}(m)$ has a minimum;

its position is shifted to the left with increasing particle size. At high porosity ($m = 0.5$) the fine crystalline PETN ($r \simeq 20\ \mu$) detonates more readily than does the coarse crystalline PETN ($r \simeq 500\ \mu$). The opposite is observed at low porosities. It can be seen that PETN with particle size $r \simeq 500\ \mu$ can pass over to detonation at very low porosities ($m \simeq 0.05$) and the induction distance does not exceed 50 mm. A further, very insignificant decrease in porosity leads to an abrupt increase in the induction distance. The porosity starting from which a considerable increase in $L_{ind}$ is observed decreases from 0.1 to 0.05 as the particle size increases from 20 to 500 $\mu$ and corresponds to approximately the same initial gas permeability of $10^{-4}$ darcy. Tests employing PETN with $r \simeq 120\ \mu$ were also performed. It was shown that the $L_{ind}(m)$ curves for particles of initial size 120 and 500 $\mu$ are practically in agreement; there is, however, a small difference for low and high porosities. This indicates that the obtained porous structures are similar to each other due to the destruction of particles during the pressing process (see section 4).

The abrupt change in $L_{ind}$ at small porosities is due to the onset of the low-velocity regime. It is not surprising that such a large scatter is observed since, as we have seen, the forms of transition to detonation are very variegated.

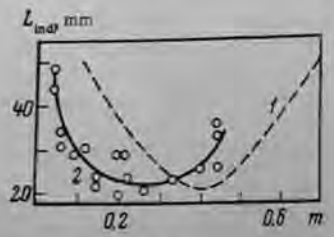


FIGURE 84. Porosity dependence of the induction distance for PETN; 1) $r = 20\ \mu$; 2) $r \simeq 500\ \mu$.

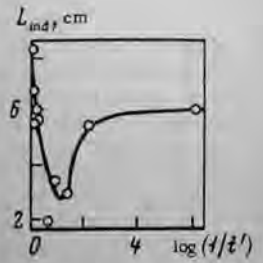


FIGURE 85. Variation in ignition distance for octogen.

Transition from deflagration of homogeneous porous explosives (octogen, hexogen, PETN and tetryl) to detonation was observed by Griffiths and Groocock /142/. The open end of the explosive charge was placed into a brass tube and ignited by lead styphnate. The effect of porosity, initial particle size of the explosive and conditions of gas removal were studied, and data reported for octogen (Figure 85) in the form of plots of $L_{ind} = \log(1/t')$, where $t'$ characterizes the gas permeability of the explosive, depending more or less on the conditions of its determination. Unfortunately, Griffiths and Groocock do not report the correlation of $(1/t')$ and the porosity and particle size of the explosive. On the other hand, the general nature of the dependence is evident. It follows from the data of Figure 85 that at constant initial particle size there is optimal explosive porosity to which the smallest induction distance corresponds. Thus, the presence of



a minimum of function $L_{ind}(m)$ is apparently a characteristic feature of homogeneous explosives.

The decrease in the initial particle size of the explosive (at a constant pressing pressure of about 150 atm) decreased the ignition distance up to a certain limit, after which $L_{ind}$ increased. The optimum particle size for octogen and hexogen was 124–251 $\mu$, and 76–124 $\mu$ for PETN /142/.

Afonina et al. /165/ studied transition from deflagration to detonation for a wide range of homogeneous explosives with constant density (0.9–1.2 g/cm$^3$). They used a 200–350-mm steel tube with inner diameter 6.4–6.8 mm (wall thickness 15 mm). A steel stopper with 2 mm channel width was employed on the ignition side. The resulting induction distances (in cm) were as follows:

| PETN | Octogen | Hexogen | DINA | Tetryl | Styphnic acid | Picric acid | TNT |
|---|---|---|---|---|---|---|---|
| 1 | 1–2.5 | 1.5–3 | 3–7 | 4–6 | 10–12 | 12–13 | >20 |

It is noteworthy that the tendency of the majority of investigated explosives to pass from deflagration to detonation increases with the heat of explosion.

No systematic research has been conducted yet on the effect of the charge diameter and conditions of gas removal. It has been noted /165/ that for low explosives (TNT, picric acid) an increase in charge diameter and closing of the open (toward the side of ignition) end of the charge brought about a shorter induction distance. The effect of the above parameters is much weaker for high explosives (PETN, hexogen).

As for the role of the casing, our tests with PETN ($\rho = 1.45$ g/cm$^3$, $r = 500\ \mu$, $d_{charge} = 5$ mm) in steel casings of different wall thickness showed that a certain minimum casing strength is necessary for transition from deflagration to detonation, and that the condition $p' > p_{cr}$ must hold. On decreasing the wall thickness $\Delta$ from 17 to 3 mm it was found that $L_{ind}$ did not change but remained 15 mm. In this case, the pressure $p'$ attained in the case prior to destruction is higher than $p_{cr}$. An increase in induction distance was observed for $\Delta < 3$ mm, when $p' \to p_{cr}$. Finally, no detonation arose in thick-walled casings ($\Delta = 0.5$–$1.0$ mm; $p' < p_{cr}$); only the low-velocity regime propagated. Burning was quenched on further decrease in $\Delta$.

Ammonium perchlorate-based mixtures /14/. Table 14 presents measured induction distance for mixed explosives (particle size of components $r \simeq 15\ \mu$). The charges were ignited at the closed end. The results represent averages of several tests conducted in steel tubes with 15–20-mm wall thickness.

For comparison, the table presents data for PETN of similar dispersity ($r \simeq 20\ \mu$). It follows that the dependence of ignition distance on porosity for mixed and homogeneous explosives differs. For mixed explosives there is an increase in induction distance with decreasing porosity over the whole range of studied porosities.

TABLE 14. Induction distance, mm

| Explosive | Porosity | | |
|---|---|---|---|
| | 0.6 | 0.45 | 0.25 |
| Stoichiometric mixture of ammonium perchlorate with polystyrene | 85 | 140 | >240 |
| The same, with TNT | 60 | 120 | >240 |
| PETN | 40 | 20 | 30 |

Ammonium nitrate-based mixtures. Sokolov et al. /144/ studied transition from deflagration of industrial $NH_4NO_3$-based explosive mixtures to detonation. The tests were carried out in thick-walled steel tubes with screw-on lids. The charges were free-flowing and were ignited on the closed side of the tube. Sokolov et al. succeeded in obtaining transition from deflagration to detonation only with tubes longer than 1–2 m. The experimental results are shown in Table 15.

The table shows that burning of mixed explosives containing the weaker oxidizer $NH_4NO_3$ is characterized by a much lesser tendency to detonate than $NH_4ClO_4$ mixtures. Burning of pure ammonium nitrate and of ammonium nitrate mixed with an inert fuel (AM-10) does not pass over to detonation in a tube shorter than 6000 mm. Introduction of active fuels (TNT, hexogen) considerably increases this tendency. Nevertheless, even for rock ammonite No. 1 the induction distance is longer than the induction distance for perchlorate mixtures. It should also be noted that values close to $L_{ind}$ are obtained for pure TNT and industrial explosives, which contain only 21% TNT (ammonite No. 6 and zernogranulite 79/21B). The authors noted a somewhat unusual effect: with increasing charge diameter the induction distance increased. In their opinion this result is due to the pointlike nature of ignition (the igniter diameter was 1 cm) and the formation of a spherical divergent flame front with the result that the pressure in the combustion zone increases more slowly. It is also noted that, at its onset, transition from deflagration of industrial explosives to detonation has an irregular statistical nature.

It should be emphasized that when deflagration of mixed explosives passes over to detonation, both physical and chemical factors (i.e., the chemical nature of the mixture constituents) are important. Moreover, processes of diffusional mixing play an important role.

We now consider briefly research on the transition from deflagration of porous explosives to detonation.

The onset of detonation ahead of the accelerating flame front and also the compression of the explosive in the transition region (see Figure 81a,d) confirm the notion that the fundamental cause of the onset of detonation is the shock wave, which is formed by coalescence of compression waves that initiate the flame front, i.e., by the classical piston mechanism, which is discussed elsewhere /121, 42, 143/.

This mechanism allows the porosity dependence of $L_{ind}$ to be clarified. The main factor determining the shock wave formation when the explosive is ignited at one end of the tube is the rate of change of the pressure ($dp/dt$) in the combustion zone. Quantity $dp/dt$ is determined by the flame surface



TABLE 15. Induction distance and detonation velocity for some industrial explosives and their individual components (TNT, $NH_4NO_3$) /144/

| Explosive and its composition | Density, g/cm³ | Weight of igniter, g | Tube diameter, mm | Tube length, mm | Number of tests | Tests terminating with detonation | Induction distance, mm | Detonation velocity, m/sec |
|---|---|---|---|---|---|---|---|---|
| Rock ammonite No. 1: 66% $NH_4NO_3$ (ZhV* + 5% TNT + 24% hexogen + + 5% aluminum | 1.07 | 2 | 23 | 2000 | 6 | 5 | ⩽300 | 4750–5000 |
| Ammonite No. 6: 79% $NH_4NO_3$ (ZhV) + + 21% TNT | 1.0 | 5 | 48 | 4000 | 1 | 1 | >1100 | – |
| | | | 34 | 2000 | 1 | 1 | 1200 | 4500–4800 |
| | | | 23 | 2000 | 2 | 2 | 600 | 4500 |
| Zernogranulite 79/21B: 79% $NH_4NO_3$ + + 21% TNT | 0.9 | 8 | 48 | 2000 | 2 | 2 | 500–700 | 3800 |
| | | | 34 | 2000 | 2 | 2 | 700 | 3800 |
| | | | 23 | 2000 | 2 | 2 | ⩽300 | 1600–1900 |
| Dinamon AM-10: 87.7% $NH_4NO_3$ (ZhV) + 10% Al + 2.3% oil | 0.95–1.05 | 16 | 48 | 6000 | 1 | 0 | – | – |
| | | | | 4000 | 1 | 0 | – | – |
| TNT | 1.1 | 5 | 34 | 3000 | 1 | 1 | 800–1000 | – |
| | | | | 2000 | 3 | 3 | 300–900 | 4800–5000 |
| Ammonium nitrate ($NH_4NO_3$) | 0.9 | 18–25 | 48 | up to 6000 | 7 | 0 | – | – |

* Water-resistant grade of ammonium nitrate containing hydrophobic and iron additives.

(specific surface of the pores and velocity of their convective ignition) and also by the pressure dependence of the burning velocity of the explosive. There exists optimal porosity and particle size for homogeneous explosives at which the induction distance is shortest. The maximum pore surface enveloped by the flame corresponds to the optimal porosity. In this connection we note that, for fine-crystalline PETN (Figure 84), satisfactory agreement is observed between the porosity values ($m = 0.3-0.5$) at which the specific pore surface (Figure 14) and the rate of convective burning (see Figure 61) attain their peak value. Crushing of the particles by the compression waves must be allowed for when analyzing function $L_{ind}(m)$ for coarse-crystalline PETN.

Unlike homogeneous explosives, function $L_{ind}(m)$ has no minimum for mixed explosives. In our opinion this difference is due to the following facts. If the velocity of layer-by-layer deflagration increases linearly with pressure for homogeneous explosives, the deflagration velocity of mixed explosives is pressure-independent at a pressure of several kilobars /23/. This, of course, brings about a slower pressure growth $dp/dt$ when mixed explosives are ignited. Moreover, with increasing density the critical diameter of detonation decreases for homogeneous /137/ and increases for mixed /108/ explosives. Furthermore, the critical pressure initiating detonation increases with the density of mixed explosives (see section 28).

This enables one to explain the high absolute induction distances of mixed explosives and the experimentally observed intensive increase in $L_{ind}$ with density. During the slow pressure increase in the combustion zone of mixed explosives, compression of the substance over a considerable charge length may lead to the inability of the system to detonate.

In order to develop a theory of transition from deflagration to detonation we require the wave pattern ahead of the flame front and the laws governing the propagation and coalescence of the compression waves that determine the formation of the critical-intensity shock wave. Unfortunately, this problem has remained virtually uninvestigated. Various ideas that were advanced were not confirmed experimentally. Existing difficulties are mainly due to the absence of data on the propagation of weak compression waves in porous condensing media.

In conclusion, we note that the "piston" mechanism is a simplified and more or less idealized mechanism. The real mechanism is much more complex. First, it must be taken into account that a shock wave of critical intensity may arise due to the localized explosion of individual volumes of the explosive.

## D. ONSET OF DETONATION BY SHOCK INITIATION

### 29. DETERMINATION OF CRITICAL PRESSURES INITIATING DETONATION

The final result of the predetonation growth of burning is the formation of a shock wave, which leads to detonation of the explosive if the amplitude of the wave reaches a value equal to the critical pressure initiating detonation (critical detonation pressure $p_{cr}$). One cannot study transition from



deflagration to detonation without knowledge of the critical detonation pressure. Shock initiation of detonation has recently been studied intensively mainly in connection with the determination of the sensitivity of different explosives to shocks.

In order to experimentally determine $p_{cr}$, we must know the shock adiabat of the explosive, i.e., the connection between the pressure and the specific volume of the substance at the shock front, or, in other words, the connection between the pressure (velocity of the shock wave) and the mass velocity of the substance. The shock adiabats (dynamic compressibility) of condensed substances were determined in many papers; they were reviewed by Al'tshuler /140/. The dynamic compressibility of TNT and hexogen at near-maximum density was investigated especially. There is a scarcity of data on the compressibility of porous explosives: PETN /150/ and ammonium perchlorate /151/ of bulk density, and pressed TNT /157/. Plotting of the shock adiabat is a complex and laborious process. For this reason, methods of calculating these adiabats of explosives are important.

Generalized shock adiabats. Gogolev et al. /145/ proved that the dynamic compressibility of some metals can be described by a single function (generalized shock adiabat) which only involves two initial parameters, namely, density $\rho_0$ and sonic velocity. They reached this conclusion after processing experimental data with the aid of a similarity law in explicit form.

Afanasenkov et al. /146/ proved the correctness of this conclusion for organic substances. It was found that, for liquids, the experimental data satisfy the expression

$$D = C_0 + 2U - 0.1\frac{U^2}{C_0}, \qquad (72)$$

where $D$ is the shock wave velocity, $U$ the mass velocity, and $C_0$ the volumetric sonic velocity subject to the initial conditions.

A similar expression was found to hold for high-density cast TNT and pressed hexogen. This, and the fact that the solid substance in the shock wave can be treated as a liquid when the yield point is surpassed, allowed relationship (72) to be recommended as the generalized shock adiabat for organic explosives. Good agreement was found between the curves calculated by (72) and the experimental curves, and enabled the shock adiabat of organic explosives to be plotted /146/. Only the volumetric sonic velocity $C_0$ need be determined in order to calculate this curve for an individual explosive.

The value of $C_0$ in a liquid is best computed by Rao's equation

$$C_0^{1/4} = \frac{p_0}{M}\sum_i y_i B_i, \qquad (73)$$

where $\rho_0$ and $M$ are the initial density and molecular weight of the substance; $y_i$ is the number of chemical bonds of given type and $B_i$ are the increments in these bonds.

The value of $C_0$ can also be determined experimentally by the ultrasonic method. In the experiment, the longitudinal ($C_l$) and transversal ($C_t$) sonic

velocities are measured in the solid and $C_0$ calculated from the relationship

$$C_0^2 = C_l^2 - {}^4/_3\, C_t^2, \qquad (74)$$

or in experiments on the isothermal compressibility of the explosive.

Afanasenkov /149/ calculated values of $C_0$ for some solid explosives and linear polymers* (Table 16).

TABLE 16. Volumetric sonic velocity in some explosives and polymers

| Substance | Density, g/cm³ | Volumetric sonic velocity, m/sec | | |
|---|---|---|---|---|
| | | after Rao | by isothermal compressibility | by experiment (ultrasonic method) |
| Nitromethane | 1.14 | 1330 | — | 1346 /149/ |
| TNT (liquid) | 1.47 | 1550 | — | — |
| TNT (crystal) | | 2200 | 2200 | 2080 /149/ |
| Hexogen | 1.80 | 2640 | 2650 | — |
| PETN | 1.77 | 2420 | 2320 | — |
| Tetryl | 1.73 | 2190 | — | — |
| Ammonium perchlorate | 1.95 | — | 2840 | — |
| Teflon | 2.236 | 1085 | 1060 | — |
| Polystyrene | 1.06 | 1710 | 1980 | — |
| Poly(methyl methacrylate) | 1.18 | 1920 | 1870 | — |
| Polyethylene | 0.917 | 2070 | 2120 | — |

Mixed systems /146, 168/. In calculating the shock adiabat of a nonporous mixture of two (or more) solid substances it was assumed that the pressure in the components at the shock wave front is equalized ($p_{mix} = p_1 = p_2$) and that there is no heat exchange between them. It follows from the laws of mass and momentum conservation at the shock front that

$$U_{mix}^2 = \alpha U_1^2 + (1-\alpha)\, U_2^2, \qquad (75)$$

where $U_{mix}$, $U_1$ and $U_2$ are the mass velocities of the mixture, and of the first and second components, respectively; $\alpha$ is the weight fraction of the first component.

The adiabat of the mixture can be plotted after the shock adiabat has been determined by (72). The curve in Figure 86 presents a comparison between calculated and experimental curves for a TNT—hexogen 30/70 composition.

Porous substances /146/. The same ideas and assumptions as those mentioned above were introduced when plotting the nonequilibrium shock adiabat. Afanasenkov et al. examined a mixture consisting of a solid phase (explosive) and air in the pores. Moreover, it was assumed that on

* Knowledge of $C_0$ for polymers makes it possible to calculate the shock adiabat of mixed powders in diverse model compositions. The shock adiabat for $NH_4ClO_4$ was expressed in the form $D = C_0 + 1.5U - 0.018U^2$.



compression the final volume of the air differs from zero, while the weight fraction of the air is negligibly small. In this case the shock adiabat has the form

$$U_p^2 = U_\gamma^2 + p(1 - 1/\gamma)(1/\rho_{0p} - 1/\rho_{0s}), \qquad (76)$$

where $\gamma = V_\varphi/V$ is the degree of air compression in the pores, $\rho_{0p}$ is the initial density of the porous product, and $\rho_{0s}$ is the initial density of the solid nonporous explosive. The values of $p$ and $U_\gamma$ were given beforehand by the shock adiabat of the solid nonporous substance. Afanasenkov et al. /146/ found best agreement between theory and experiment when $\gamma = 7$ (Figure 87). This method was also used to calculate the shock adiabats of porous explosives when determining the critical detonation pressure.

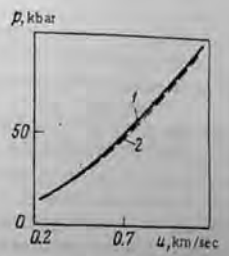


FIGURE 86. Shock adiabat of the TNT—hexogen (30/70) composition:

1) calculation; 2) experiment.

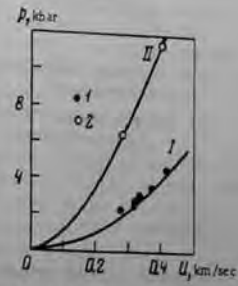


FIGURE 87. Shock adiabat of porous PETN (I) ($\rho = 1.0$ g/cm³) and TNT (II) ($\rho = 1.45$ g/cm³).

The curves represent calculated results and the points, experiment: 1) after Seay and Seely /130/; 2) after V'asil'ev /157/.

Measurement of critical detonation pressure. There are several methods of determining $p_{cr}$ /148/. In early research work the detonation was transferred from the active to the passive charge through an air gap; in recent times, however, experimental methods of determining $p_{cr}$ by an inert partition (metal, plexiglass) have become popular. The scheme of the experiment is shown in Figure 88a (1 — explosive; 2 — partition; 3 — active charge; 4 — plane-wave generator; 5 — detonator) and its graphical interpretation in Figure 88b (0I — shock adiabat of the partition material; 0II — shock adiabat of the investigated explosive; 1, 2 — isentropic curve of partition material rarefaction). A shock wave passes into the partition when the active charge detonates. The pressure in this wave is determined, if we know the shock adiabat of the explosive and the dependence of the mass velocity of the partition on the properties of the active charge. After the wave approaches the boundary separating the partition and the investigated explosive, a wave propagates in the reverse direction

away from the partition while the shock wave propagates through the explosive.

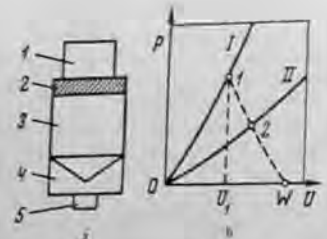


FIGURE 88. Determination of the critical detonation pressure:

a) schematic diagram of apparatus; b) its graphical interpretation.

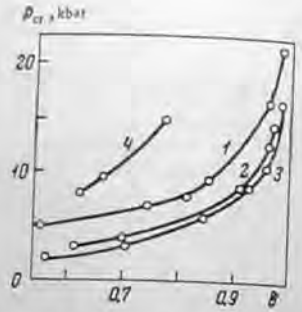


FIGURE 89. Porosity dependence of the critical detonation pressure:

1) TNT, $r < 100$ μ; 2) hexogen, $r < 100$ μ; 3) PETN, $r \simeq 20$ μ; 4) stoichiometric mixture of ammonium perchlorate and polystyrene, $r \simeq 15$ μ.

The pressure in the shock wave entering the investigated explosive is determined by the point of intersection (2) of the shock adiabat with the isentropic line of partition material rarefaction starting from point 1 (the isentropic line is the mirror reflection of the shock adiabat of the partition). The critical pressure $p_{cr}$ is determined as the minimum pressure of the wave entering the explosive for which detonation of the charge is still excited. The magnitude of $p_{cr}$ depends on the charge parameters (density, initial dimension of the particles, diameter). The profile of the initiating shock wave may also have some influence.*

Values of $p_{cr}$ measured in one design of the experiment are now examined (Figure 88). The active charge was made from TNT /147/ or from a TNT + NaCl mixture of different percentage composition /149/. The diameter and height of the active charge were 40 and 60–100 mm, respectively. A plane wave generator was used to obtain a plane detonation front. A 5-mm-thick copper plate served as partition. The passive charge of the investigated explosive (without casing) had a diameter of 20 mm and a height of 60 mm. The onset of detonation was fixed optically when photographing the charge from the lateral surface or from the front.

In the given design of the experiment the dependence of the critical detonation pressure on the relative density for TNT, hexogen /147–149/, PETN and also for a stoichiometric ammonium perchlorate-polystyrene mixture was determined.** The corresponding data are presented in Figure 89.

* Afanas'ev /143/ notes that the profile of the initiating shock wave is important in homogeneous explosives. In porous systems $p_{cr}$ is mainly determined by the amplitude of the initiating wave. This is also confirmed by the fact that the values of $p_{cr}$ for porous explosive charges of the same diameter, obtained by different methods, were found to be close to each other.

** Function $p_{cr}$ (δ) for PETN and the mixed system was obtained by A. V. Obmenin.



It follows from these data that for secondary explosives the critical pressure increases weakly with density when $\delta < 0.85$. At high densities ($\delta > 0.85$), close to the single crystal density, $p_{cr}$ rises abruptly. It is noteworthy that in accordance with data of Figure 13 at density $\delta > 0.85$ a considerable decrease in the gas permeability of the charge is observed. Thus, the presence of a low porosity has a considerable influence on the sensitivity of an explosive in the shock wave. From the investigated substances we see that the highest value of $p_{cr}$ is characteristic for the mixed system.

The charge diameter of the studied secondary explosives over the whole density range considerably surpassed the critical diameter of detonation ($d^*_{cr}$); for the mixed system ($\delta \simeq 0.75$) it was near-critical.

The fragmentary data available in the literature (e.g., /148/) indicate that an increase in the critical detonation pressure is observed at near-critical detonation conditions (at $d_{charge} \simeq d^*_{cr}$). With increasing charge diameter, function $p_{cr}$ ($d_{charge}$) becomes weaker and, when $d_{charge} \gg d^*_{cr}$, $p_{cr}$ is practically independent of the charge diameter. This is confirmed by tests that we conducted with PETN charges of different diameters (Figure 90) (for PETN with $\rho = 1.70$ g/cm$^3$, $d^*_{cr} \simeq 0.3$ mm). When $d_{charge} \gg d^*_{cr}$, the value of $p_{cr}$ is independent of the steel or plexiglass casing of the charge.

Allowance for this, and the fact that the critical detonation pressure in porous explosives is mainly determined by the amplitude of the wave (and not by its profile), gives grounds to apply the values of $p_{cr}$ obtained in tests on shock initiation to the conditions of transition from deflagration to detonation.

The initial particle size of the explosive has a peculiar effect on the sensitivity to a shock wave. We studied $p_{cr}$ (δ) for coarse-crystalline TNT with initial particle diameter $r = 0.4$–$0.8$ mm (we used uncased charges of $d_{charge} = 20$ mm; only the free-flowing charges had diameter $d_{charge} = 30$ mm). Our data are shown in Figure 91, together with other results /147–149/ for fine-crystalline TNT ($r < 0.1$ mm). It follows that the increase in initial particle diameter leads to an intensive increase in $p_{cr}$ for low-density and especially free-flowing charges. In high-density charges the effect of the initial particle diameter is much less pronounced or entirely absent. Decrease in the sensitivity of the coarse-crystalline explosive charges of free-flowing density was noted by Apin et al. /153/. This effect permits one to explain why low-density detonation in powdered explosives propagates only when particles of larger size are used. Low-velocity detonation is in this case protected from transition to normal detonation by the high value of $p_{cr}$. For TNT, the pressure in the low-velocity detonation wave (see p. 118) is much lower than the directly measured value of $p_{cr}$.

The above comments refer to pressed explosive charges with open gas-permeable porosity. In order to study the influence of the physical structure of the charge (state of aggregation), let us compare the $p_{cr}$ values for cast, pressed, molten and liquid explosives (Table 17).

The sensitivity of the explosives to the shock wave exhibits the following decreasing trend: pressed, cast, liquid explosives. Note, furthermore, that the value of $p_{cr}$ for pressed TNT with open porosity is much smaller than for cast TNT of the same density, which contains closed pores. Thus

difference is apparently related to the nature of the porosity. This is confirmed by Amster et al. /155/, who established that the sensitivity of propellant powders with closed porosity is lower than that for powders with open porosity. Thus the sensitivity of the system to the shock wave depends on the presence of porosity, its size, and also on the nature of the porosity. The structure of the charge also has a considerable influence on the formation of the detonation wave.

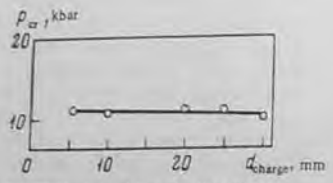


FIGURE 90. Dependence of critical detonation pressure on charge diameter (PETN, $\rho = 1.70$ g/cm$^3$, $r \simeq 20$ μ).

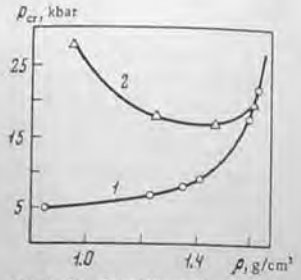


FIGURE 91. Dependence of critical detonation pressure on porosity for TNT samples of different dispersity:

1) $r < 0.1$ mm; 2) 0.4—0.8 mm.

TABLE 17. Critical detonation pressure for some explosives with different physical structures of the charge

| Explosive | Initial density, g/cm$^3$ | Diameter of free-flowing charge, mm | Critical pressure, kbar |
|---|---|---|---|
| Pressed TNT | 1.63 | 20 | 22 /147/ |
| Cast TNT | 1.62 | 20 | 115 /147/ |
| | 1.62 | 48 | 57 /224/ |
| | 1.62 | 60 | 35 /27/ |
| Fused TNT | 1.47 | 20 | 110 /147/ |
| Pressed PETN | 1.73 | 20 | 17 |
| Crystalline PETN | 1.77 | 40 | 112 /118/ |
| Pressed hexogen | 1.74 | 20 | 75 /147/ |
| Crystalline hexogen | 1.80 | 20 | 100 |
| Powdered nitroglycerin | 1.58 | 20 | 85 /147/ |
| Liquid nitroglycerin | 1.60 | 20 | 85 /147/ |
| Liquid nitromethane | 1.14 | 20 | 90 /147/ |

## 30. FORMATION OF THE DETONATION WAVE

At present much research is being carried out on the growth of the shock wave to detonation. The wave front velocity is often measured with this aim in mind.



Much information about this problem was obtained by Dremin and Koldunov /27/, who studied cast fine-crystalline and pressed TNT with initial densities of 1.62 and 1.59 g/cm$^3$, respectively. The electromagnetic method was used to determine the two parameters characterizing the shock wave, namely the velocity $D$ of the front and the time distribution $U(t)$ of the mass velocity behind the front. Also investigated was the electrical conductivity in propagating shock waves, which yielded a fairly comprehensive picture of the process behind the shock wave front. Moreover, the onset of detonation was recorded optically.

The amplitude of the initiating shock wave was 50, 35 and 20 kbar for cast TNT and 35, 18 and 12 kbar for pressed TNT. The last values were smaller than $p_{cr}$ and no onset of detonation was observed. The passive charge diameter was 60 mm, while that of the active charge (mixture of TNT with talc of different densities) was 80 mm. Plexiglass was used as the inert partition.

Measurements of $D$ and $U$ at the wave front, obtained at various distances $L$ from the partition—explosive interface, are shown in Figure 92; oscillograms of $U(t)$ are shown in Figures 93 and 94. It is seen that the growth of a shock wave into detonation proceeds by gradual changes in the values of parameters $D$ and $U$.

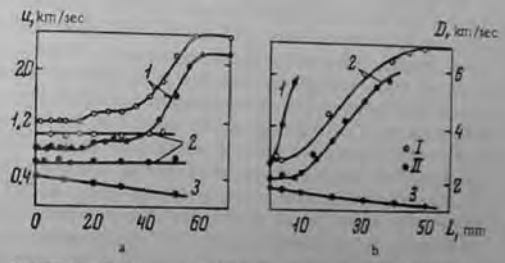


FIGURE 92. Shock wave velocity $D$ (I) and mass velocity of substances $U$ (II) at various distances $L$ from the explosive—partition interface for cast (a) and pressed (b) TNT:

a: 1) $p = 50$; 2) 35; 3) 20 kbar; b: 1) $p = 35$; 2) 18; 3) 12 kbar.


FIGURE 93. Oscillogram of the mass velocity in cast TNT (the interval between the marks corresponds to 2 μsec): $p = 50$ kbar; $L = 0$, 4, 8, 16, 30, 50 mm.


FIGURE 94. Oscillogram of the mass velocity in pressed TNT (a: $p = 18$ kbar; $L = 0, 4, 12, 18$ mm; b: $p = 12$ kbar, $L = 0, 4, 20, 40$ mm).

For cast TNT, we observe an initial section where the parameters of the shock wave that initiates detonation do not change and are given by the incoming wave. Increase in the wave parameters up to the detonation parameters begins at a certain depth, whose magnitude decreases with increasing amplitude. When the wave entering the explosive has near-critical amplitude, the onset of detonation occurs at a considerable distance from the partition (for instance, when $p = 35$ kbar the normal detonation parameters along the charge axis were fixed at depth $L \simeq 120$ mm). Photographs of the process growth showed that luminescence takes place in the predetonation stage of cast TNT and its intensity increases with time. It is of interest that, in the initial section, the velocity of the process (measured from the optical trace) is in agreement with the shock wave velocity measured by the electromagnetic method along the charge axis. These data were used to explain the nature of the low-velocity regime. It follows from Figure 93a that the shock wave in cast TNT retains its triangular profile, which is then transformed into the profile with a "shelf." This changed profile also remains when $p < p_\alpha$ and is associated by the authors with the chemical reaction behind the shock wave front.

In pressed (as opposed to cast) TNT, the tendency for the parameters to increase to detonation is observed directly at the partition – explosive interface (Figure 94a). The wave profile at the interface ($L = 0$) differs from triangular, observed when the shock wave enters the inert material. The $U(t)$ profile with the "hump" sets in when the shock wave propagates with $p > p_\alpha$. Its steepness increases, and is therefore accompanied by an increase in the mass velocity at the front ($U_f$) and at the top of the hump ($U_h$) (Figure 94a). When $p < p_\alpha$, the wave front becomes blurred and the velocity of the front drops below the sonic velocity (Figure 94b).

Electrical conductivity measurements showed that the conductivity in cast TNT begins to grow immediately behind the shock front, whereas in pressed TNT there was some delay before the conductivity increased.

All these experimental data lead to the conclusion that the detonation wave growth process in pressed TNT is more sensitive to changes in the parameters of the entering shock wave than in cast TNT. This experimental result is explained by the fact that the rate of heat release in pressed TNT depends to a considerable extent on the pressure behind the shock front.



It is now assumed that when a shock wave acts on porous explosives, the chemical reaction begins at individual hot spots and proceeds in the form of a thermal explosion. The cause for the creation and existence of hot spots are physicochemical discontinuities in the explosive. The produced reaction propagates, possibly in the form of burning, to the remaining mass of the explosive, and leads to the formation of a system of compression waves which enhance the first shock wave. This situation brings about an increase in the concentration of hot spots, pressure in the zone of reaction, and, finally, leads to detonation.

As yet, no reliable data exist about the processes taking place at the hot spot. Also, the problem of hot spot formation remains open. The following potential causes leading to the formation of individual hot spots of explosion are being considered: collision of shock waves, elastoplastic changes behind the shock front with stress localization, breaking up of flows near the discontinuities, phase transformations, and so on. Such uncertainty creates great difficulties in the development of a theory of shock initiation.

Solid (porous) explosives differ from homogeneous (liquid) explosives in this respect. In liquid explosives the entering shock wave initially propagates as in the inert medium. After some delay at the interface (at the site where the shock wave enters) thermal explosion takes place, leading to the onset of detonation in the compressed explosive, which overtakes the front of the original shock wave. Only then does normal detonation propagate over the explosive.

Research on problems involved in the stability of burning of liquid explosives gave rise to one of the most interesting and original sections of the theory of burning. Its originality is due to the fact that the fundamentals underlying the theory of the formation of instability effects were established before any experimental research or detailed investigations had been carried out. The combination of different, experimentally favorable properties of liquid explosives (such as optical transmission, stable density, wide range of possible burning velocities, possibility of changing the mobility by small additions of high polymers) enables one to perform interesting observations of the burning process.

This aspect of the theory of burning was developed by Andreev, Belyaev, Zel'dovich, Landau, and others. Soviet scientists played a leading role in this field.

Many problems discussed in this part were dealt with in various forms in Andreev's monograph /38/. However, some papers on the stability of liquid explosive burning went unmentioned in some books /37, 38/. In addition, contemporary notions about the mechanism underlying the burning stability of liquid explosives led to a new interpretation of known experimental facts. We hope that this part will be useful because it provides a summary of accumulated data and attempts to explain experimental facts from a single standpoint.

If the critical conditions of the impairment of normal burning of liquid explosives was the subject of a relatively large number of both experimental and theoretical papers, transition from deflagration to detonation has been treated only to a small extent. Few experimental investigations deal with this problem, so it is impossible to form a comprehensive picture about the process. No theory of the problem has yet been developed. The hypothesis is held that burning beyond the stability boundary may lead to spontaneous eddy formation, explosion, and even detonation. However, extrapolation of the limiting pressures to values far beyond the limiting values of the parameters is not always conclusive without theoretical justification. As a rule many factors may generate nonlinear effects, some of which may have a stabilizing influence.

The problem of burning of heterogeneous mixtures of the liquid explosive–solid compound type is relatively new. However, recent papers have established sound bases for understanding the burning mechanisms and patterns of systems of this type.

This part does not deal at all with problems involved in the burning of atomized liquid propellants. Such problems were examined in many well-known papers and books. General technical applications of the burning of liquid explosives lie outside the scope of this book.



*Chapter VI*

# *THEORY OF LIMITS OF NORMAL BURNING OF LIQUID EXPLOSIVES*

## 31. THE ANDREEV–BELYAEV AND ZEL'DOVICH THEORY

The first theory of the burning stability of explosives applied to liquid explosives was that of Andreev and Belyaev, examined in Chapter III. The main conclusion was that the possibility of stable burning at given pressure is determined by the relationship between the burning velocity (more precisely, the rate of gas formation) and the velocity of gas escape, or, more correctly, by the relationship between the acceleration of gas supply and acceleration of gas escape with pressure /38, p. 297/. To a first approximation the condition of burning stability after Andreev and Belyaev assumes the form

$$\frac{1}{A}\frac{d(u_1\rho_1)}{dp} > 1, \qquad (77)$$

where $A$ is the efflux coefficient, of the order of 7–7.6 g/cm²·sec/atm.

The burning velocity of many (but not all) liquid explosives obeys a linear function. Thus

$$B = d(u_1\rho_1)/dp \qquad (78)$$

is pressure-independent, i.e., a constant of the given substance.* Table 18 gives values of $B$ for various individual liquid explosives and mixtures, some taken from Andreev's book /38/. The table shows that the majority of liquid explosives have $B \ll A$; the ratio $A/B$ lies between $3 \cdot 10^1$ and $6 \cdot 10^2$. Hence, in order to impair the burning stability of these substances according to Andreev and Belyaev the flame surface must increase so that its area is $3 \cdot 10^1$–$6 \cdot 10^2$ times larger than the cross section of the tube. Such a large increase in the burning surface can take place only under special conditions. This problem will be considered below.

Thus, both liquid and solid explosives undergoing normal burning have values of $B$ that ensure stable burning in the sense of the Andreev–Belyaev gasdynamic mechanism.

* The dependence of $B$ on charge dimensions (which is usually weak) and initial temperature is not studied here. The introduction of these parameters changes the quantitative but not the qualitative nature of the fundamental conclusions.

TABLE 18. Coefficient $B$ (atm·g/cm$^2$·sec) for different liquid explosives

| Substance | $B$ | Substance | $B$ |
|---|---|---|---|
| Liquid nitroglycol | 0.039 | Gelatinized nitroglycol + $PbN_6$, 40:60 wt % | 0.267 |
| Gelatinized nitroglycol | 0.029 | Nitromethane | 0.0025 |
| Liquid methyl nitrate | 0.133 | Diglycol dinitrate | 0.00246 |
| Gelatinized nitroglycerin | 0.146 | Ethyl nitrate | 0.0064 |
| Gelatinized nitroglycol + $PbN_6$, 50:50 wt % | 0.148 | Nitromethane + 7 wt % pyroxylin | 0.00246 |

Belyaev's experimental research on transition from deflagration of liquid explosives (such as methyl nitrate) to detonation served as the theoretical basis for Zel'dovich's theoretical model /43/ of the burning stability of explosives possessing strong reaction in the condensed phase. The cause leading to impairment of normal burning in Zel'dovich's model is physicochemical. The essence of the mechanism is as follows. When the pressure grows due to the increasing temperature of the liquid surface, the reaction rate in the condensed phase increases and a heating wave enters the bulk of the liquid. Conversion of the vapors and the products of the condensed-phase reaction takes place in the gaseous phase. The condensed- and gas-phase reactions are considered to be independent, so a relationship can be found between the activation energies of the condensed-phase reaction and the heat of vaporization, for which the rate of heating of the liquid will be higher than the rate of vaporization. The liquid is superheated and effervesces in a layer of a certain thickness, which leads to an ejection of the liquid and its vapors into the flame zone. It is assumed that conditions for the growth of detonation are produced in this way.

The results obtained by Zel'dovich's theory are compared with experimental data and discussed in Andreev's book /38/.

## 32. LANDAU'S THEORY OF THE HYDRODYNAMIC STABILITY OF SLOW BURNING

The approach of Landau /73/ to the problem of stable burning differed from that of Andreev, Belyaev and Zel'dovich. Landau assumes the gas-phase mechanism of burning, i.e., vaporization proceeds from the liquid surface, which is sustained by heat released by chemical reactions in the vapors above the surface. Stability of the flow of combustion products is treated by small perturbation techniques with allowance for the stabilizing effect of gravitational and surface tension forces. To a first approximation, the thickness of the chemical reaction zone is neglected in comparison with the length of the perturbation wave. This also means that the processes determining the structure of the liquid-gas interface are neglected. The mathematical formulation of the problem dealing with hydrodynamic stability of the liquid-gas interface is independent of the causes of gas formation, and even of the cause of gas motion. Moreover, Landau's



problem is isobaric; gas compressibility is neglected. The solutions to Landau's problem can also be applied to other models, for example, motion of a liquid layer along the surface, blowing of gas flow past the mirror surface of a liquid.

The continuity equation and Euler's equation are solved simultaneously in order to find the critical conditions for the growth of infinitely small perturbations of the liquid-gas interface. It was found that at a sufficiently high velocity $J = u_1\rho_1$, the burning process becomes hydrodynamically unstable; small surface distortions increase. For a plane flame front to remain stable the roots of the equation

$$\Omega^2(u_1+u_2)+2\Omega k u_1u_2+\left[k^2(u_1-u_2)+\frac{gk(\rho_1-\rho_2)+\sigma k^3}{J}\right]u_1u_2=0 \quad (79)$$

must have a negative real part. This yields the following conditions for the stability of burning:

$$J^4<\frac{4\sigma g\rho_1^2\rho_2^2}{\rho_1-\rho_2}=J_*^4=(\rho_1^2u_2^2)^2, \quad (80)$$

where $u_1$ and $u_2$ are the velocities of the liquid and combustion products in a laboratory system of coordinates; $\rho_1$ and $\rho_2$ are the densities of the liquid and combustion products; $\sigma$ is the coefficient of surface tension; $J = u_1\rho_1 = u_2\rho_2$ is the mass velocity of burning; $J_*$ is the mass velocity of burning in the critical regime (critical burning velocity), equal to $u_2^2\rho_2^2$; $g$ is the free-fall acceleration; $k$ is the wave vector of liquid surface perturbation; $1/\Omega$ is the characteristic time of perturbation growth.

The main consequences of Landau's theory /177–179/ will be examined below.

### Size of the most dangerous perturbations and their growth time

Let us consider burning in a vessel of infinite diameter, in order not to be restricted initially by the permissible dimensions of the perturbations. Equation (79) will be employed to determine the size of the most dangerous perturbations, i.e., those with the shortest time of growth during burning beyond the stability limit. We introduce dimensionless quantities

$$n=\frac{J}{J_*}\sqrt{\frac{\rho_2}{\rho_1}}, \quad z=k/k_*, \quad \omega=\frac{\Omega J_*}{2g}\sqrt{\frac{1}{\rho_1\rho_2}}, \quad (81)$$

where $k_*$ is the wave number of the perturbation that grows most rapidly in the critical regime and is given by

$$k_*=\frac{J_*^2(\rho_1-\rho_2)}{2\sigma\rho_1\rho_2}=\sqrt{\frac{g}{\sigma}(\rho_1-\rho_2)}=\frac{2g\rho_1\rho_2}{J_*^2}. \quad (82)$$

When $n>1$, we take into account perturbations lying in some range of wave vectors $k$ (or wavelengths $\lambda$) depending on the burning velocity:

$$n^2-\sqrt{n^4-1}<z=k/k_*=\lambda_*/\lambda<n^2+\sqrt{n^4-1}. \quad (83)$$

When $n^4 \gg 1$ then $1/2n^3 < x < 2n^3$. Thus with increasing $n$ (burning velocity) the size range of the growing perturbations is expanded toward both long and short wave regions. When $n = 1$, the range is reduced to the point $x = 1$.

In Landau's problem, small-scale perturbations ($x > n^2 + \sqrt{n^4-1}$) are produced by surface tension forces and large-scale perturbations ($x < n^2 - \sqrt{n^4-1}$) by gravitational forces.

The size of the most dangerous perturbation, i. e., that one growing at the fastest rate, is found by determining some value $x_n$ for which $\omega$ assumes its largest value:

$$x_n = {}^1/_2 n^2 + {}^1/_2 \sqrt{4n^4 - 3} \quad \text{when } n - 1 \gg \rho_2/\rho_1. \tag{84}$$

If $\tau$ designates the growth period of perturbations with wave number $x$ at velocity $n$, then

$$\Omega = 1/\tau = \sqrt{g k_*} \sqrt{2n^2 x^2 - x - x^2}. \tag{85}$$

The value of $\tau_{min}$ for the most dangerous perturbation is determined by substituting $x_n$ for $x$. When $n^4 \gg 1$, expressions (84) and (85) simplify to the forms

$$k_n = 2\pi/\lambda_n = {}^4/_3 k_* n^2; \quad 1/\tau_{min} \simeq 1.5 (g n^2/J_*) \sqrt{\rho_1 \rho_2^*}. \tag{86}$$

It can be seen that $\lambda_n$ and $\tau_n$ decrease rapidly as the burning velocity $n$ increases. If the burning velocity is slightly higher than its critical value, i. e., if $J/J_* = 1 + \delta$, $\rho_2/\rho_1 \ll \delta \ll 1$, then

$$1/\tau_n \simeq 2\sqrt{2g} \sqrt{\rho_1 \rho_2^*} \sqrt{\delta}/J_*; \quad k_n = k_* (1 + 4\delta).$$

Near the transition from stable to unstable burning, the random perturbation varies in accordance with the law $\xi_n = \xi_0 \exp(kz - i\omega t)$. When $n < 1$, $\omega \neq 0$ and $z = 0$; when $n > 1$, $\omega = 0$ and $z \neq 0$, i. e., in the region of the stable regime the perturbations produce decaying vibrations of the liquid surface, while in the instability region the amplitude of the perturbations increases and no vibrations arise.

Table 19 presents calculated values of $\lambda_n$ and $\tau_n$ for nitroglycol as dependent on $J/J_*$. It was assumed that $\rho_1 = 1.49$ g/cm$^3$, $\sigma = 48$ dyne/cm$^2$, and $\rho_2^* = 5 \cdot 10^{-4}$ g/cm$^3$.

TABLE 19. Calculated values of parameters $\lambda_n$ and $\tau_n$

| $n$ | $J/J_*$ | $\lambda_n$, cm | $\tau_n$, sec | $\lambda_n/\tau_n$, cm/sec |
|---|---|---|---|---|
| 1.0 | 1.0 | 1.16 | $\infty$ | 0 |
| 1.05 | 1.11 | 0.97 | 0.0273 | 35.5 |
| 1.1 | 1.21 | 0.85 | 0.0180 | 47.5 |
| 1.2 | 1.44 | 0.67 | 0.0108 | 62.0 |
| 1.4 | 1.96 | 0.47 | 0.0055 | 85.5 |
| 1.5 | 2.56 | 0.35 | 0.00343 | 102 |
| 2 | 4 | 0.22 | 0.00165 | 133.5 |



Figure 95 shows the instability region (1) and the wave numbers (2) of the most dangerous perturbation. The region of absolute stability (3) lies below curve 1.

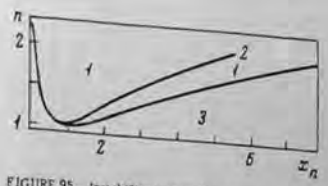


FIGURE 95. Instability region (1), wave numbers of the most dangerous perturbation (2), and region of absolute stability of burning (3).

**Effect of vessel diameter and shape on the stability limit of normal burning**

The above investigation was carried out assuming that the diameter $d$ of the vessel containing the liquid explosive is much larger than the characteristic dimension of the perturbation: $d \gg 1/k_*$.

If the diameter of the vessel containing the burning liquid is so small that this inequality is not satisfied, the size of the most dangerous perturbation $\lambda_d$ in the given case will depend on the vessel diameter and shape, and also $\lambda_d < \lambda_*$; $k_* < k_d$; $x_d > 1$.

Let us investigate qualitatively the effect of the vessel diameter on the critical burning velocity, $J_d(n_d)$. Equation (83) determines the critical burning velocity of the liquid in a tube of diameter $d$:

$$n_d = \sqrt{0.5(x_d + 1/x_d)}. \tag{87}$$

Since $x_d > 1$, $n_d > 1$, i. e., burning in a narrow vessel is more stable than in a wide vessel, due to the stabilizing effect of the walls.* It is evident that in a sufficiently narrow vessel the size of the most dangerous perturbation is proportional to the diameter, while in a sufficiently wide vessel it is diameter-independent: $1/x_d \simeq dk_*$ when $dk_* \ll 1$; $1/x_d = 1$ when $dk_* \gg 1$.

When $x_d^2 \gg 1$, expression (86) is simplified to $n_d^2 = 1/2x_d$ or $n_d^4 \simeq 1/(2dk_*)$. This expression was obtained by Landau /73/.

Let us represent the dependence of $x_d$ on $k_1 d$ by a broken line: $1/x_d = a dk_*$ when $a dk_* < 1$; $x_d = 1$ when $a dk_* \gg 1$, where $a$ is a constant that depends on the vessel shape. If (86) is taken into account we obtain

$$n_d \simeq \sqrt{0.5(a dk_* + 1/a dk_*)} \quad \text{when } ak_* d < 1,$$
$$n_d = 1 \quad \text{when } ak_* d > 1.$$

* Here, of course, secondary phenomena not relating to the hydrodynamic situation (such as heating of the liquid by the flame and heat transfer along the wall) are disregarded.

The dependence of $n_d$ on the dimensionless quantity $k_* d$ should define the general limit of stable burning of all liquid low-viscosity explosives in vessels of identical form, i. e., $n$ and $k_* d$ are dimensionless numbers. This follows from Landau's formulation, which makes it self-similar. The proportionality factor $a$ was calculated by Margolin and Chuiko /179/ for vessels of circular and rectangular cross section.

During burning in a cylindrical tube, allowance must be made for the conditions at the burning surface, and also for the boundary conditions at the tube walls, where the radial velocity component vanishes. This condition determines the permissible wave numbers $k$ of the surface perturbations:

$$k = k_{qs} = a_{qs}/R, \tag{88}$$

where $a_{qs}$ are the roots of the first derivative of the Bessel function $I_q$ of the first kind of $q$-th order; $s$ is the number of the root; $R$ is the tube radius.

The form of the elementary surface perturbations $\xi(r, \varphi)$ is given by

$$\xi \sim I_q(a_{qs} \cdot r/R)\cos q\varphi, \tag{89}$$

where $r$ is the instantaneous radius; $\varphi$ is an angle defined by integers $q$ (number of nodal diameters) and $s$ (number of nodal circles).

The critical burning velocity $J_*(R)$ is related to the tube diameter $d = 2R$ by (80) and (86). Substitution of equation (88) for $k$ into (86) yields the following relationship for burning in a cylindrical tube:

$$u^3 = \frac{J_*^2(R)}{J_*^2} = {}^1/_3\left(\frac{a_{qs}}{Rk_*} + \frac{Rk_*}{a_{qs}}\right), \quad k_*^* = \frac{\rho_1 g}{\sigma}. \tag{87a}$$

In the case of a plane-parallel vessel $a_{qs}$ is replaced by ${}^1/_2 i\pi$ ($i = 1, 2, \ldots$) in (89), while $R$ is half the larger side of the rectangular cross section of the vessel. The wave is self-excited at the stability limit, in which case $aqs/k_*R$ is very close to unity. A wave with $s = 0$ and $q = 1$ should therefore be generated at the stability limit during burning in a narrow tube ($Rk_* < 1$).

To a first approximation the dependence of the critical burning velocity on the tube radius (Figure 96) is only important in narrow tubes:

$$u^3 = J_*^2(R)/J_*^2 = 1 \quad \text{when } Rk_* > 1;$$
$$u^3 = 0.5(R_1/R + R/R_1) \quad \text{when } Rk_* < 1,$$

where $R_1 = a_{10}R_* = 1.84\, k_*$ (burning in a circular tube) and $R_1 = ({}^\pi/_2)\pi k_* \simeq 1.54\, k_*$ (for a plane vessel).

### Effect of gravitational acceleration

It follows from relationships (80) and (84) that the size of the most dangerous perturbation depends strongly on $g$ and increases with decreasing gravitational acceleration. The gravitational acceleration, however, is not important in vessels of infinite diameter. In bounded vessels with decreasing $g$, the factor stabilizing long-wave perturbations is the vessel diameter, which limits the largest dimension of the perturbation. When $g \to 0$ (neglecting interaction of the gas, liquid and vessel surface), it is assumed that

$$J_*^2 \simeq 2\sigma\rho_1^* k_*.$$

In a vessel of infinite diameter with $g \to 0$, $k \to 0$ and therefore $J_* \to 0$, i. e., burning is always unstable under the action of long-wave perturbations. In a bounded vessel the size of the perturbation $\lambda_{max} \simeq d$, while the corresponding $k_{min} \simeq 1/ad$, where $a = \text{const}$. Substitution of $k_{min}$ into (89) in place of $k_1$ shows that, when $g = 0$,

$$J_0^2 = 2\sigma\rho_1/ad.$$

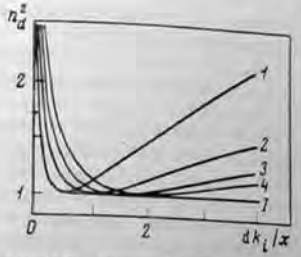


FIGURE 96. Dependence of the limits of stable burning on the reduced vessel diameter at various perturbation harmonics:

1) absolute stability curve; 1) $i = 0.5$; 2) 1.0; 3) 1.5; 4) 2.0.

Comparison of this quantity with the critical burning velocity under normal conditions yields

$$(J_0/J_*)^2 = [(\rho_1)_0/(\rho_1^*)]\,[1/(ak_* d)].$$

If we assume that $J \sim p^\nu$, the ratio of the critical pressures is given by $(p_0/p_*)^{2\nu-1} = 1/(ak_* d)$. Thus, the critical pressure (when $\nu = 1$) is inversely proportional to the vessel diameter. The ratio of the critical pressure $p_d$, determined under normal conditions in tubes of small diameter ($k_* d \ll 1$), to the critical pressure $p_0$ under free-fall conditions ($g = 0$) in a tube of diameter $d_0$ is $p_d/p_0 \simeq d_0/d$ when $ad k_* \ll 1$.

### Effect of the burning law of the liquid

It follows from equation (80) that the critical burning velocity increases with pressure:

$$J_* = C_1 p^{\nu-1}, \tag{90}$$

where $C_1$ is pressure-independent. The burning velocity of explosives can be written as

$$J = Bp^\nu. \tag{91}$$

In liquids, as a rule, $\nu = 1$.

Comparison of (90) and (91) gives

$$u' = \frac{J}{J_*} = \frac{B}{C_1} p^{\nu-0.5}. \qquad (92)$$

The requirement for stable burning is $u' < 1$. The following situations are possible, depending on the relationship between coefficients $B$ and $C_1$ and exponent $\nu$ (Figure 97):

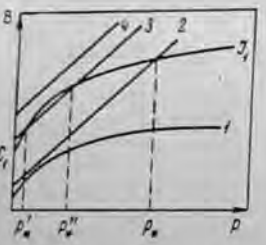


FIGURE 97. Limiting conditions of normal burning as a function of the form of the equation of the burning velocities at different pressures.

1) $C_1 > B$, $\nu < 0.5$; at all pressures $J_* > J$ and burning is stable (curve 1);

2) $C_1 > B$, $\nu > 0.5$; at pressures exceeding $p_*$ burning becomes unstable (curve 2); when $p < p_*$ burning is stable;

3) $B > C_1$, $\nu > 0.5$; two cases are possible: a) curve $J(p)$ intersects curve $J_*(p)$ at two points; burning is stable in the interval $p'_* - p''_*$ and unstable outside this interval (curve 3); b) curve $J(p)$ always lies above $J_*(p)$ (curve 4); burning is unstable at all pressures.

Coefficient $C_1$ may be calculated with the aid of the method developed by Andreev /38/. Equation (80) is simplified by using the equation connecting the parachor $P$, surface tension $\sigma$, molecular weight $M$ and density of the liquid $\rho_1$ (the Bachinskii-McLeod equation $P\rho_1/M = \sigma^{1/4}$). Andreev analyzed several possible variations and showed that his equation

$$J_* \simeq 7.91 \rho_2^{0.5} \rho_1^{1.25} (P/M)$$

actually has the form

$$J_* \simeq \beta p^{0.5},$$

where $\beta \simeq 0.25$ g/cm$^2$ · sec · atm$^{1/2}$ = const.

It follows from Andreev's data on the ratio $P/M$ that it lies between 1.7 and 1.95 for organic explosives. If we assume that $\rho_1 = 1.2 \div 1.6$ g/cm$^3$ for these substances, we see that, according to the Bachinskii-McLeod formula, $\sigma \simeq 17-94$ dyne/cm at a mean pressure of about 40 dyne/cm$^2$. This result shows that utilization of the parachor is practically equivalent to the conventional surface tension value characteristic for liquids at normal temperature. The value of coefficient $C_1$ changes very little, due to the very weak dependence of $J_*$ on $\sigma$ (i.e., on $\sigma^{1/4}$). When Andreev's data on the densities of the combustion products at $p = 1$ atm are employed, we obtain $\rho_2^0$ (1 atm) $\simeq 1.8 \cdot 10^{-4}$ g/cm$^3$. Substitution of this value together with $\rho_1 = 1.4$ g/cm$^3$ yields

$$J_* = 0.12 \sqrt[4]{\sigma} \sqrt{p}, \quad \text{g/cm}^2 \cdot \text{sec},$$



As $\sigma$ varies from 40 to 1 dyne/cm, $C_1/\sqrt{p}$ varies from 0.12 to 0.3 g/cm$^2$ · sec. Thus, to a first approximation $C_1 = 0.2$ g/cm$^2$ · sec · atm$^{1/2} \approx$ const, which is close to coefficient $\beta$. For stable burning, its velocity $J = Bp^\nu$ must satisfy

$$5Bp^{\nu-0.5} \leqslant 1. \qquad (92)$$

It can be seen from Table 18 that in noncondensed liquids the value of $5B$ at 1 atm is close to unity only for methyl nitrate. The burning stability of gelatinized explosives will be considered below.

The problem of the actual existence of considerable surface tension forces when the liquid burns is of fundamental importance. Experiments lead to the conclusion that the surface tension exists during burning and its magnitude is considerable. This was proved, in particular, by experiments in which thermocouples were introduced into the burning liquid: Steinberger /180/ and Belyaev and Lukashenya /181/ observed how liquid adheres to the junction of the thermocouple and rises to a fair height.

## 33. LEVICH'S THEORY

Whereas Landau studied the stabilizing action of surface tension and gravitational forces, Levich /74/ dealt with the hydrodynamic stability of the burning of a viscous fluid. He solved the Navier-Stokes equation by adopting some simplifications.

The critical condition of Levich has the form

$$J^3 < 3\sqrt{3} g \eta \rho_2^{1/2} \rho_1^{3/2} = J_*^3. \qquad (93)$$

The physical sense of (93) will be examined below. The fundamental consequences of Levich's theory /74/ will be dealt with now. He found fundamental laws characterizing the effect of various factors during the onset and growth of discontinuities during burning of a viscous non-Newtonian liquid. The main results of the theories of Landau and Levich are summarized in Table 20, which indicates that a considerable viscosity primarily inhibits the growth of unstable burning; the range of parameters yielding stable burning is wider. In particular, we note the considerable change in the effect of the vessel diameter, for instance at $g = 0$, from a dependence of the type $p_* \sim 1/d$ to a dependence of the type $p_* \sim 1/d^2$, which is related to the increase in the size of the most dangerous perturbation. Comparison of the effect of the vessel diameter when the influence of surface tension or viscosity predominates shows that, for some combination of the parameters, it is possible that for the same substances the function of type $p_* \sim 1/d$, which is valid in the region of larger vessel diameters, changes into the function of type $p_* \sim 1/d^2$, which is valid for small diameters. However, computation shows that the point of transition from one function to the other for conventional explosives lies in the range of very small diameters.

TABLE 20. Comparison of parameters in the problems of Landau and Levich

| Parameter | Equations expressed in terms of | |
|---|---|---|
| | $n, z$ | $n, z$ |
| Critical burning velocity | $J_*^4 = \frac{4\sigma g(\rho_1\rho_2^*)^2}{\rho_1 - \rho_2^*}$ | $J_*^3 = 3\sqrt{3}\, g\eta\rho_1^{1/2}\rho_2^{*1/2}$ |
| Characteristic dimension of perturbation | $k_* = \frac{2g\rho_1\rho_2^*}{J_*^2} = \sqrt{g\rho_1/\sigma}$ | $k_* = \frac{g^{1/2}\rho_1^{1/2}}{2\eta^{1/2}}$ |
| Boundary of perturbation spectrum | $n^2 = \frac{1}{2}(z + 1/z)$ | $n^2 = \frac{1}{3}\left(z^2 + \frac{2}{z}\right)$ |
| Size of most dangerous perturbation: | $z = \frac{2}{3}n^2 + \frac{1}{3}\sqrt{4n^4 - 3}$ | $12n^2z^4 - 8z^3 - 9n^4z^2 + 6n^2z - 1 = 0$ |
| a) $n = 1 + \delta$, $\delta \ll 1$ | $z = 1 + 4\delta$ | $z = 1 + \delta^2$ |
| b) $n^4 \gg 1$ | $z = \frac{4}{3}n^2$ | $z = \frac{\sqrt{3}}{2}n$ |
| Effect of vessel diameter | $J_*^2 \sim \frac{\sigma\rho_2}{d}$; $p \sim \frac{1}{d}$ | $J_*^3 \sim \frac{\eta^2\rho_2}{d^2\rho_1}$; $p \sim \frac{1}{d^2}$ |
| Period of perturbation growth: | $\Omega = 1/\tau = \sqrt{k_* g} \times \sqrt{2n^2z^2 - z - z^3}$ | $\Omega = \sqrt{\frac{k_* g}{2}}(-z^2 + \sqrt{3n^2z^2 - 2z})$ |
| a) $n = 1 + \delta$, $\delta \ll 1$ | $1/\tau = 2\sqrt{gk_*}\sqrt{\delta}$ | $1/\tau = 3\delta\sqrt{gk_*/2}$ |
| b) $n^4 \gg 1$ | $1/\tau \sim \sqrt{gk_*}\, n^3$ | $1/\tau \sim n^2\sqrt{gk_*}$ |
| Perturbation growth rate: | $v \sim \lambda/\tau$ | |
| a) $n = 1 + \delta$, $\delta \ll 1$ | $v = 2\sqrt{gk_*}\sqrt{\delta}/(1 + 4\delta)$ | $v = 3\sqrt{gk_*}\delta/4(1 + \delta^2)$ |
| b) $n^4 \gg 1$ | $v = 3\sqrt{gk_*}\, n/4$ | $v = 2\sqrt{gk_*}\, n/\sqrt{3}$ |
| Gravitational field absent ($g = 0$) | $J_*^2 \sim \frac{\sigma\rho_2}{d}$; $p \sim \frac{1}{d}$ | $J_*^3 \sim \frac{\eta^2\rho_2\rho_1}{d^2}$; $p \sim \frac{1}{d^2}$ |
| Surface tension absent ($\sigma \to 0$) | | |
| a) $\lambda_* < \varkappa_1/u_1$ | $J_*^2 \sim g\varkappa_1\rho_1^2\rho_2^*$ | $J_*^3 = 3\sqrt{3}\, g\eta\rho_1^{1/2}\rho_2^{*1/2}$ |
| b) $\lambda_* \ll d$ | $J_*^2 \sim g\rho_1\rho_2^* d$ | |



## 34. BURNING STABILITY AT PRESSURES ABOVE THE (THERMODYNAMIC) CRITICAL VALUE

There exist a critical pressure and a critical temperature which, when exceeded, lead to the cessation of surface tension in liquids. The critical pressure of organic liquid explosives is $p_{cr} = 40$–$50$ kg/cm$^2$. The critical temperature, on the other hand, has not been determined. Empirical expressions /182, 183/ for weakly associated liquids yield a temperature of about 250–350°C (this approach is not justified theoretically). Andreev /38/ examined burning of liquid explosives; he studied the equation of Landau and concluded that stable burning of these substances at a pressure exceeding 50 atm is impossible. Within the framework of Landau's theory, the only factor stabilizing short-wave perturbations is the surface tension and for this reason these perturbations begin to grow when $\sigma \to 0$. Allowance may naturally be made for $l_p$, the thickness of the reaction zone (in Landau's theory $l_p = 0$), and it can be assumed that perturbations of size less than $l_p$ do not affect burning. Let us write the expression for the perturbation size as $\xi \sim 1/ak_*$, while $l_p \sim \varkappa_1/u_1$. Landau's equation and Table 20 show that in order to satisfy the criterion $\xi \leqslant l_p$, the critical burning velocity when $\sigma \to 0$ must be

$$J_*^* \simeq (g\varkappa_1\rho_1^2\rho_2^*)^{1/2}. \qquad (94)$$

If $p_{cr} \simeq 50$ atm, $J_*^* \simeq 35 \cdot 10^{-2}$ g/cm$^2$ · sec, which is very low.*

The viscosity of the liquid is the other factor stabilizing short-wave perturbations. When $\xi \gg l_p$, which is allowed by the postulates of the theories of Landau and Levich, the fraction of heated liquid in the perturbation wave is insignificant. The surface tension may drop to a very small value as a result of heating of the surface; however, viscosity forces in the layer below the surface will always act. This leads to the conclusion that the viscosity may function as the stabilizer of the short-wave perturbation at supercritical pressures, whereas the critical condition for the growth of perturbations becomes the Levich criterion. Conventional liquid organic explosives have viscosities of a few centipoises at standard temperature. An estimate of quantity $J_*^*$ by Levich's equation gives $J_n^* \simeq 0.05\sqrt{p}$ ($p$, atm; $J_n^*$, g/cm$^2$ · sec), when $\eta = 10^{-2}$ poise. Thus at low $\sigma$ viscosity becomes the stabilizing factor and burning may remain stable even at pressures that are above critical in the sense considered here. However, the coefficient by which the square root of the pressure is to be multiplied (when $\eta = 10^{-2}$ poise) is somewhat lower in the problem of Levich than in the problem of Landau (when $\sigma = 30$ dyne/cm). If the burning velocity is small at the critical (thermodynamic) pressure and computation by Landau's equation gives very high values, the limiting conditions of normal burning will be determined by Levich's equation. If, on the other hand, $J_*$ according to Landau is expected to lie near the critical pressure, the limit of normal burning is given by the simultaneous action of the (decreasing) surface tension and viscosity. At high viscosities in the sense considered here, attainment of the critical pressure does not affect the stability of burning but may have some influence due to other causes (by reducing to zero the heat of vaporization of the liquid).

* Relationship (94) also holds for gases.

More complicated problems are involved in reaching the critical temperature $T_{cr}$ on the burning surface. With volatile explosives the surface temperature is limited by the boiling point, which increases with pressure. It is quite possible that $T = T_{cr}$ is reached both when $p < p_{cr}$ and $p \gg p_{cr}$. At the same time we must remember that the maximum surface temperature $T_s$ is limited by the decomposition temperature of the substance, and since ordinary explosives decompose at temperatures below the rated values $T_{cr} = 250-350°C$. $T_s$ is below $T_{cr}$. On the whole the problem remains open, since the conditions at the decomposing surface of the liquid are unclear. We can assume that the difficulties involved in attaining $T_{cr}$ stabilize burning even at pressures exceeding $p_{cr}$.

Increase in the initial temperature $T_0$ of liquid explosives has a double effect. First, the burning velocity of the liquid increases with increasing $T_0$. At the same time, too, critical conditions (80) and (93) vary due to the decrease in $\eta$ and $\sigma$ (to the same extent to which the temperature of the burning surface grows) on increasing the initial temperature (the effect of $T_0$ upon $\rho_2$ may be neglected). Analysis of the critical situation as dependent on $T_0$ shows that growth in $T_0$ considerably reduces the critical pressure $p_*$ and velocity $J$. The temperature dependence of the viscosity is exponential, so the initial temperature should affect burning of high-viscosity systems much more than burning of inviscid systems.

## 35. CRITICAL REYNOLDS NUMBER IN BURNING OF LIQUID EXPLOSIVES

According to the theory of Landau /73/, unstable burning should begin to develop at Reynolds numbers $Re_* \simeq 1$. Recent research on the stability of gas flames /184, 185/ shows that the experimental values of $Re_*$ are in good agreement with theory, if the size of the sections into which the unstable flame is divided is taken as the characteristic value. Though the actual value of $Re_*$ is $(2-4)\cdot 10^2$, the dissipative effect caused by the viscosity of the gas practically eliminates all contradictions between theory and experiment.

A similar estimation for burning of liquid explosives is of definite interest. If the aforementioned calculated values of $J_*$ are employed and the controlling dimension is taken as the wavelength of the most rapidly growing perturbation $\lambda_*$, then for the problem of Landau

$$Re_*^* \simeq \frac{J_* \lambda_*}{\eta} = \frac{2\pi \sqrt{3}}{\eta} \sqrt[4]{\frac{\sigma^3 (\rho_2^*)^2}{g \rho_1^*}}.$$

Substitution of the typical values $\eta = 2$ centipoise, $\sigma = 30$ dyne/cm and $\rho_2^* = 2 \cdot 10^{-4} \cdot p$ g/cm$^3$ for the liquid yields

$$Re_*^* \sim 10 \sqrt{p_*} = 10 - 100.$$

The Reynolds number involves the parameters of the liquid but not those of the combustion products. This confirms that the instability is generated in the liquid phase.



By a similar approach we obtain for the problem of Levich

$$Re_*^* \simeq 22 \sqrt{\rho_2^*/\rho_1} \simeq 0.25 \sqrt{p_*} \simeq 0.5 - 2.$$

Hence, as for the burning of gases, the burning of liquid explosives is characterized by critical values of the Reynolds number (of the order of unity) calculated for the most rapidly growing perturbation.

In the light of this conclusion, one can explain the unsuccessful attempt of Whittaker et al. /186/ to correlate the onset of perturbations with Reynolds numbers in the gaseous phase reaching the order of 2000 (this value is characteristic for transition from laminar to turbulent flow in a tube). Whittaker et al. /186/ correlate the onset of turbulence with the gaseous phase and take as the controlling dimension the diameter of the tube in which the explosive was ignited. However, even Whittaker et al. /186/ assume that their Reynolds number does not accurately characterize the phenomenon, and therefore introduce the effect of the thermal losses of the charge to the surroundings as the factor stabilizing burning.

Experimental data processing by means of the critical Reynolds number derived by the above technique is sometimes of definite interest.

## 36. INTERPRETATION OF THE CRITICAL CONDITIONS IN THE THEORIES OF LANDAU AND LEVICH

The physical essence of critical conditions (80) and (93) will be clarified with the aid of dimensional analysis proposed by Margolin: the magnitudes of the forces stabilizing and destabilizing the perturbation are compared with the characteristic dimension $\xi$ at the liquid surface. It should be remembered that the combustion products ($\rho_2$, $u_2$) escape from the perturbation surface, the body force $F_g \sim \xi^3 g \rho_1$ tends to "diffuse" the perturbation, while surface tension forces $F_\sigma \sim \xi\sigma$ and viscosity forces $F_\eta \sim \xi \eta W$ (where $W$ is the rate of "diffusion" of the perturbation) tend to prevent the breakup of the perturbation wave. Hence the equilibrium condition (or, more precisely, the nonaccelerated movement or relative equilibrium) in Landau's problem has the form

$$a_1 \xi^3 g \rho_1 + a_2 \sigma \xi \simeq \xi^3 \rho_1 u_2^2 \qquad (95)$$

or

$$\xi_{1,2} = \frac{1}{2a_1 g \rho_1} [\rho_1 u_2^2 \pm \Delta] \quad (a_1, a_2 - \text{const});$$

$$\Delta^2 = (\rho_1 u_2^2)^2 - 4a_1 a_2 g \rho_1.$$

The result will be studied with the plus sign selected before $\Delta$. When $J^4 = (u_2 \rho_1)^2 < 4a_2 g \rho_1 \sigma \rho_2^2 = J_*^4$, the expression for $\xi$ becomes complex and corresponds to surface vibrations with amplitude of the order of $\xi \sim u_2 u_2 / 2a_1 g$. Naturally, comparison of (95) with the expression for the perturbation wavelength (see equation (83)) $\lambda_* = \lambda_* \exp(kx - i\omega t)$, which

in a Taylor expansion near the critical point with $n < 1$ has the form $\lambda_n \simeq \lambda_* (1 - i\omega t)$, yields $\lambda_* \sim \xi = u_1 u_2 / 2a_1 g$,

$$\omega t = \sqrt{\frac{4\sigma\rho_1 a_1}{\rho_* u_*^2}} - 1 = \sqrt{g/k_*}\sqrt{(p_*/p)^2 - 1},$$

where $p_*$ and $k_*$ are the critical pressure and wave number of the perturbation. Surface vibration is interrupted at the point $J = J_*$, $\Delta = 0$, which is the critical point in Landau's problem, while the condition $J = 0$ satisfies (80). Here, $R_* = \xi_* = u_1 u_2 / 2a_1 g$. Outside the range $J > J_*$, $\xi$ increases in proportion to the increase in velocity, i. e., burning becomes unstable. When $J \gg J_*$, surface tension may be neglected and $\lim \xi = u_1 u_2 / a_1 g$ for $u_1 \to \infty$, i. e., the amplitude of the perturbation increases by a factor of two in comparison with the value at the stability limit. This corresponds to an increase in the burning surface by approximately $\xi^2$, i. e., by a factor of about 4. Quantity $\xi$ is the limiting dimension that yields the extreme estimate, and all perturbations with amplitude less than $\xi$ are permissible.

A similar consideration for Levich's problem is complicated by the fact that we do not know beforehand the "diffusion" rate $W$ of the perturbation. Therefore, the solution to the equation

$$\rho_2 u_{2n}^2 = a_3 \rho_1 g \xi^{-1} + a_4 \eta \xi W,$$
$$\xi_{1,2} = \frac{1}{2a_3 g \rho_1} [\rho_2 u_2^2 \pm \sqrt{u_2^4 \rho_2^2 - 4a_4 \eta g \rho_1 W}] \qquad (96)$$

identifies the critical condition $u_2^4 \rho_2^2 = 4a_4 \eta g \rho_1 W$ with the solution (93) of Levich, in analogy to Landau's problem. Hence $W \sim \sqrt{u_1 u_2}$ to within a factor of the order of $\sqrt{2/a_4}$.

As in Landau's problem, at subcritical burning velocities equilibrium is attained by surface vibrations; beyond the limit of stable burning the perturbation amplitude increases with burning velocity.

Introduction of the velocity of movement of the perturbation, which is the pulsation velocity of the movement of the perturbation in the liquid, allows $\xi_*$ to be expressed in the form $\xi_* = W^2 / 2a_1 g$. Comparison with Table 20 shows that $\xi_*$ is the size of the most dangerous perturbation growing at the stability limit.

The perturbation amplitude was examined earlier using only one value of $\xi$, corresponding to the minus sign before the root, i. e., long-wave perturbations were considered. The other value of the amplitude corresponds to the short-wave perturbation, which increases with burning velocity and so leads to the conclusion about the expansion of the spectrum of permissible values of $\xi$ when the burning velocity increases.

Burning will be stabilized as a result of both forces in the region where $F_\sigma \simeq F_\eta$.

Thus the critical conditions of Landau correspond to the instant at which the surface tension forces (or the viscosity forces, in the problem of Levich) no longer stabilize the movement of the surface, and its vibration passes into a continuous growth in the perturbation amplitude.

It is noteworthy that stabilization by viscosity forces in comparison with surface tension forces predominates with increasing burning velocity, since $F_\eta / F_\sigma \sim J\eta / \sigma \sqrt{\rho_1 \rho_2}$. In other words, the process is mainly stabilized by viscosity forces at higher burning velocities.



This examination shows that for the supercritical region one can select $\xi_\sigma^0$ as the measure of the perturbation amplitude in Landau's problem and $\xi_\eta^0 \sim \sqrt{\eta W / g\rho_1}$ in Levich's problem. The scale of the perturbation amplitude is $u_1 u_2 / g$ for burning up to the stability limit. The measure of the velocity of movement of the perturbation is given by $W \sim \sqrt{u_1 u_2}$ for burning beyond the stability limit and $u_2 \rho_2$ in the precritical region.

## 37. SPECIAL FEATURES OF THE BEHAVIOR OF GEL-LIKE SYSTEMS

Liquid explosives are, as a rule, Newtonian systems. The rate of their deformation is directly proportional to the applied stress. However, during condensation of liquid explosives by high polymers, the systems become non-Newtonian or even viscoplastic when the disperse phase is introduced. In non-Newtonian liquids the shearing velocity increases with stress according to a power law with exponents greater than unity, i. e., the viscosity of such systems depends on the applied stress. Therefore, in Levich's problem we must use for non-Newtonian liquids values of $\eta$ corresponding to the perturbing stress $F \sim \rho_1 (u_1 u_2)_* = J_*^2 / \rho_2$. Substitution of an expression of the type $\eta = \eta_0 F^{-s}$ in (93) yields the critical condition in this case:

$$J_*^{2+2s} = 3\sqrt{3} \eta_0 g \rho_1^s \rho_2^{(1+s)}. \qquad (97)$$

Many gel-like explosives possess plastic properties, which in simpler cases are described by the Bingham body /187, 189/. The Bingham body is characterized by a yield value $\gamma_0$. If shearing stresses $F$ less than $\gamma_0$ are applied, the substance does not flow but behaves like a solid. The experimental values of $\gamma_0$ depend on the type of gel and lie between $10^2$ and $10^5$ dyne/cm$^2$ /188/. For plastic gels the limiting velocity of normal burning when $\gamma_0 \gg \eta' g \rho_1 \rho_2 / J^2$ is $J_* = \sqrt{\gamma_0 \rho_1}$; when $\gamma_0 \ll \eta' g \rho_1 \rho_2 / J^2$ it is determined by Levich's formula (93). Here, $\eta'$ is the plastic viscosity.

There exists in gel-like systems a dynamic surface tension which is several times higher than the static surface tension. Some systems are even characterized by an ultradynamic surface tension which may be as high as 300 dyne/cm instead of the normal 30 dyne/cm. This may become an important factor of perturbation stabilization, especially if instabilities are produced by high-frequency oscillations, including those generated by the burning process itself /189/. The critical burning velocity may increase severalfold when $\sigma$ or $\eta$ increases by one order of magnitude, because the burning velocity depends weakly on surface tension and viscosity. Moreover, this is a change in the absolute value of these viscosity, which determine variations in the factors stabilizing burning quantities.

## 38. ARTIFICIAL PERTURBATIONS IN THE SUBCRITICAL BURNING REGIME

In subcritical conditions, perturbations larger than $\xi_\sigma^0 = \sqrt{\sigma / g\rho_1}$ (or $\xi_\eta^0 = \sqrt{\eta W / g\rho_1}$) may be only artificial, since they cannot be generated by

burning. Such perturbations may be introduced from the outside, for instance, by igniting the explosives or shaking the vessel containing the explosive. Artificial perturbation may either increase to a size comparable with the size of "natural" perturbations, or burn out.

At low viscosity, perturbations do not cease if $\xi < \sqrt{\sigma/g\rho_1}$. The results in section 36 allow us to state that the surface oscillates with simultaneous burning, and moreover $t_b < t_{spread}$. If $\xi \geqslant \sqrt{\sigma/g\rho_1}$, the perturbation spreads out during time $t_{spread} \sim \xi/W$. Comparison of $t_{spread}$ with the time the perturbation burns up $t_b \sim \xi/u_1$ indicates that $t_b > t_{spread}$ when $u_1 < \sqrt[4]{\sigma g/4\rho_1} \sim 5$–$10$ cm/sec and $\xi \geqslant \xi^0$. Hence large artificial perturbations in the subcritical regime practically always burn up during a period of the order of $(\xi - \xi^0)/u_1$ to dimensions of the order of $\xi^0$. Thereafter, they behave as natural perturbations. At high viscosities, the burning period of the perturbations is larger than the period of spreading and pulsations of the surface should be absent.

In the case of inviscid liquids, artificial perturbations therefore spread more quickly than they burn up, whereas the opposite applies to high-viscosity liquids. This indicates the diverse mechanism of the destruction of artificial perturbations in the subcritical region: spreading in inviscid and burning up in high-viscosity liquids.

At near-critical conditions, artificial perturbations introduced from the outside may "swing" the burning surface to the limiting amplitude, while under favorable conditions (absence of perturbing factors) the amplitude of the oscillations may not increase beyond the limits of infinitely small perturbations and burning will take place stably. Under these conditions a strong external perturbation is capable of producing eddies in the flow of combustion products, which will decay via an oscillatory regime. All this may affect the recorded burning velocity. It follows from the above that a perturbation with amplitude $\xi > \xi^0$ is a strong perturbation. Note that the value of $\xi^0$ is sometimes very small, and in experiments special measures must be taken if we wish to observe the phenomenon in its pure form. In particular, gas bubbles dissolved in the liquid may become sources of "large" perturbations.

If the conditions are such that both $\sigma$ and $\eta$ are small (low-viscosity liquid, low surface tension, high temperature of the burning surface, etc.), the perturbation spreading period is $t_{spread} \sim \sqrt{2\xi/g}$.

The theory gives no correlation between the surface oscillation frequency and the burning parameters. However, the following qualitative features can be expected. On approaching the critical point, the oscillations of the burning surface produced by the perturbations will decay at a slower rate, since equilibrium (absence of oscillations) is attained when approaching the critical point from the side of lower burning velocities. Pulsations decay rapidly in the early stage of the subcritical region, and the initial perturbations are absorbed and do not distort the growth of the burning process.

## 38. FEATURES OF BURNING IN THE SUBCRITICAL REGION

Our analysis in previous sections of this part has shown that in the subcritical region of burning the time taken to burn up the perturbations



generated by the burning process is frequently shorter than, or comparable to, the time taken by the perturbation to spread. Flame surface oscillation during simultaneous movement of the perturbation waves produces convective mixing of a thin liquid layer adhering to the flame surface. The surface perturbations promote heat exchange in the surface layer and are capable of expanding the heated layer by the addition of convective heat transfer to conductive heat transfer /38/. If weak eddy formations at the liquid surface are capable of promoting the ejection of vapors into the gaseous phase (which may be observed in substances with a hot flame), intensive mixing of the layer near the surface may cool the heated layer and the chemical reaction zone to such an extent that the thermal equilibrium conditions are impaired and burning decays.

In limiting situations, intensive mixing of the heated liquid layer with cool masses lying below the heated layer leads to thermal losses from the reaction layer. This gives rise to preconditions for a paradoxical effect: the formation of liquid perturbations near the stability limits at the site where surface oscillations exist and spreading of perturbations capable of increasing the critical burning diameter $d_{cr.b}$. This phenomenon is impossible beyond the stability limit, where such oscillations are absent.

It is natural to assume that if the perturbation amplitude is much larger than the thickness of the heated layer and the burning-up period of the perturbation is larger than the spreading period $t_{spread}$, we may expect surface oscillations to have some effect on $d_{cr.b}$, whereas decay is possible when $t_b < t_{spread}$. Comparison of the heated layer thickness $l \sim \varkappa_1/u_1$ with $\xi \sim u_1 u_2/g$ (where $\varkappa_1$ is the thermal conductivity coefficient of the liquid explosive) shows that the condition for the considered effect to arise is fulfillment of the inequalities $u_1^4 \geqslant \varkappa_1 \rho_2 g/\rho_1$ and $t_b > t_{spread}$.

The subcritical burning period, during which the liquid surface oscillates, is also characterized by the fact that in this period the burning velocity is several times higher than the normal burning velocity (without surface oscillations), due to curving of the flame surface.

On the other hand, the velocity itself depends on the introduction of artificial perturbations from outside. Transition through the critical point eliminates the indeterminacy of the size of the burning surface; it should be characterized by an abrupt break in the pressure dependence of the burning velocity, since beyond the stability limit oscillations with limited amplitude are changed (according to the theory of Landau) by the increase in the perturbation amplitude without oscillations. This permits one to consider it natural that the specified mean burning velocity of the liquid explosive charge between the region where $\varkappa_1/u_1 > (u_1 u_2/g)$ (perturbations do not affect burning) and the critical point may lie between the normal velocity and a velocity 2–4 times as high as the normal burning velocity (in proportion to the growth of the flame surface due to its bending during oscillations).

Decomposition of the standing perturbation wave (appearance of an imaginary part in the equations for the perturbation amplitude) in the subcritical burning region generates a traveling or rotary wave which, as it were, "flows over" and escapes beyond the point with the largest local pressure. Since the pressure gradient is generated by burning of the perturbation waves themselves, we shall take the rate of "spreading" as the measure for the velocity of such waves. This means that in a circular vessel, where the wave will rotate, the rotational frequency will depend on

the vessel diameter $d$ and on the burning velocity: $f \sim W/d \sim u_1\sqrt{\rho_1}/d\rho_2 \sim \sqrt{p}/d$. In a plane vessel we must expect generation of a traveling wave, whose velocity $W$ will be of the order of approximately $\sqrt{u_1 u_2}$.

## 40. POSSIBILITY OF EDDY FORMATION IN THE FUSED LAYER OF A BURNING SOLID EXPLOSIVE

Eddy formation of the melted surface layer of burning fusible explosive is sometimes regarded as one of the most important factors leading to transition from deflagration to perturbed burning and explosion /85/. Dimensional analysis relationships are employed to estimate the possibility that this effect arises.

Dimensional analysis shows that perturbations grow if the layer of melt $l_{melt}$ is thicker than the order of magnitude of the perturbation wave $\xi$. Here,

$$l_{melt} \sim \frac{\varkappa_1}{u_1} \ln T'; \quad \xi \sim \frac{u_1 u_2}{g}; \quad T' = \frac{T_* - T_{melt}}{T_{melt} - T_0},$$

where $T_*$, $T_{melt}$, $T_0$ are the surface temperature of the burning explosive, the melting point of the explosive and the initial charge temperature, respectively. Hence $l_{melt} \gg \xi$ is equivalent to the condition

$$a_1 \varkappa_1 g \rho_1^3 \rho_2 \ln T' \gg J^3,$$

where $a_1$ is a constant.

If the perturbations are stabilized by viscous forces in the melted layer of the explosive, the burning velocity for the growth of perturbation must exceed the critical value according to Levich (equation (93)). The necessary condition for perturbation of burning of the fused explosive is

$$a_1 \varkappa_1 g \rho_1^3 \rho_2 \ln T' \gg J^3 > 3\sqrt{3} g \eta \rho_1^{1/2} \rho_2^{3/2}, \tag{98}$$

or

$$\frac{a_1 \varkappa_1}{3\sqrt{3}} \frac{\rho_1^{1/2}}{\eta \rho_2^{1/2}} \ln T' \gg 1, \tag{99}$$

which (in order of magnitude) corresponds to the condition

$$\eta \sqrt{p_*} \ll a_2$$

($\eta$ in poise; $p_*$ in atm; $a_2 \simeq \text{const} \simeq 1$). When $\eta > 1$ poise, $p_* \ll 1$ atm, and high values of $p_*$ are only possible if $\eta < 1$ poise. However, it was shown above that when $\eta < 1$ poise the predominating effect is exerted by surface tension. In this case relationship (99) is replaced by an inequality of the type $a_2 u_1 / p_* \gg 1$, where $a_2$ is a constant of the order of unity and $u_1$ is the linear burning velocity; $p_*$ is given in atmospheres. Such an inequality is sometimes not satisfied in the region where $p_* > 1$ atm, since $u_1 = Bp^\nu$ ($B \simeq 10^{-1}$–$10^{-2}$ cm/sec · atm$^{1/\nu}$, $\nu \leqslant 1$).



Thus the growth of perturbations in the melted layer is unreal. Only at initial temperatures very close to the melting point ($T_0 \simeq T_{melt}$), when the substance is practically liquefied, can the considered effect take place, since in this case, in principle, there will be no difference between the substance and the viscous liquid.

## 41. STABILITY OF BURNING AT VARIABLE PRESSURE /179/

When liquid explosives burn under conditions of increasing pressure the ratio of the growth period of perturbations $t_0$ to the period of pressure change $t$ is important. If $t_0 \gg t$ the perturbation does not succeed in growing, whereas if $t_0 \ll t$ burning will be identical to constant-pressure burning. It may be assumed that the stability criterion for burning under increasing pressure conditions is

$$t_0/t \simeq \text{const} \simeq 1. \tag{100}$$

Since $t_0$ rapidly decreases with increasing pressure (see Table 20) it is sufficient to consider criterion (100) near the critical conditions characteristic for constant-pressure burning (the theories of Landau and of Levich). Suppose the critical pressure is $p_{cr}$ and the corresponding velocity $J_*$ under increasing pressure conditions. In this case

$$1/t = \dot{r} \sim \frac{1}{p_{cr}} \left(\frac{dp_{cr}}{dt}\right)_*; \quad t_0(p_{cr}).$$

When $n = J/J_* = 1 + \delta$, $\delta \ll 1$, we obtain:

a) for low viscosity ($u_1 \sim p$)

$$2\dot{r}\sqrt{\delta g k_*} = 2\dot{r}\sqrt{\delta} g^{1/4} \sqrt[4]{\rho_1/\sigma} \sim 2\dot{r} \sqrt[4]{\rho_1/\sigma} g^{1/4} \sqrt{(p_{cr} - p_*)/2p_*} \simeq \text{const} \simeq 1; \tag{101}$$

b) for high viscosity

$$^3/_2 \dot{r} \delta \sqrt{g k_*} = \frac{3}{2\sqrt{2}} \dot{r} \eta^{-1/2} g_1^{1/2} \rho_1^{1/2} (p_{cr} - p_*)/p_* \simeq \text{const} \simeq 1. \tag{102}$$

In the particular case of a liquid explosive burning in a manometric bomb and when the burning law for this explosive has the form $u_1 = Bp^\nu$, the characteristic time of pressure change is given by

$$\dot{r} = 1/t = V\rho_0^2/BSp\rho_1 = VMp^{1-\nu}/BSRT_0\rho_1,$$

where $S$ is the burning surface area, $V$ the bomb volume, $T_0$ the temperature of the combustion products, $R$ the gas constant, and M the molecular weight; for many liquid explosives, $\nu = 1$.

In other words, in a manometric bomb for low viscosity and $\nu = 1$,

$$(p_{cr} - p_*)/p_* \sim (S/V)^2,$$

whereas for high viscosity and $\nu = 1$,

$$(p_{cr} - p_*)/p_* \sim (S/V).$$

When $V \to \infty$, $p_{cr} \to p_*$, i. e., combustion takes place in a manner similar to that in the constant-pressure bomb. During burning of liquid explosives in the manometric bomb ($p_{cr} - p_*$) is larger, the faster the pressure increase in the combustion volume. Moreover, other conditions remaining unchanged, viscous systems yield a larger difference ($p_{cr} - p_*$) than do low-viscosity explosives.

Figure 98 illustrates the above results. Here, $p_*$ is the critical pressure of normal burning when $\dot{p} = 0$; in other words, in a constant-pressure bomb $p$ represents the instantaneous pressure and $\tau$ the time.


FIGURE 98. Effect of the rate of pressure change in the ignition volume on the critical pressure of normal burning.

Consider two experiments with different rates of pressure change in the bulk of the bomb: $\dot{p}_1$ and $\dot{p}_2$ (curves 1 and 2); moreover, $\dot{p}_1 < \dot{p}_2$. Time will be measured from the instant at which $p = p_*$. In $p/p_* - \tau$ coordinates, the dependence of the perturbation period in Landau's problem (curve a) and in Levich's problem (curve b) is hyperbolic, and tends asymptotically to $p/p_* = 1$ when $t \to \infty$. According to expressions (101) and (102) and Table 20, curve b lies in the region of larger times and is steeper than curve a. The points of intersection of curves 1 and 2 with curves a and b define the critical pressures observed during burning under increasing-pressure conditions. At the same time, the faster the pressure growth, the higher is the critical pressure, whereas for equal $\dot{p}$ high-viscosity systems (Levich's problem) give higher values of $p_{cr}$ than low-viscosity systems (Landau's problem).

## 42. PROBLEMS OF THE THEORY OF BURNING OF LIQUID EXPLOSIVES BEYOND THE STABILITY LIMITS

The theories of hydrodynamic stability of burning of liquid explosives, developed by Landau and Levich in the form explained above, yield stability criteria but cannot predict the nature of the process at supercritical pressure. In this sense, no theory of the growth of perturbed burning has yet been constructed.

The flow pattern of the combustion products of a perturbed liquid will be examined below. Use will be made of the results of discussions carried out elsewhere on gaseous mixtures /185/ with allowance for the fact that, unlike gaseous systems for which $\rho_1 \simeq \rho_2$, for liquids $\rho_1 \gg \rho_2$.



### Flow of combustion products during perturbed burning

When a flat unperturbed surface of a liquid surface burns, the flow of combustion products is irrotational and (neglecting lateral effects) one-dimensional. However, the flow pattern changes abruptly beyond the stability limit. The evaporation products, issuing from the curved surface when expanding during the reaction, may form eddies, since the gas flow becomes three-dimensional and is not barotropic. Calculations /185, 190/ show that the eddies spread nonuniformly over the flame surface. The highest rate of eddy formation takes place near the points of inflection of the curved profile. This process is illustrated by Figure 99 /185/, which shows that the eddies tend to develop the gas flow (with the flame) so that the convex sections advance while the curved (concave) sections lag, i. e., the initial perturbations increase. The eddies lead to pressure perturbations, the pressure gradient being directed across the flame from the convex to the concave locations. The distance between the liquid surface and the point of streamline turn depends on the thermal expansion in the flame and increases with $u_2$. Hence, the higher the pressure, the closer to the surface are the eddies initiated.

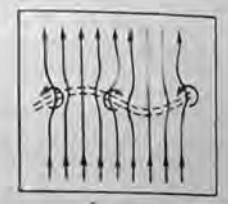

FIGURE 99. Schematic diagram of eddy formation in combustion products as a result of curved flame fronts.

The existence and behavior of the gaseous flame reproduces, as it were, in magnified form the flow pattern of the vapors from the liquid surface. Surface vibrations, mixing of the perturbation waves with the heated surface layer, all this is immediately reflected by the flame. At such moments, the gas flame in regions of intensified gas formation is ejected from the liquid surface and the flame entrained by the gas flow. A lower rate of vapor formation causes the flame moving along the gas flow to approach the surface, which in turn leads to a more intensive heat supply from the flame to the liquid, and to an accelerated vapor formation. The gas flame begins to pulsate.

It was shown earlier that the theory does not lead to any correlation between the pulsations, surface irregularities during the growth of perturbed burning, and the stability conditions. We can assume that the size of irregularities during developed perturbed burning is related to the size of the most dangerous perturbations, obtained in stability theory. A similar phenomenon arises in cellular gas flames /184, 185/, where the cell dimensions are correlated with the most rapidly growing perturbation. We may assume that there is essentially an increase in some perturbations for which (the characteristic value of) $t$ is minimum under the given conditions, while their growth suppresses the development of other perturbations. When the perturbations attain a sufficiently large amplitude their growth is interrupted as a result of nonlinear processes and a constant perturbed-burning velocity sets in.

One very important fact should not be forgotten /177/. The theories of hydrodynamic stability were developed in a linear approximation and are therefore valid for infinitely small perturbation amplitudes.

A flame instability in this approximation does not yet indicate that spontaneous eddy formation must follow. Increased perturbations may give rise to nonlinear effects, which will stabilize the curvature of the burning surface and prevent further development of perturbations.

According to the conclusions of Landau's theory, the amplitude $\lambda_n$ of the most dangerous perturbation grows beyond the stability limit. On increasing $n$, $\lambda_n$ diminishes rapidly, as does the period of its development. If $\lambda_n$ is large in comparison with the width of the burning zone (and only this case is treated in the Landau – Levich theories of the limits of stable burning), then, together with the liquid surface, the surface of chemical reaction in the gaseous phase becomes curved (we consider here the reaction zone in the vapors which are approaching the liquid surface and which most strongly affect the burning velocity of a volatile system). Naturally, comparison of the perturbation development period $t$ and the relaxation period of burning process $t_b$ shows that $t > t_b$ everywhere. It is evident that an increase in flame surface must lead to an increase in the mass velocity of burning. The effect of the curvature of the burning liquid on burning velocity has often been noted /37, 191/.

It is of interest that on passing the critical velocity the recorded velocity increases jumpwise, since immediately after $n = 1$ the flame surface begins to develop as a consequence of an increase in the amplitude of the most dangerous perturbation.

In the Landau – Levich theory, it is just this growth in amplitude that determines the development of the burning process (and hence the process pattern). Therefore, attention must be paid to the problem of how strongly surface perturbations can develop.

The growth of the perturbation amplitude in the Landau – Levich model is unlimited. However, in principle, there exist some factors which limit this growth. Hence the amplitude of the curvature of the liquid growing according to the Landau – Levich model from an infinitely small perturbation is bounded from above by the energy of the perturbing action of the flow of combustion products. The amplitude of such a perturbation $\xi$ is related to the flow velocity by the relationship

$$\xi g\rho_1 \simeq {}^1/_8 \rho_2 u_2^2,$$

which yields $\xi < u_1 u_2/2g$.

At the critical point $\xi = \xi_* \simeq (u_1 u_2)_*/2g = \lambda_* = 2\pi/k_*$. The values of $k_*$ were calculated above.

Artificial perturbations with amplitude exceeding $u_1 u_2/g$ will "spread" to these dimensions,* whereas their evolution will not differ from the growth of spontaneous perturbations. The conclusions of section 37 apply to this type of perturbation in the sense considered here.

* It is noteworthy that the effect of liquid interaction with the walls of the vessels in which it is placed is disregarded. In the case of small-diameter vessels and strong adhesion of the liquid (such as a gel-like liquid or a viscous fluid) to the vessel material, a very important factor appears and prevents spreading.



**Breakoff of droplets from a burning liquid surface**

A phenomenon which is very important in the unstable burning of liquids is now treated: the breakoff of droplets from a liquid by the action of gas flow past it. The formulation of the problem of the breakoff of droplets from a liquid surface is the same as the formulation of the problem solved by Landau /73/ and Levich /74/, if we consider the velocity of the flow past the liquid instead of the burning velocity. Dimensional analysis can be employed to this end.

If the size of droplets breaking off from the liquid surface is $r_d$, the flow velocity $u_2$, the density of the gas flow $\rho_2$ and the density of the liquid $\rho_1$, then the force acting on the liquid surface from the side of the flow is

$$F_d \sim \rho_2 u_2^2 r_d^2, \quad r_d \sim u_1 u_2/g.$$

The surface tension resisting breakoff is

$$F_\sigma \sim \sigma r_d.$$

If viscous forces prevent breakoff then

$$F_\eta \sim \eta u_2 r_d.$$

Comparison of $F_d$ with $F_\sigma$ or $F_\eta$ yields the critical breakoff condition $F_\sigma/F_d \simeq 1$ or $F_\eta/F_d \simeq 1$, which is in agreement with the Landau and Levich criteria, respectively, to within constant factors. Satisfaction of these criteria therefore denotes the beginning of the breakoff of droplets from the liquid surface. At the same time, we know that the increase in droplet size becomes considerable when the evaporation rate reaches a magnitude of the order of $5 \cdot 10^{-2}$ g/cm$^2$ · sec /192/, which is very small (much less than the ordinary condition for the burning velocity). This phenomenon may furnish an additional contribution to the entrainment of liquid droplets into the gas phase.

The flow of combustion products along the liquid surface is generated by eddy formation and the three-dimensional flow pattern of these products. The droplets break off from the crest of the perturbation waves; an irregular surface facilitates this process. The action of the eddy-containing gas flow on the liquid surface smoothens its relief.

The higher the burning velocity in comparison with the critical velocity, the smaller are the perturbations capable of developing at the surface of the burning liquid. At the same time the flow velocity increases. Actual perturbations have no time to grow and break off, and entrainment into the gaseous phase mainly takes place instead of evaporation. The heated layer in the liquid phase practically disappears. Naturally, when $u_1 \simeq 10$ cm/sec, which is experimentally realized /38, 193/, the thickness of the heated liquid layer would be about 1 $\mu$ and the time of residence in it about $10^{-5}$ sec. This is too little to enable us to assume that every substance can burn under such conditions by the conventional conductive mechanism, whereas experiment confirms the following: the ability for perturbed high-velocity burning is practically independent of the chemical nature of the liquid explosive. From this standpoint, when the original liquid explosive

burns beyond the stability limit, thermomechanical erosion takes place with subsequent processing of the explosive in the turbulent flame.

It is interesting that the burning pattern beyond the stability limit depends strongly on the burning mechanism. All the conclusions are drawn on the assumption that the fundamental reaction takes place in the gas phase. A more complicated pattern can be expected, if the explosives are subjected during burning to condensed phase reactions. In particular, impairment of thermal equilibrium in the condensed phase may lead to a decay of burning on transition to the developed perturbed regime or to a complication in ignition right up to failure.

### Burning velocity of liquid explosives beyond the stability limit

Suppose we introduce the hypothesis that processing of a liquid explosive past which flows an eddy-containing gas takes place in a turbulent high-temperature flame. In such a situation one can solve the problem about the velocity of perturbed burning, because the kinetic features of the explosive become less important in a turbulent flame. The reaction rate in the flame is very fast and does not limit processing of the original substance. The limiting stage is the increase in the perturbations, irregularities, which are "cut off" by the turbulent flow and entrained into the flame to be combusted. Consequently, the burning velocity in the perturbed regime $u_T$ is limited by the growth rate of the perturbations:

$$u_\tau \sim v_n = \lambda_n/\tau_n, \tag{103}$$

where $\lambda_n$ and $\tau_n$ are the size and period of development of the most dangerous perturbation (see Table 20) and $v_n$ is its growth rate.

The expression for $u_\tau$ is very complicated, so we shall consider the evolution of quantity $u_\tau$ using calculated data on nitroglycol (see Table 19). Figure 100 presents the dependence of $v_n$ on $J/J_* = n$ in logarithmic coordinates. On passing through $n = 1$ $v_n$ increases sharply from zero. The slope of the curve $\bar{\nu} = d(\ln u_\tau)/d(\ln n)$ characterizing the relationship $v_n \sim n^{\bar{\nu}}$ decreases from $\infty$ via intermediate values to $\bar{\nu} = 0.5$. The value approaches $\nu = 0.5$ in an asymptotic manner as $n$ increases, and $\nu = 0.5$ is reached when $n \gg 1$.

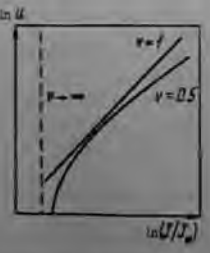


FIGURE 100. Dependence of the burning velocity beyond the stability limit on $n = J/J_*$ for nitroglycol

The expression for the limiting ($n \gg 1$) type of dependence of $u_\tau$ on the burning parameter can be derived from the following premises. The limiting magnitude of the burning velocity will be proportional to the entrainment velocity of the liquid from the surface, and is limited by the energy of the flow. At the limit, therefore,

$$(J/J_*)\sqrt{\rho_*^2/\rho_3} \gg 1, \quad (u_\tau - u_1)^2 \rho_3 \simeq \rho_* u_*^2;$$
$$(u_\tau - u_1) \simeq u_* \sqrt{\rho_*/\rho_3}. \tag{104}$$



where $u_1 = Bp^\nu$ is the normal burning velocity of the liquid in the absence of perturbations.

It is convenient to introduce the critical burning velocity and pressure $u_1^*$ and $p_*$. In this case the velocity is given by

$$u_\tau = B\left[p^\nu + \sqrt{\frac{\rho_1}{\rho_2^0}}\, p^{\nu-0.5}\right] = a(p/p_*)^\nu + a_1(p/p_*)^{\nu-0.5}$$

when

$$u_\tau \gg u_1, \quad u_\tau = a_1 \frac{u_1^*}{p_*^{\nu-0.5}} \cdot p^{\nu-0.5}, \tag{105}$$

where $a$ and $a_1$ are constants.

The velocity of the developed perturbed burning thus depends on the critical parameter $u_1^*/p_*^{\nu-0.5}$ and on the exponent ($\nu - 0.5$). Comparison of this result with calculated data for nitroglycol (see Figure 100) shows that the limiting type of function $u_\tau(p)$ obtained from expression (103) and that obtained with the help of (104) are in agreement. The same result is naturally obtained from Table 2 when $n^4 \gg 1$.

If $\lambda_n$ calculated for the infinite diameter is not realized under the given burning conditions, then the increase in $v_n$ will be slower, i.e., there is reason to believe that higher values of $J/J_*$ must be attained in order to obtain the limiting function $u_\tau(n)$.

Quantity $v_n$ for the most dangerous perturbation can be written as

$$v_n = 2\pi\sqrt{g/k_*}\cdot(z\tau)^{-1} = 2\pi\varphi\sqrt{g/k_*}, \quad \varphi = 1/z\tau.$$

The value $\varphi$ is independent of the properties of the explosive (these, however, affect the value of $k_*$). Hence universal functions $\varphi(J/J_*)$ can be derived for $\varphi_8$ in Landau's problem and for $\varphi_0$ in Levich's problem. Comparison of curves $\varphi_0(J/J_*)$ and $\varphi_8(J/J_*)$ indicates that the asymptotic dependence is reached more slowly for viscous liquids.

It is very probable that, because $\sigma \to 0$, on approaching the liquid surface temperature and the critical pressure function $\varphi(n)$ passes over from the $\varphi_8$ curve to the $\varphi_0$ curve. This gives rise to a later attainment of the limiting function by the velocity of perturbed burning.

Formula (104) was first derived from other premises by Margolin. The difficulty in using (104) is due to the fact that, when determining the velocity of burning far from the limit, we must remember that in the absence of perturbations (if suppressed somehow or other) the burning law characteristic for subcritical conditions remains in force. Constant $a$ must be determined experimentally; it indicates the ability of the liquid to be split into droplets and reflects the reaction kinetics of these droplets.

Relationship (103) holds also beyond the dependence of the predominating stabilization factor, whether surface tension or viscosity. Only the critical values are changed.

Thus, beyond the stability limits the substance burns according to the mechanism of droplet breakoff and their combustion in the turbulent gas flame. The flame becomes turbulent due to the eddies of the gas flow. The temperature in the tongue becomes homogeneous and is determined by

recirculation of the gas. The eddies of the high-temperature gas break off the liquid droplets from the perturbations and eject them into the gas, which has a temperature equal to the final temperature. The liquid is heated and combusted in this gas. Burning is of a truly turbulent nature. The gas phase is the energy source of the whole process. Recirculation of the final high-temperature combustion products ensures high efficiency of the combustion process. Since $u_т$ depends on the final temperature and composition of the combustion products as a result of its dependence on $\rho_2$, the absolute value of $u_т$ (other conditions being equal) must be higher in systems with increasing $\sqrt{RT_2/M}$, where M is the molecular weight of the combustion products, $R$ the gas constant, and $T_2$ the gas temperature. Hence, the maximum velocity of perturbed burning for mixed liquid explosives should arise near the stoichiometric ratio of the components (see section 44).

It also follows from the above that during burning beyond the stability limit particles of the original substance continuously enter the flame.

The turbulent motion of the gas can produce droplet condensation. Thermal explosion of these condensed droplets may initiate explosion, or detonation of the liquid explosive charge may even develop. This scheme of explosion initiation is assumed in almost every paper dealing with this problem. Unfortunately, the absence of direct experimental proof and the difficulties involved in obtaining it permit the possible realization of such a mechanism to be examined only indirectly.



*Chapter VII*

# *EXPERIMENTAL RESEARCH ON THE HYDRODYNAMIC STABILITY OF BURNING OF LIQUID EXPLOSIVES*

A very detailed review of experimental work dealing with research on the stability of burning of liquid explosives and transition from their deflagration to detonation can be found in the monograph of Andreev /38/. Whenever expedient, we will only refer the reader to this book. However, Andreev's book does not make reference to all the relevant work and comparison of theory with experiment is lacking.

## 43. METHODS OF INVESTIGATING BURNING OF LIQUID EXPLOSIVES

There is no need to emphasize the great influence of the experimental method used on the obtained results, and hence on the conclusions derived from the experiments. The theory of the hydrodynamic stability of burning of liquid explosives was derived on the assumption that the sizes of the acting perturbations were negligibly small in comparison with the flame front. This requirement is unfortunately difficult to fulfill in experiments serving to verify the theory, since the permissible dimensions of the perturbations introduced by the ignition system are very small. Moreover, only in individual cases do we have necessary information as to the parameters of the liquid explosive and the combustion products. This situation to some extent complicates the quantitative comparison of theory and experiment.

Burning of the liquid explosive was studied using conventional methods for determining the fundamental parameters of explosives and powders /18/. The liquid explosives are ignited in constant (or, more precisely, slowly varying) pressure bombs at both normal and elevated temperatures, in manometric bombs, or in Andreev tubes. The time (velocity) of burning is determined by techniques with burning wires, high-speed motion pictures, while at small velocities the burning period is measured by stopwatches.

The ignition method is very important. Usually, electric spirals are immersed directly into the sample material. To facilitate ignition it is useful to apply a transition layer of gelatinized nitroglycol, diglycol dinitrate, etc. However, even the intermediate gelatine layer does not ensure the absence of edge perturbations, required by the theory. The best results were obtained by the following approach. A 5–7-mm layer

of slowly burning liquid is poured onto the sample surface, the specific gravity of the liquid being less than that of the explosive sample. The auxiliary explosive must burn normally under the given experimental conditions. It is convenient to use (the liquid explosives) ethyl nitrate ($\rho_1 \simeq 1.1$ g/cm$^3$) at pressures of up to 80 atm, and nitromethane ($\rho_1 \simeq 1.12$ g/cm$^3$) at pressures between 50 and 130 atm.

Another way of ensuring the unperturbed nature of the ignition is to use a manometric bomb: ignition of the charge at a low pressure far from the limit of stable burning at a sufficiently small growth rate of the pressure in the bomb enables one to delay external perturbations associated with the ignition of the explosives until the pressures of interest are attained.

Study of temperature distributions in burning liquid explosives involves an essential difficulty: the liquid envelopes the junction of the thermocouple at the instant the latter passes over from the condensed to the gaseous phase, and this introduces distortions. Nevertheless, the maximum temperature and the heating wave profile in the condensed phase can be recorded and the results are reproducible.

Observation of the state of burning liquid explosives via a liquid layer (Figure 101) is of interest. The liquid explosive charge is poured into a glass tube with a flat bottom (3). The liquid layer is photographed by a high-speed cine camera (4) through the prism with a 45° angle. The height of the liquid layer is of the order of the depth of the field around the focusing plane (2). At 2000 frames per second and a magnification of 1.5–3 useful information can be obtained about the dynamics of the behavior of the burning liquid /178/. Stereoscopic photographs (two cameras positioned at right angles to each other) made it possible to photograph the spin of the flame /177/.

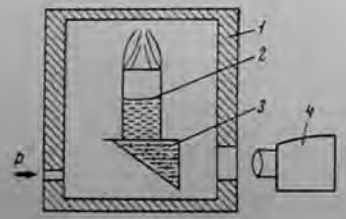


FIGURE 101. Schematic diagram of photographing liquid explosive burning through the lower end of the charge.

1) bomb; 2) surface of the burning liquid; 3) prism with a 45° angle; 4) cine camera; p denotes pressure supply.

Transition from deflagration of liquid explosives to detonation was first investigated in Andreev tubes /37/. Later /191/, constant-pressure bombs with high-speed motion picture recording was used. Some experiments were set up in a manometric bomb.



The viscosity of the liquid explosive is usually increased by dissolving a suitable high polymer (usually pyroxylin or poly(methyl methacrylate)).

Margolin et al. /177/ proposed a trace method of investigating unstable burning, based on the following principle. A very small amount (0.01–0.02%) of dye, such as nigrosin (a black organic dye), is dissolved in the liquid explosive sample (Margolin et al. /177/ used nitroglycol). After ignition of the liquid explosive with this additive, a trace remains on the walls of the beaker and reproduces the flame movement, so indicating its interaction with the flow of issuing explosive vapors. A similar method of observation is used when investigating shock waves and spin detonation.

## 44. BURNING PATTERNS OF LIQUID EXPLOSIVES

The typical scheme of variations in the burning regime as a function of the constant external pressure to which it is subjected has been often examined /38/. In general form it may be represented by the following sequence of regimes, observed when investigating the pressure dependence of burning:

1. Region of normal burning. This is characterized by a uniform flame front and steady-state propagation of burning. The pressure dependence of the burning velocity is usually very close to linear.

2. Near-critical region of transient burning. When the substance is carefully ignited (through an intermediate liquid layer) at small pressures in the beginning of this region, one can obtain metastable normal values of the burning velocity, corresponding to the normal burning region. In some cases it was possible to fix the damping of the initial perturbation over a 5–10-mm path and its transition to the normal burning velocity. The burning pattern will then be conventional and stable, and only special methods (trace methods) enable one to observe the individual features of burning. However, intensive ignition (e.g., directly by an electrical heating spiral) initiates perturbed burning of the liquid. As a rule (but not always) flame pulsations arise, while the mean burning velocity increases by a factor of no more than 2 to 4. Observations by the scheme of Figure 101 /178/ show that diverse modes of surface vibration exist.

3. Region of turbulent burning (supercritical region). This burning regime is characterized mainly by a very high burning velocity, a diffuse flame front, and small-scale eddy formation in the flame. Near the limit the pressure dependence of the burning velocity is much stronger than linear. After intensive ignition deflagration may pass over to detonation.

It is not always possible to distinguish clearly between the above burning regimes, since some may be absent (regions 1 and 2), occupy a narrow pressure interval, or overlap. The individual regimes will now be considered.

### Normal burning

Slow uniform burning is observed starting from the pressure at which the liquid explosive is ignited in a vessel of given diameter (the pressure

is determined by thermal factors) and up to a certain pressure (which varies for different explosives). For instance, according to Andreev /38/ nitroglycol burns stably in a glass tube of diameter 3–4 mm and at pressures above 0.5 atm, whereas at 1 atm the burning velocity is about 2 cm/min. The flame front is uniform, the flame itself is, as a rule, weakly luminescent, and its temperature is relatively low. Reactions in the flame do not proceed to the end; only the most active stage takes place. This is the primary flame.

As the pressure increases, the burning reaction proceeds further and the flame temperature increases; a high-temperature secondary flame is generated at a considerable distance from the surface. The appearance of the secondary flame has no influence on the burning velocity or on the pressure dependence of this velocity.

The velocity of normal burning of the liquid explosive at the given pressure depends on the initial temperature, as, in general, for all explosives. The velocity increases with this temperature; moreover, it depends on the diameter of the vessel in which the substance is ignited. The effect of the vessel diameter was examined elsewhere /138, 186, 195/ from various points of view. It appears that two phenomena must mainly be taken into account: the effect of the meniscus of the liquid upon the true area of the burning surface, and heat transfer in the liquid along the tube walls from the flame and from the liquid through the tube walls to the surroundings (heat losses). Adams and Stocks /195/ and Whittaker et al. /186/ performed experiments on the effect of the meniscus, but obtained no interesting results. Heat exchange effects are apparently more important. Heat transfer from the burning secondary flame along the walls heats the liquid explosive and increases the burning velocity; a decreasing diameter promotes this effect. It is assumed that this effect is responsible for the higher burning velocity of some liquid explosives (Figure 102) in small-diameter vessels. Heat transfer to the surroundings is especially important at low burning velocities and with incomplete heat release. At the same time, an increase in vessel diameter reduces heat losses from the gaseous phase and promotes secondary reactions. It was shown experimentally that an increase in vessel diameter reduces the pressure at which the secondary flame appears /37/. High-speed photography has indicated that artificial perturbations of the burning surface are damped in the region of normal burning.

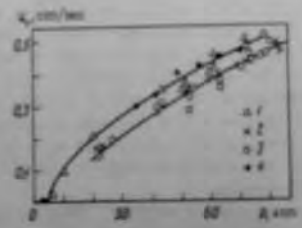


FIGURE 102. Effect of tube diameter on velocity of normal burning of ethyl nitrate: 1) d = 3.8; 2) 5; 3) 7; 4) 9 mm.

### Near-critical burning region

The theory gives a stability criterion, but cannot predict the details of the process near the critical pressure. Experiments have shown that if



the liquid surface is smooth within the limits of photographic resolution during normal burning, the burning pattern is very different in the near-critical region. The surface of the liquid explosive becomes distorted after attaining a certain burning velocity, and appears on photographic records as a blurred wavy line. From time to time the flame approaches the surface at a high velocity and returns again, or begins to revolve; the burning velocity rises abruptly and burning itself becomes nonuniform. The blurred surfaces and the roughnesses become smaller with increasing pressure. High-speed films show that pulsations are generated just as the liquid surface begins to be perturbed. Margolin et al. /177/ observed droplets of liquid explosives moving from the surface into the flame zone and concluded that eddies are formed in the gas flow starting from the surface. Figure 103 shows high-speed photographs of unstable burning of nitroglycol in a rectangular vessel of cross section 10 × 2 mm. The liquid, as it were, is pumped from one side to the other and a small-size perturbation wave travels along its surface. The period of the fundamental mode of oscillation is about 0.2 sec. The first and second harmonics of such oscillations were observed shortly after ignition. The width of the band corresponding to the liquid surface changes, which indicates surface oscillations in the direction of smaller vessel dimensions. Figure 104a shows three half-waves formed by burning nitroglycol in a rectangular vessel, while Figure 104b shows a high-speed photograph of the surface shape, characteristic for burning of liquid DINA and diglycol dinitrate. Some characteristic forms of surface distortion are observed in general during unstable burning, and can be divided into three main types /186, 196, 197/.

1. The burning liquid surface performs oscillations in the vertical direction; avalanches of droplets break off from the wave crest in the flame zone and flare up in the flame. The secondary flame pulsates, and periodically approaches the liquid surface to be ejected from it (Figure 105a). The energy for sustaining the oscillations may proceed both from the gas flame and from the burst of droplets injected into the flame. A characteristic example of this type is nitroglycol.

2. The burning liquid surface sometimes begins to perform spinning motion in the near-critical region when the flame, as it were, "screws" into the column of the liquid explosive and entrains the surface. The liquid explosive surface is generated in a position almost parallel to the normal flow direction of the combustion product. Liquid droplets broken off from this surface by the gas flow are ejected into the flame (Figures 104 and 105). Diglycol dinitrate, supercooled DINA, and some $HNO_3$-based mixtures are typical of this type of burning. It is noteworthy that when the mobility of the liquid explosive is small (condensed nitroglycerin after Andreev) the pitch of the spiral described by the flame may be considerably larger than the vessel diameter and comparable with the height of the liquid explosive column. Detonation arises in such cases (see section 48).

Whittaker et al. /186/ observed that the spin regime of motion of the burning liquid surface [helical turbulence] never passes over into the oscillatory regime, whereas the opposite variant is possible. Chuiko observed that both simple and two-head spin can be obtained by using different types of ignition of diglycol dinitrate. In the case of two-head spin the flame breaks into rotating flames.

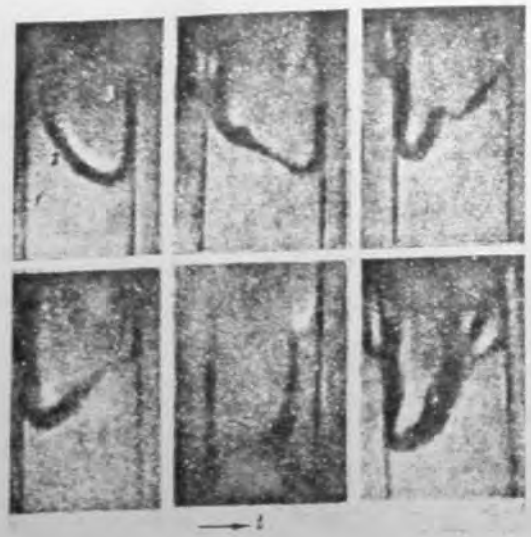

FIGURE 103. High-speed photographs of nitroglycol burning in a (2 x 10 mm) rectangular vessel:

1) substance; 2) liquid surface; 3) flame.

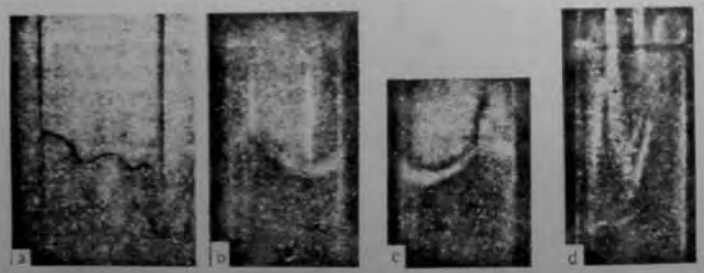

FIGURE 104. High-speed photographs of liquid explosive burning:

a) nitroglycol, 2 x 10 mm vessel, three half-waves on the burning surface; b) film of spin burning of diglycol dinitrate in a circular vessel; c) formation of a "fountain" at the tube center (diglycol dinitrate); d) breakoff of droplets from the curved surface (ethyl nitrate, 110 atm).



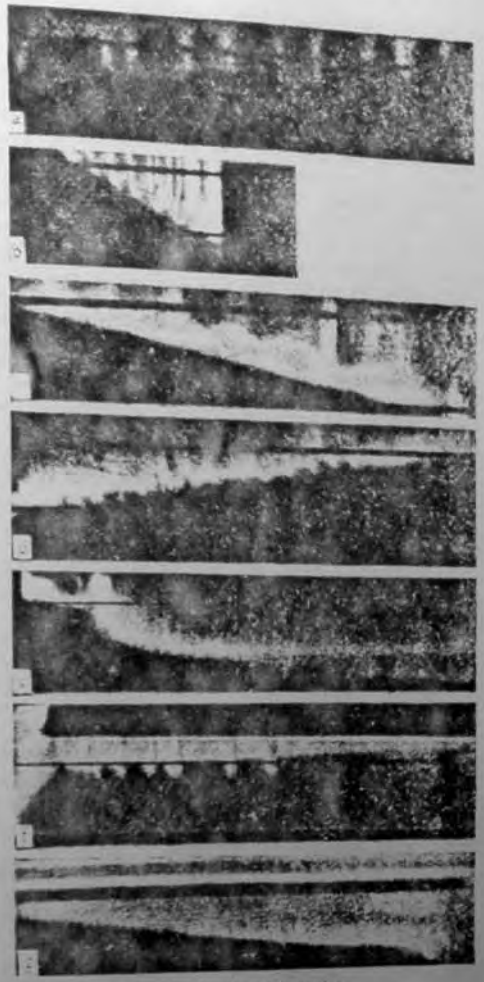

FIGURE 105. Photographs of liquid explosive burning:

a) nitroglycol, $d = 5$ mm, $p = 15$ atm, flame pulsation; b) diglycol dinitrate, $d = 5$ mm, $p = 58$ atm, two-head spin, injection of droplets from wave crest; c) diglycol dinitrate, $d = 3.8$ mm, $p = 68$ atm, two-head spin; d) ethyl nitrate, $d = 5$ mm, $p = 110$ atm, small-scale flame pulsations; e) nitromethane, $d = 8$ mm, $p = 155$ atm, damping of surface oscillations and transition to normal burning; f) nitroglycol, $d = 7$ mm, manometric bomb, liquid surface pulsations arose in the flame after normal burning, burning abruptly accelerated, explosive detonated at $p = 35$ atm; g) nitroglycol, $d = 3$ mm, $p = 10$ atm, burning accelerated near the bottom due to liquid heating along the beaker walls.

3. The third type of phenomena was described by Whittaker et al. /198/ as the formation of liquid "filaments" along the tube walls, when the surface performs wavelike motion and pumps the liquids in the form of filaments into the flame zone. Maksimov and Bairash /196/ apparently observed the same regime and called it the "gushing" regime. Their observations differ from those of Whittaker: no movement of the liquid surface was seen and the liquid moved upward at the tube center, not along the walls (Figure 104c). In both cases a large mass of droplets is ejected into the flame zone due to the collapse of the liquid jet. Accelerated combustion of these droplets ensured a high burning velocity. Transition into the gushing regime has been observed at high pressures /186/, when helical turbulence was interrupted, whereas it was observed elsewhere /196/ after the oscillatory regime.

All the investigators concluded that, in principle, the observed increase in burning velocity in near-critical regions is associated with growth of the flame surface. In accordance with an estimate (see section 38), the observed burning velocity is 2–4 times higher than the value obtained by extrapolation of data on slow burning to the near-critical region. Perturbations introduced by the ignition decay slowly in the subcritical region. Errors may therefore arise when the initial surface oscillations (associated with ignition) are assumed to be natural. Such oscillations can be distinguished with difficulty when the charges are low and the ignition pulses are intensive. Figure 105d shows a photograph of nitromethane burning in the near-critical region, and illustrates our remarks. The oscillatory regime of surface movement initiated by the igniting spiral decays after a certain time (mainly because the oscillation amplitude decreases, while the oscillation frequency does not increase) and normal burning is established.

The effect of vessel diameter on the phenomena occurring in the near-critical region can be illustrated by the example of nitroglycol and ethyl nitrate (see Figure 113) /38, 197/. An increase in vessel diameter leads to an increase in burning velocity, which is especially strong in nitroglycol.

Detailed study of the transient regions /38, 197/ showed that transition from the straight line $u(p)$ for normal burning to the straight line for developed turbulent burning is realized via a complex curve. As a rule, there is a large scatter of experimental data. For nitroglycol, nitroglycerin and DINA, the velocity in this region is larger than that corresponding to the line of turbulent burning: it is somewhat lower for diglycol dinitrate, nitromethane and ethyl nitrate in narrow tubes (4–5 mm). Both types of transient dependences are encountered in mixtures based on nitric acid. According to Andreev /38/, these features are related to the double effect of eddy formation on burning: a) eddies destroy the heated layer, make burning more difficult, and may even quench burning; b) they increase the interface between the gaseous products and liquid and may thus accelerate burning. This led to some very interesting phenomena. For example, Andreev and Bespalov /199/ observed in their experiments a considerable (2–3-fold) increase in the critical burning diameter $d_{cr}$ of gelatinized nitroglycerin (3.2–5%) during transition to the perturbed burning regime. The higher the viscosity of the gelatin, the weaker the increase in $d_{cr}$. This pattern was less pronounced in the case of nitroglycol.



though at the beginning of the near-critical region burning was frequently observed to decay at diameters several times larger than their initial values.

Attempts to correlate some hitherto unexplained facts with this phenomenon are not without interest, due to the possible effect of burning surface perturbations on the burning process (especially near the limit).

Whittaker et al. /186, 198/ observed on the $u(p)$ [consumption rate] curve of mixtures of nitric acid with some organic fuels (2-nitropropane and others) a hump (turbulence break) at some pressure (Figure 106), when the diameter of the tube in which the explosive is ignited is small (3–4 mm). On increasing the tube diameter to 5, 6 or 8 mm the hump disappears, and the $u(p)$ curve is a smooth high-pressure continuation of the consumption rate curve. Introduction into the system of 0.5% poly-(methyl methacrylate) as a condenser led to the disappearance of the hump and an approximately 40°C increase in surface temperature. Despite different experiments conducted by Whittaker et al. /186, 198/, they concluded only that the burning mechanism is changed at the hump and cannot be described by present theories of burning.

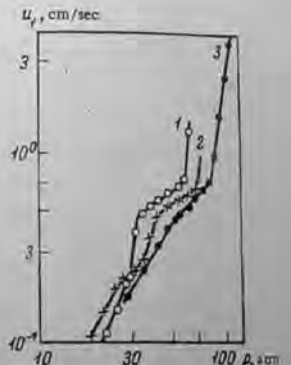


FIGURE 106. Consumption rate curves for mixed liquid explosives /186/:

1) $HNO_3$ (99%) — nitroethane; 2) $HNO_3$ (99%) — nitromethane; 3) $HNO_3$ (99%)–1-nitropropane.

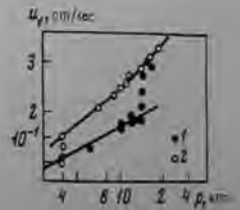


FIGURE 107. Dependence of burning velocity of hydrazine on pressure and vessel diameter /200/:

1) $d$ = 4 mm; 2) $d$ = 12.7 mm.

Many papers about burning of hydrazine were published later (see Andreev's review /38/). According to data of Antoine /200/, the burning velocity of hydrazine in 100% concentration at pressures from 1 to 14 atm in a beaker of 5.6 mm diameter is described by the equation $u_1 = 0.026\, p^{0.6}$ mm/sec. At pressures exceeding 14 atm the burning velocity is at first proportional to $p^{0.21}$, and then to $p$. As the beaker diameter increases, the burning region within which the relationship $u_1 \sim p^{0.6}$ holds becomes narrower, and transition to the curve occurs at 8 atm when the diameter equals 12.7 mm (Figure 107).

Antoine does not furnish any satisfactory explanation of this phenomenon, though he notes some change in the luminescence of the flame and in its intensity (lower flame emission brightness in the burning region up to the hump of the curve). He also observes weak turbulence of the surface and indicates that the points of the surface described a helix as the substance was combusted, regardless of the fact that, on the whole, burning took place in a steady-state fashion.

Consider the data of /198, 200/ on the basis of results derived in section 39. During burning of a low-viscosity liquid, the maximum amplitude of perturbations, which may be created by the burning process itself (below the stability limit of Landau), is defined as the height of the liquid column equilibrating the dynamic pressure of the effluent combustion products (see section 38):

$$\xi_0 \sim u_1 u_2 / 2g.$$

Evidently, no perturbations of amplitude exceeding $\xi_0$ can arise. Burning can sustain such a perturbation, if the amplitude is of the order of, or smaller than $\xi_0$. This can be achieved by providing a flow of combustion products in more than one dimension near the burning surface; this is not an exceptional phenomenon. Moreover, it follows from section 39 that the perturbation affects the burning velocity when the thickness of the combustion zone $l$ is larger than $\xi_0$. Since $l \sim \varkappa_1/u_1$, the condition $\xi_0 > l$ corresponds to the burning velocity given by

$$u_1^* = \sqrt[3]{2g\varkappa_1\rho_2/\rho_1}, \quad \text{or} \quad \frac{u_1^*}{\sqrt[3]{p_*}} = \sqrt[3]{2g\varkappa_1\rho_2^2/\rho_1}. \qquad (106)$$

Thus, "natural" perturbations of the burning surface can alter the burning velocity at a burning velocity $u_1 > u_1^*$. Decay of burning is observed when flame pulsations arise, especially for nitroglycerin and liquid (95°C) PETN. The $u$ ($p$) curve for methyl nitrate (Figure 108) after Andreev /37/, and for other (both liquid and solid) fusible substances possesses a hump and is displaced. Without excluding other possible explanations which (especially for nitroglycerin and PETN) are discussed exhaustively in Andreev's monograph /38/, we shall compare experimental and calculated data for these substances. Table 21 lists experimental burning velocities and pressures corresponding to the hump in the $u_1$ ($p$) curve; in the case of nitroglycerin and PETN they correspond to cessation of burning.

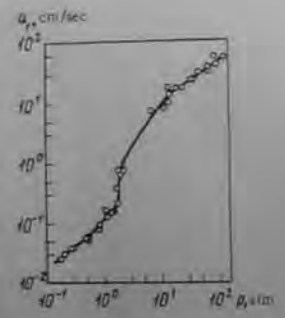


FIGURE 108. Function $u_1(p)$ for methyl nitrate when $d = 5$ mm. Data of Andreev /38/ (to $p = 2$ atm), and Belyaev and Kondrikov /206/.

For convenience, we compare values of $D = u_1/\sqrt[3]{p}$, which only depends on the thermophysical parameters of burning (see expression (106)). Experimental and theoretical data were found to be in agreement for mixtures based on nitric acid, PETN and hydrazine in a vessel of 12.7 mm diameter. In order to obtain agreement with data on nitroglycerin, we must assume that when $p \simeq 0.6$ atm the temperature of the combustion products is somewhat lower and that they contain more high-molecular fragments. If the resulting density is reduced to 1 atm, its value should be about $4.3 \cdot 10^{-4}$ g/cm$^3$ (the experimental value obtained by ignition at 1 atm is of the order of $2.1 \cdot 10^{-4}$ g/cm$^3$ /30/.



TABLE 21. Determination of the point of onset of pulsations

| Substance | Experiment | | | Calculation | Reference |
|---|---|---|---|---|---|
| | $P_*$ | $u_1^*$ | $D$ | $D_*$ | |
| Hydrazine ($d = 12.7$ mm) . . . . . | 4 | 0.06 | 0.053 | 0.056 | /205/ |
| Nitric acid—2-nitropropane . . . . | 16 | 0.163 | 0.0635 | 0.0695 | /185/ |
| Nitric acid—nitroethane . . . . . | 30 | 0.22 | 0.0707 | 0.0707 | /198/ |
| Nitric acid—dioxane . . . . . | 11 | 0.16 | 0.0805 | 0.0805 | /198/ |
| PETN . . . . . | 1 | 0.047 | 0.047 | 0.051 | /85/ |

The appearance of pulsations when $\xi_0 = l$ can be represented as follows. When $\xi_0 \ll l$ the perturbations remain inside the zone of burning (heated layer) and do not lead to essential changes in the burning velocity. When $\xi_0 \gg l$, in addition to perturbations of the surface the zone of reaction in the gaseous phase becomes curved, and the burning velocity increases in proportion to the increase in the surface. The strongest effect can be expected when $l \simeq \xi_0$, when the destruction of the heated layer may lead to the decay of burning (observed in the case of nitroglycerin).

### Limiting conditions of normal burning

Until now, we followed the fundamental papers of Andreev in the given field and referred the near-critical burning region defined by us to truly turbulent burning. In other words, the limiting velocity of normal burning was taken as the velocity above which flame pulsations and other nonsteady phenomena were observed. However, we found it necessary to make a finer subdivision of the burning regimes in the light of new ideas, and also as a result of experimental data indicating the existence of a region of metastable burning that arises in the absence of forcing perturbations of the liquid surface. The subcritical regime (decay of artificial surface perturbations) should be separated from the near-supercritical regime, where surface perturbations grow from infinitely small ones and are decomposed by nonlinear effects. In practice, available experimental data indicate that such a subdivision may be carried out only in individual cases, since the main volume of information was obtained under conditions of a strong initial perturbation.

According to the theory, the critical point will correspond to a burning velocity above which no oscillations are present, but only the perturbation amplitudes increase. This point should be determined experimentally under

conditions precluding the effect of artificial perturbations. The regime corresponding to burning in the supercritical region is characterized by a strong and monotonic dependence of the burning velocity on pressure (at least near the limit); in the subcritical region it is related to the region where slow burning depends on pressure. This fact in conjunction with photographic recording of burning enables the critical point to be found with a fair degree of accuracy.

It follows that the experimental results in the near-critical region depend strongly on the method of investigation employed, and especially on the size of the initial perturbation. Figure 105f is a photograph of nitroglycol burning in a manometric bomb. The material was ignited at 1 atm, when surface perturbations decay rapidly, while the pressure rises slowly because the combustion products of the liquid explosives are accumulated in the bulk of the bomb. With such a design of experiment the normal burning surface is retained over a considerable part of the pressure region, where perturbed burning takes place in conventional experiments. For instance, surface pulsations arose at about 19 atm in the given case, while Andreev /37/ employed a conventional design of experiment and found a value of about 13 atm. Similar observations were carried out by Whittaker et al. /186/. The method of ignition through a layer of slowly combusting liquid (ethyl nitrate) led to normal burning in a region where abrupt ignition leads to oscillatory burning. The burning velocities lay on the continuation of the $u(p)$ curve obtained by extrapolating data on normal burning to the subcritical pressure region.

In the case of low-viscosity liquid explosives, the critical pressure $p_*$ at which spontaneous eddy formation in the flame sets in under constant pressure conditions due to finite perturbations produced by the ignition process differs little (by 20–30%) from the critical pressure $p_\infty$ resulting from burning in a manometric bomb, when only infinitesimal random perturbations arise. This result indicates that the stability conditions of burning for low-viscosity liquids are practically the same as those for infinitesimal and finite perturbations. Consequently, the conclusions of the theory as regards infinitesimal perturbations are suitable for estimating the stability of burning subject to finite perturbations.

In our experiments with nitroglycol, the time taken for the pressure in the manometric bomb to increase from $p_*$ to $p_\infty$ was between 0.2 and about 1 sec (beakers of 7 mm diameter were used). The calculated period of perturbation growth (see Table 20) at $n = 1.1$ is about 0.2 sec. In another series of experiments we attempted to determine the time of perturbation growth when the explosive burned at constant pressure. The nitroglycol was ignited through a layer of ethyl nitrate, which was poured as carefully as possible onto the surface of the explosive sample. The main difficulty here was to take into account combustion of the boundary layer of the nitroglycol–ethyl nitrate mixture. We established that the experimental time for the instability to develop is about 3–7 times larger than the calculated time, while its dependence on $n$ is of the same type as the theoretical dependence.

The effect of vessel diameter on the limiting pressure of normal burning was studied with nitroglycol /178/. The points in Figure 109 correspond to the experiments, while the curve was plotted from equation (87) for a circular vessel.



Burning of ethyl nitrate in beakers of 3, 8, 7 and 5 mm diameter was investigated; limiting velocities of 0.55, 0.5 and 0.45 cm/sec were obtained at pressures of 82–85 atm. Similar results were obtained for diglycol dinitrate: the limiting velocities in beakers of the same diameter lay between 0.7 and 0.6 cm/sec, while the pressures were 52–60 atm. It is certain that the influence of side effects (such as heat transfer along the beaker walls, or heat losses to the surroundings) for slowly burning substances at a relatively low burning temperature (e. g., ethyl nitrate and diglycol dinitrate) is much stronger than for nitroglycol. Moreover, the critical velocity for the above two substances is apparently attained at pressures above the critical thermodynamic pressure; this complicates the situation even more. Whittaker et al. /186/ found that on replacing the circular vessel of 3.7 mm diameter by a rectangular vessel of cross section 10 × 1 mm the limiting pressure of normal burning decreases more strongly than the size of the vessel (ratio 10 : 3.7). This can be associated with more intensive heat transfer from the flame to the vessel wall and consequent superheating of the substance.

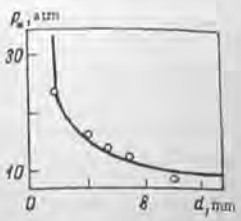


FIGURE 109. Effect of beaker diameter on the limiting pressure of normal burning nitroglycol.

The effect of the initial temperature on the limit of normal burning of nitroglycol /201/ was found to be in agreement with theory. At 12.3 atm the transition corresponds to a burning rate of 0.645 g/cm²·sec and a liquid explosive temperature of 47°C. A pressure of 17.5 atm suffices for transition to turbulent burning at 23°C, and corresponds to a rate of 0.75 g/cm²·sec. The relationship $J_*/\sqrt{p_*} \simeq C^* = \text{const}$ holds in accordance with equation (80). In this case $C^*$ is equal to 0.184 and 0.179 units, respectively.

Let us now consider the problem of agreement between experimental and computed critical conditions of normal burning. Andreev /38/ carried out such a comparison for some substances and found that in some cases very satisfactory agreement was observed between theory and experiment. We shall carry out a supplementary comparison of values characterizing limiting conditions of normal burning, some of which correspond to a high critical pressure (apparently even higher than the critical pressure calculated by Levich's formula (93) (see Table 22)). The quantity $C^* = J_*/\sqrt{p_*}$ will be used in our comparison and denoted by $C_1^*$ when following Landau's theory and by $C_2^*$ when following Levich's theory.

The pressure in Table 22 is expressed in atmospheres, and $J_*$ in grams per cm² per second. The following abbreviations were adopted: NGL – nitroglycol; MTN – methyl nitrate; DGDN – diglycol dinitrate; ETN – ethyl nitrate; NM – nitromethane; TEGDN – triethylene glycol dinitrate; DNGC – dinitroglycerin; TNM – tetranitromethane; NB – nitrobenzene; (1) – the results of the present authors; [2] – the data of Glaskova /222/ obtained with a supercooled substance; a viscosity of 30 centipoises was taken in the calculation of $C_2^*$. Figures in parentheses correspond to a rough estimate. The data of Andreev and Bespalov /198/ were used to

determine the value of $p_*$ for nitroglycerin. This value corresponds to the limit of normal burning under conditions of slowly increasing pressure. The burning rate of nitroglycerin was calculated by the equation $u = 0.23\, p^{0.793}$ g/cm$^2$ · sec.

TABLE 22. Limiting conditions of normal burning of inviscid liquid explosives

| Substance | Experiment | | | Calculation | | Reference |
|---|---|---|---|---|---|---|
| | $p_*$ | $J_*$ | $C^*$ | $C_1^*$ | $C_2^*$ | |
| NGL, 20°C, $d$ = 5 mm | 19 | 0.9 | 0.2 | 0.18 | 0.07 | /38/ |
| NGL, 23°C, $d$ = 4 mm | 17.5 | 0.75 | 0.18 | 0.18 | 0.07 | /201/ |
| NGL, 47°C, $d$ = 4 mm | 12.3 | 0.63 | 0.18 | 0.18 | (0.06) | /201/ |
| MTN, 60°C | 1 | 0.2 | 0.2 | (0.2) | (0.06) | /30/ |
| TNM, 20°C | 1.75 | 0.32 | 0.24 | 0.28 | 0.07 | /38/ |
| DGDN, $d$ = 5 mm | 85 | 1.38 | 0.15 | 0.32 | 0.15 | /197/ |
| ETN, $d$ = 7 mm | 115 | 0.67 | 0.063 | 0.23 | 0.06 | /197/ |
| NM, $d$ = 8 mm | 185 | 0.56 | 0.037 | 0.24 | 0.037 | (1) |
| DINA | 54 | 1.11 | 0.136 | (0.26) | (0.14) | (2) |
| TEGDN | 50 | 1 | 0.14 | (0.3) | (0.15) | /214/ |
| ETN/DGDN (1 : 1) | 115 | 1.11 | 0.12 | 0.29 | 0.087 | /197/ |
| DNGC | 72 | 1.43 | 0.17 | (0.2) | (0.29) | /38/ |
| TNM + benzene | 4.2 | 0.385 | 0.19 | (0.2) | (0.07) | /208/ |
| TNM + NB (3 : 2) | 3 | 0.28 | 0.164 | (0.2) | (0.07) | (1) |
| PETN, 100°C | 8.2 | 0.55 | 0.19 | (0.2) | (0.15) | /85/ |
| NGC | 1.38 | 0.296 | 0.252 | 0.33 | 0.3 | /199/ |

Table 23 shows the results of processing data /186, 198/ on the burning of mixed liquid explosives based on $HNO_3$. No data are available on the calculation of the constants, so only the value of $u_*/\sqrt{p_*} = C_0^*$ plotted from experimental data will be reported. If $\eta = 1$ centipoise and $\sigma = 16$ dyne/cm ($HNO_3$), the calculated values obtained are $C_1^* = 0.18$ units and $C_2^* = 0.06$ units.

TABLE 23. Limiting conditions of normal burning of a mixture of nitric acid and fuels /186, 198/

| Fuel | $c_{HNO_3}$ | $u_*$, cm/sec | $p_*$, atm | $C_0^*$ |
|---|---|---|---|---|
| Nitromethane | 99 | 0.6 | 85 | 0.065 |
| Nitroethane | 99 | 0.71 | 97 | 0.072 |
| 1-Nitropropane | 99 | 0.68 | 83 | 0.078 |
| 2-Nitropropane + 0.5% Lucite | 99 | 0.67 | 66 | 0.082 |
| Dioxane | 99 | 0.60 | 24 | 0.122 |
| Isobutyric acid | 99 | 0.9 | 83 | 0.099 |
| 2-Nitropropane | 100 | 1.3 | 56 | 0.174 |
| " | 97 | 0.7 | 69 | 0.084 |
| " | 95 | 0.7 | 76 | 0.080 |
| " | 90 | 0.63 | 125 | 0.056 |

The data of Tables 22 and 23 are best compared with theory using the ratio $J_*/\sqrt{p_*}$. Calculation of coefficient $C_1^*$ shows that it is of the order of



0.12–0.3 units (section 32), while coefficient $C_2^*$ is equal to 0.03–0.20 units (section 33). Comparison of these values with experiment indicates that if $p_*$ is more than 50 atm the experimental data are in best agreement if $C_1^*$ is used, whereas for low $p_*$ the experimental value of $C^*$ is closer to $C_2^*$. This fact confirms the ideas developed earlier (section 34), that when $p_*$ becomes larger than the thermodynamic critical pressure for the given liquid, in which case the surface tension becomes lower, the viscosity forces gradually become the stabilizing factor. At low pressures, stabilization of burning involves mainly the action of surface tension forces.

Further confirmation of the Landau–Levich theory was obtained in experiments on burning when the overloads that act on the liquid were changed, i. e., $g' \neq 9.8$ m/sec$^2$. First, an experiment was set up /197/ on burning of nitroglycol under free-fall conditions ($g = 0$) at 1 atm. It was found that no eddies were formed during burning in a vessel of 5 mm diameter. Comparison with theory showed /177/ that stabilization of burning was ensured in these experiments because of the small vessel diameter. For instability to develop the reaction must take place in a vessel whose diameter is of the order of 1 m. It was shown earlier /37/ that Landau's theory can be confirmed when the experiments are set up with $g' > 9.8$ m/sec$^2$, i. e., under conditions of overload. Such experiments were conducted by Ordzhonikidze et al. /202/, who experimented with nitroglycol; the explosive was ignited in a test tube of 5.5 mm diameter. When $g' = g$, i. e., under normal conditions, $p_*$ was 12 atm. When the tests were carried out with an overload equal to 300 $g$, nitroglycol burned stably over the whole pressure range under investigation (up to 140 atm). The burning velocity corresponded to values obtained by extrapolating the curve of slow burning at pressures below 12 atm under normal conditions; at 140 atm it was 3.3 cm/sec. Calculation by Landau's theory (equation (80)) shows that, at 300 $g$, transition to the turbulent regime can be expected at about 250 atm. In accordance with theory (see Table 20) it was found that $p_* \sim \sqrt{g}$.

### Burning of liquid explosives beyond the stability limit

Burning of liquid explosives beyond the stability limit is mainly characterized by high propagation velocities of the process and strong pressure dependence of the burning velocity. As a rule, the diameter of the vessel in which the explosive is ignited also considerably affects the burning velocity.

Figures 110 and 111 illustrate function $u(p)$ for some liquid explosives and their mixtures. Typical burning velocities lie between 1 and 100 cm/sec, and exponent $\nu$ in function $u(p)$ is sometimes even larger than unity. Margolin and Margulis processed the experimental data in $u/u_* - (p/p_* - 1)$ coordinates, corresponding to the theoretical function $u_\tau(p)$ (section 42). It was found (Figure 112) that far from the limit ($n \gtrsim 5$) the pressure dependence of turbulent burning is in agreement with the dependence predicted by theory.

The effect of the vessel diameter $d$ on the velocity of turbulent burning near the stability limit is illustrated by the curves of Figure 113, plotted

from data of Chuiko /197/ for nitroglycol. The equation $u_т = 0.15 + 0.032 \cdot (p-20) \cdot (d-1.7)$ cm/sec holds at pressures of 20–60 atm ($p$ is expressed in atm and $d$ in mm). If we assume that the burning velocity increases linearly with vessel diameter in the turbulent region, while under normal conditions it decreases somewhat owing to heat transfer along the vessel walls, true turbulent burning is observed above 20 atm.

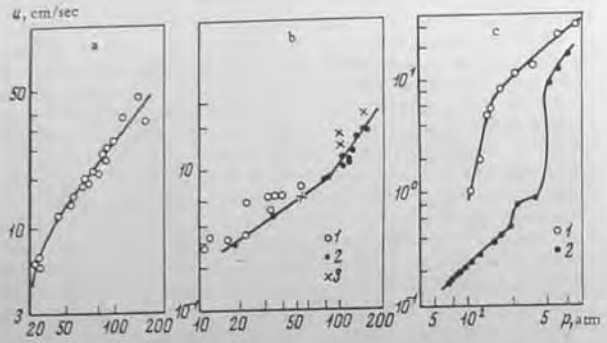


FIGURE 110. Function $u(p)$ for individual substances:

a) nitroglycol, $d = 5$ mm /206/; b) DINA (data of Glazkova): 1) supercooled explosive; 2) solid explosive; 3) DINA with 30% coloxyline; c) 1) nitromethane, according to data of Bakhman and Dubovitskii /191/ and the present authors; 2) ethyl nitrate, according to data of Bakhman and Dubovitskii /191/ and the present authors.

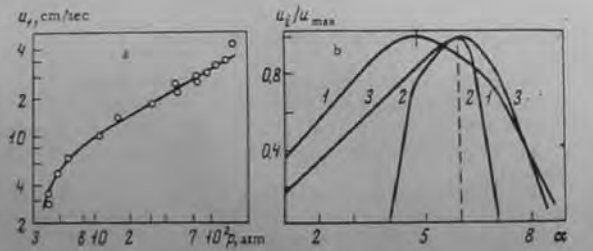


FIGURE 111. Burning velocity of mixed liquid explosives:

a) TNM–nitrobenzene (60–40), $d = 4$ mm; b) TNM–butanol at different component ratios and pressures: 1) 1 atm; 2) 2 atm; 3) 40 atm, instantaneous velocities are referred to $u_{max}$; $u_{max}$ is equal to 0.07 cm/sec at 1 atm, 2.6 cm/sec at 2 atm, and 42 cm/sec at 40 atm.



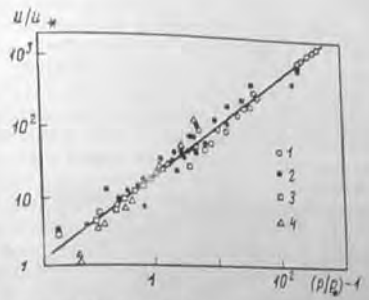


FIGURE 112. Generalized pressure dependence of liquid explosives in the turbulent regime:

1) methyl nitrate /[illegible] 206/; 2) nitroglycol /191, 193, 197, 206/; 3) ethyl nitrate /191, 197/; 4) dinitroglycol dinitrate /197/.

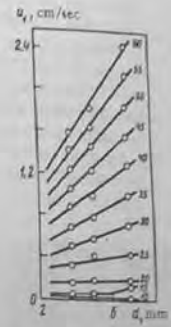


FIGURE 113. Velocity of turbulent burning of nitroglycol as a function of beaker diameter at constant pressure. Figures at the ends of the curves denote the pressure in atm.

Whittaker et al. /186/ studied burning of $HNO_3$-based liquid explosives and found that its velocity increases with vessel diameter in the region of turbulent burning. Moreover, it was found that the burning velocity in aluminum tubes is 2–3 times larger than in pyrex tubes, while in casings made from ballistite powders it was even larger. When nitroglycerin burns far from the stability limit, the velocity increases in proportion to $\sqrt{d}$ as the vessel diameter increases from 5 to 9 mm /191/.

The effect of the initial temperature on turbulent burning of liquid explosives was studied by Tereshkin and Andreev /201/. The pressure dependence of the turbulent burning velocity becomes stronger simultaneously with a decrease in the pressure at which the system passes over to the turbulent burning regime.

The effect of the initial temperature becomes weaker with distance from the stability limit. Processing of the data of Tereshkin shows that if, at a pressure of 17.5 atm, the turbulent burning velocity increases in proportion to the Kelvin temperature ($T$) raised to the power of 1.63, it increases in proportion to $T^{0.66}$ at 53.5 atm. This is due to the specific mechanism governing the turbulent burning of liquid explosives: the velocity far from the limit of normal burning is mainly determined by the energy of the combustion products, and the energy increases in proportion to the square root of the final burning temperature (see equation (104)).

It was mentioned that in experiments with nitromethane the liquid surface oscillations were observed to damp out. The rated frequency of the natural oscillations is about 15 Hz. For nitromethane burning the present authors found values of 12 Hz at 134 atm, 12 Hz at 155 atm, and 14 Hz at 208 atm. These data show that various modes of oscillations can be initiated with

pressure growth (increasing burning velocity), so altering the rhythm of the frequency changes specified in the experiments.

Some papers /186, 196/ have aimed at establishing a correlation between the observed oscillation frequencies of the burning surface (and the corresponding flame pulsations) and experimental parameters, such as pressure and vessel diameter. The results were contradictory. For instance, Maksimov and Bairash /196/ found a drop in the oscillation frequency of the surface of burning methyl nitrate; when investigating a 60 : 40 wt % tetranitromethane-nitrobenzene mixture they observed a flame pulsation of constant frequency which, however, increased with pressure ($f \sim p^{0.45}$). Chuiko /197/ observed burning of nitroglycol and found a set of frequencies which displayed a decrease in pulsations with increasing pressure. It is very likely that in these papers the parameters of different types of periodic liquid-surface distortion were fixed in different burning regions; however, it was shown above (section 38) that these distortions vary in a different manner as a function of the pressure. Data of Maksimov /196/ on the frequencies of methyl nitrate oscillations are fairly well described by the expression $f \sim 1/u_1$ and are associated with burning somewhat above the critical point. When Andreev and Tereshkin (liquid TNT) and Whittaker et al. /186/ studied the variation in the helical pitch of the burning surface and tried to correlate the angular velocity $\omega$ and pressure $b$, they found a function of the type $\omega = a - bp$, where $a$ and $b$ are constants. Thus, on increasing the pressure the frequency of revolution decreases, and at some pressure the revolution must cease; this was also observed experimentally.

Margolin et al. /177/ investigated the movement of the burning surface by a trace method (a dye was introduced into the investigated explosive). Figure 114 shows photographs of tubes in which nitroglycol containing 0.02% nigrosine (a black dye soluble in alcohol) was ignited. A trace remained on the inner walls of the (2.5 mm diameter) tubes after ignition at 20 atm (Figure 114a). The trace assumed the form of a wavelike helix with an almost constant pitch. The pitch decreases with pressure. For example, at $p = 20$ atm the pitch is about 2 mm, and at 22 atm about 1.4 mm. The largest wavelength at 20 atm is about 8 mm, and at 22 atm about 5 mm. In addition to these waves shorter ones are also observed. A trace remained on the walls of a 4-mm tube (Figure 114b) after ignition at 18 atm and had the form of a complex network of lines. The cell size is 3 × 3 mm. Such cells are obtained when the wave amplitude equals the helical pitch. The observed traces apparently reproduce the type of movement of the flame and reflect its interaction with the stream of the effluent vapors from the liquid explosive.


FIGURE 114. Photographs of beaker after nitroglycol with added dye is ignited in them:
a) $d = 2.5$ mm, $p = 24$ atm;
b) $d = 4$ mm, $p = 18$ atm.

The size of perturbations during unstable burning can be estimated from motion pictures. Such an evaluation of the wavelength yields 2–8 mm (nitroglycol, diglycol dinitrate, nitromethane). Observations of wavelengths of the order of 1 mm are less reliable. Therefore, the order of magnitude corresponds to the size of the most rapidly growing perturbations predicted by the theory (see Table 19).

In the light of contemporary ideas about the stability of the gas flow of combustion products ejected from a perturbed surface, the appearance of helical motion of the flame – surface system best reflects the results predicted by theory. In the case under consideration, stable types of motion are represented either by a revolving stream or by an annular vortex.

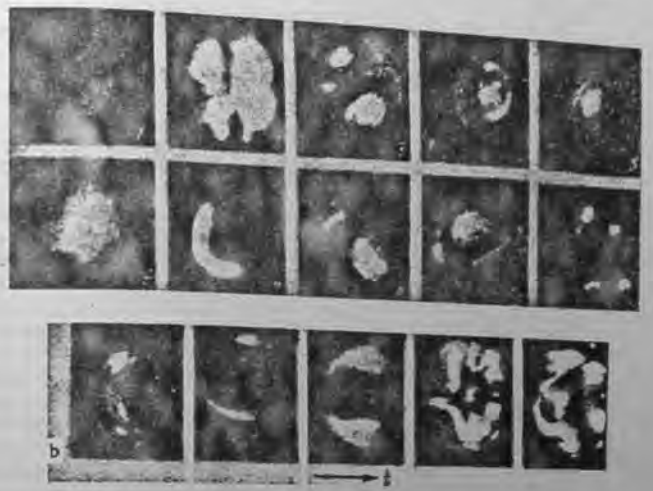


FIGURE 115. Motion pictures of the surface of liquid explosives during burning beyond the stability limits:

a) different types of surface structure; b) growth of instabilities during burning of diglycol dinitrate (62 atm, $d = 6$ mm).

As a rule, burning of liquid explosives is observed with the aid of motion pictures taken through the transparent walls of the vessel. However, Margolin and Chuiko /178/ used motion pictures taken from the end through a layer of burning liquid. In this case they cemented a flat transparent bottom to a glass tube and a test tube was fixed to a 45° prism through which the picture was taken (Figure 101). The whole assembly was placed into a constant-pressure bomb and the process photographed by a high-speed cine camera. Nitroglycol and diglycol dinitrate were investigated; for these substances, the critical pressures generating unstable burning are 15 and 54 atm, respectively (in a test tube of 6 mm diameter). The motion pictures were taken in natural light, so the light refraction at the liquid surface revealed its structure. Figure 115a shows typical motion pictures (1–10) of burning in the unstable regime. Examination of the

pictures in Figure 115a indicates that No. 1 can be compared with the mode $q = 1$, $s = 0$ (one nodal diameter) and No. 2 with the mode $q = 2$, $s = 0$ (two nodal diameters). Other pictures correspond to more complicated combination modes. Frame 1 is the most widespread pattern; such a form of perturbation is encountered in almost all the other films for both substances. The photographs taken during burning of diglycol dinitrate do not differ in appearance from photographs of burning nitroglycol. However, examination of the cine films shows that the flame revolves in this substance. This revolution is produced by the wave that travels along the tube circumference on the surface of the liquid. A characteristic process that complicates the shape of the perturbation is observed during the growth of unstable burning: two semicircles are formed, each of which is then again divided into two halves, after which the dividing process is accelerated to rapidly form a complicated combination of various modes of motion. Figure 115b shows successive pictures of such a process during burning of diglycol dinitrate at a pressure of 62 atm in a tube of 8 mm diameter. In addition to these modes, radial pulsations of the liquid were also observed sometimes (Figure 115a, No. 5).

An increase in pressure (burning velocity) leads to a decrease in the dimensions of the individual elements of the perturbations, the disappearance of large discontinuities, and the formation of a surface pattern consisting, as it were, of individual shreds. Motion pictures taken from the end make it possible to estimate the time of perturbation growth; it was about 15 msec for the situation shown in Figure 115. Photographs of the surface of the burning liquid in the perturbed regime were taken when the burning propagation velocity was ten times as large as the normal value. However, the increase in the burning surface appearing on the photographs was slight (no more than 2–3-fold). The surface visible on some photographs is probably covered with small waves. But the tenfold increase in burning velocity relative to the normal velocity cannot be explained by trivial geometric reasons alone. It would be necessary to assume that the height of the individual waves is tens of times larger than the distance between the waves. Therefore, we can conclude that the perturbed burning of the liquid is turbulent.

## 45. BURNING OF LIQUID EXPLOSIVE MIXTURES

Homogeneous stable mixtures of liquid components, such as tetranitromethane + fuels, often behave in a similar manner to the individual liquid explosives. They may burn in the normal, pulsating or turbulent regime; the critical conditions of transition to the turbulent regime are described by the theory of Landau. However, there are some differences which appear in certain circumstances. The main factor is the effect of differences in the volatility of the components and in their densities, which create prerequisites for the fractional, nonsimultaneous combustion of the components. In the absence of reaction in the condensed phase, the burning velocity will depend on the composition of the mixture in the gaseous phase. This composition may differ considerably from the original composition in the condensed phase, due to the fractional nature of evaporation.



An examination of the combustion (at 1 atm) of tetranitromethane (TNM) with such fuels as ethyl ether, benzene or acetone in tubes made of quartz, glass or metal will exhibit the following phenomenon when the mixtures are somewhat deficient in the oxidizer. A small, not bright flame is formed initially during ignition from the moderate temperature source. The flame is suspended above the tube section and is primarily responsible for burning of the fuel + air mixture. The rate of descent of the level of the liquid mixture is extremely low and comprises several hundredths of a millimeter per second. Subsequently, a bright, transparent high-temperature flame suddenly arises inside the tube and almost "rests" on the liquid surface. Intensive wavelike motion is visible on the surface of the mixture and the burning velocity increases by more than one order of magnitude (see Figure 116a). A rapid flame is formed due to burning of the mixture, which has almost the same composition as the initial mixture. Direct heating of the surface layer of the liquid by the flame and also by the wall transmitting heat from the flame enables the less readily volatile component (TNM) to vaporize at a sufficiently high rate. Application of a strong igniter permits one to immediately obtain the rapid burning regime, while low-energy ignition leads to a process involving two regimes. It should be also borne in mind that the maximum velocity of rapid burning in the normal (nonturbulent) regime corresponds approximately to the stoichiometric ratio of the components, whereas a large TNM excess makes the mixture unburnable. Observation of the dynamics of the process shows the existence of a surface layer in which intensive mixing takes place. This layer is termed the homolayer /204/ and its height is one and a half vessel diameters. In some mixtures, jets are clearly seen to fall downward from the mixing layer. Waves emerge from the tube walls inward during "rapid" burning and form cells 1–3 mm in size in 10–30 mm diameter tubes (Figure 116b). The introduction of a heat conducting rod into the liquid may accelerate the appearance of "rapid" burning. Burning continues in the rapid regime if the rod is then removed.


FIGURE 116. Photographs of burning of a liquid explosive mixture at 1 atm:

a) "slow"; b) "rapid" regime of burning of a TNM + acetone mixture; c) cells on the surface of the burning TNM + acetone mixture ($d$ = 12 mm).

The composition of the mixture is rearranged in the homolayer. The component ratio changes due to rapid consumption of the more readily

volatile component (for example, $C_6H_6$ is volatilized in the TNM + benzene mixture). At the same time, the distributions of the burning velocity, temperature, and so on, are changed. Condensation of the mixture complicates convection; the homolayer thickness decreases. The mixing intensity is a function of the ratio of the component densities. In the tests with TNM and fuel, the density of the oxidizer was always higher, and the volatility always lower, than those of the fuel. If the fuel density were higher, steady-state burning would become impossible due to the accumulation of the tetranitromethane, which is sparingly volatile and does not burn alone.

Rearrangement of the mixture during burning is proved by the following facts. When a mixture, such as TNM + benzene, is ignited, a brown layer accumulates at the end of the burning. The layer thickness is a few millimeters and the layer contains mainly TNM. In other experiments a near-stoichiometric mixture of TNM with heptane started to burn at 1 atm with a velocity of about 0.2 mm/sec. The velocity then gradually decreased and burning was quenched when 10–15 mm liquid remained in the test tube. Direct tests showed that the remaining mixture could not burn because it was enriched with TNM.

The burning regime of mixtures is determined by dynamic equilibrium between evaporation of the components, convective mixing in the surface layer, and the reaction rate in the vapor phase.

Many aspects of the deflagration of liquid mixtures and their transition to detonation were studied in depth by Gol'binder /205/. He focused his attention on the rearrangement of the mixture composition due to the fractional evaporation of components and the role of chemical factors (reaction between components, formation of active intermediate compounds, etc.). Gol'binder shows that differences between the behaviors of liquid mixtures and the individual liquid explosives are not always observed, since the mixtures frequently form chemical complexes in the liquid phase, or azeotropic systems, or continually evaporating mixtures. The differences become smaller with increasing pressure, because it is more difficult to alter the compositions of the liquid and vapor during the burning process.

Gol'binder holds the opinion that transition from deflagration of liquid mixtures to explosion or detonation includes the formation of a gas–vapor–droplet suspension (two-phase mixture). According to Andreev /38/, this layer may be stable when its thickness is somewhat below critical. Gas formation is abruptly accelerated when the thickness of the layer of the two-phase mixture in the gas phase above the burning surface exceeds the critical value. Acceleration may result from flashes or detonation, or from some intermediate regime of an explosion-like combustion of the suspension. The existence of an upper limit of detonation in terms of pressure is considered by Gol'binder as the result of a decrease in the layer thickness of the two-phase suspension: more droplets are dispersed into the gaseous phase with increasing pressure, but, in addition, their combustion period is shortened and this restricts the maximum attainable layer thickness of the suspension. This problem was treated in Andreev's book /38/, which also lists references on this topic.

Research on spontaneously igniting liquid mixtures is not treated here, because it has been examined in detail elsewhere by Gol'binder /265/ and Andreev /38/.



## 46. BURNING OF VISCOUS SYSTEMS

The stabilizing effect of condensing liquid explosives and systems is well known and has been utilized for a long time in many fields, including engineering. Many aspects of this problem have been examined in detail by, for instance, Andreev /38, 199/. Qualitatively, the effect of an increase in viscosity corresponds to the predictions of Levich's theory /74/; however, the quantitative aspect of the problem has been investigated insufficiently. Whittaker et al. /186/ condensed a mixed system ($HNO_3$–2-nitropropane) by adding the high polymer Lucite, and found that the pressure (burning velocity) at which transition to the turbulent regime proceeds increases with increasing viscosity of the mixture. The critical pressure increased in proportion to the viscosity raised to the power of 0.148. This exponent is equal to 0.33 in the theory of Levich /74/. However, analysis of Whittaker's data shows that the viscosity of the system was insufficient (less than one poise), and therefore surface tension should be the main factor stabilizing burning. Therefore, some correlation of experimental data with the theory of Landau /73/ should be sought. Whittaker's results are processed in Table 24 by computing $u_*/\sqrt{p_*}$, derived from the formula of Landau /73/ for constant surface tension and density.* This assumption is not too rough, because the amount of condensing additive is small. It can be seen from Table 24 that Landau's expression $u_*/\sqrt{p_*} \approx$ const is satisfied and Whittaker's data may be regarded as confirmation that the theory is correct. These data are not in agreement with the equation of Levich /74/.

TABLE 24. Processing of the data of Whittaker et al. /186/

| Content of Lucite, % | $\eta$ (35°C), poise | $u_*$, cm/sec | $p_*$, atm | $u_*/\sqrt{p_*}$ |
|---|---|---|---|---|
| 0.0 | 0.70 | 0.645 | 69.0 | 1.6 |
| 0.1 | 1.80 | 0.635 | 75.8 | 0.96 |
| 0.3 | 4.60 | 0.736 | 95.2 | 0.97 |
| 0.5 | 12.61 | 0.782 | 109.2 | 0.99 |
| 0.75 | 35.0 | 0.815 | 123.4 | 0.95 |

The most satisfactory confirmation of Levich's theory was obtained by Chuiko and Ivashkin (Institute of Chemical Physics of the USSR Academy of Sciences), who studied the burning stability of a 2 : 1 vol mixture of tetranitromethane (TNM) with benzene. The system was thickened by adding poly(methyl methacrylate) (PMMC). It was found that this viscous liquid system was non-Newtonian. The viscosity was measured at various shearing stresses with subsequent extrapolation to a stress of the order of $(\rho_* u_*^2)_*$, corresponding to the perturbing forces at the critical point of normal burning. Chuiko and Ivashkin succeeded in comparing theory with experiment. The mixture was ignited in beakers of 6 mm diameter and subjected to slight changes in pressures. Table 25 presents

* The relative magnitude normalized to the value for the system without an additive is reported here.

experimental data, and also critical burning velocities $J_*$ calculated by the equations of Landau and Levich. As before, the viscosity was determined by extrapolation. The differences in the values of $(\rho_1 u_1^2)_*$ were small for different systems, so the viscosity more or less corresponds to a shearing stress of the order of 1 dyne/cm$^2$. The table includes data pertaining to a mixture containing aluminum powder, which produces an additional condensation effect. If we omit the data on the mixture with 5% PMMC, Levich's equation gives a critical velocity equal to half the experimental value. The velocity calculated by Landau's equation using all the available data exceeds the experimental values by 25%. It was assumed that the surface tension of the system is constant (30 dyne/cm); this approximation may be insufficient. Thus, in this case Chuiko and Ivashkin could not make a unique choice between these theories, both of which have about the same degree of correlation with experiment.

TABLE 25. Limits of burning of viscous systems

| Content of PMMC, wt% | Experiment | | | Calculation of $J_*$ | |
|---|---|---|---|---|---|
| | % pulse | $J_*$ | $p_*$, atm | by Landau's equation | by Levich's equation |
| 1 | 9 | 0.28 | 3 | 0.433 | 0.065 |
| 2 | 32 | 0.42 | 8 | 0.71 | 0.165 |
| 3 | $2 \cdot 10^2$ | 0.77 | 10 | 0.79 | 0.725 |
| 5 | $5 \cdot 10^2$ | 1.36 | 36 | 1.8 | 18.7 |
| 5 + 5 Al | 135 | 0.645 | 11 | 0.83 | 0.31 |
| 5 + 10 Al | — | 0.38 | 56 | 1.87 | — |

Burning of the same TNM + benzene mixtures was also studied at higher pressures, when the process takes place in the turbulent regime. One of the most interesting results here was the effect of the method of mixture ignition on the burning velocity. Ignition by a weakly heated electrical spiral created burning velocities that were 2–5 times lower than values obtained by ignition with the aid of a pellet of ballistic powder (Figure 117). Comparison of different mixture velocities indicated that this difference decreases as the degree of condensation of the system with the high polymer increases; the most viscous mixtures practically no longer respond to the method of ignition. This phenomenon is apparently explained by the fact that initiation of burning by a high-intensity source (powder pellet) leads to strong distortion of the burning surface. Such distortion cannot be quickly arrested because of the increased viscosity of the system, and burning develops on the perturbed surface. The stability of such a process may be readily impaired. A strong increase in the viscosity of the system prevents distortion of the charged surface by the action of the igniter; the method of ignition becomes less important. The effect is greatest when the time required to damp surface perturbations is comparable with the time taken by the sample to burn up (compare tests on burning under increased pressure). The burning velocity data illustrated in Figure 117 correspond to a linear increase in the mean velocity of turbulent burning with pressure.



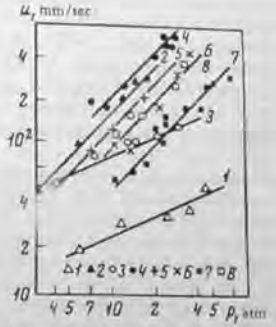


FIGURE 117. Burning velocity of 3:1 TNM—benzene mixtures as a function of the amount of condensing agent (poly(methyl) methacrylate), pressure, and method of ignition.

1 and 3) ignition by a spiral; the others — ignition by a tablet of explosive powder; 1 and 2) 1% PMMC; 3 and 4) without condensing; 5) 0.5% PMMC; 6) 2% PMMC; 7) 2% PMMC + 5% Al; 8) 5% PMMC. The exponent equals 0.5 on curves 1 and 3 and 1 on the other curves.

Experimental data obtained with mild initiation correspond to a much weaker pressure dependence of turbulent burning: the velocity for the uncondensed TNM + benzene mixture and the mixture with 1% PMMC increases in proportion to $p^{0.5}$, i. e., it corresponds to the theory of turbulent burning of liquid systems explained in section 41. It should be emphasized that the onset of the first of the considered regimes of turbulent burning with a strong pressure dependence of this process corresponds to rapid transition from deflagration to detonation, often observed during intensive ignition of liquid explosives /38, 191, 206/.

The effect of the tube height above the liquid surface has been noted by some investigators and will be examined in the light of the above data. In the high-velocity turbulent regime, burning of the droplet suspension entrained from the liquid surface far from it, e. g., into the bulk of the bomb (short tube), leads to the loss of some energy of the flow of combustion products, and the number of droplets entering the flame is restricted. The energy of the flow can be completely utilized to break off the droplets from the surface of the original liquid by increasing the tube length above the surface, and when equilibrium is impaired it may lead to the explosion of the droplet – gas mixture (section 48). As the reactivity of the system increases, so the burning temperature becomes higher, the critical tube length becomes lower, and the more readily does the mixture detonate during intensive ignition. The role of viscosity is also understandable: ultrahigh-speed turbulent burning becomes impossible when the mixture condensation is more than the limiting shear stress and reaches a value exceeding the shear stress of the turbulent flow of the combustion products. The dependence of the mechanical properties on loading rate must also be taken into account for non-Newtonian systems.

The introduction of small amounts of condensing agents into liquids frequently alters the burning velocity and its pressure dependence both in normal and turbulent burning regimes; this applies especially when additives are present in small concentrations. This effect quickly diminishes as the viscosity increases. For instance, Whittaker's data /186/ indicate that for Lucite contents of 0, 0.1, 0.3 and 0.75% in an $HNO_3$ – 2-nitropropane mixture the burning velocity is 3.9, 3.4, 2.55 and 2.4 mm/sec, respectively, at 40 atm; at 70 atm the figures are 6.5, 5.8, 4.8 and 4.6 mm/sec, respectively. The burning velocity of nitromethane with 2.8, 4.2, 7 and 9.8% pyroxyline was 1.80, 1.68, 1.42 and 1.20 mm/sec (according to data of Parfenov). It is noteworthy that uncondensed nitromethane burns at 1.5 mm/sec under these conditions. The difference in the effects of pyroxyline and Lucite is due to their different burning ability. The burning

velocity of pyroxyline is higher than that of nitromethane, whereas Lucite is essentially inert. In the tests with nitromethane, the effect of introducing an additive was to create a competing influence of two factors: increase in the velocity and energy content of the mixture when an active condensing agent is introduced, and a decrease in the velocity due to the increased viscosity of the system. Condensing of the mixture decreases the surface layer which is heated near to its boiling point (decomposition), due to the suppression of convective mixing.

The effect of viscosity on the burning velocity beyond the stability limit has remained virtually uninvestigated. It was found that the turbulent burning velocity of nitroglycol condensed by colloxylin is less pressure dependent than the corresponding quantity for uncondensed nitroglycol. The difference between the degrees of dependence increases with distance from the stability limit. The turbulent burning velocity of the TNM + benzene mixture (see Figure 110a) generally decreases with the viscosity of the system. The type of pressure dependence, however, is retained and may be approximated by the equation $u = Bp$, where $B$ decreases with increase in viscosity.

Burning of readily fusible solid substances when there is a considerable layer of the melt forms a special case. Theory shows (section 40) that eddy formation during burning by the Landau–Levich mechanism is only possible under exceptional conditions (the temperature of the substance is near its melting point). Experiments of Andreev and Popova /85/ with fused PETN indicate that the burning pattern actually corresponds to eddy formation after Landau, while the critical burning velocity is in fair agreement with the theoretical value. Glazkova's experiments /222/ with supercooled DINA also confirm that melts of explosives behave like liquid systems. Popova /85/ dealt with eddy formation during burning of solid fusible explosives by the Landau–Levich mechanism and observed that burning of solid PETN was quenched after pulsations accompanying ignition. Evidently, the melt of the layer burned up in the turbulent regime and was unable to transfer heat into the bulk of the charge, so that the melt was not continuously renewed and burning was quenched. Thus, nonquenching of turbulent burning of solid fusible explosive is impossible by the Landau–Levich mechanism. On the other hand, an abnormally large layer of the melt formed, for example, by very weak and long-term ignition may burn up in the turbulent regime, also in the form of flashes or of explosive processes.

One possible method of checking the theory is to investigate burning under increasing-pressure conditions. It was shown earlier (section 41) that high-viscosity mixtures may burn under these conditions up to pressures that considerably exceed the critical value $p_*$, determined during constant-pressure burning. Experiments with nitroglycol showed that if the pressure increases up to 20 atm/sec, $p_*$ cannot be exceeded by more than 20%, which is in agreement with theoretical predictions. Experiments were carried out with the TNM–benzene system containing 2% PMMC and 5% aluminum powder in order to check the theory for viscous systems. The mixture was ignited in a manometric bomb and the $p$ (t) curve was recorded. The mixture burned at constant pressure $p_* = 11$ atm. Figure 118a shows the variation in the critical pressure $p_{cr}$, found by tests in the manometric bomb, as a function of the reduced rate of pressure growth $\dot{r} = (1/p)(dp/dt)$,



determined on the $p$ (t) curve before the collapse of the normal pressure. The plot shows that at low growth rates a pronounced effect (predicted by theory) is observed: in the manometric bomb, $p_{cr}$ exceeds $p_*$ and increases with $\dot{r}$. Experimental data processing leads to the expression $(p_{cr} - p_*)p_*^{-1}\dot{r}^{-0.67}$. According to theory (section 41), the correlation should be performed in terms of $(p_{cr} - p_*)p_*^{-1}\eta^{-1/3} \approx \text{const}$. The investigated mixture is a non-Newtonian liquid, so its viscosity depends on the rate of shearing stress application, i. e., $\eta = \eta(\dot{r})$. If $\eta \sim \dot{r}$, the experimental data is in agreement with theory (equation (102)). The actual form of function $\eta$ ($\dot{r}$) is unknown.

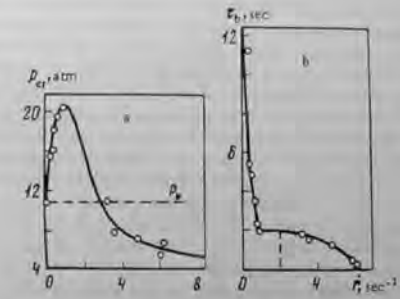


FIGURE 118. Effect of relative rate of pressure growth $\dot{r}$:

a) critical burning pressure of the 3:1 TNM–benzene mixture containing 2% PMMC and 5% Al in the manometric bomb; b) time of development of unstable burning of the same mixture.

Consider now the function $p_{cr}(\dot{r})$ at higher rates of pressure growth. The experiments show that $p_{cr} < p_*$ when $\dot{r} \gtrsim 3.1$ sec$^{-1}$. Motion pictures established that the initial perturbation produced by the igniter (gunpowder) was not quenched in these experiments and turbulent burning developed on the surface as further deepening of the roughness of the relief. In tests with a small rate of pressure increase, the initial perturbations were damped and everywhere there was a section with a smooth surface. Figure 118b shows the variation in the burning period until the instant $p_{cr}$ is reached. Comparison of Figure 118a with Figure 118b showed that the characteristic time of perturbation damping for the investigated system is about 2 sec. If the rate of pressure growth was so large that the perturbations were not damped * $p_{cr}$ was found to be smaller than $p_*$. The inequality $p_{cr} > p_*$ held during the growth of instability from normal burning. In these experiments, $p_{cr}/p_* \simeq 1.85$. Further condensation of the system will increase this ratio (for identical rates of pressure increase). At the

* This is equivalent to the requirement that the burning period of the sample should be comparable with (or lower than) the damping time of the perturbations of the mixture surface.

same time, the damping time of the initial perturbations will grow and may prevent high $p_\alpha/p_*$ values being attained. If known methods of ignition are used without considerable perturbations, the curve $p_\alpha/p_* = f(\dot{r})$ may be extrapolated to high rates of pressure increase.

## 47. BURNING OF LIQUID EXPLOSIVE CHARGES WITH HEAT-CONDUCTING ELEMENTS

The charge casing often distorts measurements when determining the burning velocity of explosives. It was found long ago that the burning velocity of charges in not too compact metallic casings is larger than in casings made of materials which are poor heat conductors /38/. The effect of heat-conducting walls was explained by Andreev /37/. A casing which is a good heat conductor (such as a metallic one) enables the heat flux into the noncombusted substance to be increased because of removal and transport of heat from the high-temperature zone into the path taken by the gaseous phase of the combustion products that conducts heat poorly. The heat is transferred over the walls and used to increase the initial charge temperatures in the surface layers which, due to the dependence of the burning rate on the explosive temperature, leads to a growth in the mean burning velocity of the charge. It is understandable that the higher the burning velocity, the smaller the amount of heat which can be transferred into the path followed by the burning front over the heat-conducting elements The temperature distribution in the gaseous phase, the presence of a reaction in the condensed phase (temperature sensitivity of the burning velocity), etc., assume considerable importance. In experiments with liquid explosives placed in (metal, quartz, glass) beakers we frequently observe boiling of the liquid at the end of low-velocity burning accompanied by flashes. For instance, a more than 100°C increase in temperature was recorded when measuring the temperature at the bottom of a beaker containing nitroglycol burning at 5 atm, long before the flame front was approached. "Edge" effects arose because an absence of heat removal leads to heat accumulation in a restricted volume and hence progressive heating of the final volume of the liquid (see Figure 105g).

The first experiments with a heat-conducting element, introduced in order to promote heat transfer from the gaseous to the condensed phase, were carried out by Kostin (cited from /37/). A copper rod was introduced into a test tube containing burning nitroglycol and sharply accelerated the burning process. At present, the introduction of heat-conducting elements into explosive charges and solid rocket propellants is one physical way of controlling their combustion velocity.

Kostin's tests were repeated by us (together with Margolin and Sokolovskii) on a 3 : 1 TNM–benzene mixture at 1 atm. Changes of the material (glass, brass, aluminum) of the charge casing affected the combustion velocity, the instant of the onset of rapid burning (section 45), and also the nature of the convective motion of the mixture in the surface layer. For instance, the "rapid" burning regime in the thin-walled aluminum casing sets in almost immediately after ignition, whereas in the quartz casing it sets in only after combustion of a liquid column whose



height is one and a half diameters of the casing. Waves are issued from the vessel walls and form cells similar to those shown in Figure 116c. The wavelike motion in the metal casing is more pronounced and proceeds more intensively than in the quartz casing. Wavelike motion is damped as the mixture becomes condensed; the high-viscosity mixture burns up more rapidly at the walls and forms a cone with vertex upward.

A copper rod was introduced into the mixture burning in the quartz beaker. Intensive convection was observed in the liquid, starting near the rod. The combustion velocity increased and transition to "rapid" burning was accelerated. A small degree of condensation of the mixtures led unexpectedly to an explosion. It was found that gas bubbles are formed in the vicinity of the rod and are a mixture of the vapors of the original liquid and the combustion products (indicated by a change in color). As the mixture was heated, the number of bubbles increased and a foamy layer accumulated; the flare-up of this layer was sometimes recorded as detonation. The localized nature of this phenomenon follows from the fact that the test tube often remained intact after the detonation, the rod was ejected, and the burning continued to propagate. The detonations were especially intensive when the rod was not introduced very far into the liquid ("edge" effect). Condensation in this case makes convective heat exchange with the cool layers more difficult; this leads to superheating of a limited volume of the mixture, its decomposition and detonation.

Systematic research on the effect of heat-conducting elements on the hydrodynamic stability of the burning of liquid explosives was conducted by Margolin et al. /208/, who used a stoichiometric tetranitromethane–benzene mixture. Their experiments made use of rectangular plexiglass or quartz test tubes (cross section 5 × 6 mm). In some experiments, copper or steel strips were introduced near both walls and served as the heat-conducting elements. The results are shown in Figure 119, from which it follows that the metallic strips considerably increased the burning velocity in the subcritical regime and the critical burning velocity; however, the critical pressure of transition to the turbulent regime remains unchanged. Consequently, the introduction of heat-conducting elements leads to an increase in the effective burning velocity of the mixture; at the same time, the burning stability of the liquid mixture is determined by the inherent fundamental velocity. In the case of powdered systems, the critical conditions governing the impairment of normal burning are also determined by the fundamental burning velocity and are independent of the physical effects, leading to an increase in the recorded burning velocity.

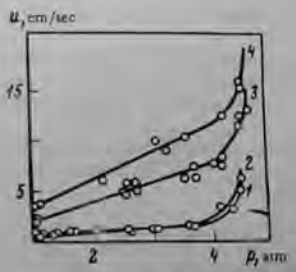


FIGURE 119. Pressure dependence of the burning velocity of the stoichiometric TNM–benzene mixture:

1) plexiglass test tube without strip; 2) 0.2-mm-thick steel strips; 3) 1.5-mm-thick copper strips; 4) 0.5-mm-thick copper strips.

Data of Margolin et al. /208/ are employed to examine the phenomena accompanying the burning of a liquid mixture into which a heat-conducting element was introduced. Heat propagates along the element from the flame zone into the bulk of the liquid. Heating of the layers adjoining the elements produced convective flows inside the liquid.

Heating of some surface layer compels it to burn in an accelerated fashion. However, at pressures below the critical pressure of transition to the turbulent regime, combustion of the superheated layer goes over to quiet burning of the unheated liquid, since in this case normal burning is characteristic under the given conditions. There then follows a period of heating of a new surface layer of the liquid by the heat transferred over the element, and the pattern is repeated. A turbulent burning regime sets in; its average velocity will be above normal due to accelerated burning of the superheated layer. Turbulent burning, which is not interrupted by normal burning periods, can develop only after the critical pressure of transition for the original mixture is exceeded in the experiments. Margolin et al. /208/ used high-speed motion pictures to experimentally confirm the above sequence of phenomena.

The effect of the heat-conducting element naturally depends on the ratio of the thermal diffusivities of the material of the element and the liquid explosive, and also on the temperature coefficient of the burning velocity of the explosive. Fractional combustion, which increases pulsations, may arise in the case of mixtures of liquids with considerably differing volatilities. Burning may become quenched when the surface layer of the mixture is enriched to an excessive extent by some component unable to burn alone. Such a situation was observed experimentally when we studied the combustion at 1 atm of a mixture of TNM and ethyl ether somewhat enriched with oxidizer.

Steady-state turbulent burning is therefore only possible when the critical value of the fundamental burning velocity is surpassed. This factor also determines the independence of the critical pressure on the presence of heat-conducting elements.

We do not examine here the potential catalytic effect of the surface of the heat-conducting element, which may sometimes considerably affect the mean burning velocity of liquid explosives.

## 48. MEANS OF TRANSITION FROM PERTURBED BURNING TO DETONATION

Research on the mechanism underlying unstable burning has always aimed at explaining transition from deflagration to explosion or detonation. Fundamental work on this problem was carried out by Andreev, Belyaev and their co-workers, and is described most exhaustively and clearly in their books /17, 59/. Nevertheless, this aspect of the theory of burning has been developed to only a slight extent at both the theoretical and experimental levels. Many of the conclusions are hypothetical and have no quantitative justification.

The theory of turbulent (perturbed) burning of liquid explosives has been examined in the previous chapters and makes it possible to somewhat



approach the solution to the problem of the conditions underlying transition from deflagration of liquid explosives to detonation. However, a final answer cannot be given mainly because there is a scarcity of experimental data.

### The Andreev–Belyaev mechanism

It was noted at the beginning of this chapter that transition from deflagration to detonation according to the Andreev–Belyaev mechanism takes place, if the acceleration of gas formation with pressure exceeds some critical value during burning.

The physical sense of this statement is clear when we examine the expression for the pressure in the volume of the vessel (tube) containing the burning explosive. If the charge diameter is equal to the tube diameter and $u_1 = Bp^\nu$, then $p_\tau = (B\rho_1/A)^{1/(1-\nu)}$. Consequently, when $B\rho_1/A > 1$ and $\nu \simeq 1$ pressure $p_\tau$ increases without limit until it destroys the casing of the charge, i.e., until detonation. Since $A \simeq 7.4$ g/cm$^2$ · sec · atm, the criterion for the onset of charge detonation will be $B\rho_1 > 7.4$ g/cm$^2$ · sec · atm, $\nu \simeq 1$. If $\nu > 1$, equilibrium is impaired in this case when the pressure exceeds $p_{cr} = (A/B\rho_1)^{1/(\nu-1)}$ (curve $m_2^*$ in Figure 120).

When $\nu < 1$, and even when $B\rho_1/A > 1$, there exists some pressure $p_1$ corresponding to an equilibrium of gas supply and gas removal. When $\nu < 1$ and $B\rho_1/A \leqslant 1$, $p_\tau$ will be practically equal to the outside pressure $p_0$.

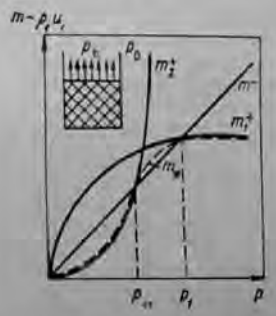


FIGURE 120. Gas supply balance during the supersonic efflux of the combustion products.

We established in the preceding section that the pressure dependence of the turbulent burning velocity has exponent $\bar{\nu}$ larger than unity, in which case intermediate values occur and at large values of $n$, $\bar{\nu} = \nu_0 - 0.5$, where $\nu_0$ characterizes unperturbed burning. As a rule, $\nu_0 \approx 1$ in liquid explosives and therefore function $u_\tau(p)$ in a developed turbulent regime has the form $u_\tau = B\,p^{0.5}$. Combustion in the developed turbulent burning regime should therefore be stable from the aspect of the Andreev–Belyaev mechanism, and also $p_1 = \left(\frac{\pi a_1}{A}\,\frac{\rho_1^{*1/\nu}}{(\rho_0^*)^{1/\nu}}\right)^{\nu}$, where $\rho_1^*$ is the density of the combustion products reduced to 1 atm. It is interesting to compare this conclusion with the data of Bakhman and Dubovitskii /191/ (see section 49).

In the transient region between $n = 1$ and $n \gg 1$ there is a pressure range over which $\bar{\nu} > 1$. If the criterion $B_*\rho_1 > A$ is satisfied, equilibrium between gas supply and removal may be impaired. However, if the casing of the explosive-containing beaker is sufficiently strong the pressure in it will increase until the onset of perturbed burning, characterized by $\bar{\nu} < 1$. This is illustrated by curve in Figure 120. Here, the gas supply exceeds the gas removal when $p < p_1$

and the pressure in the casing increases. However, transition then takes place to the saturation branch ($\bar{\nu} < 1$) and, finally, the equilibrium pressure $p_1$ is established. The casing may naturally be destroyed before $p_1$ is attained, and this will be defined as detonation.

Only one criterion of transition from deflagration to detonation by the Andreev–Belyaev mechanism was examined. The second criterion is $B_T \simeq B\sqrt{\rho_1/\rho_2} \simeq 10^3 B$. $\rho_1 B > A$. In the developed regime of perturbed burning, Comparison of this quantity with the data of Table 18 and with $A$ shows that $B_T\rho_1/A > 1$ for methylnitrate, and in this case $p_1 \simeq 3.5$ atm, while other explosives are nearer the limit. Both the order of magnitude and the numerical value of coefficient $a_1$, etc., is important here. In other words, $B_T\rho_1 > A$ may be satisfied and the subcritical burning regime may be realized, depending on the features of the situation. For instance, careless ignition, a 2–3-fold increase in the burning surface, complication of gas removal by, say, a reduction in the flow cross section of the combustion products in comparison with the surface of the charge – all these factors will cause detonation.

One important fact must be taken into account. The problem is considered in the Andreev–Belyaev theory on the assumption that the whole substance will react within the vessel in which the liquid is contained. If a considerable amount of liquid is ejected (for instance, in the form of droplets) and reacts far away from the tube, gas evolution by combustion of this amount of explosive does not enter the balance of gases determining the pressure near the surface. The height $h$ of the vessel containing the liquid explosives, which ensures complete combustion of the droplets entrained by the gas flow from the liquid surface, must evidently be no smaller than $h_*$, where

$$h > h_* \simeq \tau_{liq} u_1 = \tau_{liq} \frac{B_T}{\sqrt{\rho}} \frac{1}{\sqrt{\rho_2^0}}. \qquad (107)$$

In a first approximation, $\tau_{liq}$ is determined by the reaction kinetics of the substance and is proportional to the square of the droplet diameter; in simple combustion the exponent of the droplet diameter is unity.

FIGURE 121. Evolution of large-scale perturbation of the burning liquid surface.

The developed perturbed burning regime must be stable from the standpoint of the balance of gas supply and removal. This conclusion is drawn on the assumption that the perturbation develops from infinitesimal perturbations generated by the burning process itself, i. e., their amplitude is $\xi \ll u_1^2/g$. The larger artificial perturbations burn with spreading, as explained in section 39.

Suppose a channel was formed at the instant of intensive ignition of the liquid (Figure 121). The pressure in region $a$ will be higher than in region $b$. The excess pressure begins to extrude liquid from the vessel, atomizes it, while droplet ignition by a high-temperature flame may take place as detonation. Moreover, the wave may be unstable and instead of spreading its crest may break (see dashed curve in Figure 121). An isolated



volume is consequently formed in the bulk of the liquid and, while growing, destroys the surrounding liquid. The exterior picture of this phenomenon will be detonation of the charge.

Thus, the most favorable conditions for the development of instability in the sense of Andreev and Belyaev takes place near the limit of normal burning, when the turbulent burning regime has not yet developed. According to the Landau–Levich theory, far from the limit the burning is stable in the considered sense ($\bar{\nu} < 1$). However, we should exclude external artificial perturbations of sizes larger than about $u_1^2/g$ as these may become the causes of localized explosions.

### Thermal explosion of a suspension of liquid explosive droplets in the gaseous phase

As a result of strong turbulence, the temperature of the combustion products is close to the peak temperature and almost constant along the tongue of the flame. This ensures rapid gas-phase reactions due to the exponential temperature dependence of the reaction rate. The thermal explosion of a droplet suspension is very often regarded as the initial stage of explosion, or even detonation, of the charge. This question is now examined in somewhat more detail.

The concentration of droplets of the explosive in the gaseous phase can be assumed to be proportional to the turbulent burning velocity. If we assume that $u_1\rho_1\tau_{liq}$ grams of the substance escape into the gas phase from 1 cm$^3$ in time $\tau_{liq}$ and are distributed over a gas column of height $u_1\tau_{liq}$, we obtain $c_d = \rho_1$ g/cm$^3$.

The conditions for the thermal explosion of the suspension will be estimated on the basis of a fact determined by Rumanov and Khaikin /209/: the critical conditions for spontaneous ignition of a cluster of particles have the same form as the critical conditions for a single particle, only the heat transfer coefficient is altered. The special feature is that the thermal explosion of a cluster of droplets takes place when there is interaction between the particles. Moreover, according to Rumanov and Khaikin /209/, to a first approximation the presence of the heating and evaporation stages leads to a change in the numerical value of the critical Frank-Kamenetskii parameter $\delta_*$. The critical condition of thermal explosion can therefore be expressed in the form

$$\delta_d = \frac{E}{RT_0^2} \frac{Q\rho_1}{\lambda_1} \frac{(Nu)_d}{Nu} L^2\psi > \text{const} = \delta_*, \qquad (108)$$

where $E$ is the activation energy, $T_0$ is the temperature of the surroundings, $\psi$ is the rate of reaction, $R$ is the gas constant, $\lambda_1$ is the thermal conductivity coefficient of the droplet, $Q$ is the heat of reaction of the explosive, $(Nu)_d$ and $(Nu)$ are the Nusselt numbers for heat transfer from the particle to the gas and from the gas to the walls, respectively, $L$ is the characteristic dimension of the vessel (diameter), and $\delta_*$ is the critical parameter.

Thus, thermal explosion of a droplet suspension is only possible when inequality (108) is satisfied. This inequality contains, in particular, the vessel diameter, so thermal explosion takes place more readily when the cross-section increases. It is noteworthy that the ignition point of the particles is independent of their size /209/.

It is assumed in condition (108) that all the droplets entrained from the surface are present in the suspension. Allowance must also be made for the effect of suspension combustion during the induction period of thermal explosion /210, 211/. To a first approximation we can assume that it is sufficient to satisfy (107) and (108); the induction period of thermal explosion should be taken as $\tau_{inq}$, since the ignition period $\tau_{ig}$ is much shorter than $\tau_{inq}$.

There is another source of error that sometimes arises. A decrease in the dispersity of the particles introduced into the gas phase from the surface only changes the height of the flame tongue, but cannot impair the gas supply and removal balance. Naturally, the gas supply involves only the amount of original substance processed in the combustion products. It is impossible to impair equilibrium of the process without introducing some supplementary mechanism governing combustion of the explosive droplets and the influence of the combustion process of the suspension on the breakoff of droplets from the surface. It should be remembered that droplet breakoff is determined by the kinetic energy of the combustion products $\rho_3 u_3^2$.

Positive feedback of droplet combustion with droplet breakoff from the burning surface takes place only via an increase of pressure in the vessel, since the velocity of the combustion products no longer changes when combustion is complete (even when $\nu = 1$). Pressure increase in the vessel is possible if the time of reaction of the droplets is smaller than the efflux period of the combustion products, i. e., $D/v < h/C_3$, where $v$ is the effective rate of reaction (combustion) of droplets of diameter $D$, $h$ is the height of the free part of the tube above the liquid surface, and $C_3$ is the sonic velocity in the combustion products. If $h = 1$ cm, $C_3 = 10^5$ cm/sec and $D = 10^{-3}$ cm, we find that $v \simeq 10^2$ cm/sec. The normal burning velocity is approximately $u_1 = 3 \cdot 10^{-2} p$ cm/sec. Allowing for possible heating of the droplets, we see that $p \simeq 10^4$ atm corresponds to a velocity of 100 cm/sec. Thus, simple conductive burning of droplets at moderate pressures cannot produce a pressure jump over the burning surface. Note that the time to heat a droplet of diameter $D$ is approximately $D^2/4\mathrm{Nu}\chi_1$; when $D = 10^{-3}$ cm it is about $2 \cdot 10^{-4}$ sec, which is more than $h/C_3 = 10^{-5}$ sec. It is of interest to compare this time with the time of transition from deflagration to detonation obtained by Bakhman and Dubovitskii /191/ (see section 49).

On the whole, the question of the actual sizes of the suspension droplets remains open, since the original (broken off) droplets of the explosive may be disintegrated in the gas flow. This point is discussed in the paper of Mayer /216/.

The distance between the site at which the droplets are burned up and the surface is larger than the magnitude $\varkappa_1/u_1$, which is characteristic for the normal process. This is because vapor and cold droplets issue from the unprepared surface.

Let us now deal with the aftereffects of the thermal explosion of the suspension. If the explosion of the droplets is regarded as instantaneous,



so satisfying the condition $(u_3/C_3)(\tau_{inq}/\tau_{ig}) \geq 1$ (where $C_3$ is the sonic velocity in the combustion products), we can estimate the excess pressure created in the tongue of the flame. Since 1 cm$^3$ contains $c_3 = \rho_3 = \rho_3^0 p_0$ grams of liquid explosive, their temperature for full conversion increases from the initial value $T_0$ to the final temperature $T_3$ of explosive conversion, while the density changes from $\rho_1$ to $\rho_3$. The pressure increase $\Delta p$ in the combustion products is given by

$$\Delta p = p - p_0 = c_3 R T_3 / M \simeq p_0.$$

This quantity may be so large that the vessel is destroyed and the process will occur as an explosion. The effect of the excess pressure gradient on the original substance may destroy the liquid, atomize it, and at the same time automatically accelerate the burning process. This is due to the fact (disregarded by us) that the actual distribution of the droplet concentration over the tongue flame is not homogeneous because of the turbulent nature of the flame. Therefore, thermal explosion may arise at individual hot spots similar to the situation observed in the turbulent gas flame /185/. The difference is the (hundreds of times higher) localized pressure rise during combustion of the droplet suspension. The above inhomogeneity in the distribution causes the jet of the products of the thermal explosion to act upon the liquid surface and so impair its homogeneity.

If the time of thermal explosion growth is not too small, and if we can neglect gas efflux from the vessel during the reaction period (this implies that $u_3 \tau_{inq}/C_3 \tau_{ig} \ll 1$), then the pressure in the vessel will acquire a value of the order of $p_{ig} \leqslant (\rho_3 B_v A \rho_3^0)^{1/2}$. If the initial pressure was lower than $p_{ig}$, the result of combustion of the suspension will look like an explosion. At high pressures, the process follows that of ignition.

The reader should bear the following in mind. At pressures higher than the thermodynamic critical pressure, we have "pulse-like" evaporation of the liquid droplets after they are heated to a temperature higher than $T_{cr}$ with subsequent burning of the vapors. A total of about 5% of the droplet mass is evaporated as soon as $T_{cr}$ is attained /203/. This phenomenon can develop in many ways and may lead to a transition from turbulent burning of liquid explosives to detonation via the processes taking place in the vapor phase.

### Cavitational initiation of liquid explosives

Already in 1939, Belyaev /2/ advanced the hypothesis according to which the dynamic pressure decrease above a burning liquid surface may lead (by boiling of the liquid, after the notion of Belyaev) to the onset of detonation. The observation, that deflagration of methyl nitrate at 1 atm and 40°C goes over into detonation if the pressure is reduced during the burning process, served as the basis for this theory. Further conclusions in the light of contemporary ideas led to an unsuitable approach: the role of the rapid pressure drop was replaced by the problem of the explosion of a mixture of methyl nitrate vapor with air. An exhaustive discussion of this (second) problem is contained in the books of Andreev /37, 38/, and so will not be treated here.

We shall now examine the principle of Belyaev's hypothesis. Recent papers /212–214/ showed that a comparatively small pressure change may lead to cavitation and detonation of some explosives. According to Gordeev /213/, detonation occurs during the sudden cavitation of sufficiently large voids (cavities). The fundamentals of the mechanism are heating and ignition of the liquid vapors mixed with the dissolved gases contained in the cavity due to their rapid compression. If we take into account that heating of the vapors ($T_1/T_0$) is proportional to the compression ($p_1/p_0$) raised to the power $(\gamma - 1)/\gamma$, where $\gamma$ is the polytropic exponent, then it is convenient to have a small initial pressure $p_0$ for the given compressing pressure in order to attain the high, final temperature $T_1$. On the other hand, if the volatility is very low, the vapor pressure is negligible and the heating and ignition of the vapor will be insufficient to initiate explosion. It should be emphasized /70/ that heating by compression of the chemically active gas (like the vapor of the explosive) is more dangerous than the explosion of inert gas pockets, since the temperature of compression of the active gas will be higher due to heat evolution by the chemical reactions.

The size of the cavitational bubble may be important. Small bubbles are cooled so rapidly, that the vapors are compressed under practically isothermal conditions. For considerable heating of the bubble with the inert gas, it is necessary /70/ that the time of gas compression be $t_1 \sim p/\dot{p}$ ($\dot{p}$ is the rate of pressure growth), less than the cooling period $t_2$:

$$t_2/t_1 \simeq d^2\dot{p}/4\,\mathrm{Nu}\,\varkappa_2 p \gg 1.$$

Here, $\varkappa_2$ is the thermal diffusion coefficient of the mixture, present in the bubble; $d$ is the mean bubble diameter, and Nu is the Nusselt number for heat transfer from the bubble to the liquid.

When $d \sim 10^{-4}$ cm, we must have $\dot{p}/p > 10^5$ sec$^{-1}$, i.e., the compression must last a very short time. Heating of the compressed gas is given by $T_1/T_0 = (p_1/p_0)^{(\gamma-1)/\gamma}$. The criterion of thermal explosion of the active gas is, to a first approximation,

$$(d^2\rho_2 Q_1 E k_0/2RT_1^2\vartheta_2\,\mathrm{Nu})\exp(-E/RT_1) > 1,$$

where $k_0$ is the frequency factor, $Q_1$ is the thermal effect of chemical conversion, and $d$ is the cavity size; $\rho_2$ is the density of the liquid explosive vapors in the bubble, proportional to the vapor pressure $p_0$. It should be taken into account that $p_0 = a_1 - a_2/T_0$, where $a_1$ and $a_2$ are constants for the given substance and $T_0$ is the absolute temperature.

Thus, the critical size of the cavitational bubble depends on the volatility of the liquid and the reaction kinetics of its vapors, and may become a source of initiation of explosions for a given degree of bubble compression. Gordeev /213/ shows that any explosive liquid may detonate when a cavitational bubble collapses, the initial bubble dimensions being equal to or larger than the critical value. However, explosion cannot be initiated by cavitation in all of them, because of differences in the physicochemical properties of liquids. Substances which possess a low reaction rate of the vapors are characterized by such large critical dimensions of the cavitational bubble that explosions practically cannot take place.

Gordeev and Matveev /215/ studied the initiation of the explosion of cavities (at 1 atm) of the following liquid explosives: nitroglycerin,



tetranitromethane (TNM), nitromethane, solutions of benzene, heptane, methanol in TNM, solution of methane in liquid oxygen (at the boiling point of nitrogen), and the heterogeneous solid acetylene – liquid oxygen system (also at the boiling point of nitrogen). An original method was elaborated for producing large cavities, and first made it possible to study this phenomenon in detail. A test tube with a tight fitting piston was used; the sample was introduced beneath the piston. The liquid seal in the form of a conical funnel was filled with the same sample of the liquid explosive and enabled the liquid beneath the piston to be isolated from the atmospheric pressure for a few milliseconds. Rapid pulling out of the piston created tensile stress in the liquid. The continuity of the liquid explosive is impaired and cavities are formed.* Explosion was initiated by collapsing the cavitational bubbles in the benzene or heptane solutions in tetranitromethane. Explosions were initiated in technical nitroglycerin using a piston with a pointed end.

The effect of the initial temperature /215/ was studied with the following results. A benzene solution in TNM at temperature below 10°C, right down to the temperature of crystal precipitation, always yielded explosions. At 20°C, explosions were initiated in one-third of the experiments. The vapor pressure $p_0$ at 20°C is $p_0 = 30$ mm Hg, and at 10°C, $p_0 = 17$ mm Hg. An increase in temperature to 40°C ($p_0 = 70$ mm Hg) decreased the frequency of explosions to 3 out of 20 experiments. At 60°C ($p_0 = 160$ mm Hg) no explosion was observed in 20 experiments. A heptane solution in TNM exploded regularly at temperatures below 2°C ($p_0 = 3$ mm Hg). At 20°C ($p_0 = 14$ mm Hg), the explosion frequency was 2 out of 50 experiments and at 40°C ($p_0 = 200$ mm Hg), no explosion was observed at all in 100 experiments. A methanol solution in TNM was insensitive to initiation of explosion by cavities at temperatures of 10–50°C ($p_0 = 40$–$280$ mm Hg).

Experiments were carried out with technical and purified nitroglycerin at higher temperatures. The following fact is interesting from both the theoretical and practical standpoints: purified nitroglycerin, regardless of the very small vapor pressure (less than 0.5 mm Hg), regularly gave explosions. The technical product at 70°C exploded in two experiments out of twenty, while at lower temperatures it was insensitive to cavitational excitation.

Here, the kinetic aspect of the process definitely had some effect: the vapors of the purified nitroglycerin readily yield thermal explosions, due to their high reactivity. As regards the contaminated product, an initial temperature of at least 70°C is required for thermal explosion to grow in its cavities. It is of much interest /215/ that purified nitroglycerin becomes insensitive and its vapor pressure increases after its liquid surface is exposed to air for several hours.

The cavitational mechanism of initiating explosives must be regarded as a cause of the detonation of liquid explosives when carelessly ignited; this is especially true with respect to burning of explosives in an enclosed space. The rapidly burning igniter and the ignition of the thick, heated, explosive layer generate acoustic vibrations whose propagation can produce cavities in the liquid and initiate explosion of the whole charge.

* The tensile strength of liquids depends very strongly on the contents of dissolved gases. Saturation of a liquid with a gas sharply reduces its strength and leads to cavity formation.

Let us now return to the paper of Belyaev /2/ on the initiation of detonation of methyl nitrate, and to the supplementary paper of Andreev /37/. It was found that ignition of methyl nitrate vapors and methyl nitrate vapors mixed with air (when the methyl nitrate level is higher than 70%) produces strong detonation. Moreover, it is possible to produce detonation of liquid methyl nitrate alone when igniting the vapor–air mixture over the liquid surface. As regards these experimental results, Andreev /37/ notes that explosion of gaseous vapors can produce a slight pressure rise, which, however, is sufficient for the onset of detonation. There is reason to believe that the pressure jump created by the gaseous vapors generates acoustic vibrations in the liquid, its cavitation, and initiates explosion by the above mechanism.

However, some experimental observations indicate that explosion may be initiated also by another mechanism. For instance, we ignited nitroglycol in a small (about 200 $cm^3$) constant-pressure bomb. The nitroglycol was placed in a beaker of 5 mm diameter and 30 mm height. When we ignited the explosive by a weighed amount of gunpowder that burned up in a time of the order of 50 msec, the whole charge regularly exploded over the surface of the liquid explosive. However, normal deflagration was initiated just by protecting the liquid surface with a layer of gelatinized nitroglycol or fixing a transition layer of nitroglycerin powder. Normal burning was also obtained when the charge was ignited carefully by an electric spiral. If, on the other hand, the spiral was immersed deeply into the liquid, detonation occurred again. In the absence of special experiments, we can only assume the probability of the initiation of explosion by the cavities. Apparently, gelatin prevented the destruction of the surface by the combustion product jets of the igniter. The role of cavities in the process of initiation of explosion and the propagation of low-velocity detonation processes in liquid explosives was considered elsewhere /122, 212, 214, 215, 217/. The mechanism of initiation of detonation via cavities is one of the most frequent approaches to the transition from deflagration of liquid explosives to detonation, apparently due to the weak impulses required for its realization. Unfortunately, we do not yet have experimental data on their realization under different burning conditions.

Turbulent burning of liquid explosives beyond the stability limit leads to the generation of eddies in the gaseous phase, as mentioned above. If the steady-state process of eddy formation is impaired for one reason or another, a rarefaction wave enters the liquid from the gaseous phase. However, the pressure necessary for the onset of turbulence is, as a rule, 10 atm or more. It is therefore difficult to attain considerable compression of cavitational bubbles, so the cavitational mechanism of initiating detonation via pressure pulsations in the combustion products is rather unlikely. At the same time, some detonation in rapidly burning liquids that yield perturbed burning at low pressures (methyl nitrate, mixture of tetranitromethane with some hydrocarbon fuels) may be initiated by the cavitational mechanism.



## 49. TRANSITION FROM DEFLAGRATION OF LIQUID EXPLOSIVES TO DETONATION AT HIGH PRESSURES

The detailed research of Bakhman and Dubovitskii /191/ on the transition from deflagration of some nitro esters at high pressures to detonation is the only work dealing with this problem. The authors used constant-pressure bombs that permitted experiments to be carried out at pressures up to 800 atm. Two drum-type photorecorders (for the low-velocity and detonation processes) ensured recording of the process dynamics. Moreover, Bakhman and Dubovitskii used high-speed (2000–4000 frames per second) photography. Some results of this research will be examined below.

1. It was found that transition from deflagration of methyl nitrate to detonation (ignition in thin-walled glass tubes of diameter 5 mm and height $h_0 = 20$ mm) is only observed in the pressure range $70 \leqslant p \leqslant 350$ atm; between 350 and 800 atm the explosive only burns at a velocity of several meters per second.

2. Burning of nitroglycol at pressures above 50 atm takes place in two stages.* The first stage is characterized by a distinct front and, on the whole, by a relatively constant velocity over the height of the liquid column. In the second stage, which occurred only when $h_0 > 40$–60 mm, either a burning regime differing from the first stage was generated, or a jumpwise onset of detonation was observed.

3. It was observed that transition from almost regular deflagration to detonation occurs during a time $\leqslant 10^{-3}$ sec, which corresponds to the combustion of a layer of nitroglycol that is 1–2 mm thick.

4. Detonation sometimes did not occur at charge heights below some limiting value $h_*$. When $h > h_*$, the probability of its initiation no longer depended on the height, but increased with increasing charge diameter $d$ and ignition pressure $p_0$. We report data of Bakhman and Dubovitskii /191/ on the probability of initiation of detonation (explosion) of nitroglycol at different $d$ and $p$ (the numerator denotes the total number of experiments; the denominator denotes the number of experiments with onset of detonation):

| Pressure, atm | Inner diameter of test tube, mm | | | |
|---|---|---|---|---|
| | 3 | 5 | 6 | 8 |
| 50 | — | 0/6 | 0/7 | 0/4 |
| 100 | 0/4 | 0/5 | 2/9 | 2/2 |
| 200 | 0/4 | 15/17 | 36/20 | 2/2 |

The jumpwise transition from deflagration of nitroglycol to detonation is reported /191/; this paper also contains exposures of the experiments performed at various speeds. The hot-spot structure and traces of the completion of burning behind the detonation front are noteworthy.

5. In some experiments, burning with an eroded front sets in during the second stage of burning (after an almost uniform process) and is

* Similar observations were also made when studying burning of methyl nitrate and nitroglycerin.

characterized by an absence of definite photographic traces of the flame front and large-size luminous hot spots. This type of burning did not always go over into detonation. In narrow tubes ($d < 5$ mm) and at 150–200 atm another type of burning is noted: uniform deflagration goes over into turbulent burning, which may gradually be both accelerated and retarded. Bakhman and Dubovitskii /191/ are of the opinion that an increase in charge height (using a test tube with $h \leq 120$ mm) could lead to increased frequency of transition from deflagration to detonation.

6. When $h_0 \leq 120$ mm, transition from deflagration to detonation was observed only for nitroglycol. First, the low-velocity process sets in; its propagation velocity is of the order of a few hundred meters per second. The velocity in the 20–30 $d$ section is, as a rule, sufficiently constant over the height and damping of the process was never observed.

7. In some experiments with wide ($d > 5$ mm) test tubes, the authors observed branching of the leading, weakly luminescent wave advancing at 700–750 m/sec (as against 400–500 m/sec at the main front). This wave forms a weakly luminous region ahead of the main detonation front. In one experiment, the branch wave was reflected from the bottom of the test tube and produced charge detonation that propagated with the same velocity of 400–500 m/sec toward the main front.

8. Thickening and strengthening of the test tube walls did not affect the limiting height of onset of detonation; neither did it change the velocity of the almost uniform burning, but it considerably increased the velocity of unsteady detonation and also shrinkage of the lead column, which was put beneath the test tube as a tracer of the intensity of the explosive processes.

Let us now interpret the results. Bakhman and Dubovitskii /191/ are of the opinion that, during burning of liquid explosives beyond the stability limit, the conditions required for the onset of detonation may be created in individual small volumes of the liquid explosive situated near the flame front. As proof, they report the results of high-speed photography of burning that demonstrates the existence of a strongly curved (usually conical) flame front. Since the dynamic pressure of the combustion products of the liquid explosives issuing from the curved surface can equilibrate a very large column of the liquid, and also because of the nonuniform ignition pattern, asymmetric displacement of the liquid from the test tube and formation of a curved flame front is a natural result. Bakhman and Dubovitskii then compared initiation of detonation by shock and friction from localized hot spots with the process of unstable burning of liquids. It is assumed that the strong curvature of the flame front may cause isolated volumes of the high-temperature combustion products to be formed ahead of this front. Growth of burning inside these volumes increases the pressure and temperature. Onset of detonation is possible, if they reach sufficiently high values prior to the hot spot destruction.

In addition to the aforementioned ideas, we can supplement them in the light of more up-to-date information. The nature of the detonation processes of liquid explosives observed by Bakhman and Dubovitskii /191/ give reason to believe that the cavitational mechanism plays the leading role. In particular, this is proved by the strong influence of the casing thickness on the process rate.

From our standpoint, the source of acoustic vibrations of the test tube containing the liquid explosive consists of sonic oscillations generated by



the efflux of combustion products from the test tube. Thickening of the test tube walls, placing the test tube within a steel casing, all this promotes the transfer of sonic oscillations from the mouth of the test tube into the liquid. When $h \sim 5$ cm, $p_0 = 200$ atm, $u_1 = 80$ cm/sec and $\rho_1 = 1.5$ g/cm$^3$, the oscillation frequency is $f \sim u_1/h \simeq 700$ Hz. The acoustic vibrations of nitroglycol apparently create small cavitational bubbles, the continuity of the liquid is impaired, and the burning process becomes, in a certain sense, similar to the burning of porous, powdered explosive charges. Comparison of the observations of Bakhman and Dubovitskii /191/ with research work on low-velocity detonation processes /122, 212/ reveals that they have much in common.

The photographs of Bakhman and Dubovitskii /191/ can be interpreted as proof of the uneven, cellular structure of the flame front. The characteristic size of the initial cells is of the order of 0.2–0.5 mm (at 350 atm). Using the data of Tables 19 and 20 and taking into account that the critical pressure for nitroglycol is about 17 atm, we find that

$$\xi_n \simeq \frac{1.16 \cdot 3 \cdot 17}{4 \cdot 350} = 0.4 \text{ mm},$$

which is in agreement with experiment.

The ignition process doubtlessly has much influence on the recorded propagation of unstable burning. Only application of transition charges from normally burning substances permits one to avoid the effect of such a strong perturbation as the ignition process on the detailed growth pattern of burning, since strong perturbations cannot damp out far beyond the critical burning region.

The critical charge height, observed by Bakhman and Dubovitskii /191/ and below which no detonation arose, can be identified with the combustion height of the suspension of the liquid droplets broken off the surface. In such a case, the combustion period of the suspension when $h_0 = 5$ cm is $\tau_{1n} \sim h/u_2 = h\rho_2/(\rho u)_1 \simeq 2 \cdot 10^{-3}$ sec. When the droplet diameter is of the order of 0.8 mm (the wavelength of the most rapidly growing perturbation), the combustion velocity of the droplets is $\Phi \simeq 20$ m/sec. Extrapolation of the normal burning velocity of nitroglycol to 200 atm yields $u_1 = 5.2$ cm/sec. Allowance for droplet heating does not alter this value. One may therefore assume that crushed droplets of size somewhat less than $\xi_n$ enter the gaseous phase, or that the mechanism of their combustion is explosive and not thermally conductive. The fact that the charge diameter affects the specific detonation features also speaks in favor of the hypothesis about the initiation of detonation of explosives via thermal explosion of the droplet suspension in the gas phase. Specific detonation features are characteristic for the "collective effect" of the thermal explosion of a cluster of particles. It is noteworthy that the charge height affects the frequency of initiation of detonation independently of the charge diameter; this does not contradict relationship (108) (see also section 48).

The jumpwise onset of detonation is in agreement with the hypotheses about the development of detonation via thermal explosion of the explosive particles and intermediate combustion products in the gaseous phase, subject to conditions under which the original liquid is prepared by acoustic vibrations of the test tube that are generated by the efflux of the combustion

products. The branch wave advancing ahead of the main front may be identified with propagation of the cavitation front, and the luminescence with heating of the cavitational bubbles. Modern research techniques will doubtless shed new light on this problem.

We mention the following approaches. Leipunskii and Korotkov ignited nitroglycol at pressures of up to 2000 atm and found that, when dissolved air is thoroughly exhausted from the liquid, deflagration proceeds at a few meters per second without transition to explosion or detonation. Since a manometric bomb was used in the experiments of Leipunskii and Korotkov, the sample was ignited at low pressures and hence definitely excluded outside perturbations (and removed air bubbles), increased the tensile strength of the liquid explosive, and consequently the stability of turbulent burning.

The above comments do not exclude the possible growth of detonation from the combustion hot spot formed in the bulk of the liquid under suitable conditions. The only question is how the hot spot is created. The experiments of I. A. Voskoboinikov (Institute of Chemical Physics, USSR Academy of Sciences, 1962), who used a stoichiometric tetranitromethane–nitrobenzene mixture, are a fine illustration of the nontrivial mechanism of the initiation of detonation. The ignition hot spot comprised a droplet of metallic sodium which was dropped into the test tube with the mixture. Photographic recording showed that, initially, low-velocity burning arose near the droplet. Inertial forces ensure for a short time (about 50 μsec) the potential development of an isolated hot spot of burning in the bulk of the liquid under increasing pressure. The high burning velocity of the TNM–nitrobenzene mixture makes possible the development of turbulent burning even at these low pressures (2–5 atm) and short periods, characteristic for the given experiment. Photographic tracing of the process shows that a detonation wave traveling with a speed of the order of 7000 m/sec arises in the mixture. This experiment clearly demonstrates the fundamental possibility of the onset of detonation from the isolated combustion hot spot inside the liquid explosive, though additional research is necessary for a definite solution to the problem.

## 50. BURNING OF TWO-PHASE SYSTEMS

Margolin et al. /218/ conducted experimental and theoretical research on a very simple, two-phase porous charge – slit charge model. The slit charge consisted of two plane-parallel plates separated by a gap into which liquid was poured. One (or both) of the plates was prepared from powder. At normal burning, the liquid prevents penetration of the flame into the gap and the powder plate burns at the face. Under certain conditions the planar surface of the liquid becomes unstable, waves arise on it, droplets and jets are formed and entrained by the stream of combustion products. The fresh, bare sections of the powder plate are again ignited and burning penetrates into the bulk of the slit. This pattern reminds one of turbulent burning of liquid explosives, the difference being that the energy source in this case is the burning of the bare part of the lateral surface of the slit. The theory of turbulent burning of a slit powder charge filled with liquid was constructed /218/ similarly to the theory of turbulent burning of liquid explosives.





The following model of turbulent burning is adopted. Pulsations in the velocity of the combustion products are of the order of magnitude of the mean gas velocity and lead to pulsations in the velocity of the liquid. The plate surface laid bare is instantaneously ignited. To a first approximation, the velocity of turbulent burning equals the velocity of liquid pulsations. When turbulent motion passes from the gas to the liquid, the pulsations of the pressure, and not of the velocity, are retained. Therefore, the boundary condition on the burning surface has the form

$$\rho_g W_g^2 = \rho_l W_l^2 + k_1\sigma/\xi + k_2\rho_l g\xi + k_3\eta W_l\xi/\delta^2, \qquad (109)$$

where $W_l$ is the pulsation velocity in the liquid, $W_g$ is the pulsation velocity of the gas, $\rho_l$ is the density of the liquid, $\rho_g$ is the density of the gas, $\xi$ is the turbulence scale, $\sigma$ is the coefficient of surface tension, $g$ is the gravitational acceleration, $\eta$ is the viscosity of the liquid, $\delta$ is the width of the gap of the slit, and $k_1$, $k_2$ and $k_3$ are coefficients.

The pulsation velocity of the gas motion has scale $\xi$ and is proportional to the velocity of gas motion at this distance from the surface:

$$W_g = k_0 J\xi/\rho_l\delta, \qquad (109a)$$

where $k_0$ is a coefficient, and J is the mass velocity of burning of the powder.

Substitution of (109a) into equation (109) yields

$$(nk_0\xi J/\delta)^2/\rho_g = \rho_l W_l^2 + k_1\sigma/\xi + k_2\rho_l g\xi + k_3\eta W_l\xi/\delta^2; \qquad (110)$$

$n = 1$ or 2 is the number of powder plates.

In reality, we have a whole spectrum of pulsations. The growth of pulsations with different wavelengths $\xi$ takes place at various velocities. The velocity of turbulent burning is determined primarily by the pulsations which develop with maximum velocity. Analysis of (109) shows that the pulsation velocity increases continuously with increasing $\xi$, and therefore pulsations with the largest wavelength, i.e., with $\xi \simeq L$ (the slit width) are the most important for our purpose. If $\xi$ in equation (109) is replaced by $L$, we obtain a quadratic equation in $W_l$ with which to determine $W_g$ as a function of the pressure, slit dimensions and burning velocity of the powder. The critical condition for the onset of turbulent burning follows from (110) when $\xi = L$ and $W_l = 0$.

For a sufficiently large charge diameter $L$, where

$$L \gg \sqrt{\sigma k_1/\rho_l g k_2} \qquad (111)$$

(condition (111) is satisfied when $L > 5$ mm), the equation of transition from laminar to turbulent burning has the form

$$n^2 J^2/\rho_l = (k_1/k_0^2)(\rho_l). \qquad (112)$$

Insertion of $J = Bp^{\nu}$ and $\rho_1 = ap$ into this equation gives the critical transition pressure

$$p_{cr} = (ak_2\rho_1 g\delta^3/B^2k_0^2n^2)^{1/(2\nu-1)}. \qquad (113)$$

Two limiting cases can be distinguished in the solution of equation (110). In the case of a relatively low turbulent burning velocity, the last term in the right-hand part of (110) is much larger than the first term, i.e., viscous forces are larger than inertia forces:

$$W_1 = ALJ^2n^2/\eta\rho_1 - C\rho_1 g\delta^2/\eta \qquad (114)$$

when

$$\frac{k_0}{k_2}\sqrt{\rho_1/\rho_2}\,\delta Jn/\eta < 1. \qquad (115)$$

Here

$$A = k_0^2/k_2; \quad C = k_2/k_3.$$

If viscous forces are neglected in comparison with inertia and gravitational forces for very large turbulent burning velocities, we have

$$W_1 = k_0 JLn/\delta\sqrt{\rho_1\rho_2}$$

when

$$\frac{k_0}{k_2}\sqrt{\frac{\rho_1}{\rho_2}}\frac{\delta Jn}{\eta} > 1; \quad \frac{k_0^2J^2n^2L}{k_2\rho_1\rho_2 g\delta^2} > 1.$$

Experiments were carried out /218/ in a constant-pressure bomb in a nitrogen atmosphere. The charge consisted of two plane-parallel plates separated by a gap into which liquid was poured. One of the plates consisted of gunpowder, and the other of plexiglass, through which motion pictures were taken or the process recorded photographically. The width of the plates was from 10 to 37 mm, the height 60 mm, the thickness 2 mm, and the gap between the plates 0.1–0.8 mm. It was found that such a charge may either burn in the normal regime, when the presence of the slit filled with the liquid does not affect the burning velocity of the charge, or in the turbulent regime, when the propagation velocity of the flame is many times larger than the normal velocity. The motion pictures and photographic recording showed that under identical conditions the turbulent velocity is the same from experiment to experiment and is independent of the charge length.

The dependence of the burning velocity of nitroglycerin powder ($u_1 = 0.47\,p^{0.75}$ cm/sec at 1 kg/cm$^2$ $< p <$ 150 kg/cm$^2$) on the pressure in the bomb was also studied /218/. The gap between the plates was filled with water. Estimates show that condition (115) was always satisfied in these experiments. Therefore, the theoretical burning velocity, calculated from (114) when $n = 1$, must be compared with experiment.



Coefficients $A$ and $C$ entering (113) were determined as follows. In accordance with (114), all the experimental data were plotted (Figure 122) in dimensionless coordinates $W_1\eta/\rho_1 g\delta^2$ and $LJ^2/\rho_1\rho_2 g\delta^2$; they fitted a straight line. Coefficient $A$ (equal to $3 \cdot 10^{-4}$) is given by the slope of this line. Coefficient $C$ (equal to $3 \cdot 10^{-2}$) is determined by the intercept of the straight line on the ordinate axis.

An increase in the gap (Figure 123) and also an increase in the liquid viscosity brings about a decrease in the velocity of turbulent burning, while an increase in slit width increases the velocity.

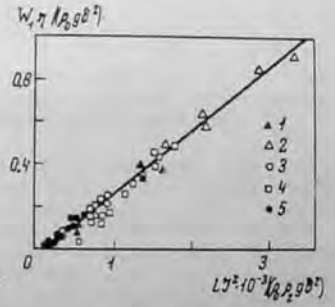


FIGURE 122. Generalized curve for the velocity of turbulent burning of slit charges: 1) $\delta$ = 37 mm, $L$ = 0.37 mm; 2) $\delta$ = 20 mm, $L$ = 0.2 mm; 3) $\delta$ = 20 mm, $L$ = 0.37 mm; 4) $\delta$ = 10 mm, $L$ = 0.2 mm; 5) $\delta$ = 10 mm, $L$ = 0.37 mm.

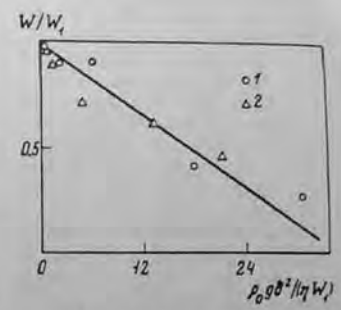


FIGURE 123. Turbulent burning velocity as a function of the gap in the slit: 1) $L$ = 10 mm; $p$ = 100 atm; 2) $L$ = 20 mm, $p$ = 60 atm.

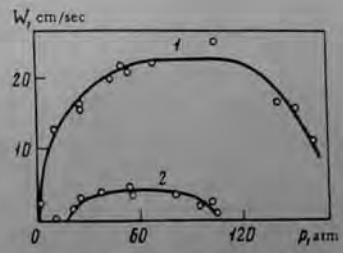


FIGURE 124. Experimental pressure dependences of the turbulent burning velocity for powders with variable $\nu$ larger and smaller than 0.5.

Analysis of equations (110) and (114) shows that, when slit-type powder charges burn with $\nu > 0.5$, turbulent burning sets in when the pressure exceeds some critical value. Further pressure increase leads to an increase in the turbulent burning velocity. If, on the other hand, $\nu < 0.5$, the theory forecasts that the onset of the turbulent regime should take place when the pressure is decreased to some subcritical value and that the turbulent burning velocity should increase with decreasing pressure. This theoretical conclusion was confirmed experimentally. Figure 124 shows pressure dependences of the burning velocity of slit charges. Curve 1 relates to a powder whose burning velocity is determined by the expression $u_1 = 0.56\ p^{0.28}$ cm/sec at 10 atm $< p <$ 140 atm, while curve 2 relates to a powder with $u_1 = 0.32\ p^{0.17}$ cm/sec at 15 atm $< p <$ 140 atm. Over the pressure range from 1 to 10–15 atm, $\nu$ varies from unity to 0.28 for the first powder, and from 0.8 to 0.17 for the second.

The experimental relationships shown in Figure 124 are in qualitative agreement with theory. At low pressures, the turbulent burning velocity increases with pressure since $\nu > 0.5$; turbulent burning is damped with pressure at high pressures ($\nu < 0.5$).

The measured turbulent velocities were lower than the calculated values. This is explained by the fact that here the slit was filled with kerosene, which, unlike water, wets the powder. Therefore, a liquid film whose thickness depends on the velocity of movement of the liquid and its parameters forms on the surface of the powder /220/, and also leads to a decrease in the velocity of turbulent burning /218/. Confirmatory experiments showed that a severalfold decrease in the turbulent burning velocity was observed whenever a wettable liquid was used instead of a nonwettable liquid to fill the slit.

### Experimental research on burning of two-phase systems

When a porous charge is filled with a liquid, a mobile two-phase system is formed and its burning is accompanied by some interesting properties. A stable or a perturbed turbulent burning regime is generated, depending on the ability of the system components to burn and on their physicochemical properties.

Mixtures of gunpowder with nitroglycerin (contents from 10 to 60%) were combusted normally at atmospheric pressure /37/; the burning velocity was lower than the calculated additive value. Higher nitroglycerin concentrations did not ensure mobility of the system and its combustion did not differ from the burning pattern of ordinary heterogeneous systems.

The experiments of Kondrikov /87, 221/ are of greater interest. He studied the behavior of some initiating explosives in mixtures with gelatinized nitro esters and found that burning is unstable at atmospheric or moderately elevated pressures: burning is quenched or detonation sets in when the mixture is ignited. A pressure increase stabilizes burning. For instance, a mixture of weakly gelatinized nitroglycol with 10 wt % lead azide in charges of 5 mm diameter begins to burn stably at pressures above $p_\alpha = 6$ atm at a velocity that is practically equal to the burning velocity of



gelatin. An increased lead azide content up to 75 wt % brings about an increase in $p_\alpha$ according to Kondrikov /221/. $p_\alpha = 4.10 \exp(1.32\ m)$ kg/cm$^2$, where $m$ is the content of lead azide in the mixture (g/cm$^3$). The burning velocity of the mixture is approximately proportional to the pressure, while coefficient $B$ in the equation $u_1 = Bp^\nu$ depends on $m$ in a similar manner to $p_\alpha$ (Figure 125).

Mixtures of lead azide with other liquid nitro esters and also mixtures of nitro esters with lead trinitroresorcinolate (Figure 126) and potassium picrate (Figure 127) exhibit, on the whole, the same pattern of pressure dependence on stable burning; however, the most typical effect here is for burning to be quenched. The onset of detonation was found to be promoted by direct ignition of the mixture by a heated spiral, and by the presence of clusters of the initiating substance in the mixture.

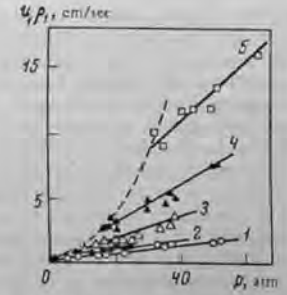


FIGURE 125. Pressure dependence of the burning velocity of a mixture of lead azide with gelatinized nitroglycol.

Lead azide content: 1) 0; 2) 10; 3) 30; 4) 50; 5) 60%. The mixture detonates or burning is quenched above the broken line /221/.

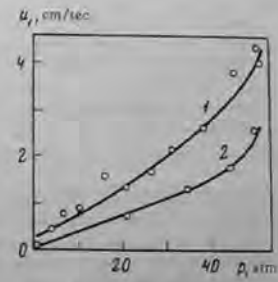


FIGURE 126. Pressure dependence of the burning velocity of a mixture of lead trinitroresorcinolate with gelatinized nitroglycol:

1) 50; 2) 30%.

Kondrikov /221/ explains the peculiar behavior of the mixture with the aid of a hypothesis about the onset of detonation of a mixture containing a sufficiently large number of explosive particles dispersed from the charge surface. It is assumed that the decisive factor for the onset of detonation is not the pressure, but the "thickness of the heated and reacted layer as long as it exists."

Another attempt at explaining the peculiar region of unstable burning of heterogeneous mixtures containing rapidly burning particles is interesting. Suppose, in accordance with published data /87, 221/, it is assumed that deflagration of pure lead azide readily goes over into detonation (apparently due to the intensive dispersion and explosion of the particle suspension). When the ozide level in the mixture with the nitro ester is low, each particle represents a heat sink in relation to the nitro ester surrounding it.

The "pores" between the particles filled with liquid may burn, if the thermal equilibrium is balanced in the heated layer. In other words, the "pore diameter" should correspond to the burning velocity of the liquid at the given pressure in approximately the same way as the critical diameter of burning $d_{cr.b}$. The "pore diameter" at low burning velocities may be small (this was also found in the experiments of Kondrikov) and insufficient for steady-state burning of the liquid base. Mixing of the heated layer by microignitions of accelerated particles also may prevent burning /221/. The effect of the charge diameter, whose decrease always led to quenching of burning, speaks for the thermal nature of the phenomenon. Burning is quenched after combustion (or ignition) of the heated layer, due to the action of these above factors during ignition from a weak source. On the other hand, intensive ignition brings about vaporization of the liquid explosives, the unprotected initiating substance becomes bare, and detonation sets in by the mechanism for the pure lead azide. At high pressure, when the burning velocity is sufficiently large, separate burning of the liquid "skeleton" of the mixture sets in and the azide particles are entrained into the gaseous phase, where they burn one by one. An increase in the content of the solid phase (the particle size remains constant) decreases the diameter $d_p$ of the pores filled with the liquid, since $d_p \sim (1-\Delta)/\Delta$, where $\Delta$ is the volume content of the solid phase. If $d_p > d_{cr}$ for solid burning and, after Kondrikov /221/, $d_{cr.b} \sim p^{-\psi}$, where $\psi = 0.6-1.48$ (the average value of $\psi$ is unity), then

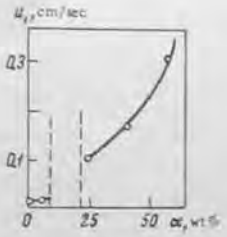


FIGURE 127. Dependence of the burning velocity at 1 atm of a mixture of potassium picrate with gelatinized diglycol dinitrate on the composition.

α denotes the content of potassium picrate.

$$p_{cr}\,\Delta/(1-\Delta) \simeq \text{const}, \quad p_{cr}\,d_p \simeq \text{const}. \qquad (116)$$

Processing of Kondrikov's data /221/ using (116) shows that this expression describes the experimental data fairly well.

If the advanced hypothesis is correct, an increase in, for example, the initial temperature should narrow the pressure range of unstable burning because of the increase in the burning velocity of the liquid explosive and the decrease in its value of $d_{cr.b}$. Changes in the particle size $D$ of the solid phase while its content remains constant should affect $d_p$, due to the variation in the effective diameter of liquid layers; it is expected that the relation $p_{cr}\,D = \text{const}$ will be fulfilled when $\Delta = \text{const}$.

Kondrikov's tests /221/ on the burning of a 50 : 50 wt % nitroglycerin – lead azide mixture are a good illustration of the effect of the vessel diameter. It is known /38, 189/ that nitroglycerin does not burn in some pressure ranges. Andreev attributed this phenomenon to intensive eddy formation in the heated layer in accordance with the Landau–Levich mechanism. Lead azide in pure form does not burn at all, but detonates. Condensation of nitroglycerin by lead azide leads to its stable burning. Moreover, in the developed regime of perturbed burning this additive



halves the burning velocity of nitroglycerin. Introduction of the concept of an effective diameter of the liquid layers in the mixture with the solid filler allows these facts to be explained by the dependence of the limiting conditions on the diameter (thickness) of these layers.

Margolin et al. /219/ studied the burning regimes of two-phase systems comprising a solid and a liquid explosive charge. A glass tube was filled with grains of nitroglycerin powder ($u_1 = 0.47 \cdot p^{0.78}$ cm/sec when 1 kg/cm$^2$ < $p$ < 150 kg/cm$^2$) or of ammonium perchlorate. The gaps between the grains were filled with liquid (water, alcohol, benzine, glycerin). The charges were ignited in a bomb in a nitrogen atmosphere at pressures of 1 to 120 kg/cm$^2$.

Figure 128 illustrates the pressure dependence of the burning velocity of a charge consisting of cylindrical grains (the grain diameter is equal to its height) of nitroglycerin powder placed in a tube of 6.5 mm inner diameter. The charges were filled with water or alcohol; the liquid occupied 30–40 vol % of the charge. At pressures above $p_{cr}$, burning took place in the turbulent regime at velocities considerably exceeding the burning velocity of the powder alone. At pressures below $p_{cr}$, burning was not sustained because the water (or alcohol) drenched the grains and prevented flame propagation from grain to grain. The burning velocity of water-filled charges is more than that of alcohol-filled charges, because alcohol wets the pores to a much greater extent than water. As the tube diameter increases, the burning velocity at the beginning increases and then remains constant.

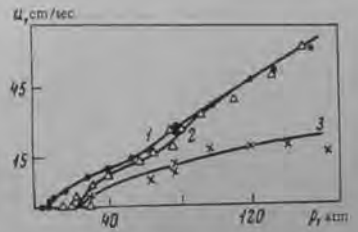


FIGURE 128. Pressure dependence of the burning velocity of two-phase charges comprising nitroglycerin powder and water.

1) grains of 1 mm diameter with water; 2) grains of 3 mm diameter with water; 3) grains of 1 mm diameter with alcohol.

Solutions of various glycerin concentrations in water were used to study the effect of the viscosity of the liquid filling the gaps. When the filler liquid is more viscous, the velocity of turbulent burning remains constant at the beginning. Then, it drops abruptly (Figure 129) until it is quenched or attains a normal burning velocity of the powder grains, when the filler is immobile.

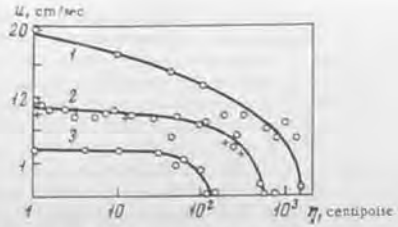


FIGURE 129. Dependence of the burning velocity of two-phase charges of nitroglycerin powder (grain diameter 1 mm) on the viscosity of the filler liquid:

1) 80; 2) 50; 3) 25 atm.
Crosses refer to experimental data for grains of 3 mm diameter at 50 atm.

Turbulent burning was also observed in a mixture of ammonium perchlorate grains with benzene (20 wt %) (Figure 130). The turbulent burning velocity decreases with decreasing size of the perchlorate grains. It is known that the velocity of layer-by-layer deflagration of ammonium perchlorate with solid fuels increases when the size of the oxidizer particles decrease /44/. Figure 130 also shows the pressure dependence of a mixture of ammonium perchlorate with benzene, condensed by rubber (rubber cement). It can be seen that turbulent burning of a mixture of the oxidizer with the mobile liquid fuel propagates much more rapidly than normal burning of the mixture with the viscous fuel. The burning velocity of the mixture with rubber cement is approximately equal to the burning velocity of the ammonium perchlorate mixed with a solid organic fuel /44/.


FIGURE 130. Pressure dependence of the burning velocity of two-phase charges of ammonium perchlorate with benzene (1—3) and rubber cement (4—5) for different ammonium perchlorate grains:

1 and 5) 1—3.6 mm; 2) 0.25—0.63 mm; 3 and 4) 0.1—0.25 mm.



These experiments show that turbulent burning may arise in two-phase systems consisting of powder explosives or propellant powders filled with liquid, and also in charges consisting of solid oxidizer and liquid fuel.

The onset of turbulent burning can be explained as follows. Under certain conditions normal burning becomes unstable, gaseous combustion products penetrate into the pores of the charge and displace the liquid and ignite the pore walls. The displaced liquid in other places is ejected into the stream of combustion products, the flame zone moves ahead due to the convective motion in the pores and not as a result of heating of fresh portions of the liquid by the conductive heat-transfer mechanism. Photographs show that the leading front of turbulent burning leaves behind a zone consisting of deflagrating explosive grains and pores; the liquid in this zone has already been removed from the pores. A liquid film should remain on the grains; the film thickness depends on the velocity of movement and the liquid parameters /220/.

The presence of a mechanical binder between the particles affects the turbulent burning process. A charge consisting of powder grains cemented together with acetone and filled with water burns more rapidly than a similar free-flowing charge. This effect of cemented grains is also found when a porous (gas-filled) powdered charge burns. Dispersion of non-cemented charges evidently reduces the intensity of the action of the combustion products upon the fresh mixture. Burning propagates over the interface of components in a system that cannot burn independently.

Photographic recording of the development of the process in different systems also shows that the liquid in the turbulent burning regime near the critical pressure is ejected from the slit charge as a fountain from the middle of the slit or near its edge. During the growth of turbulent burning (the velocity is 10—30 times as high as the normal burning velocity) the liquid is ejected in the form of thin jets and droplets. It is easy to see here some similarity with the turbulent burning of individual liquid explosives or of their mixtures (see section 44).

The presence of a dry section of the slit over the liquid surface promotes the growth of turbulent burning, but the velocity remains unchanged. An increase in slit length to a certain value facilitates the onset of turbulent burning, due to the increase in the velocity of the combustion products in the gap.

The data of Whittaker et al. /198/ about the role of the volatility of the components are very interesting. They studied this problem with a mixture of nitric acid and solid fuel, and noted that the evaporation rate of all the components must be equal to the burning velocity in the case of steady-state normal burning. It was found that a mixture of nitric acid with m-dinitrobenzene cannot burn normally, but at high pressures it is combusted in the turbulent regime. For comparison, Whittake et al. investigated a mixture of nitric acid and sebaconitrile, which has a vapor pressure of 1 μ Hg at 45°C; it therefore has the same vapor pressure as m-dinitrobenzene. This mixture was also unable to burn in the normal regime, but after a pressure of 154 atm is reached it is ignited and combusted in the turbulent regime. Thus mixtures with very low vapor pressures have only a turbulent burning region, when the particles and droplets of the mixture enter the high-temperature flame and are vaporized there, and retain the original

ratio of the components in the flame. The surface temperature of the charge reached in the normal burning regime is too small to ensure transport of the sparingly volatile component into the gas phase. Though the experiments of Whittaker et al. /198/ were conducted on mixtures with a solid fuel, their conclusions remain valid also for liquid components. For instance, tetranitromethane mixtures with a fuel enriched by the oxidizer does not burn, but they are completely combusted in the turbulent regime if burning takes place at higher pressures.



*BIBLIOGRAPHY*


1. Belyaev, A. F. – Dokl. Akad. Nauk SSSR, Vol. 18: 267. 1938.
2. Belyaev, A. F. – Dokl. Akad. Nauk SSSR, Vol. 24: 253. 1939.
3. Belyaev, A. F. Sbornik statei po teorii VV (Collection of Papers on the Theory of Explosives), p. 7. – Moskva, Oborongiz. 1940.
4. Belyaev, A. F. – Dokl. Akad. Nauk SSSR, Vol. 28: 715. 1940.
5. Belyaev, A. F. Doctoral Thesis. – Inst. Khim. Fiz. AN SSSR, Moskva. 1946.
6. Andreev, K. K. – Dokl. Akad. Nauk SSSR, Vol. 29: 469. 1940.
7. Andreev, K. K. Sbornik statei po teorii VV (Collection of Papers on the Theory of Explosives), p. 39. – Moskva, Oborongiz. 1940.
8. Andreev, K. K. – Dokl. Akad. Nauk SSSR, Vol. 51: 29. 1946.
9. Pâtry, M. Combustion et détonation des substances explosives. – Paris, Herman et Cie. [Russian translation, 1938.]
10. Belyaev, A. F., A. I. Korotkov, and A. A. Sulimov. – Fizika Goreniya i Vzryva, No. 3: 47. 1966.
11. Bobolev, V. K., S. V. Chuiko, and L. F. Chekirda. – Prikl. Mekh. i Tekhn. Fiz., No. 4: 99. 1963.
12. Belyaev, A. F., A. I. Korotkov, A. V. Obmenin, A. A. Sulimov, and M. K. Sukoyan. – Fizika Goreniya i Vzryva, No. 1: 8. 1969.
13. Gipson, R. W. and A. Maček. – Eighth Intern. Sympos. on Combustion, p. 847. The Williams and Wilkins Company. 1962.
14. Korotkov, A. I., A. A. Sulimov, V. F. Obmenin, V. F. Dubovitskii, and A. I. Kurkin. – Fizika Goreniya i Vzryva, No. 3: 315. 1969.
15. Bowden, F. P. and A. D. Yoffe. Initiation and Growth of Explosion in Solids. – Cambridge University Press. 1952.
16. Bobolev, V. K. and A. V. Dubovik. – Prikl. Mekh. i Tekhn. Fiz., No. 2: 150. 1965.
17. Dubovik, A. S. Fotograficheskaya registratsiya bystroprotekayushchikh protsessov (Photographic Recording of High Speed Processes). – Moskva, "Nauka." 1964.
18. Pokhil, P. F., V. M. Mal'tsev, and V. M. Zaitsev. Metody issledovaniya protsessov goreniya i detonatsii (Methods for the Study of Deflagration and Detonation Processes). – Moskva, "Nauka." 1969.
19. Salamandra, G. D., T. V. Bazhenova, S. G. Zaitseva, R. I. Soloukhin, I. M. Naboko, and I. K. Sevast'yanova. Nekotorye metody issledovaniya bystroprotekayushchikh protsessov (Methods for the Study of High Speed Processes). – Moskva, Izdatel'stvo AN SSSR. 1960.
20. Gal'perin, L. N. and K. K. Shvedov. – Zhurn. Fiz. Khim., Vol. 37: 1182. 1963.

21. Amster, A. B., P. A. Kendall, L. I. Vallette, and B. B. Harrell. – Rev. Scient. Instrum., Vol. 31: 188. 1960.
22. Gibson, F. G., M. I. Bowser, and G. A. Mason. – Rev. Scient. Instrum., Vol. 30: 916. 1959.
23. Belyaev, A. F., A. I. Korotkov, A. K. Parfenov, and A. A. Sulimov. – Zhurn. Fiz. Khim., Vol. 37: 150. 1963.
24. Bridgman, P. W. Advanced Studies in the Field of High Pressure. [Russian translation, 1948.]
25. Sokolik, A. I. and A. I. Stanilovskii. Dvukhkanal'nyi p'ezoelektricheskii izmeritel' davlenii PID-9 (PID-9 Two-channel Piezoelectric Pressure Detector). – Moskva, Izdatel'stvo Filiala Vses. Inst. Nauch. Tekhn. Informatsii Gos. Komiteta Soveta Ministrov SSSR po Nauke i Tekhnike i Akad. Nauk SSSR. 1957.
26. Zaitsev, V. M., P. F. Pokhil, and K. K. Shvedov. – Dokl. Akad. Nauk SSSR, Vol. 132: 1339. 1960.
27. Dremin, A. N. and S. A. Koldynov. – In: "Vzryvnoe delo," No. 63/20: 37. Moskva, "Nedra," 1967.
28. Scheidegger, A. E. Physics of Flow through Porous Media, rev. ed. – Univ. Toronto Press, 1960.
29. Leibenzon, L. S. Dvizhenie prirodnykh zhidkostei i gazov v poristoi srede (Movement of Natural Liquids and Gases in a Porous Medium). – Moskva, Gostoptekhizdat. 1947.
30. Zabrodskii, S. S. Gidrodinamika i teploobmen v psevdoozhizhennom sloe (Hydrodynamics and Heat Exchange in a Fluidized Bed). – Moskva, Gosenergoizdat. 1963.
31. Afanas'ev, G. T. and V. K. Bobolev. Initsiirovanie tverdykh VV udarom (Shock Initiation of Solid Explosives). – Moskva, "Nauka," 1968.
32. Andreev, K. K. and S. V. Chuiko. – Zhurn. Fiz. Khim., Vol. 37: 6. 1963.
33. Aleksandrov, E. N., V. A. Veretennikov, A. N. Dremin, and K. K. Shvedov. – Fizika Goreniya i Vzryva, No. 3: 400. 1968.
34. Orr, Clyde Jr. and J. M. Dalla Valle. Fine Particle Measurements. Size, Surface and Pore Volume. – New York, Macmillan. 1959.
35. Andreev, K. K. – Zhurn. Fiz. Khim., Vol. 20: 467. 1946.
36. Andreev, K. K. – Dokl. Akad. Nauk SSSR, Vol. 1: 220. 1935.
37. Andreev, K. K. Termicheskoe razlozhenie i gorenie VV (Thermal Decomposition and Combustion of Explosives). – Moskva–Leningrad, Gosenergoizdat. 1957.
38. Andreev, K. K. Termicheskoe razlozhenie i gorenie VV (Thermal Decomposition and Combustion of Explosives). – Moskva, "Nauka." 1966.
39. Sulimov, A. A. and A. I. Korotkov. – Materialy 11-i Vsesoyuznoi konferentsii po voprosam goreniya dispersnykh sistem, p. 40. Odessa, Izdatel'stvo Odesskogo Gosudarstvennogo Universiteta. 1972.
40. Annikov, V. E. and B. N. Kondrikov. – Fizika Goreniya v Vzryva, No. 3: 350. 1968.
41. Zel'dovich, Ya. B. and N. N. Semenov. – Zhurn. Eksp. Teoret. Fiz., Vol. 10: 1116: 1940.



42. Frank-Kamenetskii, D. A. Diffuziya i teploperedacha v khimicheskoi kinetike (Diffusion and Heat Transfer in Chemical Kinetics). – Moskva, Izdatel'stvo AN SSSR. 1947.
43. Zel'dovich, Ya. B. – Zhurn. Eksp. Teoret. Fiz., Vol. 12: 498. 1942.
44. Bakhman, N. N. and A. F. Belyaev. Gorenie geterogennykh kondensirovannykh sistem (Combustion of Heterogeneous Condensed Systems). – Moskva, "Nauka," 1967.
45. Belyaev, A. F. and N. N. Bakhman. – Fizika Goreniya i Vzryva, No. 1: 22. 1966.
46. Novikov, S. S., P. F. Pokhil, and Yu. S. Ryazantsev. – Fizika Goreniya i Vzryva, No. 4: 469. 1966.
47. Novozhilov, B. V. – Fizika Goreniya i Vzryva, No. 4: 482. 1966.
48. Pokhil, P. F., L. D. Romodanova, and O. P. Rysakova-Romashkan. – Zhurn. Fiz. Khim., Vol. 36: 1331. 1962.
49. Belyaev, A. F. and A. E. Belyaeva. – Zhurn. Fiz. Khim., Vol. 20: 1381. 1946.
50. Pokhil, P. F. – In: "Fizika vzryva," No. 2: 181. Moskva, Izdatel'stvo AN SSSR. 1953.
51. Maksimov, E. I., A. G. Merzhanov, and V. M. Shkiro. – Fizika Goreniya i Vzryva, No. 1: 24. 1965.
52. Maksimov, E. I. and A. G. Merzhanov. – Fizika Goreniya i Vzryva, No. 1: 47. 1966.
53. Belyaev, A. F. and L. D. Komkova. – Zhurn. Fiz. Khim., Vol. 24: 1302. 1950.
54. Beckstead, M. W. and J. D. Hightower. – AIAA, Vol. 5: 1785. 1967.
55. Pokhil, P. F. – Fizika Goreniya i Vzryva, No. 3: 439. 1969.
56. Kondrikov, B. N. – In: "Teoriya VV," p. 198. Moskva, "Vysshaya shkola," 1967.
57. Bakhman, N. N. – Prikl. Mekh. i Tekhn. Fiz., No. 1: 106. 1965.
58. Maksimov, E. I. – Fizika Goreniya i Vzryva, No. 2: 203. 1968.
59. Belyaev, A. F. Gorenie, detonatsiya i rabota vzryva kondensirovannykh sistem (Deflagration, Detonation and Explosion of Condensed Systems). – Moskva, "Nauka," 1968.
60. Belyaev, A. F., A. I. Korotkov, and A. A. Sulimov. – Prikl. Mekh. i Tekhn. Fiz., No. 5: 117. 1963.
61. Bobolev, V. K., A. D. Margolin, and S. V. Chuiko. – Dokl. Akad. Nauk SSSR, Vol. 162: 388. 1965.
62. Bobolev, V. K., A. D. Margolin, and S. V. Chuiko. – Fizika Goreniya i Vzryva, No. 4: 24. 1966.
63. Bobolev, V. K., I. A. Karpukhin, and S. V. Chuiko. – Nauchno-Tekhnicheskie Problemy Goreniya i Vzryva, No. 1: 44. 1965.
64. Andreev, K. K. and V. V. Gorbunov. – Zhurn. Fiz. Khim., Vol. 37: 9. 1963.
65. Andreev, K. K. and V. V. Gorbunov. – In: "Teoriya VV," p. 138. Moskva, "Vysshaya shkola," 1967.
66. Andreev, K. K. and V. V. Gorbunov. – Ibid., p. 149.
67. Andreev, K. K. and V. M. Rogozhnikov. – Ibid., p. 163.
68. Andreev, K. K. and V. M. Rogozhnikov. – Ibid., p. 176.
69. Andreev, K. K. and V. M. Rogozhnikov. – Ibid., p. 190.
70. Margolin, A. D. and S. V. Chuiko. – Fizika Goreniya i Vzryva, No. 3: 27. 1965.

71. Belyaev, A. F. – Zhurn. Prikl. Khim., Vol. 23: 432. 1950.
72. Andreev, K. K. – Izv. AN SSSR, Otdel. Tekhn. Nauk, Energetika i Avtomatika, Vol. 4: 188. 1959.
73. Landau, L. D. – Zhurn. Eksp. Teoret. Fiz., Vol. 14: 240. 1944.
74. Levich, V. G. – Dokl. Akad. Nauk SSSR, Vol. 109: 975. 1956.
75. Shchelkin, K. I. Bystroe gorenie i spinovaya detonatsiya gazov (Rapid Combustion and Spin Detonation of Gases). – Moskva, Izdatel'stvo Ministerstva Vooruzhennykh Sil SSSR. 1949.
76. Zel'dovich, Ya. B. – Zhurn. Tekhn. Fiz., Vol. 17: 1. 1947.
77. Barenblatt, G. I. – Izv. AN SSSR, Otdel. Tekhn. Nauk, Vol. 6: 97. 1954.
78. Belyaev, A. F. – Dokl. Akad. Nauk SSSR, Vol. 29: 406. 1940.
79. Edwards, G. – Trans. Faraday Soc., Vol. 49: 152. 1953.
80. Glazkova, A. P. and I. A. Tereshkin. – Zhurn. Fiz. Khim., Vol. 35: 1622. 1961.
81. Summerfield, M., G. S. Sutherland, M. J. Webb, H. J. Taback, and K. P. Hall. Burning Mechanism of Ammonium Perchlorate Propellants. – In: ARS Progress in Astronautics and Rocketry: Solid Propellant Rocket Research, edited by M. Summerfield, Vol. 1, pp. 141–182. New York – London, Academic Press. 1960.
82. Taylor, T. W. – Combust. Flame, Vol. 6: 103. 1962.
83. Pokhil, P. F., V. M. Mal'tsev, and G. V. Lukashenya. – Dokl. Akad. Nauk SSSR, Vol. 135: 913. 1960.
84. Sulimov, A. A. and A. I. Korotkov. – Zhurn. Fiz. Khim., Vol. 38: 331. 1963.
85. Andreev, K. K. and P. P. Popova. – Zhurn. Fiz. Khim., Vol. 35: 9. 1961.
86. Shchelkin, K. I. and Ya. K. Troshin. Gazodinamika goreniya (Gas Dynamics of Combustion). – Moskva, Izdatel'stvo AN SSSR. 1963.
87. Andreev, K. K. and B. N. Kondrikov. – Dokl. Akad. Nauk SSSR, Vol. 137: 130. 1961.
88. Bowden, F., B. Evans, and A. Yoffe. – 6th Intern. Sympos. on Combustion, p. 609. New York – London, Reinhold Publishing Corporation. 1957.
89. Margolin, A. D. – Dokl. Akad. Nauk SSSR, Vol. 140: 4. 1961.
90. Margolin, A. D. and S. V. Chuiko. – Fizika Goreniya i Vzryva, No. 3: 119. 1966.
91. Kondrikov, B. N. and Ma Chinyun'. – In: "Teoriya VV," p. 207. Moskva, "Vysshaya shkola," 1967.
92. Leipunskii, O. I. Doctoral Thesis. – Inst. Khim. Fiz. AN SSSR. Moskva. 1945.
93. Belyaev, A. F. and A. I. Korotkov. – In: "Fizika vzryva," No. 1: 177. Moskva, Izdatel'stvo AN SSSR. 1952.
94. Sorkin, R. E. Gazotermodinamika raketnykh dvigatelei na tverdom toplive (Gas Dynamics of Solid-Propellant Rocket Engines). – Moskva, "Nauka," 1967.
95. Irwin, O. R., P. K. Salzman, and W. H. Andersen. – 9th Intern. Sympos. on Combustion, p. 358. New York – London, Academic Press. 1963.
96. Whittaker, A. G. and D. C. Barham. – ARSJ, Vol. 8: 1273. 1962.



97. Andreev, K. K. and V. V. Gorbunov. – In: "Teoriya VV," p. 558. Moskva, Oborongiz. 1963.
98. Zel'dovich, Ya. B. – Dokl. Akad. Nauk SSSR, Vol. 150: 2. 1963.
99. Hicks, B. L. – J. Chem. Phys., Vol. 22: 414. 1954.
100. Averson, A. E., V. V. Barzykin, and A. G. Merzhanov. – Dokl. Akad. Nauk SSSR, Vol. 178: 131. 1968.
101. Rozenband, V. I., V. V. Barzykin, and A. G. Merzhanov. – Fizika Goreniya i Vzryva, No. 2: 171. 1968.
102. Librovich, V. B. – Prikl. Mekh. i Tekhn. Fiz., No. 6: 74. 1963.
103. Merzhanov, A. G. and F. I. Dubovitskii. – Uspekhi Khimii, Vol. 35: 4. 1966.
104. McAlevy, R. F., P. L. Cowan, and M. Summerfield. See /81, p. 623/.
105. Baer, A. D., N. W. Ryan, and D. L. Salt. See /81, p. 653/.
106. Raizberg, Yu. A. – Fizika Goreniya i Vzryva, No. 4: 568. 1968.
107. Zel'dovich, Ya. B. – Prikl. Mekh. i Tekhn. Fiz., No. 1: 10. 1963.
108. Belyaev, A. F. – In: "Voprosy teorii VV," p. 29. Moskva–Leningrad, Izdatel'stvo AN SSSR. 1947.
109. Bakhman, N. N. – Zhurn. Fiz. Khim., Vol. 35: 4. 1961.
110. Belyaev, A. F., A. I. Korotkov, A. A. Sulimov, and M. K. Sukoyan. – Fizika Goreniya i Vzryva, No. 2: 166. 1970.
111. Serebryakov, M. E. Vnutrennyaya ballistika stvol'nykh sistem i porokhovykh raket (Interior Ballistics of Barrel Systems and Powder Rockets). – Moskva, Oborongiz. 1962.
112. Andreev, K. K. and V. M. Rogozhnikov. – In: "Teoriya VV," p. 288. Moskva, "Vysshaya shkola." 1967.
113. Kutateladze, S. S. Osnovy teorii teploobmena (Fundamentals of Heat Transfer Theory). – Moskva, Mashgiz. 1962.
114. Kirsanova, Z. V. and O. I. Leipunskii. – Fizika Goreniya i Vzryva, Vol. 1: 72. 1970; Tezisy dokladov i Vsesoyuznogo simpoziuma po goreniyu i vzryvu. Moskva, "Nauka." 1968.
115. Barenblatt, G. I. – Prikl. Mekh. i Tekhn. Fiz., No. 4: 102. 1961.
116. Mushkelishvili, N. I. Nekotorye osnovnye zadachi matematicheskoi teorii uprugosti (Some Basic Problems of the Mathematical Theory of Elasticity). – Moskva, "Nauka." 1966.
117. Kirsanova, Z. V. Tezisy dokladov II Vsesoyuznogo simpoziuma po goreniyu i vzryvu (Synopses of Reports of the Second All-Union Symposium on Deflagration and Detonation). – Erevan, "Nauka." 1969.
118. Campbell, A. W., W. C. Davis, and J. R. Travis. – Physics of Fluids, Vol. 7: 498. 1961.
119. Kuznetsov, N. M. – Prikl. Mekh. i Tekhn. Fiz., No. 1: 45. 1968.
120. Obmenin, A. V., A. I. Korotkov, A. A. Sulimov, and V. F. Dubovitskii. – Fizika Goreniya i Vzryva, No. 4: 461. 1969.
121. Maček, A. – J. Chem. Phys., Vol. 31: 162. 1959.
122. Dubovik, A. V. Candidate Thesis. – Inst. Khim. Fiz. AN SSSR. Moskva. 1965.
123. Merzhanov, A. G., V. V. Barzykin, and V. T. Gontkovskaya. – Dokl. Akad. Nauk SSSR, Vol. 148: 380. 1963.
124. Bills, K. W. and J. H. Wiegand. – AIAA, Vol. 1: 130. 1963.
125. Price, D. and L. F. Wehner. – Combust. Flame, Vol. 8: 73. 1963.

126. Afanas'ev, G. T., V. K. Bobolev, A. V. Dubovik, and V. S. Zhuchenko. – In: "Vzryvnoe delo," No. 63/20: 86. Moskva, "Nedra." 1967.
127. Bobolev, V. K., A. V. Dubovik, I. A. Karpukhin, and V. V. Rybakov. – Fizika Goreniya i Vzryva, No. 3: 331. 1969.
128. Obmenin, A. V., A. I. Korotkov, and A. A. Sulimov. Tezisy dokladov II Vsesoyuznogo simpoziuma po goreniyu i vzryvu (Synopses of Reports of the Second All-Union Symposium on Deflagration and Detonation). – Erevan, "Nauka." 1969.
129. Obmenin, A. V., V. A. Balykov, A. I. Korotkov, and A. A. Sulimov. – Fizika Goreniya i Vzryva, No. 4: 571. 1970.
130. Zel'dovich, Ya. B. and Yu. P. Raizer. Fizika udarnykh voln i vysokotemperaturnykh gidrodinamicheskikh yavlenii (Physics of Shock Waves and High-Temperature Hydrodynamic Phenomena). – Moskva, Fizmatgiz. 1963.
131. Babaitsev, I. V., B. N. Kondrikov, Z. V. Paukova, and V. F. Tyshevich. – Fizika Goreniya i Vzryva, No. 3: 326. 1969.
132. Apin, A. Ya. and V. K. Bobolev. – Dokl. Akad. Nauk SSSR, Vol. 458: 241. 1947.
133. Lyakhov, G. M. and G. I. Pokrovskii. Vzryvnye volny v gruntakh (Detonation Waves in Soils). – Moskva, Gosgortekhizdat. 1962.
134. Parfenov, A. K. and A. Ya. Apin. – Nauchno-Tekhnicheskie Problemy Goreniya i Vzryva, No. 1: 109. 1965.
135. Parfenov, A. K. Candidate Thesis. – Inst. Khim. Fiz. AN SSSR, Moskva. 1947.
136. Dubovik, A. V. and V. K. Bobolev. – In: "Vzryvnoe delo," No. 63/20: 72. Moskva, "Nedra." 1967.
137. Bobolev, V. K. – Dokl. Akad. Nauk SSSR, Vol. 57: 789. 1947.
138. Soloukhin, R. I. Udarnye volny i detonatsiya v gazakh (Shock Waves and Detonation in Gases). – Moskva, Fizmatizdat. 1963.
139. Bobolev, V. K., V. A. Burov, and A. V. Dubovik. – Fizika Goreniya i Vzryva, No. 1: 124. 1968.
140. Al'tshuler, L. V. – Usp. Fiz. Nauk, Vol. 85: 197. 1965.
141. Oppenheim, A., N. Manson, and H. Wagner. – AIAA, No. 1: 2243. 1963.
142. Griffiths, N. and I. M. Groocock. – J. Chem. Soc., Vol. 11: 4154. 1960.
143. Sokolov, A. V. and Yu. N. Aksenov. – In: "Vzryvnoe delo," No. 52/9. Moskva, Gosgortekhizdat. 1963.
144. Sokolov, A. V., I. V. Mil'chakov, and L. K. Dubnov. – In: "Vzryvnoe delo," No. 63/20. Moskva, "Nedra." 1967.
145. Gogolev, V. M., V. G. Myrkin, and G. I. Yablokova. – Prikl. Mekh. i Tekhn. Fiz., No. 5: 93. 1963.
146. Afanasenkov, A. N., V. M. Bogomolov, and I. M. Voskoboinikov. – Fizika Goreniya i Vzryva, No. 3: 4. 1967.
147. Ilyukhin, V. S. and P. F. Pokhil. – Dokl. Akad. Nauk SSSR, Vol. 140: 179. 1961.
148. Afanasenkov, A. N., V. M. Bogomolov, and I. M. Voskoboinikov. – In: "Vzryvnoe delo," No. 68/25.68. Moskva, "Nedra." 1970.
149. Afanasenkov, A. N. Candidate Thesis. – Inst. Khim. Fiz. AN SSSR. Moskva. 1969.
150. Seay, G. E. and L. B. Seely. – J. Appl. Phys., Vol. 32: 1092. 1961.



151. Evans, M. W., B. O. Reese, and L. B. Seely. – 4th Intern. Sympos. on Detonation, p. 359. Maryland. 1965.
152. Belyaev, A. F., M. A. Sadovskii, and I. I. Tamm. – Prikl. Mekh. i Tekhn. Fiz., No. 1: 2. 1960.
153. Apin, A. Ya., A. N. Afanasenkov, G. V. Dimza, and V. I. Stafeev. – Dokl. Akad. Nauk SSSR, Vol. 147: 1141. 1962.
154. Bolkhovitinov, L. G. and V. A. Vasil'ev. – Fizika Goreniya i Vzryva, Vol. 4: 587. 1969; Referaty dokladov na II Mezhdunarodnom kollokviume po gazodinamike vzryva i reagiruyushchikh sistem. Novosibirsk. 1969.
155. Amster, A. B., E. C. Noonan, and G. J. Bryan. – ARSJ., Vol. 30: 960. 1960.
156. Wasley, R. J. and F. E. Walker. – J. Appl. Phys., Vol. 40: 2639. 1969.
157. Vasil'ev, M. Ya. – Fizika Goreniya i Vzryva, No. 3: 43. 1965.
158. Glazkova, A. P. – Prikl. Mezh. i Tekhn. Fiz., No. 5: 121. 1963.
159. Babaitsev, I. V., B. N. Kondrikov, and V. F. Tyshevich. – In: "Vzryvnoe delo," No. 68/25: 215. Moskva, "Nedra." 1970.
160. Anders[illegible], W. H. and R. F. Chaiken. – ARSJ., Vol. 31: 1379. 1961.
161. Mal'tsev, V. M. Candidate Thesis. – Inst. Khim. Fiz. AN SSSR. Moskva. 1961.
162. Krasnov, Yu. K., V. M. Margulis, A. D. Margolin, and P. F. Pokhil. – Fizika Goreniya i Vzryva, No. 3: 290. 1970.
163. Zenin, A. A. – Fizika Goreniya i Vzryva, No. 3: 67. 1966.
164. Bryan, C. I. and E. C. Noonan. – Proc. R. Soc., Vol. A246: 167. 1958.
165. Afonina, L. V., I. V. Babaitsev, and B. N. Kondrikov. – In: "Vzryvnoe delo," No. 68/25: 149. Moskva, "Nedra." 1970.
166. Sulimov, A. A., A. V. Obmenin, and A. I. Korotkov. – Trudy III Vses. Simpoz. po goreniyu i vzryvu, p. 464. Moskva, "Nauka." 1972.
167. Apin, A. Ya. – Dokl. Akad. Nauk SSSR, Vol. 24: 922. 1939.
168. Dremin, A. N. and I. A. Karpukhin. – Prikl. Mekh. i Tekhn. Fiz., No. 3: 184. 1960.
169. Margolin, A. D. and V. M. Margulis. – Fizika Goreniya i Vzryva, No. 1: 15. 1969.
170. Landau, L. D. and E. M. Lifshits. Mekhanika sploshnykh sred (Mechanics of Continuous Media). – Moskva, Gostekhteorizdat. 1953.
171. Babaitsev, I. V., V. V. Gorbunov, B. N. Kondrikov, and V. A. Ponomarev. – Materialy X Vsesoyuznoi konferentsii po aktual'nym voprosam ispareniya, goreniya i gazovoi dinamiki dispersnykh sistem, p. 51. Odessa. Izdatel'stvo Odesskogo Gosudarstvennogo Universiteta im. D. I. Mechnikova. 1970.
172. Andreev, K. K. – Combust. Flame, Vol. 7: 175. 1963.
173. Liddiard, T. P. – 4th Sympos. on Detonation. Maryland. 1965.
174. Irwin, O. R., P. K. Salzman, and W. H. Andersen. – AIAA, Vol. 1: 2260. 1963.
175. Margolin, A. D. and E. E. Kiselev. – Fizika Goreniya i Vzryva, No. 4: 83. 1965.

176. Taylor, W. – Trans. Faraday Soc., Vol. 58: 561. 1963.
177. Margolin, A. D., L. F. Chekirda, and S. V. Chuiko. – Inzhener. Zh., Vol. 3: 460. 1963.
178. Margolin, A. D. and S. V. Chuiko. – Prikl. Mekh. i Tekhn. Fiz., No. 1: 104. 1966.
179. Margolin, A. D. and S. V. Chuiko. – Trudy Tsentr. Nauchno-Issled. Proektno-Konstrukt. Kotlo-Turbinnyi Inst. im. I.I. Polzunova, Vol. 64: 75. 1965.
180. Steinberger, R. – 4th Intern. Sympos. on Combustion, p. 205. Baltimore, The Williams and Wilkins Co. 1953.
181. Belyaev, A. F. and G. V. Lukashenya. – Prikl. Mekh. i Tekhn. Fiz., No. 6: 114. 1966.
182. Spravochnik khimika (The Chemist's Handbook), 2nd edition, Vol. 3. – Moskva - Leningrad, "Khimiya," 1964.
183. Hála, E., J. Pick, V. Fried, and O. Vilim. Vapour-Liquid Equilibrium. – New York, Pergamon Press. 1958.
184. Shchelkin, K. I. – Fizika Goreniya i Vzryva, No. 4: 455. 1968.
185. Istratov, A. G. and V. B. Librovich. Itogi nauki. Gidromekhanika (Progress in Science. Hydromechanics). – Moskva, Izdatel'stvo Vses. Inst. Nauch. Tekhn. Informatsii Gos. Komiteta Soveta Ministrov SSSR po Nauke i Tekhnike AN SSSR. 1966.
186. Whittaker, A. G. et al. – J. Phys. Chem., Vol. 60: 904. 1956.
187. Eirich, F. R. Rheology: Theory and Application, Vol. 1. 1956; Vol. 2. 1958; Vol. 3. 1960. – New York, Academic Press. 1960.
188. Reiner, M. Deformation, Strain and Flow. – Interscience. 1960.
189. McLain, W. H. – AIAA-Paper, No. 64: 368. 1964.
190. Darriens, G. – 6th Intern. Congress Appl. Mech., p. 24. Paris, Dunod. 1946.
191. Bakhman, N. N. and F. I. Dubovitskii. – In: "Fizika vzryva," No. 4: 102. Moskva, Izdatel'stvo AN SSSR. 1955.
192. Chem. Engng. Handbook, No. 7: 436. 1956.
193. Andreev, K. K., I. A. Tereshkin, and A. P. Glazkova. – Zhurn. Fiz. Khim., Vol. 35: 426. 1961.
194. Paushkin, Ya. M. Khimiya reaktivnykh topliv (Chemistry of Rocket Propellants). – Moskva, Izdatel'stvo AN SSSR. 1962.
195. Adams, G. K. and G. W. Stocks. – 4th Intern. Sympos. on Combustion, p. 239. The Williams and Wilkins Co. 1953.
196. Maksimov, E. I. and A. A. Bairash. – Fizika Goreniya i Vzryva, No. 1: 76. 1969.
197. Chuiko, S. V. Thesis. – Inst. Khim. Fiz. AN SSSR. Moskva. 1959.
198. Whittaker, A. G. et al. – J. Phys. Chem., Vol. 62: 908. 1958.
199. Andreev, K. K. and G. H. Bespalov. – In: "Teoriya vzryvchatykh veshchestv," p. 430. Moskva, Oborongiz. 1963.
200. Antoine, A. C. – Combust. Flame, Vol. 6: 363. 1962.
201. Andreev, K. K. *See* /199, p. 416/.
202. Ordzhonikidze, S. K., A. D. Margolin, and P. F. Pokhil. – Trudy III Vses. Simpoz. po goreniyu i vzryvu, p. 83. Moskva, "Nauka," 1972.
203. Wieber, P. R. – AIAA, Vol. 1: 2764. 1963.
204. Blinov, V. I. and G. N. Khudyakov. Diffuzionnoe gorenie zhidkostei (Diffusional Combustion of Liquids). – Moskva, Izdatel'stvo AN SSSR. 1961.



205. Gol'binder, A. I. *See* /199, pp. 468, 499/.
206. Belyaev, A. F. and L. D. Komkova. – Zhurn. Fiz. Khim., Vol. 45: 3696. 1950.
207. Golub, A. – J. Spacecraft and Rockets, Vol. 4: 562. 1965.
208. Margolin, A. D., V. M. Margulis, and P. F. Pokhil. – Fizika Goreniya i Vzryva, No. 4: 426. 1968.
209. Rumanov, E. N. and B. I. Khaikin. – Fizika Goreniya i Vzryva, No. 1: 129. 1969.
210. Grigor'ev, Yu. M. et al. – Fizika Goreniya i Vzryva, No. 4: 526. 1968.
211. Merzhanov, A. G., B. M. Slutsker, and A. S. Shteinberg. – Fizika Goreniya i Vzryva, No. 4: 540. 1968.
212. Dubovik, A. V. and V. K. Bobolev. – Ibid., p. 493.
213. Gordeev, V. E. Candidate Thesis. – Inst. Khim. Fiz. AN SSSR. Moskva. 1967.
214. Dubovik, A. V., I. M. Voskoboinikov, and V. K. Bobolev. – Fizika Goreniya i Vzryva, No. 1: 105. 1966.
215. Gordeev, V. E. and Yu. S. Matveev. – Fizika Goreniya i Vzryva, No. 4: 589. 1966.
216. Mayer, A. – ARSJ, Vol. 31: 1783. 1961.
217. Dremin, A. N., O. K. Rozanov, S. D. Savrov, and V. S. Trofimov. – Fizika Goreniya i Vzryva, No. 3: 291. 1969.
218. Margolin, A. D., V. M. Margulis, and P. F. Pokhil. – Dokl. Akad. Nauk SSSR, Vol. 137: 130. 1961.
219. Margolin, A. D., V. M. Margulis, and N. V. Solov'ev. – Fizika Goreniya i Vzryva, No. 3: 272. 1970.
220. Levich, V. G. Fiziko-khimicheskaya gidrodinamika (Physico-chemical Hydrodynamics). – Moskva, Fizmatgiz. 1959.
221. Kondrikov, B. N. *See* /199, p. 443/.
222. Glazkova, A. P. – Fizika Goreniya i Vzryva, No. 1: 62. 1971.
223. Chaudri, M. M. and I. E. Field. Preprints of Papers to be Presented at Fifth Symposium on Detonation. Pasadena, 18–21 August 1970.
224. Cook, A., D. Pack, and W. McEwan. – Trans. Faraday Soc., Vol. 56: 1028. 1960.